

STRUCTURE AND FUNCTION OF THE INFLUENZA MEMBRANE PROTEIN M2 BY
MAGIC ANGLE SPINNING NMR AND DYNAMIC NUCLEAR POLARIZATION

by

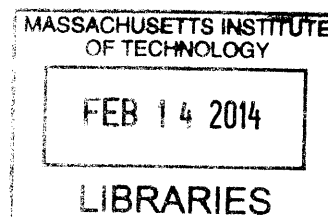
Loren B. Andreas

B.A., Chemistry (2007)
Oberlin College

Submitted to the Department of Chemistry
in Partial Fulfillment of the Requirements for the Degree of
Doctor of Philosophy in Chemistry

at the
Massachusetts Institute of Technology
February, 2014

ARCHIVES



© 2014 Massachusetts Institute of Technology. All rights reserved.

Signature of Author _____ Department of Chemistry

Certified by _____ Professor Robert G. Griffin
Thesis Supervisor

Accepted by _____
Chairman, Department Committee on Graduate Students

This doctoral thesis has been examined by a committee of the department of chemistry as follows:

Professor Robert W. Field____
Chairman

Professor Robert G. Griffin____
Thesis Supervisor

Professor Jianshu Cao____

Structure and function of the Influenza Membrane Protein M2 by Magic Angle Spinning NMR and Dynamic Nuclear Polarization

by

Loren B. Andreas

Submitted to the Department of Chemistry
on December 6th, 2013 in Partial Fulfillment of the Requirements of the
Degree of Doctor of Philosophy in Chemistry

Abstract

Determination of the 3D structure of membrane proteins is a frontier that is rapidly being explored due to the importance of membrane proteins in regulating cellular processes and because they are the target of many drugs. In addition, measuring and understanding how these proteins interact with ligands and other molecules is of critical importance to the design of the next generation of therapeutic agents.

With this motivation, we report new methods for the structural characterization of proteins using magic angle spinning (MAS) nuclear magnetic resonance (NMR) applied to the membrane protein M2 from Influenza A, a small helical transmembrane proton transporter that is the target of adamantane based inhibitors but which is now drug resistant due primarily to the point mutation S31N. The development of techniques that boost the sensitivity of NMR are key to its extension to larger molecules such as membrane proteins, and two such methods, dynamic nuclear polarization (DNP) and proton detection, are applied herein. We report the measurement of the distance between the amine of the inhibitor rimantadine and the pore of M2 using DNP.

We have applied recoupling techniques to assign the spectra and measure internuclear distances in the drug resistant S31N mutant of M2 in lipid bilayers. Attenuation of strong proton dipole couplings with 60 kHz spinning has allowed us to detect well-resolved proton spectra, and with the higher receptivity of protons, we measured interhelical distances with a methyl-methyl 4D spectrum. Synthesis of the information resulted in a high resolution structure of S31N M2.

Thesis Supervisor: Robert G. Griffin

Title: Professor of Chemistry and Director of the Francis Bitter Magnet Laboratory

Table of Contents

Abstract	3
List of Figures	7
Acknowledgements	12
Chapter 1 : Introduction	14
2.1 Motivation	14
2.2 Magic Angle Spinning NMR Theoretical Background	16
Two or more spins	18
Spinning about the Magic Angle	21
2.3 Recoupling	22
Heteronuclear Dipolar Recoupling: REDOR.....	22
Homonuclear Dipolar Recoupling: RFDR.....	24
2.4 Thesis Outline	26
2.5 References	26
Chapter 2 : Magic Angle Spinning NMR Investigation of Influenza A M2₁₈₋₆₀: Support for an Allosteric Mechanism of Inhibition	30
2.1 Introduction	30
2.2 Results and Discussion	30
2.3 Methods and Spectral Assignments	36
2.4 References	39
Chapter 3 : Dynamic Nuclear Polarization Study of Inhibitor Binding to the M2₁₈₋₆₀ Proton Transporter from Influenza A	42
3.1 Introduction	42
3.2 Methods	45
The DNP enhanced ZF-TEDOR experiment	45
Optimization of Radical Concentration	45
M2 Sample Preparation.....	46
NMR, Hardware, Referencing, and Processing	46
3.3 Results	47
3.4 Discussion	54
3.5 Supporting Information	56
3.6 Conclusions	59
3.7 References	60
Chapter 4 : MAS NMR of the Drug Resistant S31N M2 Proton Transporter from Influenza A	64
4.1 Introduction	64
4.2 Results and Discussion	65
4.3 Methods	69
4.4 Supporting Information	70
Table of Chemical Shifts	71
4.5 Conclusion	77
4.6 References	78

Chapter 5 : MAS NMR Structure of the Drug Resistant S31N M2 Proton Transporter from Influenza A in A Lipid Bilayer	82
5.1 Introduction	82
5.2 Results and Discussion	83
5.3 Methods	88
5.4 Supporting Information	100
5.5 References	148
Chapter 6 : Synthesis and physical properties of Deuterated 1,2-Diphytanoyl-<i>sn</i>-glycero-3-phosphocholine Lipid	152
6.1 Introduction	152
6.2 Results and Discussion	154
6.3 Methods	157
NMR Spectroscopy	157
Differential Scanning Calorimetry	158
Synthesis of DPhPC	158
Sample Preparation	159
6.4 References	161
Chapter 7 : ²H-DNP-enhanced ²H-¹³C solid-state NMR correlation spectroscopy	164
7.1 Introduction	164
7.2 Results and Discussion	166
Polarizing Agents and DNP-Enhancement Profiles	166
² H-DNP Enhanced ² H- ¹³ C Correlation Spectroscopy	170
Spectral Linewidths	172
Sensitivity Gain Through DNP	173
7.3 Methods	175
Sample Preparation	175
DNP Spectroscopy	175
EPR Spectroscopy	176
7.4 Conclusions	176
7.5 References	176
Chapter 8 : Paramagnetic Signal Quenching in MAS-DNP of Homogeneous Solutions	180
8.1 Introduction	180
8.2 Background and Theory	182
Mechanisms of DNP	182
Electron-nuclear interactions during MAS DNP	183
Properties of the polarizing agents	184
Transverse paramagnetic relaxation	186
8.3 Methods	187
Instrumentation	187
Sample preparation	187
Data acquisition and analysis	188
8.4 Results and Discussion	190
Determination of paramagnet induced relaxation rates	191
T ₁ relaxation and build-up of polarization	192
T ₂ and homogeneous linewidth	195
T _{1ρ} relaxation	197
DNP enhancement factor	199
Signal quenching	201
Overall sensitivity enhancement	204

Electron Decoupling	205
8.5 Supporting Information	205
Synopsis	205
Choice of internal standard	206
Determination of internal standard signal amplitude of undoped samples	207
Determination of urea signal amplitude of doped samples	208
Correction for varying polarization times used in measurement of internal standard signal amplitude of undoped samples	208
Final correction of NMR signal bleaching data using internal standard signal amplitude ..	210
Supplementary Tables	213
8.6 Conclusions	216
8.7 References	217
Chapter 9 : High-Resolution Solid-State NMR Structure of Alanyl-Prolyl-Glycine.....	222
9.1 Introduction	222
9.2 Results and Discussion	223
CSA parameters for precise R ² W fitting	224
Carboxyl terminus	225
Constraints effect on structural quality	226
9.3 Conclusions	228
9.4 Experimental Methods.....	228
Sample preparation	229
Assignments	229
NCCN Local Field Correlations	229
Rotational Resonance Width.....	230
DANTE-REDOR	231
9.5 Supporting Information	234
APG Single Crystal Data	234
9.6 References	242
Curriculum Vitae.....	244

List of Figures

<i>Figure 1.1.</i> A static phosphorus spectrum of a phospholipid, and an isotropic spectrum acquired under 6.3 kHz MAS.	22
<i>Figure 2.1.</i> TEDOR spectrum of M2 ₁₈₋₆₀ showing large chemical shift changes upon addition of rimantadine.	31
<i>Figure 2.2.</i> Chemical shift perturbations ($\Delta\delta = \delta_{\text{bound}} - \delta_{\text{apo}}$) are distributed across the channel and support an allosteric effect upon drug binding.	32
<i>Figure 2.3.</i> TEDOR spectra of M2 acquired at 0, 1, and 4 Rmt molecules per channel	33
<i>Figure 2.4.</i> ¹³ C- ¹³ C PDSM spectra of POPC embedded (red) and DPhPC embedded (black) M2 show nearly identical spectra	35
<i>Figure 2.5.</i> The 1-bond ¹³ C ¹⁵ N TEDOR spectrum presented in <i>Figure 2.1</i> is expanded to show peak doublings.	38
<i>Figure 2.6.</i> A Drug titration of M2 in DPhPC lipids is detected in a ¹⁵ N CPMAS experiment.....	39
<i>Figure 3.1.</i> Schematic of the DNP enhanced TEDOR experiment.....	45
<i>Figure 3.2.</i> PDSM spectra of M2 acquired under four sample conditions show that chemical shifts are unperturbed by 60% glycerol if glycerol is the last component added to the sample.....	48
<i>Figure 3.3.</i> ZF-TEDOR spectra acquired at 278 K (red) show one set of cross-peaks, and those acquired at ~90 K using DNP (blue) show additional peaks.	49
<i>Figure 3.4.</i> ZF-TEDOR spectra show that the pore binding site is correlated with chemical shift changes.....	50
<i>Figure 3.5.</i> DNP enhanced ZF-TEDOR spectra (five mixing points) recorded at 600 MHz with DNP are used to measure a drug-protein distance.	52
<i>Figure 3.6.</i> A structural model of the pore binding site is shown using distance constraints from DNP enhanced TEDOR experiments, 278 K TEDOR experiments, and previously reported data.	54
<i>Figure 3.7.</i> Spectra of ¹³ C-ILFY reverse labeled M2 (blue) show identical crosspeaks as FY reverse labeled M2 (red).	56
<i>Figure 3.8.</i> The double mutant used in this work is functional and drug sensitive.	57
<i>Figure 3.9.</i> An illustration of the tilt angle measured by Hong and coworkers for Amantadine and Rimantadine	57
<i>Figure 3.10.</i> The Proton Driven Spin Diffusion (PDSM) pulse program	58

Figure 3.11. The z-filtered transferred echo double resonance (ZF-TEDOR) pulse program.....	58
Figure 4.1. ZF-TEDOR spectra of S31N M2 ₁₈₋₆₀ are shown in the presence (blue) and absence (red) of the inhibitor Rmt.....	65
Figure 4.2. An aromatic-aromatic ¹³ C correlation spectrum using 400 ms of proton driven spin diffusion mixing shows cross-peaks between the two sets of chemical shifts.	66
Figure 4.3. 3D ZF-TEDOR-RFDR pulse sequence used for assignments.	68
Figure 4.4. Slices are shown from the NCACX and NCOCX regions of a 3D ZF-TEDOR-RFDR spectrum used for sequential assignments.	69
Figure 4.5. Histidine resonances are shown from the 1.2 ms ZF-TEDOR spectrum of Figure 4.1	73
Figure 4.6. The effect of temperature changes on the chemical shift is investigated in overlaid ¹³ C- ¹³ C correlation spectra at two different temperatures.	74
Figure 4.7. Peak doubling, $ \delta_{\text{prime}} - \delta $ in ppm, is displayed as a function of residue number for ¹³ C resonances of WT M2 ₁₈₋₆₀ . The average value between the drug bound and apo samples is displayed.	75
Figure 4.8. Peak doubling, $ \delta_{\text{prime}} - \delta $ in ppm, is displayed as a function of residue number for ¹⁵ N resonances of WT M2 ₁₈₋₆₀ . The average value between the drug bound and apo samples is displayed.	75
Figure 4.9. Chemical shift changes with addition of the inhibitor rimantadine are plotted against residue number for the S31N mutant of M2 ₁₈₋₆₀	76
Figure 4.10. A reproduction of the spectrum in Figure 4.2 with aromatic assignments listed on the diagonal. We thereby show that the critical interhelical contact between C δ 2 and C ϵ 1 of H37 is far removed from tryptophan peaks.	77
Figure 5.1. Dimer of dimers structure of M2.....	84
Figure 5.2. Side chain conformations of the S31N M2 tetramer.	85
Figure 5.3. Explanation of drug resistance.	86
Figure 5.4. PAR spectrum with 15 ms mixing recorded at a ¹ H frequency of 900 MHz and 20 kHz MAS. A four-fold molar excess of rimantadine drug was present in the sample.	89
Figure 5.5. The Ca-Ca region of a PDS spectra with 400 ms mixing were recorded at 750 MHz spinning at 14.287 kHz. A four-fold molar excess of rimantadine drug was present in the sample.	90
Figure 5.6. ¹⁵ N-aliphatic correlations from a ¹⁵ N- ¹³ C TEDOR spectrum of a 1:1 mixture of ¹⁵ N and 1,6- ¹³ C glucose labeled M2. 14.336 ms of TEDOR mixing was applied.	90

Figure 5.7. ^{13}C - ^{13}C RFDR spectrum of 1,6- ^{13}C Glucose labeled M2 showing inter-helical cross-peaks	91
Figure 5.8. Selected planes from a proton detected 4D using an 8 ms RFDR period of ^1H - ^1H mixing, and J-coupling based transfers for CH correlation.	92
Figure 5.9. Timing diagram for the 4D methyl-methyl HCHHCH spectrum shown in Figure 5.8	92
Figure 5.10. The N- $^{13}\text{C}\alpha$ plane from the TEDOR spectrum of U- ^{13}C , ^{15}N S31N M2. 1.2 ms of mixing was applied in order to observe only one bond transfer.	93
Figure 5.11. Selected strips from the 3D TEDOR-RFDR spectrum show the consecutive assignment of residues P25 to I33.	94
Figure 5.12. A cross polarization based HN spectrum showing the completed backbone amide assignments.	95
Figure 5.13. Selected strips from the HCaNH spectrum of ^2H M2.	95
Figure 6.1 Protonated DPhPC (top) and DPPC (bottom).	153
Figure 6.2. Temperature dependent ^2H spectra of DPhPC, DPhPC:M2, and DPPC.	154
Figure 6.3. The ^2H spectrum of DPhPC at 173 K overlapped with that of 208 K on an absolute scale. The isotropic peak emerges while the powder pattern is reduced by 50%.	155
Figure 6.4. Differential scanning calorimetry (DSC) trace of ^2H DPhPC in 60:40 glycerol:water (vol).	156
Figure 6.5. The ^2H NMR spectrum of chain deuterated DPhPC at 290 K.	157
Figure 6.6. Proton spectrum (a) of acyl chain deuterated (d78) DPhPC demonstrating a purity by NMR of above 85%. In (b), a thin layer chromatogram shows a single spot with the same retention time as commercial protonated DPhPC.	159
Figure 6.7. Phosphorus spectrum of alkyl chain deuterated (d78) DPhPC.	160
Figure 6.8. Comparison of M2 ₁₈₋₆₀ spectra in ^2H DPhPC and in commercial ether linked DPhPC.	161
Figure 7.1. Molecular structures of the two polarizing agents TOTAPOL and OX063.	166
Figure 7.2. Trityl EPR spectra and ^2H enhancement profiles.	167
Figure 7.3. Comparison of the steady-state ^2H signal intensity for TOTAPOL (A) and OX063 (B).	168
Figure 7.4. ^2H bulk-polarization build-up curve showing an enhancement of 700.	169

Figure 7.5. Direct ^{13}C DNP-enhanced MAS-NMR spectra of U- $[\text{}^2\text{H}_7, \text{}^{13}\text{C}_5]$ -proline taken (A) without decoupling and (B) with 83 kHz of TPPM ^2H decoupling.	170
Figure 7.6. Direct and ^2H -CP ^{13}C MAS-NMR spectra of U- $[\text{}^2\text{H}_7, \text{}^{13}\text{C}_5]$ -proline taken at 90 K....	171
Figure 7.7. Pulse sequence to record a ^2H double-quantum, ^{13}C correlation spectrum.	171
Figure 7.8. Determination of the DQ efficiency for U- $[\text{}^2\text{H}_7, \text{}^{13}\text{C}_5]$ -proline from DNP enhanced spectra.	172
Figure 7.9. Two-dimensional DNP-enhanced ^2H -DQ- ^{13}C correlation spectrum of U- $[\text{}^2\text{H}_7, \text{}^{13}\text{C}_5]$ -proline recorded at 90 K	173
Figure 8.1. Polarizing agents investigated in this study.	185
Figure 8.2. Pulse sequence used for relaxation time measurements.....	189
Figure 8.3. DNP enhanced ^{13}C - ^1H CP spectra of ^{13}C -urea in 60/30/10 (vol.-%) d_8 -glycerol/ $\text{D}_2\text{O}/\text{H}_2\text{O}$	190
Figure 8.4. Equilibrium signal intensity (top) and T1 (bottom) are compared for a 20 mM trityl sample and a 10 mM TOTAPOL sample under static and MAS conditions.....	191
Figure 8.5. ^1H DNP build-up time constant T_B (top) and paramagnetically enhanced buildup rate constant $\tilde{\Gamma}_B$	193
Figure 8.6. Electron spin longitudinal relaxation time constant T_{1S} (top) and transverse relaxation time constant T_{2S} (bottom) as a function of electron spin concentration of various polarizing agents measured at 140 GHz EPR frequency.	194
Figure 8.7. ^{13}C transverse relaxation time constant T_2 (top) and the related rate constant $\tilde{\Gamma}_2$...	196
Figure 8.8. ^1H (top) and ^{13}C (bottom) $\tilde{\Gamma}_{1\rho}$ at a spin-lock field of $\omega_{\text{SL}}/2\pi = 50$ kHz as a function of electron spin concentration of various polarizing agents.....	198
Figure 8.9. Characterization of sensitivity gain by DNP.....	200
Figure 8.10. Relative off-signal intensity not affected by paramagnetic quenching ($1-\xi$) as a function of the electron spin concentration c_s normalized to the absolute magnetization of each electron spin.....	203
Figure 9.1. Crystal structure of APG 13 showing the 11 SSNMR experimental constraints used in the structural refinement.	223
Figure 9.2. a) Relative orientations of the Proline C' and C $_{\gamma}$ CSAs	225
Figure 9.3. Crystal lattice of APG showing competing intermolecular distances to the long-range internuclear distance that could be used for structural refinement.	226
Figure 9.4. 20 lowest energy structures of APG using simulated annealing	227

Figure 9.5. a) Contour plot of the root mean square deviation between experimental and simulated R ² W profiles for P ₀ to P _γ as a function of distance and relaxation.....	228
Figure 9.6. Dephasing curves for extraction of Ψ torsion angle.....	230
Figure 9.7. R ² W spectra at 5 spinning frequencies.....	231
Figure 9.8. The χ ² surface for azimuthal (α) and polar (β) angles of the CSA-dipole orientation	232

Acknowledgements

I would like to thank Prof. Robert Griffin, my research supervisor, for material and scientific support, and for providing a flexible research environment. I have had the opportunity to pursue topics that interest me because Bob's encouragement and the independence that he fosters in the lab.

I have been fortunate to learn from many fellow Ph.D. students and postdoctoral researchers during my time at MIT. Dr. Matthew Eddy helped get me started with high field spectroscopy and the M2 project, and we continued to work together on many projects. Dr. Alexander Barnes was instrumental in the design and implementation of the DNP application of M2. Ta-Chung Ong took the lead in the acquisition of ²H spectra of lipid samples. Dr. Marcel Reese helped with M2 structure calculations and the analysis of spectra that resulted in highly ambiguous restraints, and Eric Miller contributed to both sample preparation and data analysis. In addition, I have benefitted from insightful discussion from many other researchers, including Dr. Andy Smith, Dr. Marvin Bayro, Dr. Galia Debelouchina, Dr. Evgeny Markhasin, Dr. Bjorn Corzilius, Qing Zhe Ni, Thach Can, Dr. Yongchao Su, Dr. Jennifer Mathies, Dr. Eugenio Daviso, Dr. Michael Colvin, Dr. Vladimir Michaelis, Dr. Kendra Frederick, and Angela Jacavone.

I am truly grateful for the many collaborations I have had, in particular the collaboration with Prof. James Chou and his former graduate student, Dr. Rafal Pielak who taught me the protocol for M2 production and purification. I am thankful for the helpful discussion and advice of all the other members of the Chou lab, particularly Dr. Marcelo Berardi, Dr. Remy Sounier, Dr. Matthew Call, and Jessica Williamson. I also had the great opportunity to bring samples to France for the acquisition of proton detected spectra with Prof. Guido Pintacuda and Lyndon Emsley.

I would like to thank Prof. Vladimir Gelev for reigniting my interest in organic chemistry. Without his help, the synthesis of deuterated lipids would not have been a success.

The technical support and guidance I have received from Ajay Thakkar, Mike Mullins, Ron Derocher, Jeff Bryant, Dr. Tony Bielecki, Dr. Chris Turner, and Dr. David Ruben is gratefully acknowledged.

I also thank my undergraduate advisor, Prof. Manish Mehta, for sending me on my current trajectory in magic angle spinning NMR.

Finally, thanks to my wife Samina Ali, my son Zian, my parents, and my brothers.

Chapter 1: Introduction

2.1 Motivation

Proteins provide the basis for a multitude of important processes that support life. They are found as soluble proteins, such as enzymes, membrane associated proteins that interact with specific locations in the cell, and transmembrane proteins that often serve as the gatekeepers of cells and cellular compartments. Membrane proteins comprise 20 to 30 percent of all proteins,¹ are vital for mediating entry and exit of molecules across membranes, signaling, and cell adhesion. Important classes of membrane proteins include G-protein coupled receptors (GPCRs), involved in signaling and cellular response, Aquaporins, which are selectively permeable to water and small molecules such as glycerol, and transporters and symporters, which move small molecules across membranes. Membrane proteins comprise over 50 percent of drug targets.²

Determination of protein structures is the first step toward the rational development of inhibitors. Diffraction methods and solution NMR have provided insight into membrane protein function through the determination of structures, the identification of ligand binding sites and equilibria, and measurement of dynamic information. For example, the Nobel Prize in chemistry was awarded recently for successful determination of crystal structures of GPCR membrane proteins because they are so difficult to study using diffraction methods due to the necessity of coaxing the protein into a highly ordered crystal. Solution NMR structures of small membrane proteins has been highly successful, but extension to much larger molecules is not possible due to an increase in line width with molecular size due to slowed molecular tumbling. Although solution NMR and crystallization methods have made progress in the area of membrane protein structure, there is still a paucity of solved transmembrane protein structures, which occupy less than one percent of the protein data bank although they represent approximately 20 to 30 percent of all proteins. There is therefore a crying need for a reliable and efficient method for membrane protein structure determination.

High-resolution solid-state NMR is rapidly emerging as a powerful structural tool in chemistry and biology to access at the atomic-level substrates that traditionally escape solution NMR and X-ray crystallography.³⁻²⁵ Steadily ongoing methodological developments combined with tremendous engineering advances in probe and spectrometer hardware, and notably increased magnetic field strengths, have paved the way for studying structure and dynamics of solid chemical and biological samples at atomic resolution. A variety of strategies

for resonance acquisition and assignment has led to the first 3D structure determinations of model macromolecules in the solid state at atomic resolution, spanning a broad atlas of structures ranging from non-crystalline or poorly-crystalline materials to protein aggregates or membrane proteins.^{3, 4, 23, 26-29} Solid-state NMR also has a unique ability to supplement the determination of protein folds with data on dynamics, spanning a timescale of events which is potentially broader than that probed by solution NMR.³⁰⁻³² The possibility of accessing structural and dynamic information is particularly interesting for membrane proteins because their function often involves conformational plasticity, either for transport of small molecules, or for signaling across the membrane.

It thus appears that solid-state NMR is uniquely positioned to answer key questions about structure and function of membrane proteins, and to complement diffraction-based techniques and solution NMR spectroscopy in order to understand their mode of action in mechanistic and structural terms.

However, these determinations are far from routine. Today only a very small handful of examples have been published involving structures of membrane proteins. The development of a robust, rapid general protocol is now required for solid-state NMR to become a widespread tool for the structural biology of membrane systems. The chapters in this thesis provide a demonstration of such new methods applied to the membrane protein M2 from Influenza.

The M2 protein from Influenza A is a single pass membrane protein that assembles as a tetramer and conducts protons at low pH, which is used to trigger unpacking of the virus in the endosomal pathway for infection. The full length protein is 97 residues, but a 43 residue section comprising the transmembrane helix and a C-terminal amphipathic helix is sufficient for proper pH dependent proton conduction in liposomes and in oocyte assays.^{33, 34} Additionally, inhibitor binding was observed at two different sites in the protein, and the location of functional binding was under intense discussion. Several mutants, notably S31N are resistant to these inhibitors. The relatively small size of this protein coupled with a high degree of interest from the biological and medical communities made this protein an ideal case for the demonstration of magic angle spinning NMR for protein structure determination. The results of NMR measurements presented herein have unequivocally determined the structure of the S31N mutant of M2, and determined the site of functional inhibitor binding.

One of the advantages of NMR is that the energies associated with transitions in nuclear magnets are small. This results in minimal perturbation of a chemical system when it is probed with radio frequency (RF) pulses to determine structural information. No chemical bonds risk being broken,

and typically a small amount of energy is delivered to the sample in the form of heating. The disadvantage is that with small energy spacing, Boltzmann polarization is small near ambient temperatures. For this reason, a continual problem in NMR is sensitivity. Several ways to overcome the sensitivity problem are applied in this thesis, including dynamic nuclear polarization (DNP) at low temperatures, acquisition at higher and higher field, and the detection of a high-gamma nucleus such as ^1H .

The following paragraphs describe the fundamentals of the spin physics behind the NMR based determination of molecular structure used in this thesis. The primary focus of the subsequent chapters is to apply NMR methodology to gain insight into the function of the M2 protein from influenza A through structure determination by (i), assignment of the resonances and chemical shift based secondary structure prediction (ii), determination of distances with dipolar recoupling (iii), construction of the full molecular geometry in simulation.

2.2 Magic Angle Spinning NMR Theoretical Background

Theoretical treatment of NMR follows the Quantum Mechanical description that can be found in a variety of texts.³⁵⁻³⁸ A brief introduction is presented here. In the simplest NMR experiment, a sample of many non-interacting spins is placed in a large static field \mathbf{B}_0 and the interaction between the spin and the magnetic field is the Zeeman interaction. The magnetic moment (μ) is related to spin angular momentum by:

$$\mu = \gamma \mathbf{S} \quad (1.1)$$

The gyromagnetic ratio γ is dependent on the type of nucleus, ^1H , ^{13}C , ^{15}N , ^{31}P , etc. The energy associated with the interaction of the quantum magnet and the static magnetic field is:

$$H = -\boldsymbol{\mu} \cdot \mathbf{B} = -\gamma \mathbf{B} \cdot \mathbf{S} \quad (1.2)$$

When \mathbf{B} is in the z direction with magnitude B_0 then:

$$H = -\gamma B_0 S_z \quad (1.3)$$

For spin 1/2, as commonly encountered in biological molecules, this becomes:

$$H = -\frac{\gamma B_0 \hbar}{2} \begin{pmatrix} 1 & 0 \\ 0 & -1 \end{pmatrix} \quad (1.4)$$

Which clearly has eigenvalues of $\pm\gamma B_0 \hbar / 2$. Inserting the stationary states associated with these eigenvalues into the time dependent Schrödinger equation, we see that the spin precesses at the Larmor frequency:

$$\omega = \gamma B_0 \quad (1.5)$$

At equilibrium, the net magnetic moment is determined by the population difference between the up and down states, which follows the Boltzmann distribution. The net polarization difference is typically small in NMR, in which case the polarization difference can be approximated with a Taylor expansion of the exponential:

$$P = \frac{\gamma \hbar B_0}{2kT} \quad (1.6)$$

This net polarization lies along z at equilibrium. In order to detect the NMR signal, a radio frequency pulse (RF) is applied at or near the Larmor frequency, which tips the magnetization into the xy-plane where it oscillates and is detected by the current induced in a coil. The effect of an oscillating field in the xy-plane is described by the hamiltonian:

$$H = -\gamma B_0 S_z - \gamma B_1 (S_x \cos \omega t + S_y \sin \omega t) \quad (1.7)$$

then, using $S_x \cos \omega t + S_y \sin \omega t = \exp(-iS_z \omega t) S_x \exp(iS_z \omega t)$:

$$H = -\gamma B_0 S_z - \gamma B_1 (e^{-iS_z \omega t} S_x e^{iS_z \omega t}) \quad (1.8)$$

Typically the result of the RF is shown using a rotating frame transformation:

$$\Psi' = e^{i\omega_z t S_z} \Psi \quad (1.9)$$

Then

$$-\frac{i}{\hbar} \frac{\partial \Psi'}{\partial t} = -[\omega + \gamma B_0 S_z + \gamma B_1 S_x] \Psi' \quad (1.10)$$

and the time dependence has been eliminated. On resonance then, this Hamiltonian, $H' = -[\gamma B_1 S_x]$, results in a rotation about I_x in the rotating frame. If the oscillating field is left on for the correct time, this produces a magnetic moment in the xy-plane that precesses at the Larmor frequency and is detected in a coil.

Two or more spins

Interactions between spins are critically important for the use of NMR as a tool for structural biology because they encode geometrical quantities (distance and orientation). In this case the full Hamiltonian contains terms that arise from interaction between spins:

$$H = H_z + H_{RF} + H_{CS} + H_J + H_D + H_Q \quad (1.11)$$

Where H_z is the Zeeman Hamiltonian, H_{RF} is Hamiltonian describing time dependent application of radio frequency pulses, H_{CS} is the anisotropic chemical shift interaction. H_J H_D and H_Q are interaction between spins: the scalar, dipolar, and quadrupolar Hamiltonian, respectively.

The local electronic environment surrounding a nucleus results in an orientation dependent shift in the magnetic field felt by the spin, with the magnitude of the shift typically being parts per million (ppm) of the applied field. This effect on a spin S is described by the chemical shift hamiltonian:

$$H_{CS} = -\gamma \mathbf{S} \cdot \boldsymbol{\sigma} \cdot \mathbf{B}_0 \quad (1.12)$$

Where σ is a second rank tensor. The chemical shift can be used when the sample is aligned for determination of relative orientations between the molecular frame and the external field. In addition, the isotropic part of the chemical shift still gives detailed information about the electronic environment, and is particularly useful for distinguishing different atomic sites, for example a carbonyl from an aliphatic ^{13}C , or the $^{13}\text{C}\alpha$ of valine from the $^{13}\text{C}\alpha$ of leucine.

Two spins S and I interact via the J coupling, an interaction that is mediated by electrons in chemical bonds:

$$H_J = 2\pi\mathbf{S}\cdot\mathbf{J}\cdot\mathbf{I} \quad (1.13)$$

Under static sample conditions, \mathbf{J} is a tensor, however, under isotropic tumbling or MAS it reduces to a number J. In the high field approximation, it becomes even simpler:

$$H_J = 2\pi\mathbf{J}S_xI_x \quad (1.14)$$

It is useful for transfer of magnetization over 1 bond in solids, and generally does not provide 3D structural information.

The dipole coupling Hamiltonian between two spins I and S, H_D , is probably the most important term for structure determination by SSNMR:

$$H_D = -\frac{\mu_0\hbar^2\gamma_I\gamma_S}{4\pi r^3}(3(\mathbf{I}\cdot\mathbf{e})(\mathbf{S}\cdot\mathbf{e})-\mathbf{I}\cdot\mathbf{S}) \quad (1.15)$$

Where μ_0 is the magnetic constant, r is the internuclear distance, and e is the internuclear unit vector. In spherical coordinates and using raising and lowering operators:

$$\begin{aligned}
H_D &= \frac{\mu_0 \hbar^2 \gamma_I \gamma_S}{4\pi r^3} (A + B + C + D + E + F) \\
A &= I_z S_z (1 - 3 \cos^2 \theta) \\
B &= -\frac{1}{4} (I^+ S^- + I^- S^+) (1 - 3 \cos^2 \theta) \\
C &= -\frac{3}{2} (I^+ S_z + I_z S^+) \sin \theta \cos \theta e^{-i\phi} \\
D &= -\frac{3}{2} (I^- S_z + I_z S^-) \sin \theta \cos \theta e^{i\phi} \\
E &= -\frac{3}{4} I^+ S^+ \sin^2 \theta e^{-2i\phi} \\
F &= -\frac{3}{4} I^- S^- \sin^2 \theta e^{2i\phi}
\end{aligned} \tag{1.16}$$

In the homonuclear case, the term A is diagonal, and the term B is off diagonal but connecting states of equal energy. According to perturbation theory, these terms will produce a significant effect. The terms C through F, on the other hand, connect states that differ in energy, and according to perturbation theory will have a small effect on the correction to the energies and states. The terms C through F are thus typically dropped from the dipole Hamiltonian in the zero order approximation:

$$H_{D,\text{homo}}^0 = \frac{\mu_0 \hbar^2 \gamma_I \gamma_S}{4\pi r^3} \frac{1}{2} (3I_z S_z - \mathbf{I} \cdot \mathbf{S}) (1 - 3 \cos^2 \theta) \tag{1.17}$$

In the heteronuclear case, the B term is also truncated, and the Hamiltonian becomes:

$$H_{D,\text{hetero}}^0 = \frac{\mu_0 \hbar^2 \gamma_I \gamma_S}{4\pi r^3} (2I_z S_z) (1 - 3 \cos^2 \theta) \tag{1.18}$$

The dipole coupling term is strong enough to provide internuclear distance information on a length scale that encodes meaningful distances in proteins. The dipole coupling is used in this thesis for measurement of ^1H - ^1H , ^{13}C - ^{13}C , and ^{13}C - ^{15}N distances.

Spinning about the Magic Angle

When the sample is spun about an axis that makes an angle θ_R with B_0 , the dipole coupling takes on a time dependence that can be analyzed by rotating the coordinate system from the spinning axis back to the B_0 frame:

$$\cos\theta = \begin{bmatrix} 0 & 0 & 1 \end{bmatrix} \begin{bmatrix} \cos\theta_R & 0 & -\sin\theta_R \\ 0 & 1 & 0 \\ \sin\theta_R & 0 & \cos\theta_R \end{bmatrix} \begin{bmatrix} \cos\omega t \sin\gamma \\ \sin\omega t \sin\gamma \\ \cos\gamma \end{bmatrix} \quad (1.19)$$

where we have chosen the y axis as identical in both frames, and the angle β is the angle between the internuclear axis and the rotation axis. Note that Eqn (1.19) is a simplification of the general case of rotating a tensor. For an arbitrary tensor, two rotations must be applied, first rotation from the molecular frame into the MAS frame and then into the lab frame.

If the sample rotation is sufficiently fast, we can replace the term $(1 - 3\cos^2\theta)$ in the dipole Hamiltonian with its time average. Using the expression above for $\cos^2\theta$ and averaging over one rotation:

$$\langle 1 - 3\cos^2\theta \rangle = (1 - 3\cos^2\theta_R) \left(\frac{3\cos^2\gamma - 1}{2} \right) \quad (1.20)$$

If the angle θ_R is chosen such that $(1 - 3\cos^2\theta_R) = 0$, then the term vanishes. This angle is 54.74° , the magic angle. Since the chemical shift anisotropy also has an orientation dependence of the same form, spinning about the magic angle at a sufficient frequency results in narrow line spectra similar to the result of molecular tumbling in solution. An example of this phenomenon is presented in *Figure 1.1*. The static spectrum spans about 50 ppm, and with MAS, the spectrum is narrowed to a fraction of 1 ppm.

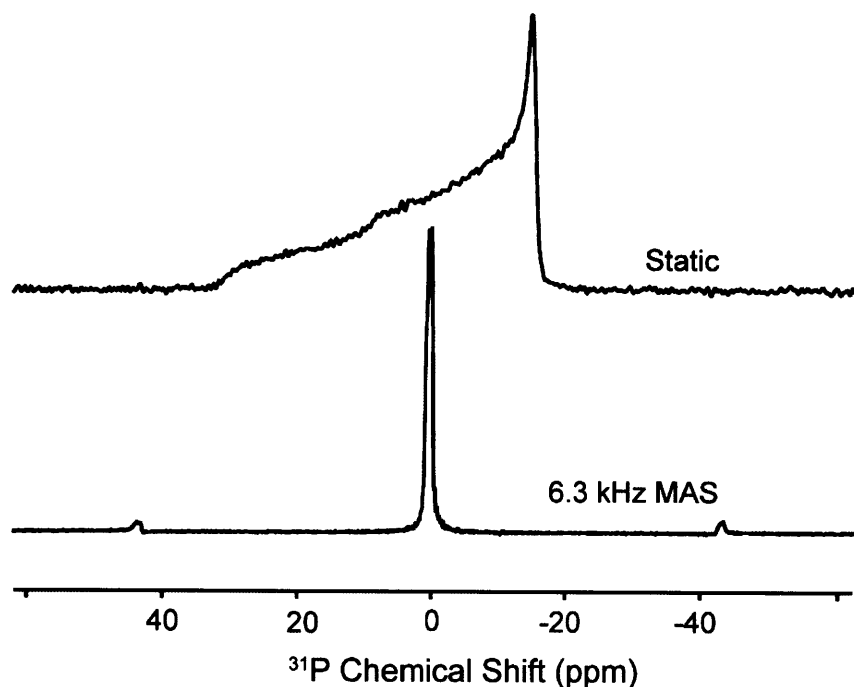


Figure 1.1. A static phosphorus spectrum of a phospholipid, and an isotropic spectrum acquired under 6.3 kHz MAS.

2.3 Recoupling

Modern methods, such as MAS and decoupling can remove interactions such as CSA, dipole coupling, and J coupling, resulting in high-resolution spectra where hundreds of atomic sites can be distinguished. In MAS experiments, the sample rotation is the primary method of removing these couplings in order to improve the spectral resolution. However, it is the dipole couplings and CSAs that contain valuable structural information, and that information is lost under MAS. Fortunately, application of carefully timed RF pulses allows selective reintroduction of terms in the Hamiltonian that carry structural information. This selective switching of terms in the Hamiltonian forms the Foundation of modern MAS NMR, allowing for example, dipole couplings to be measured in one dimension of a spectrum and isotropic chemical shift to be correlated in the second dimension. In addition, recoupling can be used to drive transitions between coupled spins. Recoupling sequences used in this thesis are both heteronuclear and homonuclear dipolar recoupling.

Heteronuclear Dipolar Recoupling: REDOR

When RF pulses are applied concurrently with sample rotation, we must analyze the time dependent interactions.³⁹ An arbitrary sequence of RF pulses can produce a non-zero average

Hamiltonian, as is the case for REDOR, described below. The dipole coupling as a function of time under sample rotation is, from Eqns. (1.18) and (1.19):

$$\begin{aligned}
 H_D &= d(t)S_zI_z \\
 d(t) &= d\left\{\sin^2\beta\cos 2(\alpha+\omega_R t)-\sqrt{2}\sin 2\beta\cos(\alpha+\omega_R t)\right\} \\
 d &= \frac{\mu_0\hbar^2\gamma_I\gamma_S}{2\pi r^3}
 \end{aligned}
 \tag{1.21}$$

where α describes the initial orientation of the internuclear vector with respect to the rotor, and β is the angle between the internuclear vector and the MAS axis, as before. As determined before in Eqn. (1.20), the average dipole coupling over one rotor cycle is zero.

Importantly, the dipole coupling varies *coherently* with sample rotation, with a characteristic frequency of ω_R or $2\omega_R$. The ω_R component of $d(t)$ changes sign twice per rotor period. The spin part of the dipole Hamiltonian (S_zI_z) can be manipulated with RF pulses. If π -pulses on S_z are applied twice per rotor period, then both the spatial and spin part of the Hamiltonian change sign twice per rotor period, and there is a net non-zero Hamiltonian. This is the REDOR Hamiltonian. To determine the average REDOR Hamiltonian, we integrate $d(t)$ for one rotor period:

$$\begin{aligned}
 \bar{H} &= \left[\frac{1}{\tau_R} \int_0^{\tau_R/2} d(t) dt - \frac{1}{\tau_R} \int_{\tau_R/2}^{\tau_R} d(t) dt \right] S_z I_z \\
 \bar{H} &= -\frac{d}{\pi} \sqrt{2} \sin 2\beta \sin \alpha \cdot 2S_z I_z
 \end{aligned}
 \tag{1.22}$$

The density operator (starting with I_x at time 0) is then:

$$\begin{aligned}
 \rho(t) &= e^{-\frac{i\bar{H}t}{\hbar}} I_x e^{\frac{i\bar{H}t}{\hbar}} \\
 \rho(t) &= e^{-\frac{i\phi \cdot 2S_z I_z}{\hbar}} I_x e^{\frac{i\phi \cdot 2S_z I_z}{\hbar}} \\
 \rho(t) &= \cos\phi I_x + 2\sin\phi S_z I_y \\
 \phi &= -\frac{dN_c\tau_R}{\pi} \sqrt{2} \sin 2\beta \sin \alpha
 \end{aligned}
 \tag{1.23}$$

Where N_c is the number of rotor cycles applied, and ϕ is the accumulated phase that the initial state has acquired. In a REDOR measurement, the reduction of the $\cos\phi$ term is observed

(typically as a function of the REDOR time), which can provide a highly accurate method for measuring the dipole coupling, and hence the internuclear distance for an isolated spin pair. In the related TEDOR measurement, the $2\sin\phi$ term is observed (indirectly) in order to correlate the chemical shifts of the coupled S and I spins. The TEDOR experiment can be used in 2D for assignments, or it can be used to measure distance by measuring peak intensity in multiple 2D spectra at different mixing times. In this thesis, samples have no preferential orientation, and the $\cos\phi$ or $2\sin\phi$ terms must be averaged over all molecular orientations.

A final note about REDOR is that in principle, the π pulses can be applied on either the I or S channel for dipolar recoupling. However, the sequence must be designed to avoid unwanted recoupling and to refocus the chemical shift. For example, if pulses are split on both channels such that each channel has one π pulse per rotor period, this can lead to homonuclear recoupling. At least one pulse is applied to each of the channels in order to refocus chemical shift.

Homonuclear Dipolar Recoupling: RFDR

Homonuclear recoupling is based on the same principles as heteronuclear recoupling, in that the with the RF manipulation of the spin part of the Hamiltonian interferes with the coherent averaging of the spatial part due to MAS, resulting in a non-zero average. (In this case we consider only the first order average, although higher order terms in the Magnus Expansion are necessary for the analysis of some NMR pulse sequences such as Third Spin Assisted Recoupling¹²). For the homonuclear case, the pulse sequence design must consider that RF pulses are typically non-selective and therefore manipulate both spins simultaneously.

We illustrate homonuclear dipolar recoupling with RFDR⁴⁰. This pulse sequence can be analyzed with delta pulses or with finite pulses. Here we present the treatment of finite pulses, which becomes important at higher spinning frequencies.⁴¹

From Eqn 1.21, $d(t)$ has terms that oscillate at ω_R and $2\omega_R$, which will be multiplied by the spin part of the Hamiltonian.

$$\begin{aligned}
 H_{D,\text{homo}} &= d(t) \frac{1}{2} (3I_z S_z - I \cdot S) \\
 d(t) &= d \left\{ \sin^2 \beta \cos 2(\alpha + \omega_R t) - \sqrt{2} \sin 2\beta \cos(\alpha + \omega_R t) \right\} \\
 d &= \frac{\mu_0 \hbar^2 \gamma_I \gamma_S}{2\pi r^3}
 \end{aligned} \tag{1.24}$$

The pulse sequence consists of a pi-pulse of duration τ_p placed at the beginning of each rotor period and alternating in phase between x and y. For the calculation of the average Hamiltonian, we first determine the action of the pulses over 4 rotor periods.

$$U_{RF} = \begin{cases} e^{-i\pi(I_X+S_X)t/\tau_p} & 0 < t < \tau_p \\ e^{-i\pi(I_X+S_X)} & \tau_p < t < \tau_R \\ e^{-i\pi(I_Y+S_Y)(t-\tau_R)/\tau_p} e^{-i\pi(I_X+S_X)} & \tau_R < t < \tau_R + \tau_p \\ e^{-i\pi(I_Y+S_Y)} e^{-i\pi(I_X+S_X)} = e^{i\pi(I_Z+S_Z)} & \tau_R + \tau_p < t < 2\tau_R \\ e^{-i\pi(I_X+S_X)(t-2\tau_R)/\tau_p} e^{i\pi(I_Z+S_Z)} & 2\tau_R < t < 2\tau_R + \tau_p \\ e^{-i\pi(I_X+S_X)} e^{i\pi(I_Z+S_Z)} & 2\tau_R + \tau_p < t < 3\tau_R \\ e^{-i\pi(I_Y+S_Y)(t-3\tau_R)/\tau_p} e^{-i\pi(I_X+S_X)} e^{i\pi(I_Z+S_Z)} & 3\tau_R < t < 3\tau_R + \tau_p \\ e^{i2\pi(I_Z+S_Z)} & 3\tau_R + \tau_p < t < 4\tau_R \end{cases} \quad (1.25)$$

Then the average Hamiltonian is:

$$\begin{aligned} \bar{H} &= \frac{1}{4\tau_R} \left\{ \int_0^{\tau_p} \tilde{H}_D(t) dt + \int_{\tau_p}^{\tau_R} \tilde{H}_D(t) dt + \dots \right\} \\ &= \frac{1}{4\tau_R} \left\{ \int_0^{\tau_p} \frac{d(t)}{2} e^{i\pi(I_X+S_X)t/\tau_p} 3I_z S_z e^{-i\pi(I_X+S_X)t/\tau_p} dt + \right. \\ &\quad \left. \int_{\tau_p}^{\tau_R} \frac{d(t)}{2} 3I_z S_z dt + \dots \right\} \end{aligned} \quad (1.26)$$

Which reduces to:

$$\bar{H} = \frac{1}{4\tau_R} \left\{ 4 \int_0^{\tau_p} \frac{d(t)}{2} 3I_z S_z \cos \frac{2\pi t}{\tau_p} dt + 4 \int_{\tau_p}^{\tau_R} \frac{d(t)}{2} 3I_z S_z dt + \right. \\ \left. 2 \int_{\tau_p}^{\tau_R} \frac{d(t)}{2} 3(I_X S_X + I_Y S_Y) dt \right\} \quad (1.27)$$

And after integration:

$$\bar{H} = \left\{ \begin{aligned} &\frac{3\omega_1^2}{\pi(\omega_R^2 - 4\omega_1^2)} [\sin(\omega_R \tau_p + \gamma) - \sin \gamma] \cdot A + \\ &\frac{3\omega_1^2}{8\pi(\omega_R^2 - \omega_1^2)} [\sin(2\omega_R \tau_p + 2\gamma) - \sin 2\gamma] \cdot B \end{aligned} \right\} \cdot \left(I_z S_z - \frac{1}{2} [I_X S_X + I_Y S_Y] \right) \quad (1.28)$$

$$A = d \sin^2 \beta$$

$$B = -\sqrt{2} \sin 2\beta$$

The result is a scaling of the static homonuclear dipole coupling, with a scaling factor that goes to zero as τ_p goes to zero. RFDR is a useful recoupling sequence with low RF power requirement, allowing it to be applied even at a spinning frequency of 60 kHz. It is applied in this Thesis for long range recoupling of ^{13}C at 20 kHz MAS and recoupling of ^1H at 60 kHz, allowing the extraction of useful distance information.

2.4 Thesis Outline

Chapters 2 through 5 concern the measurement of structural properties of the M2 proton transporter from influenza A. In chapter 2, the interaction of an inhibitor is investigated on the wild type protein, which shows a large-scale reorganization of the channel upon drug binding. In chapter 3, the location of the functional binding site was determined using dynamic nuclear polarization (DNP). This measurement resolved a controversy concerning the location of drug binding, and demonstrated the utility of DNP for characterization of ligand-protein interaction. In chapter 4, focus is turned to a drug resistant mutant of M2, which arises from a single point mutation S31N, and is widely circulated in the present influenza population. In the same lipid preparations as used for the study of drug binding in WT M2, nearly no change is observed in the spectrum on addition of inhibitor. In order to shed light on the molecular basis for drug resistance, the structure of S31N M2 was solved using MAS and the result is presented in chapter 5. Chapter 5 is the culmination of multiple lines of analysis involving many differently labeled samples of both protein and lipid. In addition, chapter 5 includes proton detected measurements of proton-proton distances using exciting new hardware that allows spinning at 60 kHz.

Chapters 6 through 9 concern the methodological development of techniques for MAS NMR. Chapter 6 details the synthetic route used in the synthesis of deuterated lipids for ^1H detected measurements. Chapter 7 presents the use of ^2H DNP and ^2H - ^{13}C correlation as an alternate method to the commonly used ^1H DNP. Chapter 8 is a detailed look at signal quenching and relaxation in homogeneous solutions under DNP conditions, and is useful for the optimization of sample conditions for DNP. Finally, Chapter 9 is a structure determination of the model peptide APG, which was used as a model system to compare the restraining power of different NMR measurements on this particular molecular structure.

2.5 References

- (1) Almen, M. S.; Nordstrom, K. J.; Fredriksson, R.; Schioth, H. B., Mapping the human membrane proteome: a majority of the human membrane proteins can be classified according to function and evolutionary origin. *BMC Biol* **2009**, *7*, 50.
- (2) Overington, J. P.; Al-Lazikani, B.; Hopkins, A. L., How many drug targets are there? *Nat Rev Drug Discov* **2006**, *5* (12), 993-6.
- (3) Knight, M. J.; Felli, I. C.; Pierattelli, R.; Emsley, L.; Pintacuda, G., Magic Angle Spinning NMR of Paramagnetic Proteins. *Acc Chem Res* **2013**.
- (4) Yan, S.; Suiter, C. L.; Hou, G.; Zhang, H.; Polenova, T., Probing Structure and Dynamics of Protein Assemblies by Magic Angle Spinning NMR Spectroscopy. *Acc Chem Res* **2013**.
- (5) Andreas, L. B.; Barnes, A. B.; Corzilius, B.; Chou, J. J.; Miller, E. A.; Caporini, M.; Rosay, M.; Griffin, R. G., Dynamic nuclear polarization study of inhibitor binding to the m218-60 proton transporter from influenza a. *Biochemistry* **2013**, *52* (16), 2774-82.
- (6) Huber, M.; Hiller, S.; Schanda, P.; Ernst, M.; Bockmann, A.; Verel, R.; Meier, B. H., A proton-detected 4D solid-state NMR experiment for protein structure determination. *Chemphyschem* **2011**, *12* (5), 915-8.
- (7) Bayro, M. J.; Debelouchina, G. T.; Eddy, M. T.; Birkett, N. R.; Macphee, C. E.; Rosay, M.; Maas, W. E.; Dobson, C. M.; Griffin, R. G., Intermolecular structure determination of amyloid fibrils with magic-angle spinning and dynamic nuclear polarization NMR. *J Am Chem Soc* **2011**, *133* (35), 13967-74.
- (8) Cady, S.; Wang, T.; Hong, M., Membrane-dependent effects of a cytoplasmic helix on the structure and drug binding of the influenza virus M2 protein. *J Am Chem Soc* **2011**, *133* (30), 11572-9.
- (9) Cady, S. D.; Wang, J.; Wu, Y.; DeGrado, W. F.; Hong, M., Specific binding of adamantane drugs and direction of their polar amines in the pore of the influenza M2 transmembrane domain in lipid bilayers and dodecylphosphocholine micelles determined by NMR spectroscopy. *J Am Chem Soc* **2011**, *133* (12), 4274-84.
- (10) Eddy, M. T.; Ong, T. C.; Clark, L.; Teijido, O.; van der Wel, P. C.; Garces, R.; Wagner, G.; Rostovtseva, T. K.; Griffin, R. G., Lipid dynamics and protein-lipid interactions in 2D crystals formed with the beta-barrel integral membrane protein VDAC1. *J Am Chem Soc* **2012**, *134* (14), 6375-87.
- (11) Etzkorn, M.; Bockmann, A.; Lange, A.; Baldus, M., Probing molecular interfaces using 2D magic-angle-spinning NMR on protein mixtures with different uniform labeling. *J Am Chem Soc* **2004**, *126* (45), 14746-51.
- (12) Lewandowski, J. R.; De Paepe, G.; Griffin, R. G., Proton assisted insensitive nuclei cross polarization. *J Am Chem Soc* **2007**, *129* (4), 728-9.
- (13) Marulanda, D.; Tasayco, M. L.; McDermott, A.; Cataldi, M.; Arriaran, V.; Polenova, T., Magic angle spinning solid-state NMR spectroscopy for structural studies of protein interfaces. resonance assignments of differentially enriched *Escherichia coli* thioredoxin reassembled by fragment complementation. *J Am Chem Soc* **2004**, *126* (50), 16608-20.
- (14) Zhou, D. H.; Nieuwkoop, A. J.; Berthold, D. A.; Comellas, G.; Sperling, L. J.; Tang, M.; Shah, G. J.; Brea, E. J.; Lemkau, L. R.; Rienstra, C. M., Solid-state NMR analysis of membrane proteins and protein aggregates by proton detected spectroscopy. *J Biomol NMR* **2012**, *54* (3), 291-305.
- (15) Linsler, R.; Chevelkov, V.; Diehl, A.; Reif, B., Sensitivity enhancement using paramagnetic relaxation in MAS solid-state NMR of perdeuterated proteins. *J Magn Reson* **2007**, *189* (2), 209-16.
- (16) Reif, B., Ultra-high resolution in MAS solid-state NMR of perdeuterated proteins: implications for structure and dynamics. *J Magn Reson* **2012**, *216*, 1-12.
- (17) Hu, K.-N.; Yu, H.-h.; Swager, T. M.; Griffin, R. G., Dynamic nuclear polarization with biradicals. *J. Am. Chem. Soc.* **2004**, *126* (35), 10844-10845.

- (18) Rosay, M.; Lansing, J. C.; Haddad, K. C.; Bachovchin, W. W.; Herzfeld, J.; Temkin, R. J.; Griffin, R. G., High Frequency Dynamic Nuclear Polarization in MAS Spectra of Membrane and Soluble Proteins. *J. Am. Chem. Soc.* **2003**, *125*, 13626-27.
- (19) Bajaj, V. S.; Hornstein, M. K.; Kreischer, K. E.; Sirigiri, J. R.; Woskov, P. P.; Mak, M.; Herzfeld, J.; Temkin, R. J.; Griffin, R. G., 250 GHz Gyrotron for Dynamic Nuclear Polarization in Biological Solid State NMR. *J. Mag. Res.* **2007**, *190*, 86-114.
- (20) Barnes, A. B.; Mak-Jurkauskas, M. L.; Matsuki, Y.; Bajaj, V. S.; van der Wel, P. C. A.; DeRocher, R.; Bryant, J.; Sirigiri, J. R.; Temkin, R. J.; Lugtenburg, J.; Herzfeld, J.; Griffin, R. G., Cryogenic sample exchange NMR probe for magic angle spinning dynamic nuclear polarization. *J. Mag. Res.* **2009**, *198* (2), 261-270.
- (21) Bajaj, V. S.; Mak-Jurkauskas, M. L.; Belenky, M.; Herzfeld, J.; Griffin, R. G., DNP enhanced frequency-selective TEDOR experiments in bacteriorhodopsin. *Journal of Magnetic Resonance* **2010**, *202* (1), 9-13.
- (22) Rosay, M.; Zeri, A. C.; Astrof, N. S.; Opella, S. J.; Herzfeld, J.; Griffin, R. G., Sensitivity-enhanced NMR of biological solids: Dynamic nuclear polarization of Y21M fd bacteriophage and purple membrane. *Journal of the American Chemical Society* **2001**, *123* (5), 1010-1011.
- (23) Yao, Y.; Ding, Y.; Tian, Y.; Opella, S. J.; Marassi, F. M., Membrane protein structure determination: back to the membrane. *Methods Mol Biol* **2013**, *1063*, 145-58.
- (24) Cady, S. D.; Schmidt-Rohr, K.; Wang, J.; Soto, C. S.; DeGrado, W. F.; Hong, M., Structure of the amantadine binding site of influenza M2 proton channels in lipid bilayers. *Nature* **2010**, *463* (7281), 689.
- (25) Ritter, C.; Maddelein, M. L.; Siemer, A. B.; Lhrs, T.; Ernst, M.; Meier, B. H.; Saupe, S.; Riek, R., Correlation of structure and infectivity of the HET-s prion. *Nature* **2005**, *435* (7043), 844.
- (26) Tang, M.; Comellas, G.; Rienstra, C. M., Advanced Solid-State NMR Approaches for Structure Determination of Membrane Proteins and Amyloid Fibrils. *Acc Chem Res* **2013**.
- (27) Asami, S.; Reif, B., Proton-Detected Solid-State NMR Spectroscopy at Aliphatic Sites: Application to Crystalline Systems. *Acc Chem Res* **2013**.
- (28) Sengupta, I.; Nadaud, P. S.; Jaroniec, C. P., Protein Structure Determination with Paramagnetic Solid-State NMR Spectroscopy. *Acc Chem Res* **2013**.
- (29) Murray, D. T.; Das, N.; Cross, T. A., Solid State NMR Strategy for Characterizing Native Membrane Protein Structures. *Acc Chem Res* **2013**.
- (30) Giraud, N.; Bockmann, A.; Lesage, A.; Penin, F.; Blackledge, M.; Emsley, L., Site-specific backbone dynamics from a crystalline protein by solid-state NMR spectroscopy. *J Am Chem Soc* **2004**, *126* (37), 11422-3.
- (31) Lewandowski, J. R., Advances in Solid-State Relaxation Methodology for Probing Site-Specific Protein Dynamics. *Acc Chem Res* **2013**.
- (32) Munowitz, M. G.; Griffin, R. G.; Bodenhausen, G.; Huang, H., Two-dimensional rotational spin-echo nuclear magnetic resonance in solids: correlation of chemical shift and dipolar interactions. *J Am Chem Soc* **1981**, *103* (10), 2529-2533.
- (33) Ma, C.; Polishchuk, A. L.; Ohigashi, Y.; Stouffer, A. L.; Schon, A.; Magavern, E.; Jing, X.; Lear, J. D.; Freire, E.; Lamb, R. A.; DeGrado, W. F.; Pinto, L. H., Identification of the functional core of the influenza A virus A/M2 proton-selective ion channel. *Proc Natl Acad Sci U S A* **2009**, *106* (30), 12283-8.
- (34) Pielak, R. M.; Schnell, J. R.; Chou, J. J., Mechanism of drug inhibition and drug resistance of influenza A M2 channel. *Proc Natl Acad Sci U S A* **2009**, *106* (18), 7379-84.
- (35) Cohen-Tannoudji, C.; Diu, B.; Laloe, F., *Quantum Mechanics*. 1992.
- (36) Griffiths, D. J., *Introduction to Quantum Mechanics*. 2004.
- (37) Sakurai, J. J.; Napolitano, J. J., *Modern Quantum Mechanics*. 2010.
- (38) Slichter, C. P., *Principles of Magnetic Resonance*. 1990.

- (39) Gullion, T., Introduction to rotational-echo, double-resonance NMR. *Concepts in Magnetic Resonance* **1998**, *10* (5), 277-289.
- (40) Bennett, A. E.; Rienstra, C. M.; Griffiths, J. M.; Zhen, W. G.; Lansbury, P. T.; Griffin, R. G., Homonuclear radio frequency-driven recoupling in rotating solids. *Journal of Chemical Physics* **1998**, *108* (22), 9463-9479.
- (41) Ishii, Y., C-13-C-13 dipolar recoupling under very fast magic angle spinning in solid-state nuclear magnetic resonance: Applications to distance measurements, spectral assignments, and high-throughput secondary-structure determination. *Journal of Chemical Physics* **2001**, *114* (19), 8473-8483.

Chapter 2: Magic Angle Spinning NMR Investigation of Influenza A M2₁₈₋₆₀: Support for an Allosteric Mechanism of Inhibition

2.1 Introduction

The M2 protein from influenza A virus is a single pass membrane protein that assembles as a tetramer to form a H⁺ selective channel that functions at low pH and is critical in the viral lifecycle. A class of aminoadamantyl inhibitors has become ineffective against many influenza strains due to mutations in the N-terminal region of the channel¹, thus stimulating great interest in identification of the pharmacologically relevant binding site and the mechanism of inhibition and drug resistance. Discussion of an external, lipid-facing site and a pore-blocking site is ongoing²⁻⁸. A solution NMR structure⁷ in DHPC micelles of M2₁₈₋₆₀ showed an external binding site at D44 via direct NOE measurement; however, the pharmacological relevance of this binding pocket was questioned due to possible detergent effects, such as hydrophobic mismatch, which may impact structure, dynamics, and binding affinity⁴. Pioneering solid state NMR experiments by Cross, et al.⁹ using a shorter TM construct, M2₂₂₋₄₆, in lipid environments^{3, 10} were followed by diffraction studies in detergent⁸. Some of these results and more recent NMR experiments³ suggest S31 as a binding site. Recently, an elegant ¹³C-²H REDOR experiment using ²H labeled drug and ¹³C labeled peptide on M2₂₂₋₄₆ in lipids detected inhibitor near S31, and at higher drug concentrations, near D44⁴. However, M2₂₂₋₄₆ exhibits reduced function and drastically reduced inhibition by drug when compared with M2₁₈₋₆₀⁶. Furthermore the similar construct, M2₂₁₋₆₁ has indistinguishable conduction compared to the full length protein⁵. It is presently unclear whether the discrepancy between the two observed binding sites arises due to detergent effects, the highly truncated construct, or other factors. We therefore initiated investigations of the fully functional construct, M2₁₈₋₆₀ in lipid bilayers with magic angle spinning (MAS) NMR. Our chemical shift data reveal global conformational changes upon drug binding that suggest an allosteric mechanism of inhibition, and peak doubling, indicating a twofold symmetric tetramer.

2.2 Results and Discussion

Figure 2.1 (top) shows a ¹⁵N-¹³C one-bond zf-TEDOR^{11, 12} correlation spectrum of M2₁₈₋₆₀ in 1-palmitoyl-2-oleoyl-*sn*-glycero-3-phosphocholine (POPC) bilayers, demonstrating spectral assignments in both the absence (red) and presence (blue) of the inhibitor rimantadine (Rmt).

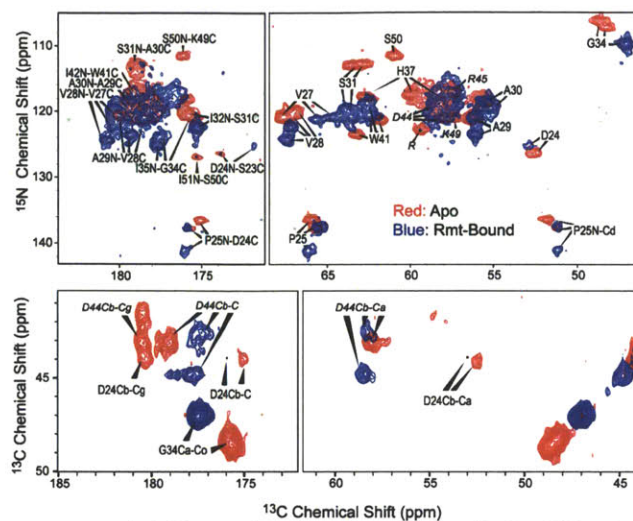


Figure 2.1. TEDOR spectrum of $M2_{18-60}$ showing large chemical shift changes upon addition of rimantadine. (top) ^{15}N - ^{13}C zf-TEDOR spectra ($\tau_{\text{mix}} = 1.3$ ms) showing assignments of ^{13}C , ^{15}N [^{12}C , ^{14}N -ILFY] $M2_{18-60}$ in the drug bound (blue) and unbound (red) states. Unless otherwise indicated, cross peaks arise from 1-bond N-Ca magnetization transfer. (bottom) ^{13}C - ^{13}C PDS spectra ($\tau_{\text{mix}} = 50$ ms) showing Asp and Gly cross-peaks of these samples. Sizable chemical shift changes are observed in the N and or Ca sites for residues 25, 27, 28, 31, 34, 35, 37, and 41. Many peaks are doubled (see **Figure 2.5** for expansion), notably P25 and A29, supporting the existence of a two-fold symmetric tetramer. Spectra were recorded ~ 0 °C, just above the phase transition of pure POPC lipids. Labels such as D44 are shown in italics to indicate less certainty in assignments (see Methods Section).

Linewidths of ~ 1 ppm for both ^{15}N and ^{13}C are observed at 700 MHz for both drug-bound and apo samples, indicating conformational homogeneity. This narrow linewidth also indicates that the dynamics of this system are favorable for investigation by MAS NMR. The similar linewidths in the bound and apo states is in contrast to results with $M2_{22-46}$ where drug binding significantly narrowed the spectra³, and the improvement using $M2_{18-60}$ could be attributed to the larger construct, which remains tetrameric even in an SDS detergent environment⁶.

Upon Rmt binding, we observe substantial (>1 ppm $^{13}\text{C}\alpha/\text{C}\beta$, >2 ppm ^{15}N) chemical shift changes from residues 24 to 41, distributed across the entire range of unambiguously assigned residues and nearly spanning the transmembrane helix. Significant perturbations occur for pore lining residues 27, 34, 37, 41 and from residues 24, 25, 28, 29, 31, 32, 35, which are found in the helix-helix interface and lipid facing sites⁷. Only two assigned residues, 30 and 42, show no chemical shift perturbations >1 ppm in $^{13}\text{C}\alpha/\text{C}\beta$ or >2 ppm in ^{15}N . In **Figure 2.2** these chemical shift perturbations are shown as a function of residue number and demonstrate significant changes on a length scale many times larger than the ~ 5 Å Rmt drug, indicating allostery. We note that the ~ 7 ppm shift change at S31 that was observed for $M2_{22-46}$ using Amt³ is also observed here for $M2_{18-}$

60 using Rmt. In addition, we also observe a ~ 3.5 ppm shift in H37 C α , which is comparable considering the ~ 2 fold increase in chemical shift variability of ^{15}N compared to $^{13}\text{C}\alpha$. Thus, chemical shift data supports an allosteric effect, but does not locate the drug; it is therefore consistent with proposed sites of pharmacological relevance, S31 and D44.

An allosteric effect is also in agreement with previous measurements of aligned samples that detected a kink at G34 in amantadine (Amt) bound M2₂₂₋₄₆ and a modified conformation with

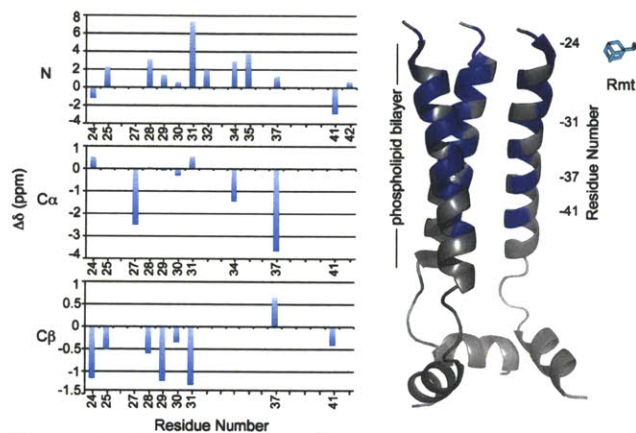


Figure 2.2. Chemical shift perturbations ($\Delta\delta = \delta_{\text{bound}} - \delta_{\text{apo}}$) are distributed across the channel and support an allosteric effect upon drug binding. (left) Chemical shift perturbations as a function of residue number. (right) A comparison of the Rmt drug size with the transmembrane tetramer assembly from the solution structure. Blue residues indicate a shift of >2 ppm in N and or >1 ppm in C α /C β . One of the four helices has been removed for clarity.

drug binding¹³. A backbone structure of amantadine bound M2 was calculated in this previous study; however, broad apo spectra compromised a complete structural analysis of that state. From the present spectra, it is clear that the allosteric changes extend across the entire TM domain.

This conclusion relies on the significance of the chemical shift differences between the bound and apo states. Chemical shift changes can arise from several factors, which include changes in secondary structure but can also include variations in solvents, temperature, and pH. Comparisons of chemical shifts between solution and microcrystalline preparations of the same model proteins reported strong agreement (~ 1 ppm and less for ^{13}C and $^{13}\text{C}\alpha$, ~ 2 ppm and less for ^{15}N) in the protein core, with somewhat larger differences observed for sites forming crystal contacts in the solid state preparations¹⁴⁻¹⁷. Temperature and pH are constant for all of the data reported herein, and the possibility of nonspecific binding and membrane changes are addressed below and in **Figure 2.3** and **Figure 2.4**; we have therefore excluded these potential sources for chemical shift perturbations.

The solution NMR structure showed an external binding site with a specific interaction between the amine group of Rmt and D44 C γ . Therefore, we have also examined the Asp region of ^{13}C - ^{15}N proton driven spin diffusion¹⁸ (PDS) spectra shown in **Figure 2.1 (bottom)** for perturbations. The G34 C α -C' peak exhibits a well-resolved movement on drug binding and intense peaks in both states, suggesting that it is in a position in the peptide that is not influenced by dynamics. In contrast, Asp C β -C' and C β -C γ peaks show reduced intensity that is likely due to motion interfering with cross-polarization (CP) and decoupling^{19, 20}. Addition of Rmt causes a 2-fold further decrease in these peak intensities and chemical shift changes of several ppm. A direct H-bond between the drug amine and an Asp C γ carboxyl, can explain these effects. However, these effects can also be explained by a large-scale reorganization of the channel resulting in altered conformation and dynamics in the vicinity of the Asp residues.

In **Figure 2.3**, zf-TEDOR spectra are shown at 0, 1, and 4 Rmt molecules per channel in order to investigate binding stoichiometry and rule out the possibility of nonspecific binding. **Figure 2.3a** shows an apo spectrum. Upon addition of one Rmt molecule per channel (**Figure 2.3b**), resonances of the Rmt-bound form appear and with approximately 25% of total intensity. At four

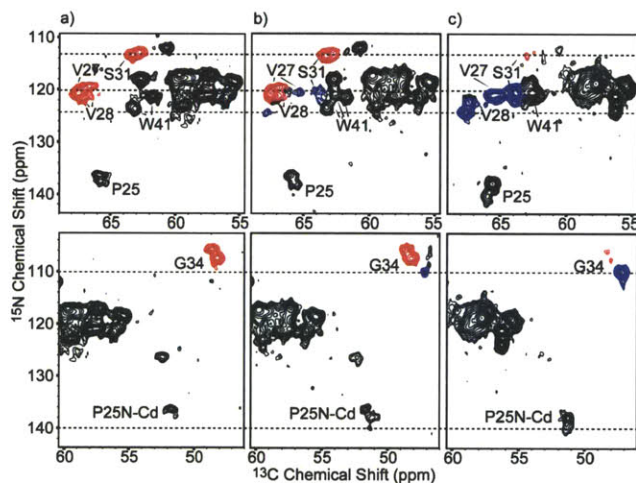


Figure 2.3. TEDOR spectra of M2 acquired at 0, 1, and 4 Rmt molecules per channel in a, b, and c, result in cross peaks due to M2 bound to Rmt and present at ~0%, 25% and >90%, respectively. The apo spectrum is simultaneously observed at 100%, 75% and <10% of total site-specific signal intensity. Unless otherwise indicated, cross peaks arise from 1-bond N-C α magnetization transfer. Resonances that clearly show the titration are displayed in red (unbound form) and blue (Rmt bound resonances). Dashed lines at G34 and other resonances serve as a guide. Signal to noise is ~10 for strong signals. M2 samples used in the titration were embedded in DPhPC lipids and show nearly identical spectra as those recorded in POPC lipids (see **Figure 4**).

Rmt molecules per channel (**Figure 2.3c**), resonances arising from Rmt-bound M2 are primarily observed, with apo resonances still detected at <10 % total intensity. No gradual change in chemical shifts is observed; rather the resonances of the bound form appear in concert and increasing intensity with increasing Rmt. At 16 Rmt molecules per channel, the effect is saturated and only the bound form is observed (**Figure 2.1, blue**). If these chemical shift changes are due to specific binding, then resonance intensities suggest a binding stoichiometry of >1 molecule per channel. Notably, pore facing residues such as G34 and V27, which are unlikely to be affected by any nonspecific hydrophobic interactions or changes in lipid composition, clearly demonstrate the changes. Furthermore, although Rmt partitions strongly to membrane²¹, at one drug per channel it occupies only 2 mol percent of the *non-protein* membrane components. Neither protein nor M2 tetramer is in excess, yet all of the chemical shift perturbations are observed. Therefore if we assume that the pharmacological binding site has high affinity, then nonspecific binding and changes in membrane composition are excluded.

Sensitivity to membrane composition was further investigated by collecting TEDOR and PDS D spectra in another lipid, 1,2-diphytanoyl-*sn* glycerol-3-phosphocholine (DPhPC). Spectra recorded in DPhPC are remarkably similar to spectra of POPC embedded M2, with maximum chemical shift differences of 0.3 ppm and 0.7 ppm for ¹³C and ¹⁵N, respectively. PDS D Spectra recorded in these two lipids are overlaid in **Figure 2.4**. The fact that this change in membrane composition causes small changes in the spectra provides further evidence that drug induced chemical shift changes are caused by a specific drug interaction and not caused by altering the membrane composition. Clearly the state of this construct of M2 in lipids is stable to the change in membrane composition between DPhPC and POPC.

Two distinct sets of peaks are observed for many residues in both apo and drug bound M2₁₈₋₆₀, with approximately equal intensity, providing evidence that the tetramer is twofold symmetric. These are most obvious in the P25 cross peaks in **Figure 2.1 (top)**, but are also apparent in more crowded regions of the spectra. Multiple peak sets could indicate the presence of multiple conformations or arise due to incomplete drug binding. However, peak doubling appears with equal intensity between the two sets of peaks, and is found in *both* the apo and drug bound states, suggesting that the tetrameric assembly has twofold symmetry, which may arise due to packing of bulky W41 and H37 side chains. This is in agreement with previous work, which showed that the doubly protonated state of M2 contains two imidazole-imidazolium dimers of H37 and is therefore twofold symmetric at this position²². It is also qualitatively consistent with the diffraction structure at neutral pH, which shows conformational heterogeneity in the C-terminal region⁸. Other structural studies have assumed fourfold symmetry. For example, a single set of resonances was observed for this construct in DHPC micelles⁷ and may be the result of fast interconversion between two states at higher temperatures. Also, peak doubling may be present and within the linewidth observed in previous MAS NMR studies.

Dimerization of two tetramer channels could also lead to two sets of resonances, with different chemical shifts at the interface. However, some of the largest separations in doubled peaks appear

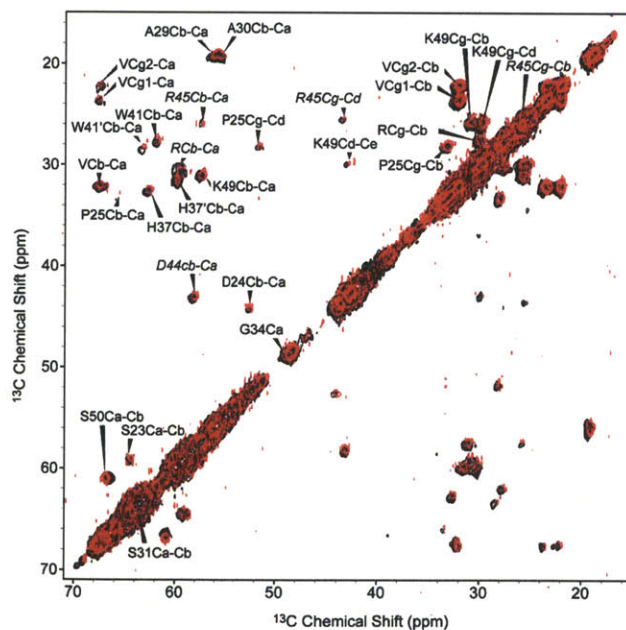


Figure 2.4. ¹³C-¹³C PDSM spectra of POPC embedded (red) and DPhPC embedded (black) M2 show nearly identical spectra with maximum chemical shift differences of 0.3 ppm. With 15 ms mixing, mostly 1-bond correlations are observed.

at residues inside the channel such as H37 and W41. We therefore find that the most likely explanation for the peak doubling is a twofold symmetric channel.

2.3 Methods and Spectral Assignments

Synthesis of U=¹³C,¹⁵N[¹²C,¹⁴NILFY]M2₁₈₋₆₀: Synthesis and reconstitution of M2₁₈₋₆₀: Preparation of M2₁₈₋₆₀ by overexpression in *E. coli* has been described previously^{6, 7}. Briefly, M2₁₈₋₆₀ was overexpressed in *e-coli* BL-21DE3 as a fusion with trpLE with a N-terminal His₉-tag. Protein synthesis was induced with an IPTG concentration of 150uM at an OD₆₀₀ of 0.75. The protein was purified on a Ni²⁺ affinity column and cleaved with 0.35 g CNBr in 2.5 mL 70% formic acid per liter of cell culture. Finally, pure protein was isolated on a C4 reverse phase HPLC column. For reverse labeling, 1L of M9 culture was divided into two parts. A 700 mL portion was inoculated and grown to an OD₆₀₀ of 0.7. Natural abundance amino acids ILFYS (Sigma) were dissolved in the remaining 300 mL, and added to the 700 mL portion bringing the OD to ~0.5 prior to induction at OD₆₀₀ of 0.75. Induction conditions were at 18 °C and for 14-18 hours.

M2 bilayer preparation: Pure peptide was dispersed in either 1-palmitoyl-2-oleoyl-*sn*-glycero-3-phosphocholine (POPC) or 1,2-diphytanoyl-*sn* glycerol-3-phosphocholine (DPhPC) purchased from Avanti. Bilayer samples were prepared by detergent dialysis. Peptide and lipid were dissolved separately in ~14 mg per mL Octyl Glucopyranoside (OG) detergent (Sigma), then combined at a lipid to protein molar ratio of 14 (POPC) and 12 (DPhPC). Detergent was removed by dialyzing against 2 L of buffer with 2 buffer changes per day using a 3.5 kDa cutoff. Dialysis buffer contained 40 mM phosphate, 30 mM glutamate and 3 mM sodium azide at pH 7.8. After 5 days of dialysis, the sample was pelleted by centrifugation at 100 000 × g and packed into the MAS rotor. For POPC imbedded samples with drug, dry lyophilized Rimantadine (see synthesis below) was added to the membrane pellet at a 4:1 Drug:M2 molar ratio. Lyophilized drug was buffered using phosphate to insure the correct pH was maintained. In the rimantadine titration, the calculated molar quantity of 15 mg/mL rimantadine at pH 7.8 was added to the membrane pellet.

Synthesis of ¹⁵N rimantadine: Rimantadine was synthesized from the 1-adamantyl methyl ketone precursor by a Leukart-Wallach reaction²³. 2 g ketone, 3.4 g sodium formate and 2.67 g ammonium chloride were dissolved in 20 ml diethylene glycol at ~100 °C and reacted for 2 hours. Successful reaction was verified by solution NMR and mass spec.

NMR: NMR spectra were recorded at 700 Mhz ¹H frequency using a home built spectrometer courtesy of David Rubin and a triple channel Varian 3.2 mm HCN probe. ¹³C and ¹⁵N chemical shifts were referenced using the published shifts of adamantine relative to DSS for ¹³C

referencing²⁴ and the IUPAC relative frequency ratios between DSS (¹³C) and liquid ammonia (¹⁵N)^{25, 26}. All spectra were acquired at a MAS rotational frequency of 12.5 kHz. 83 kHz TPPM proton decoupling was used in all experiments. Z filtered transferred echo double resonance (TEDOR¹¹) were acquired using 1.4 ms mixing with 50 kHz ¹³C and ¹⁵N pi pulses. Proton driven spin diffusion (PDS¹⁸) spectra were collected with 20ms 50ms and 200ms mixing. Two-dimensional versions of the correlation experiments NCACX and NCOCX were acquired using a 6ms specific ¹⁵N to ¹³C CP transfer²⁷ and 20ms and 100ms of PDS mixing. Spin locking frequencies during the ¹⁵N to ¹³C CP transfer were ~43 and 30 kHz for ¹³C and ¹⁵N, respectively using a 3 kHz ramp on ¹³C. All spectra were recorded with VT gas regulated at -6 °C approximately one inch from the stator. With frictional heating, we estimate the sample temperature to be ~0 degrees. The POPC lipids have a transition temperature of -2 °C and therefore are assumed to be in the liquid phase. Spectra were processed using the NMRPipe²⁸ software package and displayed and assigned using Sparky (Goddard and Kneller, University of California, San Francisco).

Assignments and Chemical Shift Changes: Assignments relied on PDS spectra to identify spin systems and residue types and TEDOR, NCACX and NCOCX to link these spin systems. Five spin systems were assigned and are isolated from each other due to natural abundance labeling of residues ILFY. These are S₂₃D₂₄P₂₅, V₂₇V₂₈A₂₉A₃₀S₃₁[¹⁵N]I₃₂, G₃₄[¹⁵N]I₃₅, H₃₇ and W₄₁[¹⁵N]I₄₂. The spin system S₂₃D₂₄P₂₅ was easily identified due to the unique proline nitrogen chemical shift. V₂₇V₂₈A₂₉A₃₀S₃₁[¹⁵N]I₃₂ is identified since these are the only alanine and valine residues in the sequence. G₃₄[¹⁵N]I₃₅ was identified as the only glycine residue without an N-C' contact. (The other glycine in the sequence, G58 would be connected to H57, however, neither of these residues appear in the spectra). H₃₇ was identified as the only remaining histidine in the sequence. W₄₁[¹⁵N]I₄₂ was identified since W₄₁ is the only tryptophan in M2₁₈₋₆₀. Isoleucine residues were found to be transaminated, and amide shifts were identified as contacts to S₃₁, G₃₄ and W₄₁. In addition, resonances from S₂₃, D₄₄, and R₄₅ are present, but are ambiguously assigned due to spectral overlap. There are three aspartic acid residues in the sequence. D24 is assigned. D21 is in the N-terminal region of the peptide, which does not appear in the spectra (residues 18-22 are not observed). Therefore the aspartic acid peaks in the spectrum are likely from D44. An NCOCX contact to D44 The K₄₉S₅₀ spin system was identified in the apo spectra, but not in the drug bound spectra, although a lysine spin system was observed. Where peak doubling was encountered, the two sets of resonances are not contiguously assigned due to gaps caused by the labeling. When two sets of resonances were observed, the average was used in calculating chemical shift changes.

Peak Doubling: An expansion of the TEDOR spectrum from *Figure 2.1* is presented below (*Figure 2.5*) to show some of the observed peak doublings. Peak doubling is clearly evident for P25, V27, V28, A29, A30, S31, G34, and W41, and occur in both apo and drug-bound spectra.

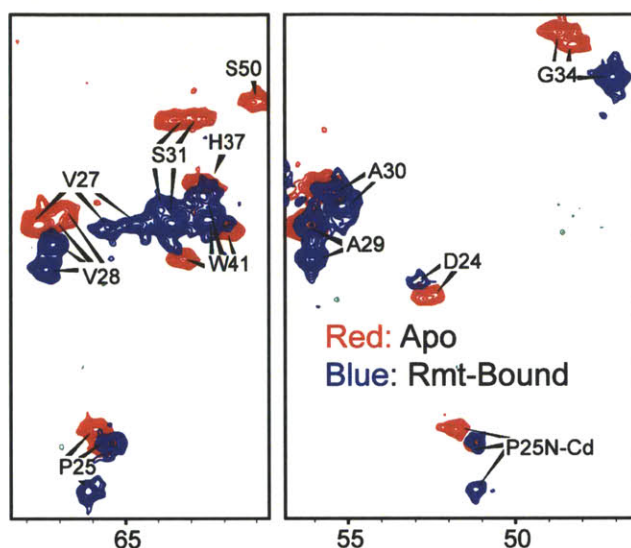


Figure 2.5. The 1-bond ^{13}C ^{15}N TEDOR spectrum presented in *Figure 2.1* is expanded to show peak doublings. Doublings are observed for both apo and drug-bound spectra at many residue positions. Note, for example, P25 and S31 which show doubling in *both* apo and drug-bound spectra.

Rimantadine titration: An NMR detected titration of rimantadine was carried out by directly adding the relative molar quantity of 15 mg/mL rimantadine solution at pH 7.8 to DPhPC membrane pellet and incubating for several hours. The increase in ^{15}N labeled rimantadine was detected at 39 ppm in a ^{15}N CPMAS NMR spectrum (*Figure 2.6*). Although this experiment is not quantitative due to possible changes in CP efficiency and dynamics, the ^{15}N rimantadine signal is ~0:1:4 in the three samples, as expected.

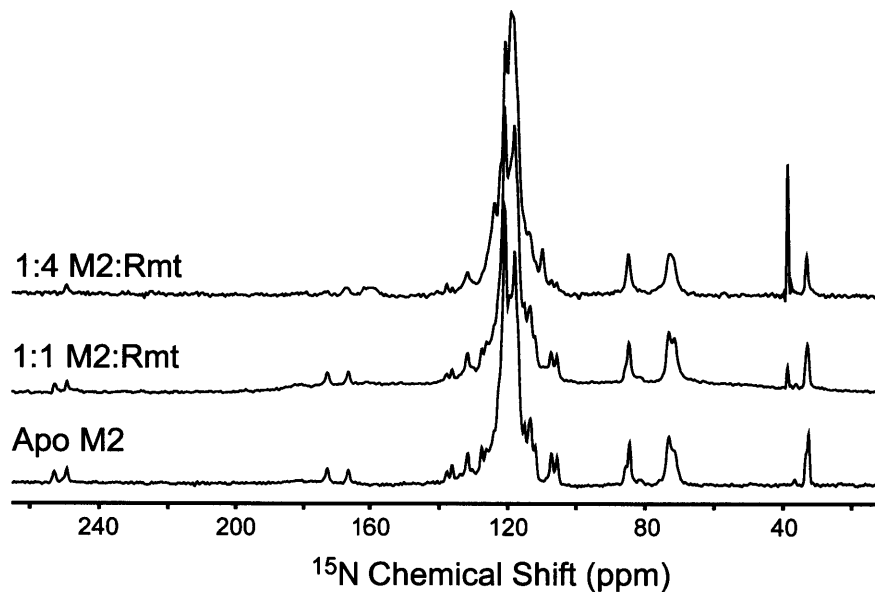


Figure 2.6. A Drug titration of M2 in DPhPC lipids is detected in a ^{15}N CPMAS experiment. Lower, middle, and Upper spectra show, respectively, 0, 0.25 and 1 rimantadine:M2 molar ratios, corresponding to 0, 1 and 4 drug molecules per channel. The drug signal at 39 ppm shows the expected increase in intensity, and drug induced changes in the spectra are evident even in the 1D spectrum. The spectra were processed using a 20 kHz sinebell windowing function and linear prediction of the first two points.

In summary, large drug induced chemical shift changes observed across the entire TM region support a large-scale reorganization of the channel by an allosteric mechanism. In addition, doubling of peaks is likely due to a twofold symmetric tetramer and drug titration data are consistent with a binding stoichiometry of >1 Rmt molecule per channel. Determination of the inhibitor binding site based on maximal chemical shift perturbation alone is not possible given the magnitude and distribution of chemical shift changes. Therefore, a direct dipolar coupling measurement⁴ between the drug and the M2 is needed to determine the binding location(s) and thereby elucidate the mechanism of inhibition in a construct, such as M2_{18-60} , that retains full function in conductance assays.

Acknowledgement. We thank Marcelo Berardi, Alexander Barnes and Eric Miller for helpful discussion. This work was supported by the National Institute of Health (EB001960 and EB002026). L.B. Andreas was supported by a National Science Foundation Graduate Research Fellowship.

2.4 References

- (1) Bright, R. A.; Shay, D. K.; Shu, B.; Cox, N. J.; Klimov, A. I., Adamantane resistance among influenza A viruses isolated early during the 2005-2006 influenza season in the United States. *JAMA* **2006**, *295* (8), 891-4.
- (2) Pielak, R. M.; Chou, J. J., Flu Channel Drug Resistance: A tale of two sites. *Protein & Cell* **2010**, *1* (3), 246-258.
- (3) Cady, S. D.; Luo, W.; Hu, F.; Hong, M., Structure and function of the influenza A M2 proton channel. *Biochemistry* **2009**, *48* (31), 7356-64.
- (4) Cady, S. D.; Schmidt-Rohr, K.; Wang, J.; Soto, C. S.; DeGrado, W. F.; Hong, M., Structure of the amantadine binding site of influenza M2 proton channels in lipid bilayers. *Nature* **2010**, *463*, 689-692.
- (5) Ma, C.; Polishchuk, A. L.; Ohigashi, Y.; Stouffer, A. L.; Schon, A.; Magavern, E.; Jing, X.; Lear, J. D.; Freire, E.; Lamb, R. A.; DeGrado, W. F.; Pinto, L. H., Identification of the functional core of the influenza A virus A/M2 proton-selective ion channel. *Proc Natl Acad Sci U S A* **2009**, *106* (30), 12283-8.
- (6) Pielak, R. M.; Schnell, J. R.; Chou, J. J., Mechanism of drug inhibition and drug resistance of influenza A M2 channel. *Proc Natl Acad Sci U S A* **2009**, *106* (18), 7379-84.
- (7) Schnell, J. R.; Chou, J. J., Structure and mechanism of the M2 proton channel of influenza A virus. *Nature* **2008**, *451* (7178), 591-5.
- (8) Stouffer, A. L.; Acharya, R.; Salom, D.; Levine, A. S.; Di Costanzo, L.; Soto, C. S.; Tereshko, V.; Nanda, V.; Stayrook, S.; DeGrado, W. F., Structural basis for the function and inhibition of an influenza virus proton channel. *Nature* **2008**, *451* (7178), 596-9.
- (9) Kovacs, F. A.; Cross, T. A., Transmembrane four-helix bundle of influenza A M2 protein channel: structural implications from helix tilt and orientation. *Biophys J* **1997**, *73* (5), 2511-7.
- (10) Wang, J.; Kim, S.; Kovacs, F.; Cross, T. A., Structure of the transmembrane region of the M2 protein H(+) channel. *Protein Sci* **2001**, *10* (11), 2241-50.
- (11) Jaroniec, C. P.; Filip, C.; Griffin, R. G., 3D TEDOR NMR experiments for the simultaneous measurement of multiple carbon-nitrogen distances in uniformly (13)C,(15)N-labeled solids. *J Am Chem Soc* **2002**, *124* (36), 10728-42.
- (12) Hing, A. W.; Vega, S.; Schaefer, J., Transfer-echo double-resonance NMR. *J Magn Reson* **1992**, *96*, 205-209.
- (13) Hu, J.; Asbury, T.; Achuthan, S.; Li, C.; Bertram, R.; Quine, J. R.; Fu, R.; Cross, T. A., Backbone structure of the amantadine-blocked trans-membrane domain M2 proton channel from Influenza A virus. *Biophys J* **2007**, *92* (12), 4335-43.
- (14) Franks, W. T.; Zhou, D. H.; Wylie, B. J.; Money, B. G.; Graesser, D. T.; Frericks, H. L.; Sahota, G.; Rienstra, C. M., Magic-angle spinning solid-state NMR spectroscopy of the beta1 immunoglobulin binding domain of protein G (GB1): 15N and 13C chemical shift assignments and conformational analysis. *J Am Chem Soc* **2005**, *127* (35), 12291-305.
- (15) Igumenova, T. I.; Wand, A. J.; McDermott, A. E., Assignment of the backbone resonances for microcrystalline ubiquitin. *J Am Chem Soc* **2004**, *126* (16), 5323-31.
- (16) Seidel, K.; Etzkorn, M.; Heise, H.; Becker, S.; Baldus, M., High-resolution solid-state NMR studies on uniformly [13C,15N]-labeled ubiquitin. *Chembiochem* **2005**, *6* (9), 1638-47.
- (17) van Rossum, B. J.; Castellani, F.; Pauli, J.; Rehbein, K.; Hollander, J.; de Groot, H. J.; Oschkinat, H., Assignment of amide proton signals by combined evaluation of HN, NN and HNCA MAS-NMR correlation spectra. *J Biomol NMR* **2003**, *25* (3), 217-23.
- (18) Szeverenyi, N. M.; Sullivan, D.; Maciel, G. E., Observation of spin exchange by two dimensional fourier-transform C-13 Cross polarization magic angle spinning. *J Magn Reson* **1982**, *47*, 462-475.
- (19) Long, J. R.; Sun, B. Q.; Griffin, R. G., Molecular Dynamics and Magic Angle Spinning NMR. *J Am Chem Soc* **1994**, *116* (26), 11950-11956.
- (20) Maus, D. G.; Copie, V.; Sun, B. Q.; Griffiths, J. M.; Griffin, R. G.; Luo, S.; Schrock, R. R.; Liu, A. H.; Seidel, S. W.; Davis, W. M.; Grohmann, A., A Solid-State NMR Study of

Tungsten Methyl Group Dynamics in [Weta(5)-C(5)Me(5)Me(4)]. *J Am Chem Soc* **1996**, *118* (24), 5665-5671.

(21) Wang, J.; Schnell, J. R.; Chou, J. J., Amantadine partition and localization in phospholipid membrane: a solution NMR study. *Biochem Biophys Res Commun* **2004**, *324* (1), 212-7.

(22) Hu, J.; Fu, R.; Nishimura, K.; Zhang, L.; Zhou, H. X.; Busath, D. D.; Vijayvergiya, V.; Cross, T. A., Histidines, heart of the hydrogen ion channel from influenza A virus: toward an understanding of conductance and proton selectivity. *Proc Natl Acad Sci U S A* **2006**, *103* (18), 6865-70.

(23) Polis, Y. J., Grava, Ilze Yanovna Method of Producing Alpha-Methyl-1Adamantylmethyl-amine Hydrochloride. 1974.

(24) Morcombe, C. R.; Zilm, K. W., Chemical shift referencing in MAS solid state NMR. *J Magn Reson* **2003**, *162* (2), 479-86.

(25) Markley, J. L.; Bax, A.; Arata, Y.; Hilbers, C. W.; Kaptein, R.; Sykes, B. D.; Wright, P. E.; Wuthrich, K., Recommendations for the presentation of NMR structures of proteins and nucleic acids. IUPAC-IUBMB-IUPAB Inter-Union Task Group on the Standardization of Data Bases of Protein and Nucleic Acid Structures Determined by NMR Spectroscopy. *J Biomol NMR* **1998**, *12* (1), 1-23.

(26) Harris, R. K.; Becker, E. D.; Cabral de Menezes, S. M.; Goodfellow, R.; Granger, P., NMR Nomenclature: Nuclear Spin Properties and Conventions for Chemical Shifts. IUPAC Recommendations 2001. *Solid State Nucl Magn Reson* **2002**, *22* (4), 458-483.

(27) Baldus, M.; Petkova, A. T.; Herzfeld, J.; Griffin, R. G., Cross Polarization in the tilted frame: Assignment and spectral simplification in heteronuclear spin systems. *Molecular Physics* **1998**, *95* (6), 1197-1207.

(28) Delaglio, F.; Grzesiek, S.; Vuister, G. W.; Zhu, G.; Pfeifer, J.; Bax, A., NMRPipe: a multidimensional spectral processing system based on UNIX pipes. *J Biomol NMR* **1995**, *6* (3), 277-93.

Chapter 3: Dynamic Nuclear Polarization Study of Inhibitor Binding to the M2₁₈₋₆₀ Proton Transporter from Influenza A

Adapted from Andreas, LB; Barnes, AB; Corzilius, B; Chou, JJ; Miller, EA; Caporini, M; Rosay, M; Griffin, RG; Biochemistry, 2013, 52(16):2774-82.

3.1 Introduction

Magic angle spinning (MAS) NMR is a powerful analytical technique well suited for dynamic and structural characterization of membrane proteins and amyloid fibrils at atomic resolution¹⁻³. In contrast with solution NMR, the ability to investigate systems of larger molecular mass without an inherent broadening of resonances is a major advantage of MAS NMR. However, the decreased molecular site concentration of larger molecules and detection of smaller magnetic moments of ¹³C and ¹⁵N spins means that sensitivity limits the application of traditional MAS NMR experiments. Dynamic nuclear polarization (DNP) can greatly increase the sensitivity of NMR by transferring the substantially higher polarization found in the electron spin reservoir to nuclear spins. DNP was first demonstrated at a magnetic field of 3.03 mT using a static sample of a metal¹; these seminal studies also experimentally verified the Overhauser effect as an efficient polarization transfer mechanism. In the 1980's, DNP experiments performed on dielectric solids were integrated with MAS at 1.2 T, a low magnetic field by current standards²⁻⁵. The extension of DNP to magnetic field strengths used in contemporary NMR (≥ 5 T) has been achieved with the implementation of gyrotron oscillators as microwave power sources. Additional advances in NMR probe technology and development of stable organic radicals serving as the source of electron polarization have stimulated more widespread adoption of the approach and recently sparked considerable interest in the biological solid state NMR community. DNP in conjunction with MAS NMR has now been proven to yield considerable gains in sensitivity making possible a 25-10,000 fold reduction in experiment time in studies of membrane proteins, amyloid fibrils, and peptide nanocrystals at 9 Tesla^{6, 7}. Cryogenic MAS studies with improved probe technology on crystalline peptides demonstrated that resolution need not be compromised at low temperature^{8, 9}. MAS-DNP experiments on bacteriorhodopsin, a helical 7 transmembrane protein, have exploited both the sensitivity available from DNP as well as the cryogenic temperatures employed in such experiments to trap intermediates of its proton pumping cycle to better characterize the mechanism of ion translocation^{10, 11}. Experiments on the amyloid protein PI3-SH3 have shown

that additional cross-peaks appear at low temperatures due to changes in protein dynamics, and the DNP enhanced spectra were useful in determining details of the fibril structure¹². In some, but not all cases, the cryogenic sample temperature leads to inhomogeneous line broadening and reduced resolution. Therefore application of DNP to biological systems of broad interest typically relies on well-resolved chemical shifts from spins found in unique chemical environments, or specific isotopic labeling of a cofactor, inhibitor, or residues to generate site-specific resolution. With the present state of the art and fields of about 9 T to 14 T, successful application will likely involve carefully labeling the protein and ligand to make use of spectra with approximately 1.5 (¹³C) and 3 (¹⁵N) ppm linewidths^{8, 13}.

In this study, we demonstrate that DNP can be used to elucidate ligand-protein interactions even in the weak (mM) binding regime using the proton transporter M2₁₈₋₆₀ from Influenza A virus and the inhibitor rimantadine. We present direct measurement of membrane protein-ligand interaction using MAS dipolar recoupling and DNP to detect the sites of drug binding in the tetrameric proton channel M2₁₈₋₆₀ in the non-conducting, high pH state. This method is generally applicable to the study of drug or ligand binding, particularly for weak binding because general application of MAS NMR dipolar recoupling techniques to weak binding ligands requires the temperature to be lowered in order to quench dynamic exchange processes¹⁴. Although we stress the importance of low temperatures to quench exchange processes, binding sites can be detected while undergoing exchange using NOE measurements or dephasing experiments in which the exchange term commutes with the Hamiltonian. However, experiments such as ZF-TEDOR^{15, 16} that rely on transverse mixing do not commute with exchange terms and are made accessible by the low temperatures and DNP.

The M2 proton channel from Influenza A is inhibited by the antiviral drugs rimantadine (Rmt) and amantadine (Amt). The full protein is 97 amino acids, and a construct comprising residues 21-61 has been shown to retain proton conductivity and inhibition by Amt and Rmt¹⁷. This construct and a similar 18-60 construct contain a single pass transmembrane helix and an amphipathic helix, which has been shown to stabilize the tetrameric assembly. An even shorter construct, M2₂₂₋₄₆, comprising the transmembrane segment, shows reduced inhibition by drug, but remains drug sensitive. A controversy regarding the site of pharmacological inhibition arose from the observation of two different binding sites in various constructs of M2. Prevalence of n terminal resistance mutations¹⁸ and drug induced changes in the pKa of H37¹⁹ suggested binding in the pore of the channel. However, structural studies showed multiple binding sites. An external site near D44 and R45 was observed by NOE in a solution NMR structure²⁰ of M2₁₈₋₆₀. On the other hand, an internal site in the pore near residues V27, S31, and G34A was proposed in a 3.5 Å

diffraction structure of M2₂₂₋₄₆ at pH 5.3²¹, and also observed in REDOR recoupling experiments²². When the drug was first detected in the pore of M2₂₂₋₄₆ in lipid bilayers, it was unclear if the conflicting results were due to truncating the protein near the external site, the particular micelle environment of the solution NMR structure, or other differences in sample preparations. The drug has now been shown to bind to the pore of M2₂₁₋₆₁²³ ruling out problems with protein truncation. It is therefore known that the aminoadamantyl inhibitors Amt and Rmt bind to the pore of fully functional constructs in lipids, and the lack of pore NOE measurements in the solution NMR is likely due to the specific sample environment.

Nevertheless, since the drug has been shown to bind to both sites, the important remaining question was to definitively determine the site(s) responsible for inhibition. The pharmacological significance of each binding site has been supported based on resistance mutations and binding affinities, yet there is not yet consensus regarding interpretation of the functional data^{24, 25}. Perhaps the strongest support for functional pore binding came from an interesting drug-sensitive chimera protein containing C-terminal residues from influenza B M2 and thus lacking the external binding site²⁶. A recent study using this AM2-BM2 chimera solved a detailed structure of the tetramer with Rmt bound inside the pore²⁷.

Given the existing evidence for multiple binding sites, most likely of differing affinity, we investigated M2₁₈₋₆₀ in lipid bilayers to explore the benefits of cryogenic DNP and to determine the locations of the functionally important drug amine group when bound to the protein. We present direct measurement of the drug in both binding sites, and correlate pore binding with widespread chemical shift changes that have been interpreted as an indicator of structural rearrangement and functional binding^{14, 28}.

We used both wild type (WT) M2 and the D21G, D24G double mutant to study drug binding. The use of the double mutant is justified by noting that the mutations occur outside the lipid embedded channel region. In addition, the mutant shows proton conduction and inhibition similar to the WT protein in liposome assays (see *Figure 3.8* in the supporting information). Additionally, in all samples, cysteins 19 and 50 were changed to serine with no loss of function²⁴ in order to prevent uncontrolled disulphide bond formation. The two mutations from D to G remove ambiguity in potential cross-peaks arising from D44 in the external binding site. Thus, the WT₁₈₋₆₀ sequence used in this work is RSN DSSDPLVVAA SIIGILHLIL WILDRLFFKS IYRFFEHLGLK.

3.2 Methods

The DNP enhanced ZF-TEDOR experiment

In our DNP enhanced ZF-TEDOR experiment (*Figure 3.1*), spin polarization is transferred several times before final detection. First, electron polarization on biradicals²⁹ such as TOTAPOL³⁰ is transferred to nearby protons via the cross effect³¹ under the application of CW microwave irradiation and concurrently transferred to more distant protons via spin diffusion. The microwave irradiation frequency is set to 28.0498 GHz/Tesla to maximize DNP efficiency using TOTAPOL. Next, ¹H polarization is transferred to ¹³C in a cross polarization step. The previous steps serve to increase the initial ¹³C polarization and increase the sensitivity of the experiment. Finally, ZF-TEDOR recoupling¹⁵ is used to transfer carbon polarization to ¹³C-¹⁵N two-spin order, the nitrogen chemical shift is encoded, and the two-spin order is reconverted into ¹³C single quantum coherence for direct detection. It is in this final ZF-TEDOR step that the interaction between ¹³C labeled protein and ¹⁵N labeled drug is observed.

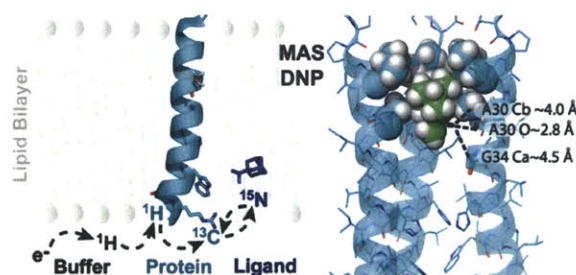


Figure 3.1. Schematic of the DNP enhanced TEDOR experiment showing transfer of polarization from electrons to protons via the cross effect, from matrix protons to protein protons via ¹H-¹H spin diffusion, from ¹H to ¹³C via cross polarization, and from protein ¹³C to ¹⁵N ligand via TEDOR. This allows the measurement of protein-drug distances, as illustrated on the right.

Optimization of Radical Concentration

A low concentration of 4 mM TOTAPOL was used in order to ensure that the radical induced only minimal paramagnetic relaxation effects on the protein. Particularly, reduction in transverse relaxation during long mixing periods could reduce signal intensity. Average carbonyl ¹³C T₂ relaxation times of only ~2 ms were found in a 40 mM TOTAPOL M2 sample with DNP enhancements of 26. A T₂ of 13 to 14 ms was found using 4 mM, similar to the T₂ value at 278 K. These effects are particularly pronounced in this relatively small protein, and appear to be much less significant in previous studies that used 40 mM TOTAPOL to probe details of the active site of bacteriorhodopsin, which is shielded from close approach of radical by a larger (26 kD)

protein⁸. General optimization of radical concentration for DNP is the subject of ongoing discussion.

M2 Sample Preparation

Pure M2₁₈₋₆₀ peptide was prepared by expression in *E. coli* as a fusion protein to TrpLe with a His 9 tag, and purified with a nickel affinity column followed by chemical cleavage with cyanogen bromide in 70 % formic acid and final purification on a C4 reverse phase HPLC column^{20, 28}. The Udorn strain of influenza was chosen, but with C19S and C50S mutations to prevent unwanted disulphide bond formation. Indicated samples additionally contained the D21G and D24G mutations.

M2 samples were prepared for MAS NMR as described previously²⁸ with modification to cryoprotect the sample in a glassy matrix^{32, 33} containing TOTAPOL for DNP. DPhPC lipid (Avanti Polar Lipids) and lyophilized M2₁₈₋₆₀ were dissolved in denaturing buffer (6M guanidine, 40 mM phosphate, 30 mM glutamate, 3 mM sodium azide, pH 7.8, ≥ 33 mg/mL octyl glucoside (OG) detergent) with a lipid to protein ratio of 2:1 by weight. Buffer components were purchased from Sigma, and detergent from Affymetrix. The resulting solution was then dialyzed in a 3.5kD cutoff dialysis cassette (Thermo) against 1 L of sample buffer (40 mM phosphate, 30 mM glutamate, 3 mM sodium azide, pH 7.8) for 7 days with 2 dialysis buffer changes per day. Lipid/M2 bilayers formed a white precipitate after approximately 24 hours. Solid material was pelleted by centrifugation at $\sim 100\,000 \times g$ in a Beckmann ultracentrifuge. For pore-bound samples, a fourfold molar excess of ¹⁵N Rmt was added directly to the membrane pellet and incubated for 2 days at room temperature (~ 22 °C). The pellet was then mixed with 2 mL of DNP buffer (60:40 by volume glycerol-d₈:75 % deuterated sample buffer and 4 mM TOTAPOL³⁰) and separated by centrifugation at $450\,000 \times g$ for 12 hours. DNP buffer was drained from below the sample and the sample was packed in a 4mm (Revolution NMR) or 3.2 mm (Bruker) sapphire MAS rotor. For pore-unbound samples, the membrane pellet was first mixed with DNP buffer and centrifuged at $450\,000 \times g$. A fourfold molar excess of ¹⁵N Rmt was then added to the sample immediately before packing into a sapphire MAS rotor.

NMR, Hardware, Referencing, and Processing

Standard NMR spectra were recorded using Cambridge Instruments spectrometers (courtesy of D.J. Ruben) operating at 500, 700, and 750 MHz ¹H frequencies and using triple channel Varian 4 mm (500 MHz), Varian 3.2 mm (700 MHz), and Bruker 3.2 mm e-free (750 MHz) probes. DNP

NMR spectra were acquired at 211 MHz using a Cambridge Instruments spectrometer and triple channel HCN probe equipped with a 4 mm MAS stator and waveguide for delivery of microwave irradiation from a gyrotron oscillator at 139.66 GHz³⁴. Additional DNP spectra were recorded using a commercial DNP spectrometer³⁵ at 400MHz ¹H frequency and 263 GHz for the microwaves (Bruker, Billerica, MA).

Chemical shifts were referenced using the published shifts of adamantane relative to DSS for ¹³C referencing³⁶ and the IUPAC relative frequency ratios between DSS (¹³C) and liquid ammonia (¹⁵N)^{37, 38} for ¹⁵N referencing. DNP spectra were referenced using the known chemical shifts of G34 at 278 K. Additional experimental details such as pulse sequences, NMR field strengths, and spinning frequencies are indicated in the figure captions. Spectra were processed using the NMRPipe³⁹ software package and visualized and assigned using Sparky (Goddard and Kneller, University of California, San Francisco). Spectra collected at 600 MHz were processed with 150 Hz Gaussian apodization in both ¹³C and ¹⁵N dimensions to improve the signal to noise ratio of the buildup curve. All other TEDOR spectra were processed with a 100 Hz Gaussian apodization window in the ¹³C dimension, and 150 Hz (cryogenic DNP) and 30 Hz (278 K) in the ¹⁵N dimension to improve sensitivity. Spectra in **Figure 3.2** were processed with 30 Hz of Gaussian apodization. TPPM⁴⁰ Decoupling field strengths of ~100 kHz were used during TEDOR mixing periods, and either 100 kHz or 83 kHz were used during acquisition. Power levels of 50 to 83 kHz were used for ¹³C pulses, and 20 to 40 kHz for ¹⁵N pulses. Further details of the pulse sequences are provided in the supporting information.

3.3 Results

The DNP experiments are performed at low temperatures of ~80-100 K where ice crystals would form from buffers commonly used for room temperature experiments. The samples are thus cryoprotected using 60% glycerol by volume. We show in **Figure 3.2** that the chemical shifts are unperturbed by the addition of 60% glycerol, both for the apo and the functionally-bound states at ~278 K. The spectra provide a fingerprint that can be used to distinguish between apo M2 and functionally-bound M2, where functional binding is determined by large chemical shift changes^{14, 19, 28}. Previous reports found that addition of the aminoadamantyl drugs Rmt and Amt cause widespread chemical shift changes of up to several ppm to occur and a functionally drug-bound spectrum is easily distinguished from an apo spectrum. Based on these fingerprint spectra, we conclude that the glycerol does not cause any significant change in these states of the protein. However, we find that glycerol increases the energy barrier for functional drug binding. In

samples with drug added *before* glycerol, the drug-bound set of shifts was observed. In samples with drug added *after* glycerol, the apo set of peaks was observed. Since the final composition of both samples is the same, we conclude that the difference is attributed to kinetically trapping the apo state and that the barrier for drug binding is increased by glycerol.

Spectra in **Figure 3.2** were assigned using ZF-TEDOR^{15, 16} and PDSD^{41, 42} correlation experiments as was reported for WT₁₈₋₆₀²⁸, and by observation of only minor differences in chemical shift between WT₁₈₋₆₀ and the D21G and D24G double mutant spectra of **Figure 3.2**. As with WT, we observe membrane embedded resonances from approximately residue 25 to 50 at 278 K. These observed residues span both proposed binding sites. Residue 24 appears weakly in some spectra, and residues 18-23 and 54-60 are not detected due to unfavorable mobility of this part of the protein. Spectra recorded at low temperature and with DNP were assigned based on the room temperature resonances for G34, and by using the observed range of chemical shifts reported in the BioMagResBank⁴³ for cross-peaks that do not show up at high temperature. These low temperature cross-peaks could not be uniquely assigned; therefore all possible assignments are indicated.

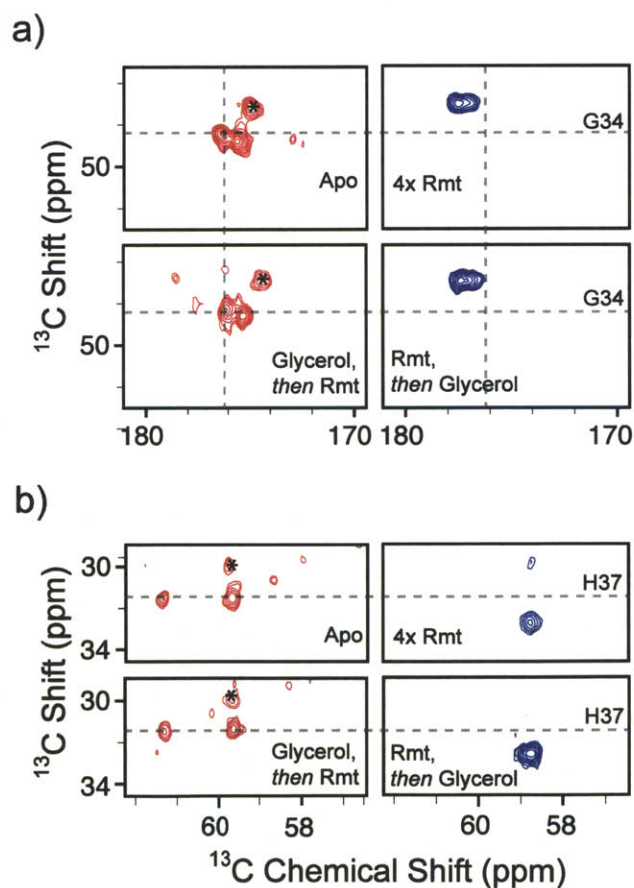


Figure 3.2. PDSD spectra of M2 acquired under four sample conditions show that chemical shifts are unperturbed by 60% glycerol if glycerol is the last component added to the sample. In a) and b) are shown

cross-peaks of G34 and H37, respectively in uniformly ^{13}C labeled samples. The first three panels were recorded using a 700 MHz instrument with a Varian 3.2 mm triple channel probe spinning at 12.5 kHz. The fourth panel (4x Rmt then 60% glycerol) was recorded at 750 MHz with a triple channel Bruker e-free probe spinning at 13.4 kHz. These spectra of the D21G and D24G double mutant were recorded at ~ 278 K using 15 ms of mixing. Peaks of G34 and H37 are displayed because of the excellent resolution in these regions of the spectrum, and a clear change in frequency upon drug binding. Peaks other than those from G34 and H37 are indicated with an asterisk.

In order to observe a dipolar coupling between uniformly ^{13}C labeled protein and ^{15}N labeled inhibitor Rmt, we used a ^{13}C - ^{15}N ZF-TEDOR experiment with 8.8 ms of mixing. Near room temperature (~ 278 K), the spectrum shows only two correlations to ^{15}N labeled drug after 23 days of acquisition (**Figure 3.3**, red). In contrast, DNP enhanced TEDOR spectra with 8.7 ms mixing at low (80-105 K) temperatures showed several additional cross-peaks (**Figure 3.3 and Figure 3.4**, blue) and required only 2 days of acquisition due to the reduction in temperature and a signal enhancement factor of 11. Assignments consistent with the observed cross-peaks are indicated in the figures, and clearly show that at room temperature the drug is observed in the pore near G34 and A30. The G34 cross-peak is unambiguously assigned at 278 K, based on the known unique resonances of G34 at this temperature. The A30 cross-peak is assigned by ruling out the only other alanine, A29, as a possible assignment because this residue is found on the outside of the channel far from G34, and the simplest interpretation of the data is that we are observing a single binding site in the pore.

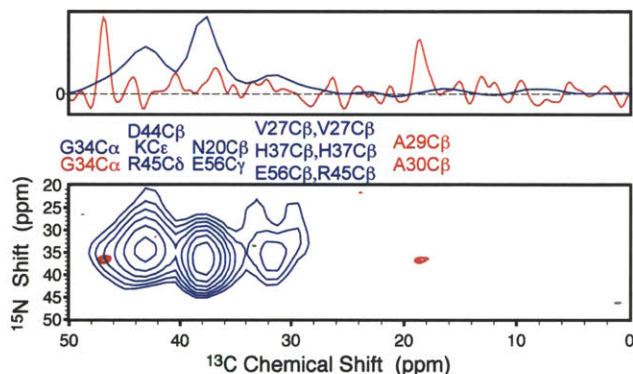


Figure 3.3. ZF-TEDOR spectra acquired at 278 K (red) show one set of cross-peaks, and those acquired at ~ 90 K using DNP (blue) show additional peaks. In red is shown an 8.8 ms TEDOR experiment acquired at 500 MHz and 10 kHz MAS with a sample temperature of 278 K. In blue is shown an 8.72 ms TEDOR experiment acquired at 211 MHz and 4.587 kHz MAS using DNP at 90 K. The 278 K spectrum was recorded in 23 days and the 90 K DNP spectrum in 2 days. Both spectra were acquired using the same sample of D21G-D24G M2 packed in a 4 mm sapphire rotor. ^{15}N labeled Rmt was added before glycerol, and binding reached $\sim 70\%$ (as indicated by fingerprint spectra such as in **Figure 3.2** before glycerol kinetically trapped the remaining 30% in the pore-unbound state. Possible assignments are indicated.

At low temperature and using DNP, the drug is also observed on the periphery of the protein, consistent with the external site near D44 that was previously observed using solution NMR. In addition, cross-peaks are observed that are consistent with drug associating to E56 or N20, which may be another site of weak drug-protein association. The sample in **Figure 3.3** was approximately 70% functionally bound before glycerol was added and the remaining 30% was trapped in the apo state. The amount of functionally bound protein is less than 100% because it can take days for drug to penetrate and fully bind to the thick membrane pellet. Once glycerol is added, further binding is kinetically prevented. We used spectra similar to those shown in **Figure 3.2**, and the known chemical shifts of the apo and bound M2 to determine the extent of drug binding.

In **Figure 3.4**, we show that if the protein is kinetically trapped in the apo state with drug present in the sample, the drug is observed only outside the pore. Isoleucine and leucine residues were ruled out as possible assignments by reverse labeling of these residue types with ^{12}C and observation of the same peaks (see **Figure 3.7** in the supporting information).

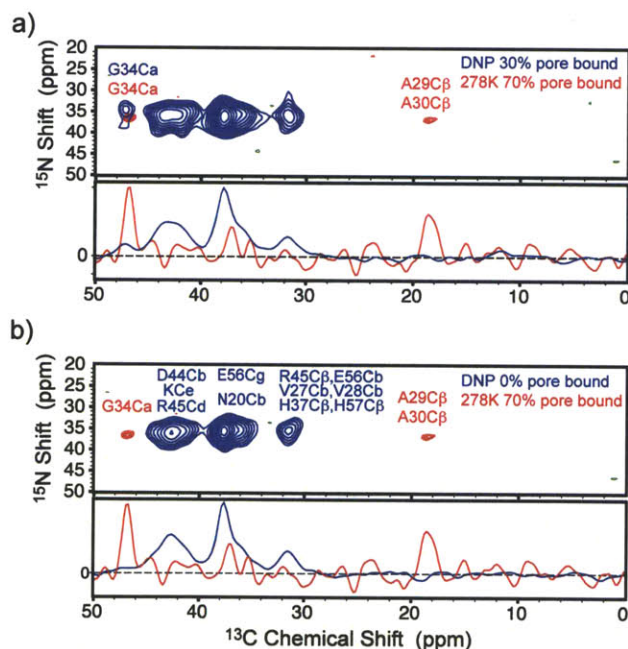


Figure 3.4. ZF-TEDOR spectra show that the pore binding site is correlated with chemical shift changes. A 400 MHz DNP enhanced TEDOR spectrum (a) with 12.5 ms mixing is shown in blue. The wild type M2 sequence was used, and ~30% of the sample was drug bound as indicated by chemical shifts. In b), a similar spectrum is shown of D21G, D24G M2 but with the protein kinetically trapped in the apo state. Notably, the pore site at G34 is not detected in the functionally unbound sample shown in blue in (b). In red, the TEDOR spectrum acquired at ~278 K, 500 MHz, and 8.8 ms mixing of D21G, D24G M2 is presented for comparison. All possible assignments are listed for each peak in blue (DNP) and red (non-DNP).

The resolution of the DNP enhanced spectrum at 211 MHz is significantly reduced compared to the 278 K spectrum acquired at 500 MHz, but the DNP enhanced spectrum has much higher signal to noise, and the contours are displayed at a lower level. Therefore, the 2D spectra should not be used to infer resolution and we include 1D slices below the 2D spectrum to show the inherent ^{13}C resolution in the spectra. We also see that the Ala C β resonance does not appear in the DNP spectrum. This is typical of $-\text{CH}_3$ groups at temperatures of $\sim 100\text{-}200$ K and results from three-fold hopping at a rate that interferes with ^1H decoupling. Acquisition at temperatures where the methyl dynamics are much slower than the decoupling field results in a return of signal intensity and ^2H labeling of the methyl group has a similar effect by reducing the couplings.⁴⁴

In the 211 MHz DNP enhanced spectrum (*Figure 3.2*), the G34C α resonance is not resolved, but appears as a shoulder on a larger nearby peak. In *Figure 3.3 (a)*, we show a similar DNP spectrum, this time acquired at 400 MHz and applying 12.5 ms of mixing. The spectrum clearly shows a peak at G34C α even though this sample had not equilibrated before addition of glycerol, and only $\sim 1/3$ of the sample showed drug binding as measured by the chemical shift changes. The spectrum in *Figure 3.4 (b)* shows that when glycerol is added before the inhibitor, only the external binding site(s) are observed, once again indicating that the protein is trapped in the pore-unbound state by 60% glycerol. Pore binding is therefore correlated with chemical shift changes. Coupled with a recent report showing that the drug resistant S31N mutant of M2 does not exhibit chemical shift changes with the addition of rmt,⁴⁵ the evidence points convincingly to the pore site as responsible for inhibition in agreement with recent reports^{23, 27}. Despite other glycines in the sequence of M2, the glycine cross-peaks in the DNP spectra can be uniquely assigned to the pore glycine, G34, because glycine peaks are missing from the spectrum when the protein is trapped in the pore-unbound state; the weaker association of the drug on the periphery of the channel does not result in detection of TEDOR cross-peaks to glycine C α s.

With this unique ^{15}N Rmt to G34 C α assignment under DNP conditions, we can proceed with standard MAS NMR experiments designed to measure internuclear distances. In *Figure 3.5*, we show the results of a ZF-TEDOR buildup curve recorded at 600 MHz with DNP using uniformly ^{13}C labeled WT M2₁₈₋₆₀ in a sample with nearly saturated binding to the pore. The maximum signal to noise ratio in the DNP enhanced TEDOR experiment was 15 at 11.52 ms of mixing, which is sufficient to measure a distance using an analytical fitting procedure described previously¹⁵. The data are inconsistent with a drug amine centered in the channel, and the fit distance depends somewhat on whether the amine is near two or one helices. A fit of 4.3 or 4.0

$\pm 0.2 \text{ \AA}$ was found for fits with two and one G34 C α s, respectively. Details of the fit are described below.

An overall scaling factor, λ , is used in the fit to account for an unknown cross polarization intensity and experimental imperfections. Fortunately, we can reduce the number of free parameters in the fit by using the known distance associated with a 1-bond cross-peak from G34C α to G34N to determine λ . A natural abundance of 0.36 percent for ^{15}N was used to scale this peak in the fit, and both the short distance of 1.5 \AA , and the long distance of interest were simulated simultaneously using the same value for λ . The fit parameter Γ_2 is an exponential relaxation term that is dominated by ^{13}C transverse relaxation and was therefore fit using one value for both curves. The average ^{13}C Γ_2 of the sample was determined to be above 100 s^{-1} using

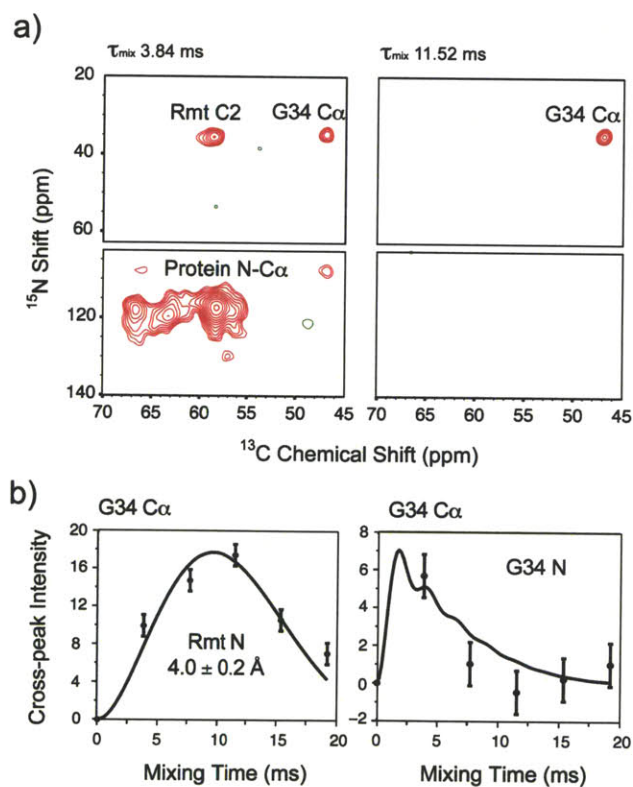


Figure 3.5. DNP enhanced ZF-TEDOR spectra (five mixing points) recorded at 600 MHz with DNP are used to measure a drug-protein distance. Spectra are contoured at two mixing times in (a), and displayed for the G34 cross-peak as a function of mixing time in (b). At 3.84 ms mixing (a, left), one bond cross-peaks are detected due to the natural abundance of $\sim 1\%$ ^{13}C Rmt drug, and $\sim 0.36\%$ ^{15}N protein. By 11.52 ms (a, right), these natural abundance cross-peaks have decayed, and only the cross-peak of interest remains. In (b), the G34 cross-peak intensity is shown as a function of mixing time (points \pm the spectrum rms noise level), with the best-fit simulation as described in the text (smooth curve). The fit resulted in a distance of $4.0 \text{ \AA} \pm 0.2 \text{ \AA}$. The G34 N-C α cross-peak was simultaneously fit (b, right) to reduce the degrees of freedom in the fit. A low natural abundance of ^{15}N ($\sim 0.36\%$) accounts for the reduced signal of this curve. The spectra were recorded in ~ 4 days at a spinning frequency of 12.5 kHz and a temperature of $\sim 100 \text{ K}$. The DNP enhancement factor was 2.5.

an echo experiment, justifying fitting over a range of Γ_2 values between 50 and 150 s^{-1} , as done for crystalline peptides¹⁵. The one bond J coupling of G34 was varied over a wide range of 40 to 60 Hz in the fit, but influenced the fit distance by less than 0.1 Å. Typical values of $^1J_{C-C\alpha}$ are about 55 Hz⁴⁶. Two percent of the sample was assumed to have no J coupling based on an estimate of 98% enrichment of ^{13}C using 99% ^{13}C glucose and a ^{12}C starter culture. A Monte Carlo approach was used to estimate the measurement error by refitting 1000 times with the addition of the appropriate noise level of the spectrum¹⁵ to each curve. The resulting distribution was used to calculate the rms deviation. All error estimates are reported at 1 rmsd.

The final consideration in properly fitting the distance is to determine how many of the helices in the tetramer are close enough to contribute to the cross-peak. If we assume all four are equidistant from the drug amine, then a fit distance of 4.8 ± 0.2 Å is found. With the drug amine positioned between G34 C α and A30 C β , this distance is incompatible with the solution constraints, which allow a minimum distance of about 5.5 Å, and certainly incompatible with the more loosely packed diffraction structures. If we fit the data with two G34 C α s equidistant from the drug amine, and the other two at a reasonable distance of 6.5 Å or above, we determine a fit distance of 4.3 ± 0.2 Å. Finally, if we assume the ^{15}N interacts primarily with one helix, with the other G34 C α s at reasonable distances of 5.5 Å, 6.5 Å, and 6.5 Å, the fit distance is 4.0 ± 0.2 Å. This fit is shown in **Figure 3.5(b)**.

In order to visualize the pore binding site for which we found unambiguous constraints, we have performed a simulated annealing using the program XPLOR-NIH⁴⁷. In addition to the two new constraints from ZF-TEDOR at ~278 K and with cryogenic DNP, we used structural constraints from a solution NMR structure²⁰ and a constraint based on previously reported 2H - ^{13}C REDOR experiments.^{22, 48} Based on the DNP enhanced buildup curve, an upper limit of 4.5 Å was allowed for the Rmt amine to G34 C α . Similar constraints, entered in the calculation as 3.5 ± 1 Å, were entered for ^{15}N -Rmt to A30 C β based on the similar intensity of this cross-peak at room temperature. Constraints of 3.5 ± 1 Å were also applied between the V27 C γ 1 and Rmt CH₂ groups farthest from the amine in order to orient the adamantyl cage consistent with a recent report using the 22-46 construct⁴⁸. Drug constraints were introduced to only one of the four strands of the protein. Given the symmetry of the channel, and the fact that we observe two sets of chemical shifts, the drug amine may hop between 2 or 4 of the helices and thus prevent

breaking of the two-fold symmetry of the channel. A representative result from the simulated annealing is shown in *Figure 3.6*.

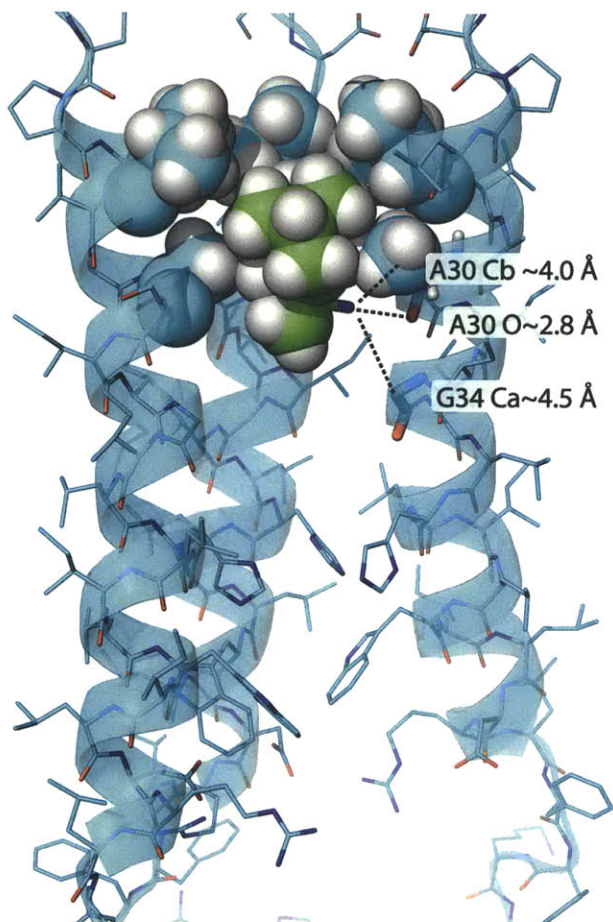


Figure 3.6. A structural model of the pore binding site is shown using distance constraints from DNP enhanced TEDOR experiments, 278 K TEDOR experiments, and previously reported data. The structural model was calculated using XPLOR-NIH and converged to a set of similar structures with 0 violations. A representative structure is shown with drug in green and protein in blue. Three distances to the drug ^{15}N are shown, two of which (A30 C β and G34 C α) are the result of TEDOR measurements. The third distance is a result of the structure calculation and suggests a possible hydrogen bond between the drug amine and the protein at A30 carbonyl oxygen. The constraints deposited in the protein data bank for the solution NMR structure 2RLF²¹ were used to define the tetrameric assembly. Distance constraints of $3.5 \pm 1 \text{ \AA}$ were introduced between the drug ^{15}N and A30 C β and between drug ^{15}N and G34C α based on TEDOR spectra. Finally, constraints of $3.5 \pm 1 \text{ \AA}$ were introduced between the V27 C $\gamma 1$ and Rmt CH₂ groups farthest from the amine in order to orient the adamantyl cage consistent with previously reports.

3.4 Discussion

In previous experiments, two binding sites have been observed, a pore site in M2₂₂₋₄₆ and M2₂₂₋₆₂, and an external site in M2₁₈₋₆₀, M2₂₂₋₄₆. We have confirmed the internal site in the M2₁₈₋₆₀ construct using DNP MAS at 100 K. Additionally, a drug-protein association is observed on the periphery of the channel, consistent with the external site, however, the location and affinity are

not determined. The pore site was found to have a significantly higher barrier, causing the protein to be kinetically trapped near room temperature in the pore-unbound state using 60% glycerol. Pore-bound Rmt was observed in a standard ZF-TEDOR experiment at ~278 K, indicating that the drug is exchanging with the free population slower than the millisecond timescale. In contrast, the external association was only observed at the low temperatures used in DNP experiments, indicating that drug exchange likely results in loss of signal at 278 K. The external site is observed even when the protein has been kinetically trapped in the pore-unbound state (as determined by chemical shift changes) indicating that this site has a low barrier, is not responsible for chemical shift changes, and is most likely not responsible for pharmacological binding.

Measurements of the external binding site(s) of the protein appear to have some specificity even though they are not unambiguously assigned. For example, we see a cross-peak to E56 or N20, but not to neighboring H57 and G58, or S19, S22, and S23 residues. A completely nonspecific interaction should result in some detection of these external glycine and serine residues. Still, partitioning of the drug into the interfacial region of the membrane may significantly enhance population of these sites. Whether the observation of specificity at these weaker sites requires a slow cooling rate and annealing of the protein remains an open to further investigation.

Although binding to the pore of the channel has been observed previously, the present work is the first to our knowledge to directly determine the position of the drug amine group between residues 30 and 34. A previous report in bilayers determined the correct orientation of the drug in the channel, but placed the amine group about a half helical turn towards the carboxy terminus of the protein compared to our measurements⁴⁸. Additionally, our data suggests a hydrogen bond between the drug amine and the A30 carbonyl. Out of 30 calculated structures that did not violate any of the constraints, the distance between the drug amine nitrogen and the A30 carbonyl oxygen was found to vary between 2.4 and 3.5 Å, suggesting a hydrogen bond between drug and protein at this location. Though this agrees with a previously observed conformational heterogeneity at A30's hydrogen bonding donor G34 among drug bound and apo samples⁴⁹, and with a recent solution NMR structure of a chimera protein containing C-terminal residues from Influenza-B M2²⁷, it is the first time this specific interaction has been observed using WT protein. The structural model presented here is consistent with previous measurements on the Rmt tilt angle in the pore of M2₂₂₋₄₆⁴⁸ determined using measurements of the scaled ²H quadrupole splitting of ²H labeled Rmt. The amine was found to point towards the C-terminal end of the channel with a 13° angle between the bilayer normal and the adamantyl group. Rmt is tilted by up to ~35° in the structural model shown in *Figure 3.6*, with most of the ensemble clustered within about 12°. A large distribution in the tilt angle is not surprising because we have not made

measurements to determine this angle, with the adamantyl cage instead being positioned by steric crowding within the channel. Interestingly, the tilt angle of the related drug Amt was previously found to be a much larger 37° ²², suggesting that the shorter link between the adamantyl group and the amine in Amt might force the adamantyl group to rotate so that both the amine and the adamantyl cage can occupy approximately the same locations in the channel for both drugs (see *Figure 3.9* in the supporting information). The evidence for a drug-protein hydrogen bond at A30 carbonyl (both the tilt angle of Amt and the TEDOR measurements on Rmt) could help inform molecular dynamics simulations of this channel that have instead proposed hydrogen bonding to water and a small tilt angle⁵⁰ or even found the amine group pointing towards the nitrogen terminus of the protein⁵¹.

3.5 Supporting Information

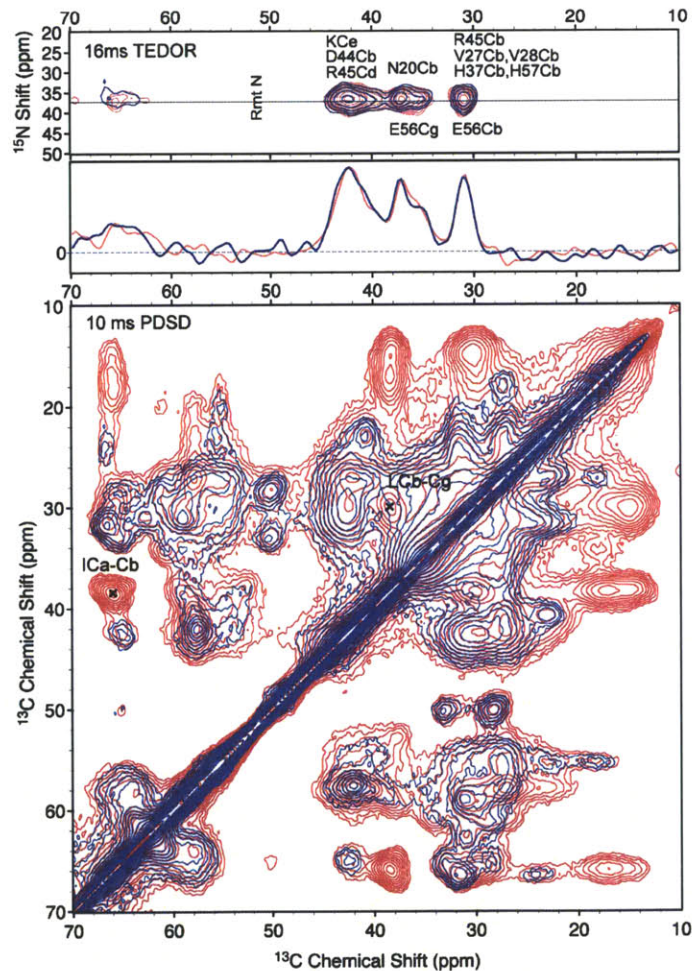


Figure 3.7. Spectra of ^{13}C -ILFY reverse labeled M2 (blue) show identical crosspeaks as FY reverse labeled M2 (red). Top: 16 ms ZF-TEDOR with A 1D slice from the 2D spectrum displayed. Bottom: A 10 ms PDSM spectrum demonstrates successful labeling for these samples since Ile and Leu cross peaks are absent from the blue spectrum. Spectra were recorded at 400 MHz, 9009 kHz MAS, and a temperature of

~105 K. D21G-D24G M2 was used, and ^{15}N was incorporated into the backbone of the protein with ^{15}N Leucine.

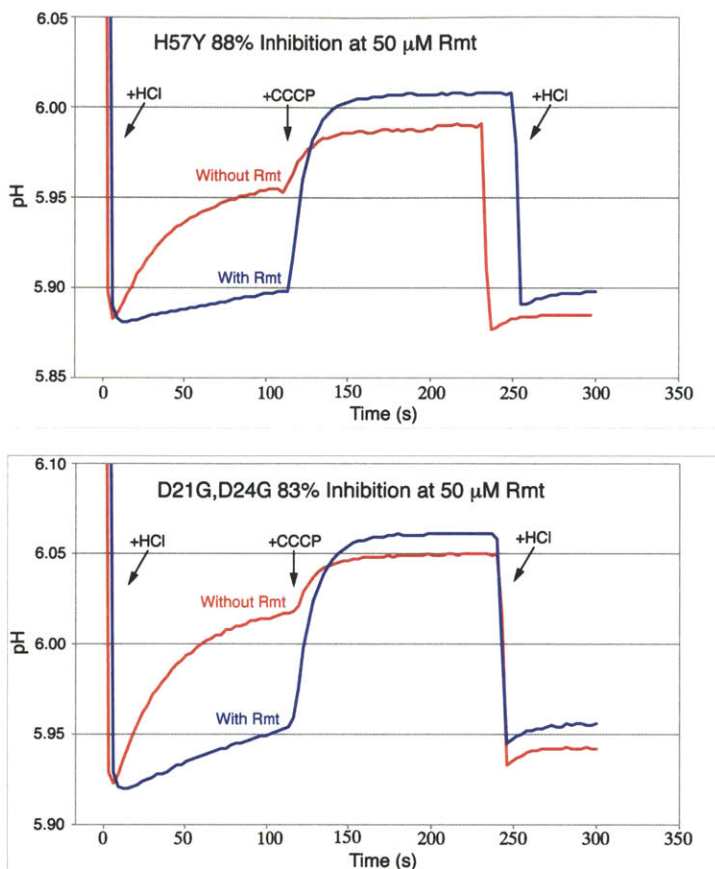


Figure 3.8. The double mutant used in this work is functional and drug sensitive. Channel current is measured indirectly by pH in a liposome assay described previously.²⁴ Briefly, M2 is prepared in liposomes, and the pH outside the liposomes is measured as a function of time. Addition of HCl initiates channel conduction of protons into the liposomes, the initial slope of which is used as a measure of proton flux. The proton flux per channel was calculated using CCCP to equalize the pH inside and outside the liposome, followed by addition of a known amount of HCl to calculate the total buffering capacity. The D21G,D24G double mutant and the H57Y mutant are drug sensitive, with ~80-90% reduction in proton current in the presence of 50 μM Rimantadine, similar to wild type protein.

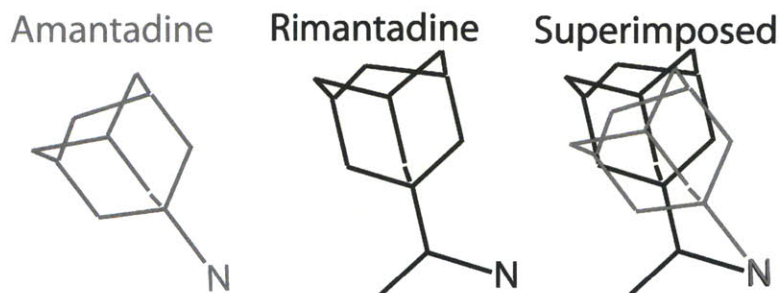


Figure 3.9. An illustration of the tilt angle measured by Hong and coworkers for Amantadine and Rimantadine^{22,48}. Amantadine is tilted 37° from the bilayer normal, while Rimantadine is tilted by only 13° .

In both cases, the amine and adamantyl ends of the molecule occupy similar positions relative to the membrane normal. The illustration was generated using a single internuclear distance and ideal angles of 120° for the projection of tetrahedral geometry in 2 dimensions.

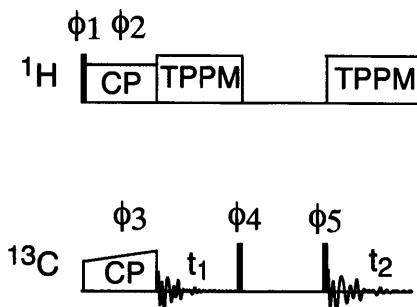


Figure 3.10. The Proton Driven Spin Diffusion (PDS) pulse program used in Figure 1 is depicted as previously described^{41,42}. Narrow rectangles represent 90° pulses. A ^1H flip and decoupling power level of 83 kHz was used. Two pulse phase modulation⁴⁰ (TPPM) was optimized with phases of 18 and 0 degrees, and a pulse length of 5.8 μs . 83 kHz of ^{13}C was used for flip pulses. Cross polarization (CP) was applied for 1.5 to 2 ms with constant irradiation at ~ 70 kHz on ^1H and with an optimized ramp on ^{13}C centered at one rotor frequency below the proton nutation frequency. The phase cycle was: $\phi_1 = 13$, $\phi_2 = 2$, $\phi_3 = 1133$, $\phi_4 = 2$, $\phi_5 = 1111\ 3333\ 2222\ 4444$, $\phi_{\text{receiver}} = 2442\ 4224\ 3113\ 1331$, where $x=1$, $y=2$, $-x=3$, $-y=4$.

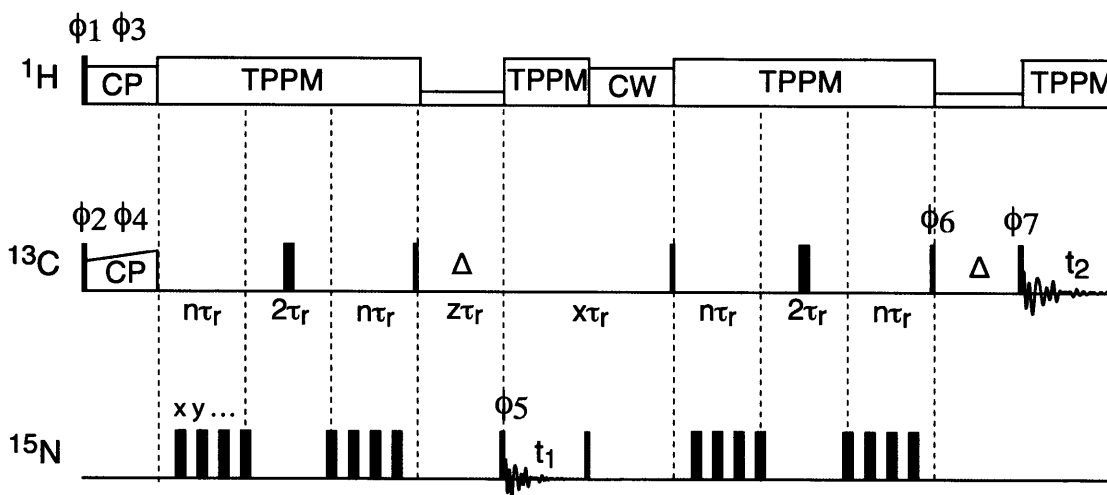


Figure 3.11. The z-filtered transferred echo double resonance (ZF-TEDOR) pulse program used in Figures 2-4 is depicted as previously described¹⁵. Narrow rectangles represent 90° pulses, and broad rectangles represent 180° pulses. A ^1H flip and decoupling power level of 83 to 100 kHz was used during evolution, and ~ 100 kHz was applied during mixing. Two pulse phase modulation (TPPM) was optimized with phases of 18 and 0 degrees, and a pulse length of 5.8 μs (83 kHz) or 4.8 μs (100 kHz). 50 to 83 kHz of ^{13}C was used for flip pulses. A power level of 20 to 40 kHz was typical for flip pulses on the ^{15}N channel. At 278 K, cross polarization (CP) was applied for 1.5 to 2 ms with constant irradiation at ~ 70 kHz on ^1H and with an optimized ramp on ^{13}C centered at one rotor frequency below the proton nutation frequency. At low temperature, 0.9 ms of CP was used. The phase cycle was: $\phi_1 = 16x(1)\ 16x(3)$, $\phi_2 = 16x(4)\ 16x(2)$, $\phi_3 = 2$, $\phi_4 = 1$, $\phi_5 = 13$, $\phi_6 = 2244$, $\phi_7 = 1111\ 2222\ 3333\ 4444$, $\phi_{\text{receiver}} = 4224\ 1331\ 2442\ 3113\ 2442\ 3113\ 4224$

1331, where $x=1$, $y=2$, $-x=3$, $-y=4$. The initial flip pulse on the ^{13}C channel was omitted for spectra acquired at ~ 100 K. Rotor synchronization is indicated under the ^{13}C channel in the figure. Mixing times ($4n\tau$) are indicated in the manuscript. Z-filters of 2 to 4 rotor periods were sufficient to suppress unwanted coherences.

3.6 Conclusions

We have shown that DNP can be used with MAS for the identification of ligand-protein interactions. The low temperatures used for DNP quenches dynamic processes that interfere with dipolar recoupling experiments, particularly for weakly bound ligands. These effects were demonstrated in M2, in which the pore binding site is evident at 278 K, and weaker binding to the periphery of the protein is only observed at cryogenic temperatures. In addition, we found that glycerol can be used to kinetically prevent the drug from entering the pore, thereby allowing us to make samples with the pore unoccupied, but with drug bound to the external site. With these samples, we have correlated chemical shift changes with binding in the pore. In addition, we located the position of the functionally important drug amine group in relation to specific protein ^{13}C atoms, placing the amine close enough to A30 carbonyl to form a hydrogen bond. Further experiments could include BASE-TEDOR experiments¹⁵ to improve precision of the distance measurements, as well as unambiguous assignment experiments to precisely determine the external binding site(s).

ACKNOWLEDGMENT

We thank Rafal Pielak for help running the liposome assay and help with sample preparation. We thank Marvin Bayro and Galia Debelouchina for help with the DNP acquisition at Bruker Biospin, Remy Sounier, and Marcelo Berardi for helpful discussion regarding sample preparation. Matthew Eddy and Yongchao Su are gratefully acknowledged for help in testing TEDOR fitting code against a known system. This work was supported by NIH grants EB-001960, EB-002026, AI-067438, and GM-094608.

3.7 References

- (1) Carver, T. R.; Slichter, C. P., Polarization of Nuclear Spins in metals. *Physical Review* **1953**, *92*, 212-213.
- (2) Afeworki, M.; Mckay, R. A.; Schaefer, J., Selective Observation of the Interface of Heterogeneous Polycarbonate Polystyrene Blends by Dynamic Nuclear-Polarization C-13 Nmr-Spectroscopy. *Macromolecules* **1992**, *25* (16), 4084-4091.
- (3) Afeworki, M.; Vega, S.; Schaefer, J., Direct Electron-to-Carbon Polarization Transfer in Homogeneously-Doped Polycarbonates. *Macromolecules* **1992**, *25*, 4100-4106.
- (4) Macho, V.; Kendrick, R.; Yannoni, C. S., Cross Polarization Magic-Angle Spinning NMR at Cryogenic Temperatures. *Journal of Magnetic Resonance* **1983**, *52*, 450-456.
- (5) Wind, R. A.; Anthonio, F. E.; Duijvestijn, M. J.; Smidt, J.; Trommel, J.; Vette, G. M. C. d., Experimental Setup for Enhanced ¹³C NMR Spectroscopy in Solids Using Dynamic Nuclear Polarization. *Journal of Magnetic Resonance* **1983**, *52*, 424-434.
- (6) Debelouchina, G.; Bayro, M.; van der Wel, P.; Caporini, M.; Barnes, A.; Rosay, M.; Maas, W.; Griffin, R., Dynamic nuclear polarization-enhanced solid-state NMR spectroscopy of GNNQQNY nanocrystals and amyloid fibrils. *Phys. Chem. Chem. Phys.* **2010**, *12*, 5911-5919.
- (7) Bajaj, V. S.; Mak-Jurkauskas, M. L.; Belenky, M.; Herzfeld, J.; Griffin, R. G., DNP enhanced frequency-selective TEDOR experiments in bacteriorhodopsin. *Journal of Magnetic Resonance* **2010**, *202* (1), 9-13.
- (8) Barnes, A. B.; Corzilius, B.; Mak-Jurkauskas, M. L.; Andreas, L. B.; Bajaj, V. S.; Matsuki, Y.; Belenky, M.; Lugtenburg, J.; Sirigiri, J. R.; Temkin, R. J.; Herzfeld, J.; Griffin, R. G., Resolution and Polarization Distribution in Cryogenic DNP/MAS Experiments. *Physical Chemistry and Chemical Physics* **2010**, submitted.
- (9) Barnes, A. B.; Mak-Jurkauskas, M. L.; Matsuki, Y.; Bajaj, V. S.; van der Wel, P. C. A.; DeRocher, R.; Bryant, J.; Sirigiri, J. R.; Temkin, R. J.; Lugtenburg, J.; Herzfeld, J.; Griffin, R. G., Cryogenic sample exchange NMR probe for magic angle spinning dynamic nuclear polarization. *J. Mag. Res.* **2009**, *198* (2), 261-270.
- (10) Bajaj, V.; Mak-Jurkauskas, M.; Belenky, M.; Herzfeld, J.; Griffin, R., Functional and shunt states of bacteriorhodopsin resolved by 250 GHz dynamic nuclear polarization-enhanced solid-state NMR. *Proc. Natl. Acad. Sci.* **2009**, *106* (23), 9244.
- (11) Mak-Jurkauskas, M. L.; Bajaj, V. S.; Hornstein, M. K.; Belenky, M.; Temkin, R. J.; Griffin, R. G.; Herzfeld, J., Energy Transformations Early in the Bacteriorhodopsin Photocycle Revealed by DNP-Enhanced Solid State NMR. *Proc. Natl. Acad. Sci. U. S. A.* **2008**, *105* (3), 883-888.
- (12) Bayro, M. J.; Debelouchina, G. T.; Eddy, M. T.; Birkett, N. R.; Macphee, C. E.; Rosay, M.; Maas, W. E.; Dobson, C. M.; Griffin, R. G., Intermolecular structure determination of amyloid fibrils with magic-angle spinning and dynamic nuclear polarization NMR. *J Am Chem Soc* **2011**, *133* (35), 13967-74.
- (13) Rosay, M.; Zeri, A. C.; Astrof, N. S.; Opella, S. J.; Herzfeld, J.; Griffin, R. G., Sensitivity-enhanced NMR of biological solids: Dynamic nuclear polarization of Y21M fd bacteriophage and purple membrane. *Journal of the American Chemical Society* **2001**, *123* (5), 1010-1011.
- (14) Cady, S. D.; Hong, M., Amantadine-induced conformational and dynamical changes of the influenza M2 transmembrane proton channel. *Proceedings of the National Academy of Sciences* **2008**, *105* (5), 1483.
- (15) Jaroniec, C. P.; Filip, C.; Griffin, R. G., 3D TEDOR NMR experiments for the simultaneous measurement of multiple carbon-nitrogen distances in uniformly (¹³C,¹⁵N)-labeled solids. *J Am Chem Soc* **2002**, *124* (36), 10728-42.

- (16) Hing, A. W.; Vega, S.; Schaefer, J., Transferred-Echo Double-Resonance Nmr. *Journal of Magnetic Resonance* **1992**, *96* (1), 205-209.
- (17) Ma, C.; Polishchuk, A. L.; Ohigashi, Y.; Stouffer, A. L.; Schon, A.; Magavern, E.; Jing, X.; Lear, J. D.; Freire, E.; Lamb, R. A.; DeGrado, W. F.; Pinto, L. H., Identification of the functional core of the influenza A virus A/M2 proton-selective ion channel. *Proc Natl Acad Sci U S A* **2009**, *106* (30), 12283-8.
- (18) Holsinger, L. J.; Nichani, D.; Pinto, L. H.; Lamb, R. A., Influenza A virus M2 ion channel protein: a structure-function analysis. *J Virol* **1994**, *68* (3), 1551-63.
- (19) Hu, J.; Fu, R. Q.; Cross, T. A., The chemical and dynamical influence of the anti-viral drug amantadine on the M-2 proton channel transmembrane domain. *Biophysical Journal* **2007**, *93* (1), 276-283.
- (20) Schnell, J.; Chou, J., Structure and mechanism of the M2 proton channel of influenza A virus. *Nature* **2008**, *451* (7178), 591-595.
- (21) Stouffer, A. L.; Acharya, R.; Salom, D.; Levine, A. S.; Di Costanzo, L.; Soto, C. S.; Tereshko, V.; Nanda, V.; Stayrook, S.; DeGrado, W. F., Structural basis for the function and inhibition of an influenza virus proton channel. *Nature* **2008**, *451* (7178), 596-9.
- (22) Cady, S. D.; Schmidt-Rohr, K.; Wang, J.; Soto, C. S.; DeGrado, W. F.; Hong, M., Structure of the amantadine binding site of influenza M2 proton channels in lipid bilayers. *Nature* **2010**, *463* (7281), 689.
- (23) Cady, S.; Wang, T.; Hong, M., Membrane-dependent effects of a cytoplasmic helix on the structure and drug binding of the influenza virus M2 protein. *J Am Chem Soc* **2011**, *133* (30), 11572-9.
- (24) Pielak, R. M.; Schnell, J. R.; Chou, J. J., Mechanism of drug inhibition and drug resistance of influenza A M2 channel. *Proc Natl Acad Sci U S A* **2009**, *106* (18), 7379-84.
- (25) Jing, X.; Ma, C.; Ohigashi, Y.; Oliveira, F. A.; Jardetzky, T. S.; Pinto, L. H.; Lamb, R. A., Functional studies indicate amantadine binds to the pore of the influenza A virus M2 proton-selective ion channel. *Proc Natl Acad Sci U S A* **2008**, *105* (31), 10967-72.
- (26) Ohigashi, Y.; Ma, C.; Jing, X.; Balannick, V.; Pinto, L. H.; Lamb, R. A., An amantadine-sensitive chimeric BM2 ion channel of influenza B virus has implications for the mechanism of drug inhibition. *Proc Natl Acad Sci U S A* **2009**, *106* (44), 18775-9.
- (27) Pielak, R. M.; Oxenoid, K.; Chou, J. J., Structural Investigation of Rimantadine Inhibition of the AM2-BM2 Chimera Channel of Influenza Viruses. *Structure* **2011**, *19* (11), 1655-1663.
- (28) Andreas, L. B.; Eddy, M. T.; Pielak, R. M.; Chou, J.; Griffin, R. G., Magic Angle Spinning NMR Investigation of Influenza A M2(18-60): Support for an Allosteric Mechanism of Inhibition. *Journal of the American Chemical Society* **2010**, *132* (32), 10958-10960.
- (29) Hu, K.-N.; Yu, H.-h.; Swager, T. M.; Griffin, R. G., Dynamic nuclear polarization with biradicals. *J. Am. Chem. Soc.* **2004**, *126* (35), 10844-10845.
- (30) Song, C.; Hu, K. N.; Joo, C. G.; Swager, T. M.; Griffin, R. G., TOTAPOL: a biradical polarizing agent for dynamic nuclear polarization experiments in aqueous media. *J Am Chem Soc* **2006**, *128* (35), 11385-90.
- (31) Wollan, D. S., Dynamic Nuclear Polarization with an Inhomogeneously Broadened ESR Line. I Theory. *Phys. Rev. B* **1976**, *13*, 3671-3685.
- (32) Rosay, M.; Lansing, J. C.; Haddad, K. C.; Bachovchin, W. W.; Herzfeld, J.; Temkin, R. J.; Griffin, R. G., High Frequency Dynamic Nuclear Polarization in MAS Spectra of Membrane and Soluble Proteins. *J. Am. Chem. Soc.* **2003**, *125*, 13626-27.
- (33) Bajaj, V. S.; Hornstein, M. K.; Kreisler, K. E.; Sirigiri, J. R.; Woskov, P. P.; Mak, M.; Herzfeld, J.; Temkin, R. J.; Griffin, R. G., 250 GHz Gyrotron for Dynamic Nuclear Polarization in Biological Solid State NMR. *J. Mag. Res.* **2007**, *190*, 86-114.
- (34) Joye, C. D.; Griffin, R. G.; Hornstein, M. K.; Hu, K. N.; Kreisler, K. E.; Rosay, M.; Shapiro, M. A.; Sirigiri, J. R.; Temkin, R. J.; Woskov, P. P., Operational Characteristics of a 14-

- W 140-GHz Gyrotron for Dynamic Nuclear Polarization. *IEEE Trans Plasma Sci IEEE Nucl Plasma Sci Soc* **2006**, *34* (3), 518-523.
- (35) Rosay, M.; Tometich, L.; Pawsey, S.; Bader, R.; Schauwecker, R.; Blank, M.; Borchard, P. M.; Cauffman, S. R.; Felch, K. L.; Weber, R. T., Solid-state dynamic nuclear polarization at 263 GHz: spectrometer design and experimental results. *Phys. Chem. Chem. Phys.* **2010**, *12* (22), 5850-5860.
- (36) Morcombe, C. R.; Zilm, K. W., Chemical shift referencing in MAS solid state NMR. *J Magn Reson* **2003**, *162* (2), 479-86.
- (37) Markley, J. L.; Bax, A.; Arata, Y.; Hilbers, C. W.; Kaptein, R.; Sykes, B. D.; Wright, P. E.; Wuthrich, K., Recommendations for the presentation of NMR structures of proteins and nucleic acids. IUPAC-IUBMB-IUPAB Inter-Union Task Group on the Standardization of Data Bases of Protein and Nucleic Acid Structures Determined by NMR Spectroscopy. *J Biomol NMR* **1998**, *12* (1), 1-23.
- (38) Harris, R. K.; Becker, E. D.; Cabral de Menezes, S. M.; Goodfellow, R.; Granger, P., NMR Nomenclature: Nuclear Spin Properties and Conventions for Chemical Shifts. IUPAC Recommendations 2001. *Solid State Nucl Magn Reson* **2002**, *22* (4), 458-483.
- (39) Delaglio, F.; Grzesiek, S.; Vuister, G. W.; Zhu, G.; Pfeifer, J.; Bax, A., NMRPipe: a multidimensional spectral processing system based on UNIX pipes. *J Biomol NMR* **1995**, *6* (3), 277-93.
- (40) Bennett, A. E.; Rienstra, C. M.; Auger, M.; Lakshmi, K. V.; Griffin, R. G., Heteronuclear Decoupling in Rotating Solids. *Journal of Chemical Physics* **1995**, *103* (16), 6951-6958.
- (41) Szeverenyi, N. M.; Sullivan, M. J.; Maciel, G. E., Observation of Spin Exchange by Two-Dimensional Fourier Transform ¹³C Cross Polarization-Magic-Angle-Spinning. *J Mag Res* **1982**, *47*, 462-475.
- (42) Szeverenyi, N. M.; Bax, A.; Maciel, G. E., Proton-Exchange Rates in Solid Tropolone As Measured via ¹³C CP/MAS NMR. *J Am Chem Soc* **1983**, *105* (9), 2579-82.
- (43) Ulrich, E. L.; Akutsu, H.; Doreleijers, J. F.; Harano, Y.; Ioannidis, Y. E.; Lin, J.; Livny, M.; Mading, S.; Maziuk, D.; Miller, Z.; Nakatani, E.; Schulte, C. F.; Tolmie, D. E.; Kent Wenger, R.; Yao, H.; Markley, J. L., BioMagResBank. *Nucleic Acids Res* **2008**, *36* (Database issue), D402-8.
- (44) Maus, D. C.; CopiÈ, V.; Sun, B.; Griffiths, J. M.; Griffin, R. G.; Luo, S.; Schrock, R. R.; Liu, A. H.; Seidel, S. W.; Davis, W. M., A Solid-State NMR Study of Tungsten Methyl Group Dynamics in [W (5-C5Me5) Me4][PF6]. *Journal of the American Chemical Society* **1996**, *118* (24), 5665-5671.
- (45) Andreas, L. B.; Eddy, M. T.; Chou, J. J.; Griffin, R. G., Magic-Angle-Spinning NMR of the Drug Resistant S31N M2 Proton Transporter from Influenza A. *Journal of the American Chemical Society* **2012**, *134* (17), 7215-7218.
- (46) Chen, L.; Kaiser, J. M.; Lai, J.; Polenova, T.; Yang, J.; Rienstra, C. M.; Mueller, L. J., J-based 2D homonuclear and heteronuclear correlation in solid-state proteins. *Magnetic Resonance in Chemistry* **2007**, *45* (S1), S84-S92.
- (47) Schwieters, C. D.; Kuszewski, J. J.; Tjandra, N.; Clore, G. M., The Xplor-NIH NMR molecular structure determination package. *Journal of Magnetic Resonance* **2003**, *160* (1), 65-73.
- (48) Cady, S. D.; Wang, J.; Wu, Y.; DeGrado, W. F.; Hong, M., Specific binding of adamantane drugs and direction of their polar amines in the pore of the influenza M2 transmembrane domain in lipid bilayers and dodecylphosphocholine micelles determined by NMR spectroscopy. *J Am Chem Soc* **2011**, *133* (12), 4274-84.
- (49) Yi, M.; Cross, T. A.; Zhou, H. X., Conformational heterogeneity of the M2 proton channel and a structural model for channel activation. *Proc Natl Acad Sci U S A* **2009**, *106* (32), 13311-6.
- (50) Wang, J.; Ma, C.; Fiorin, G.; Carnevale, V.; Wang, T.; Hu, F.; Lamb, R. A.; Pinto, L. H.; Hong, M.; Klein, M. L.; DeGrado, W. F., Molecular dynamics simulation directed rational design

of inhibitors targeting drug-resistant mutants of influenza A virus M2. *J Am Chem Soc* **2011**, *133* (32), 12834-41.

(51) Leonov, H.; Astrahan, P.; Krugliak, M.; Arkin, I. T., How do aminoadamantanes block the influenza M2 channel, and how does resistance develop? *J Am Chem Soc* **2011**, *133* (25), 9903-11.

Chapter 4: MAS NMR of the Drug Resistant S31N M2 Proton Transporter from Influenza A

Adapted from Andreas, LB; Eddy, MT; Chou, JJ; Griffin, RG; J. Am. Chem. Soc., 2013, 134(17):7215-8.

4.1 Introduction

The M2 proton transporter from Influenza A conducts at low pH and is the target of aminoadamantyl inhibitors rimantadine (Rmt) and amantadine (Amt) whose activity is believed to arise from binding to the pore of the channel.¹⁻⁶ The inhibitors reduce the rate of proton conduction, thereby interfering with the unpacking of the viral particle in the endosomal pathway for infection. However, a single mutation from serine 31 to asparagine (S31N) renders these inhibitors ineffective for many current influenza A infections⁷ and therefore understanding the structure of the S31N mutant and the structural basis for resistance could guide the design of more potent inhibitors that would target current flu variants. In addition, since the S31N mutation is far more prevalent than the commonly studied Udorn (WT) strain of M2, the structure of S31N M2 is more relevant for the design of novel inhibitors that might exploit a new mechanism.

A segment of the protein comprising residues roughly 18-60 of the full 97 amino acid sequence has been shown to retain the critical function of proton conduction and inhibition by Amt and Rmt.^{8,9} Several structures and structural models of WT M2 have been reported using solution NMR,¹⁰ oriented sample NMR,⁵ crystallography,⁴ and solid state NMR that combined oriented sample constraints¹¹ and magic angle spinning (MAS).¹² Yet there have been few investigations of the S31N mutant. A solution NMR structure of S31N M2 has been reported,⁹ however, it was solved using a detergent and buffer system that did not support Rmt binding in the pore of WT M2. Thus, it appears that M2 structure and inhibition are sensitive to membrane mimetic environment. Therefore, an investigation of the S31N variant in fully hydrated lipid bilayers could reveal new functionally relevant structural features.

Additionally, the S31N mutant can be used as a negative control for experiments that investigate the effects of drug binding. It was previously shown that large and widespread chemical shift changes occur upon binding of Rmt to WT M2₁₈₋₆₀¹³ and similar changes occur in a shorter construct comprising residues 22-46.¹⁴ Since S31N M2₁₈₋₆₀ is drug resistant, chemical shift

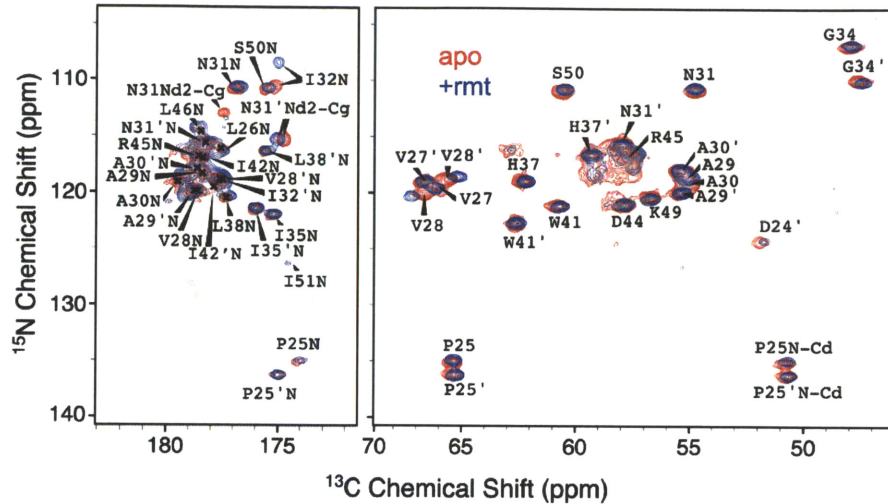


Figure 4.1. ZF-TEDOR spectra of S31N M₂₁₈₋₆₀ are shown in the presence (blue) and absence (red) of the inhibitor Rmt. Spectra were recorded at a ¹H frequency of 900 MHz and demonstrate ~0.7 ppm and ~0.5 ppm ¹⁵N and ¹³C backbone linewidths, respectively. Labels correspond to N-C α cross-peaks (right) and nitrogen i of N_i-C_{i-1} cross-peaks (left) unless otherwise indicated. The sample temperature was ~30 °C, the spinning frequency was 20 kHz, and the TEDOR mixing time was 1.2 ms.

changes due to nonspecific effects should remain upon addition of drug, and the functionally important chemical shift changes should be absent. Therefore, the S31N mutant can assist in differentiating between binding and non-specific hydrophobic effects that may be present due to a large excess of inhibitor used in the MAS NMR experiments.

4.2 Results and Discussion

Here we report the initial NMR spectra of S31N M₂₁₈₋₆₀ reconstituted into lipid bilayers, from which we derive interesting details of the channel structure. Spectra of S31N M₂₁₈₋₆₀ at 900 MHz (**Error! Reference source not found.**) exhibit high resolution of ~0.7 and 0.5 ppm for ¹⁵N and ¹³C backbone linewidths, respectively. This allowed all strong resonances in this ZF-TEDOR^{15, 16} spectrum to be assigned based on sequence information and sequential correlations in a 3D ¹⁵N-¹³C-¹³C chemical shift correlation experiment using ZF-TEDOR and RFDR^{17, 18} (**Figure 4.3** and **Figure 4.4**, assignments in **Table S4.2**). Full assignments were made for 14 of the 43 residues, and an additional 7 ¹⁵N assignments were made due to transamination of isoleucine and leucine residues such that these residues were ¹⁵N labeled despite addition of natural abundance amino acids prior to protein expression (details below). The ¹³C signal was suppressed for these residues.

A second set of resonances of comparable amplitude (denoted with a prime in the figures) was assigned for each residue in the transmembrane region of the peptide between residues 25 and 42, similar to what was observed for WT M2.¹³

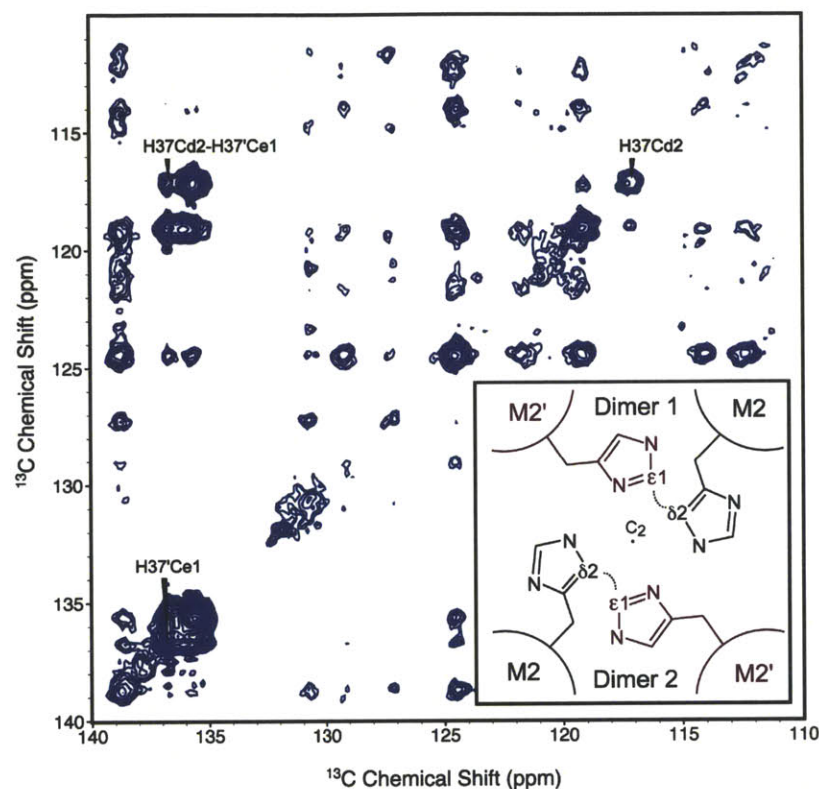


Figure 4.2. An aromatic-aromatic ^{13}C correlation spectrum using 400 ms of proton driven spin diffusion mixing shows cross-peaks between the two sets of chemical shifts. The sample temperature was $\sim 10^\circ\text{C}$ and the spinning frequency was 14.287 kHz. The inset shows an illustration of a C_2 symmetric channel composed of a dimer of dimers viewed along the C_2 axis with the four alpha helices at the corners. The observed intermolecular correlation between carbons $\delta 2$ and $\epsilon 1'$ is also depicted in the inset.

This extensive doubling of cross-peaks suggests that the channel assembles as a C_2 symmetric tetramer in a dimer of dimers configuration, rather than a C_4 symmetric tetramer. The C_2 symmetry was previously proposed as the best explanation to WT spectra that also demonstrated similar intensities between the two sets of peaks.¹³ Nevertheless, there remained the possibility that the doubled peaks were caused by two different populations of protein that happened to have similar intensity. We exclude the possibility of multiple separate tetramer conformations by showing a cross-peak between the two sets of chemical shifts in a 400 ms PDS spectrum recorded at 750 MHz (**Figure 4.2**, **Figure 4.10**). The cross-peak labeled in the figure is between H37 C $\delta 2$ and H37' C $\epsilon 1$. Since H37 is a pore-facing residue known to play a critical role in ^1H selectivity and the pH dependence of ^1H conduction,^{19, 20} we conclude that this cross-peak is within a single tetramer, and not a possible tetramer-tetramer contact. In other parts of the

molecule, we do not see analogous cross-peaks, indicating that the two sets of shifts do not exchange on this timescale. We therefore conclude that in lipid bilayers, as opposed to detergent, the protein is resolved as a dimer of dimers with C_2 symmetry on the NMR timescale.

Unlike WT M2, only relatively minor changes in chemical shift (<2 ppm ^{15}N , <1 ppm ^{13}C) are observed with addition of a four-fold molar excess of the inhibitor Rmt. Notably, the ~ 7 ppm change in the ^{15}N shift of residue 31 and the ~ 3.5 ppm change in the shift for H37 $\text{C}\alpha$ are absent in S31N M2. The largest chemical shift changes occur in lipid facing residues such as V28 $\text{C}\alpha$ and I32 ^{15}N that also lie near the lipid head groups where the amphiphilic Rmt is expected to partition. Since the inhibitor partitions strongly to membranes,²¹ it occupies $\sim 7\%$ of the total membrane components by mass (~ 35 mol %). Therefore the shift changes can be attributed to nonspecific differences in the membrane composition upon addition of drug.

The program TALOS+ was used to predict the backbone torsion angles ϕ and ψ for both sets of chemical shifts and the results are listed in Table S4.1 of the supporting information. Since TALOS+ makes predictions based on sequential amino acid triplets, the current labeling restricted the analysis to the longest stretch of continuously labeled and assigned residues 27-31, VVAAN. As expected, the results show an alpha helical conformation. More interestingly, the two sets of chemical shifts are separate enough to show a difference in predicted torsion angles. The predicted values of ϕ, ψ differ by 13, 14 degrees, respectively for the key resistance residue N31 suggesting that the symmetrically inequivalent helices may have significantly different secondary structure.

The widespread cross-peak doubling and C_2 structure is thus far uniquely resolved for the 18-60 construct in lipid bilayers. In solution, only a single set of resonances was observed, indicating that if two conformations exist, they are exchanging faster than the nmr timescale. This resulted in C_4 symmetric structural constraints.⁹ Crystal structures of WT M2₂₂₋₄₆ showed some conformational heterogeneity, but a C_2 axis was apparently not evident, as channel models based on the crystal structure were constructed with C_4 symmetry.⁴ Peak doubling was not resolved by MAS NMR of the shorter construct of WT M2₂₂₋₄₆,¹² however, doubling may be present beneath the significantly broader line widths that were reported for the 22-46 construct. The dimer of dimers topology is in qualitative agreement with a previous MAS NMR study that proposed an imidazole-imidazolium dimer in M2₂₂₋₄₆,¹⁹ implying C_2 symmetry at H37. However, at pH 7.8, we observe neutral His (based on sidechain nitrogen shifts near 250 ppm, **Figure 4.5**) for both sets of chemical shifts, in contrast with the imidazole-imidazolium dimers that were reported to form when the tetramer is doubly protonated with a pKa of 8.2. Nevertheless, it is possible that the

previously reported dimerization and the widespread doubling of peaks are manifestations of the same underlying structural feature and that the pKa is sensitive to the sample differences.

Existing evidence points to several possible modes by which the S31N mutation confers drug resistance. The larger sidechain of asparagine might prevent the drug from binding by reducing the space in the pore, and this mode of resistance was supported by surface plasmon resonance measurements in which binding was not observed for the S31N mutant.^{22, 23} On the other hand, structures solved by solution NMR show residue 31 in the helix-helix interface,^{3, 9, 10} suggesting that the mutation might severely weaken channel-drug interactions by altering helix packing. The widespread doubling of resonances, and the 13°,14° difference in the predicted value of ϕ, ψ for N31 suggest that detailed understanding of the drug resistant structure may include twofold channel symmetry.

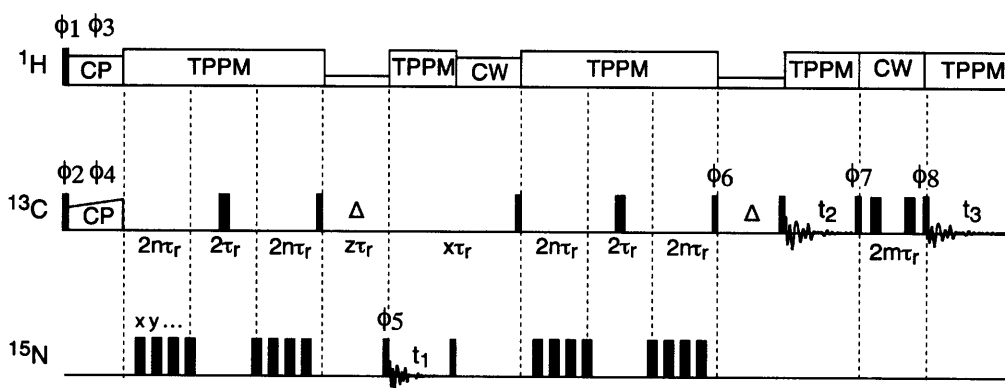


Figure 4.3. 3D ZF-TEDOR-RFDR pulse sequence used for assignments. Narrow and broad bars represent pulses of 90 and 180 degree nutation respectively. Vertical dashed lines indicate rotor synchronization. The parameter n determines the total TEDOR mixing time, and the parameter m likewise determines the RFDR mixing, by extension of the respective pulse trains. The phase cycle was $\phi_1=(16 \times 1)(16 \times 3)$, $\phi_2=(16 \times 4)(16 \times 2)$, $\phi_3=2$, $\phi_4=1$, $\phi_5=13$, $\phi_6=2244$, $\phi_7=1133$, $\phi_8=1111222233334444$, $\phi_{rec}=4242\ 1313\ 2424\ 3131\ 2424\ 3131\ 4242\ 1313$. The REDOR mixing in ZF-TEDOR used xy -4, and the RFDR mixing used xy -16 phase alternation. All other pulses had a phase of 1. The phases of the pulses after t_1 evolution and before t_2 evolution were incremented for phase sensitive detection. Due to time constraints, only the first 4 values of the phase cycle were used.

Chemical shift assignments were achieved via 3D ^{15}N - ^{13}C - ^{13}C spectra using one bond ^{15}N - ^{13}C ZF-TEDOR mixing followed by ^{13}C - ^{13}C RFDR mixing, similar to previously described 2D experiments²⁴ and the commonly used N-C cross-polarization (DCP) based experiments.²⁵⁻²⁸ The sequence is depicted in **Figure 4.3** and allows both the NCOCX and NCACX connectivity experiments to be efficiently acquired in a single spectrum (**Figure 4.4**). Efficient NCACX and NC δ CX transfers are demonstrated for Pro, a residue that is often difficult to observe in DCP spectra due to weak H-N cross-polarization to the Pro nitrogen. The ZF-TEDOR transfer avoids

this problem because the experiment begins with an H-C cross-polarization step. In principle, this experiment should also provide assignment information originating from sidechain ^{15}N 's in residues such as histidine, tryptophan, lysine, and arginine. However, we found that these transfer efficiencies were reduced and their detection would have required significantly longer experiment times. In order to avoid excessive spectral widths in the indirect ^{13}C dimension, we folded the carbonyl resonances onto the spinning side band just higher than the aliphatic resonances, by applying a dwell time matching the rotor period. A spinning frequency corresponding to ~ 90 ppm was useful for this reduction in the sweep width, and also avoids strong rotational resonance conditions.²⁹⁻³¹

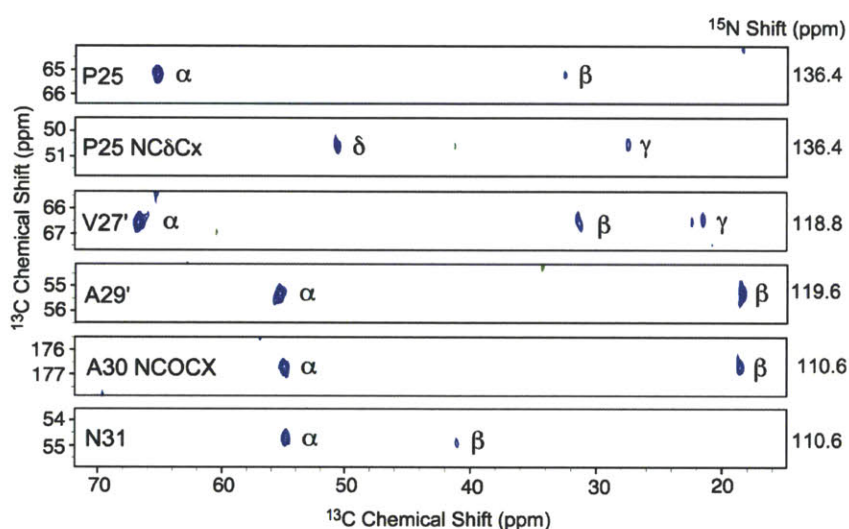


Figure 4.4. Slices are shown from the NCACX and NCOCX regions of a 3D ZF-TEDOR-RFDR spectrum used for sequential assignments. For P25, the NC δ transfer was also efficient (second panel). 1.2 ms of TEDOR mixing and 4.8 ms of RFDR mixing with 83 kHz pulses were used. The direct acquisition used a 6 μs dwell time and 3072 points (~ 18.4 ms), the indirect ^{13}C dimension was acquired with a 50 μs dwell time and 180 complex points (9 ms), and the ^{15}N dimension used a 150 μs dwell time and 74 complex points (11.1 ms). The carrier frequency was set to 100 ppm for ^{15}N , and 89 ppm for ^{13}C . The spectrum was acquired in ~ 5 days and provided useful NCACX and NCOCX connectivity information. The sample temperature was ~ 30 $^{\circ}\text{C}$, and the spinning frequency was 20 kHz.

4.3 Methods

M2₁₈₋₆₀ was prepared by over expression in E. Coli as described previously^{10, 13} with C19S and C50S mutations to prevent unwanted disulphide bond formation. The resulting sequence with the S31N mutation was RSNDSDDLPLV VAANIIGILH LILWILDRLF FKSIYRFFEH GLK. In order to simplify the spectra, residues ILFY were unlabeled by addition of the natural abundance amino

acids to the culture approximately 1 hour prior to induction. Bilayer protein samples were prepared by adding 1,2-di-O-phytanoyl-*sn*-glycero-3-phosphocholine (DPhPC) lipid (Avanti) and lyophilized M2₁₈₋₆₀ at a lipid to protein ratio of 1:1 by weight (~6:1 by mol) both dissolved in denaturing buffer (6M guanidine, 40 mM phosphate, 30 mM glutamate, 3 mM sodium azide (Sigma-Aldrich), pH 7.8, >=33mg/mL OG detergent (Anatrace)). The resulting solution was dialyzed in a 3.5kD cutoff dialysis cassette (Thermo) against 1 L of sample buffer (40 mM phosphate, 30 mM glutamate, 3 mM sodium azide, pH 7.8) for 7 days with 2 dialysis buffer changes per day. A white precipitate was observed after approximately 24 hours. Solid membrane material was pelleted by centrifugation at ~100 000 x g. Samples with rmt had a four-fold molar excess added directly to the membrane pellet.

The NMR spectrum in **Figure 4.2** was recorded on a 750 MHz spectrometer courtesy of David Ruben and all other spectra were recorded using a Bruker 900 MHz spectrometer (Bruker Biospin). Each instrument employed a Bruker 3.2 mm HCN e-free probe. Referencing was performed using the chemical shifts of adamantane relative to DSS for ¹³C³² and the relative frequency ratios between DSS (¹³C) and liquid ammonia (¹⁵N)^{33,34} for ¹⁵N referencing. The sample temperature was estimated using the chemical shift of ⁷⁹Br in KBr to determine heating due to sample spinning.³⁵ (See **Figure 4.6** for a comparison of spectra recorded at 10 and 30 °C, the temperatures used for PDS and assignment, respectively) Spectra were processed with NMRPipe³⁶ and displayed and assigned using Sparky (Goddard and Kneller, University of California, San Francisco).

4.4 Supporting Information

Residue	ϕ (°)	ψ (°)	SD ϕ (°)*	SD ψ (°)*
V28/V28'	-60/-61	-47/-41	6/6	8/9
A29/ A29'	-62/-62	-38/-43	5/9	9/10
A30/ A30'	-67/-63	-36/-37	11/8	6/8
N31/ N31'	-79/-66	-29/-43	15/20	19/10

Table S4.1. The ϕ and ψ torsion angles predicted by the program TALOS+ using chemical shifts from residues V27 to I32. A difference of 13 and 14° is predicted for ϕ and ψ , respectively at residue N31 due to the substantial peak doubling at this residue.

*The standard deviation among the 10 best matches as reported by TALOS+.

Table of Chemical Shifts

	N	C'	C α	C β	C γ , γ 1	C γ 2, C δ , δ 1	C δ 2	C ϵ , ϵ 1, ϵ 2	C ϵ 3	C ζ 2	C ζ 3	C η 2, N δ 1	N δ 2, ϵ , ϵ 1, ϵ 2, ζ
D24	x	174.2	x	x	x	-	-	-	-	-	-	-	-
D24'	124.2	175.0	52.0	41.9	179.2	-	-	-	-	-	-	-	-
D24	x	174.0	x	x	x	-	-	-	-	-	-	-	-
D24'	124.2	175.0	51.7	41.9	179.2	-	-	-	-	-	-	-	-
P25	135.2	177.7	65.3	32.7	27.5	50.7	-	-	-	-	-	-	-
P25'	136.2	177.5	65.3	32.6	27.5	50.6	-	-	-	-	-	-	-
P25	134.9	178.0	65.3	32.6	27.5	50.7	-	-	-	-	-	-	-
P25'	136.3	177.5	65.2	32.5	27.5	50.6	-	-	-	-	-	-	-
L26	116.0	-	-	-	-	-	-	-	-	-	-	-	-
L26'	116.2	-	-	-	-	-	-	-	-	-	-	-	-
L26	115.7	-	-	-	-	-	-	-	-	-	-	-	-
L26'	116.4	-	-	-	-	-	-	-	-	-	-	-	-
V27	119.3	178.6	66.1	31.8	23.1	21.6	-	-	-	-	-	-	-
V27'	119.1	177.7	66.6	31.5	22.4	21.5	-	-	-	-	-	-	-
V27	119.6	179.1	66.1	31.7	23.0	21.5	-	-	-	-	-	-	-
V27'	119.0	177.6	66.6	31.4	22.3	21.5	-	-	-	-	-	-	-
V28	120.0	178.3	66.7	31.3	22.5	21.8	-	-	-	-	-	-	-
V28'	118.8	178.7	65.6	31.6	22.5	21.4	-	-	-	-	-	-	-
V28	120.3	178.0	67.2	31.2	22.5	22.4	-	-	-	-	-	-	-
V28'	118.6	178.7	65.2	31.5	22.3	21.5	-	-	-	-	-	-	-
A29	118.4	179.4	55.1	18.5	-	-	-	-	-	-	-	-	-
A29'	119.9	178.6	55.4	18.4	-	-	-	-	-	-	-	-	-
A29	118.4	179.4	55.2	18.5	-	-	-	-	-	-	-	-	-
A29'	119.9	178.7	55.3	18.4	-	-	-	-	-	-	-	-	-
A30	119.1	177.0	55.0	18.6	-	-	-	-	-	-	-	-	-
A30'	117.9	178.3	55.4	18.7	-	-	-	-	-	-	-	-	-
A30	118.6	176.8	54.9	18.5	-	-	-	-	-	-	-	-	-
A30'	118.0	178.4	55.3	18.5	-	-	-	-	-	-	-	-	-
N31	110.8	175.1	54.7	40.6	177.5	-	-	-	-	-	-	-	113.0
N31'	115.6	177.5	58.0	40.0	174.8	-	-	-	-	-	-	-	115.3
N31	110.7	175.0	54.7	41.1	177.4	-	-	-	-	-	-	-	113.4
N31'	115.8	177.5	58.0	39.8	175.0	-	-	-	-	-	-	-	115.4
I32	110.5	-	-	-	-	-	-	-	-	-	-	-	-
I32'	118.9	-	-	-	-	-	-	-	-	-	-	-	-
I32	108.4	-	-	-	-	-	-	-	-	-	-	-	-
I32'	118.8	-	-	-	-	-	-	-	-	-	-	-	-
G34	106.8	175.2	48.0	-	-	-	-	-	-	-	-	-	-
G34'	109.9	176.0	47.6	-	-	-	-	-	-	-	-	-	-
G34	106.8	175.2	47.9	-	-	-	-	-	-	-	-	-	-
G34'	110.1	176.0	47.4	-	-	-	-	-	-	-	-	-	-
I35	122.0	-	-	-	-	-	-	-	-	-	-	-	-
I35'	121.4	-	-	-	-	-	-	-	-	-	-	-	-

	N	C'	C α	C β	C γ , γ 1	C γ 2, C δ , δ 1	C δ 2	C ϵ , ϵ 1, ϵ 2	C ϵ 3	C ζ 2	C ζ 3	C η 2, N δ 1	N δ 2, ϵ , ϵ 1, ϵ 2, ζ
I35	122.0	-	-	-	-	-	-	-	-	-	-	-	-
I35'	121.4	-	-	-	-	-	-	-	-	-	-	-	-
H37	118.9	177.3	62.3	31.3	135.8	-	117.1	135.7	-	-	-	251.6	167.1
H37'	116.6	175.6	59.3	30.3	136.3	-	119.2	136.9	-	-	-	251.0	173.5
H37	119.0	177.2	62.3	31.2	135.7	-	117.2	135.6	-	-	-	251.4	167.1
H37'	116.6	175.4	59.2	30.1	136.2	-	119.1	136.8	-	-	-	251.1	173.6
L38	120.5	-	-	-	-	-	-	-	-	-	-	-	-
L38'	116.4	-	-	-	-	-	-	-	-	-	-	-	-
L38	120.1	-	-	-	-	-	-	-	-	-	-	-	-
L38'	116.4	-	-	-	-	-	-	-	-	-	-	-	-
W41	121.1	178.6	60.7	28.2	111.8	125.1	129.3	138.7	119.7	114.0	121.7	124.4	128.9
W41'	122.7	177.8	62.6	27.6	111.1	127.3	130.9	138.8	121.0	114.9	120.9	123.8	129.9
W41	121.2	178.1	60.6	28.2	112.1	124.6	129.1	138.8	119.6	114.1	121.8	124.5	128.7
W41'	122.6	177.5	62.6	27.4	111.3	127.3	130.7	138.9	121.2	114.9	120.3	123.6	129.8
I42	116.9	-	-	-	-	-	-	-	-	-	-	-	-
I42'	119.6	-	-	-	-	-	-	-	-	-	-	-	-
I42	116.7	-	-	-	-	-	-	-	-	-	-	-	-
I42'	119.4	-	-	-	-	-	-	-	-	-	-	-	-
D44	121.0	178.5	57.9	42.8	180.2	-	-	-	-	-	-	-	-
D44	121.0	178.6	57.8	42.7	180.3	-	-	-	-	-	-	-	-
R45	116.8	178.5	57.8	29.6	25.9	42.7	-	-	-	-	-	-	84.5
R45	116.4	178.6	57.4	29.3	25.3	42.2	-	-	-	-	-	-	84.2
L46	114.6	-	-	-	-	-	-	-	-	-	-	-	-
L46	114.2	-	-	-	-	-	-	-	-	-	-	-	-
K49	120.3	175.7	56.8	30.4	25.2	29.3	-	42.5	-	-	-	-	32.3
K49	120.5	175.5	56.7	30.3	25.1	29.2	-	42.3	-	-	-	-	32.4
S50	110.9	174.5	60.6	66.9	-	-	-	-	-	-	-	-	-
S50	110.7	174.6	60.5	66.4	-	-	-	-	-	-	-	-	-
I51	126.1	-	-	-	-	-	-	-	-	-	-	-	-
I51	126.4	-	-	-	-	-	-	-	-	-	-	-	-

Table S4.2. Chemical shifts (ppm) of M2 S31N₁₈₋₆₀ in the presence (blue) and absence (red) of the inhibitor rimantadine. A second set of chemical shifts is observed between residue 25 and 42 as indicated by a prime. Missing assignments are marked by an (x), and those that are not expected (not labeled or not existent in the sequence) are marked with a (-). Assignments are missing for the side chain of R45 beyond Ne.

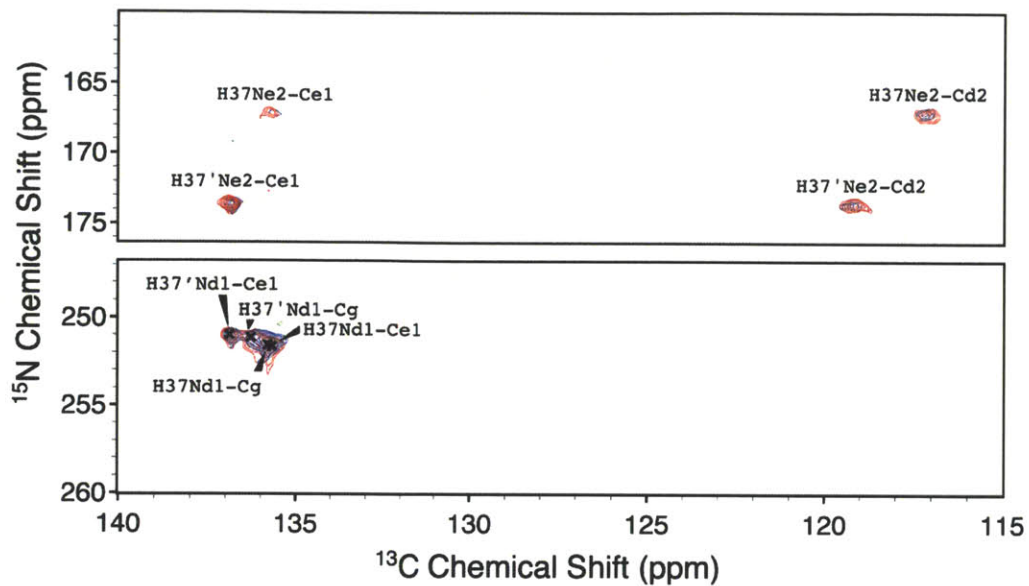


Figure 4.5. Histidine resonances are shown from the 1.2 ms ZF-TEDOR spectrum of **Figure 4.1**. The sample was S31N M2₁₈₋₆₀ in DPhPC bilayers both in the presence (blue) and absence (red) of rimantadine at pH 7.8. For both sets of chemical shifts, a deprotonated N δ 1 resonance is observed near 250 ppm, while the N ϵ 2 resonance is observed near 170 ppm and therefore protonated. This indicates that both sets of chemical shifts correspond to imidazole sidechains that are neutral and in the τ tautomeric state.

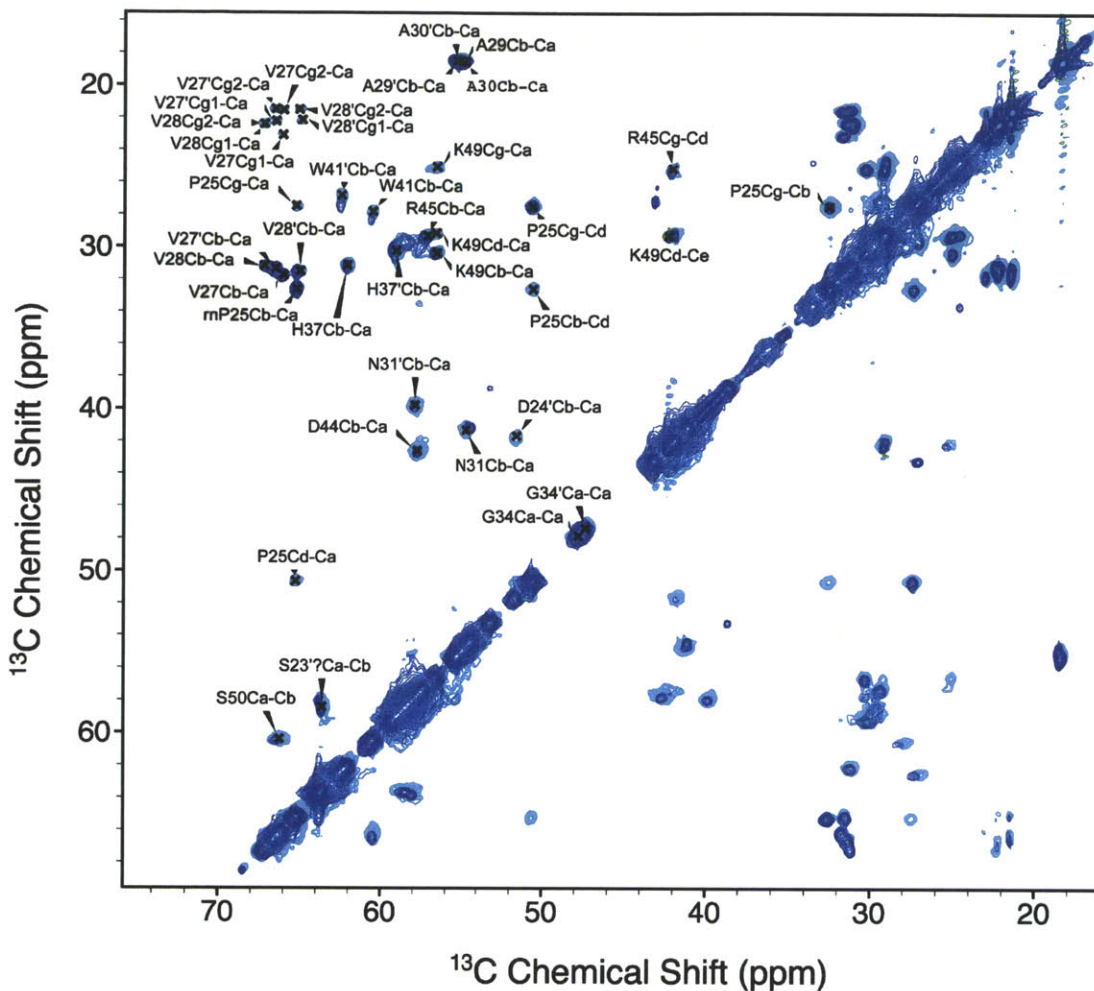


Figure 4.6. The effect of temperature changes on the chemical shift is investigated in overlaid ^{13}C - ^{13}C correlation spectra at two different temperatures. A 25 ms PDS spectrum (light blue) was collected at 10 °C and a field corresponding to a 750 MHz ^1H frequency and 14.287 kHz MAS. A 1.6 ms RFDR spectrum (dark blue) was collected at 30 °C and a field corresponding to 900 MHz ^1H frequency and 20 kHz MAS. No significant differences in chemical shift are detected except for a ~ 0.5 ppm (~ 100 Hz) shift in the C β resonances of W41. Since W41C β is only 1 to 2 kHz from a 1 bond rotational resonance condition to W41C γ in these spectra, but on opposite sides of the condition, the discrepancy may be explained by the effect of rotational resonance³⁷.

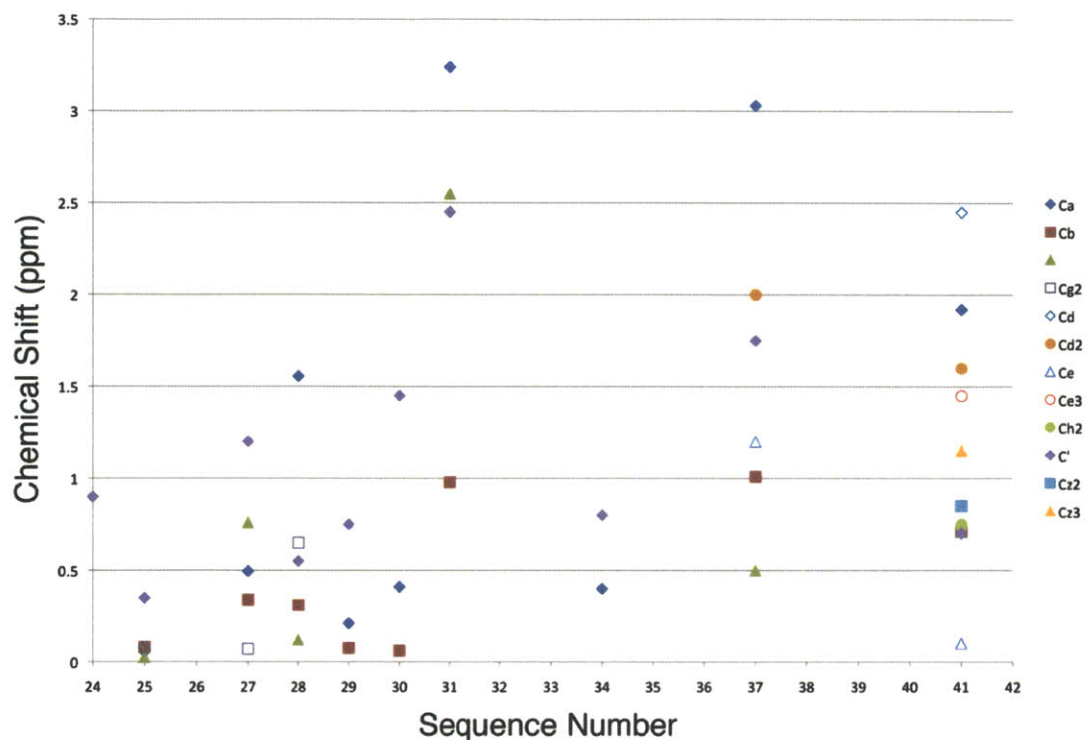


Figure 4.7. Peak doubling, $|\delta_{\text{prime}} - \delta|$ in ppm, is displayed as a function of residue number for ^{13}C resonances of WT M2₁₈₋₆₀. The average value between the drug bound and apo samples is displayed.

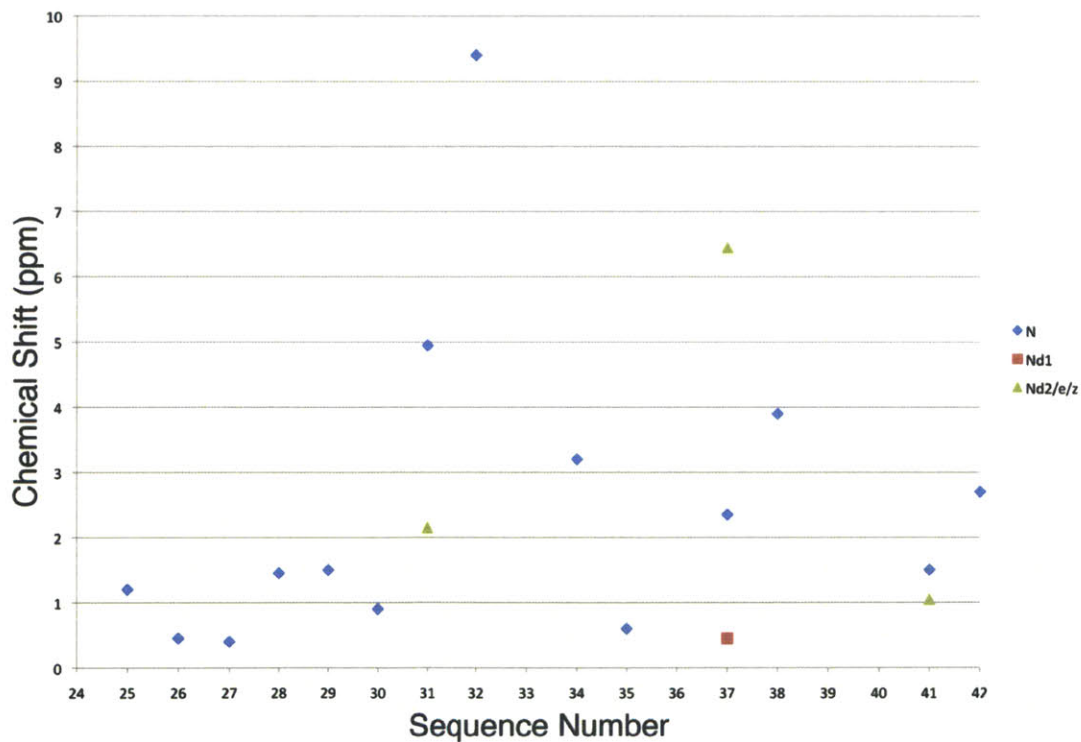


Figure 4.8. Peak doubling, $|\delta_{\text{prime}} - \delta|$ in ppm, is displayed as a function of residue number for ^{15}N resonances of WT M2₁₈₋₆₀. The average value between the drug bound and apo samples is displayed.

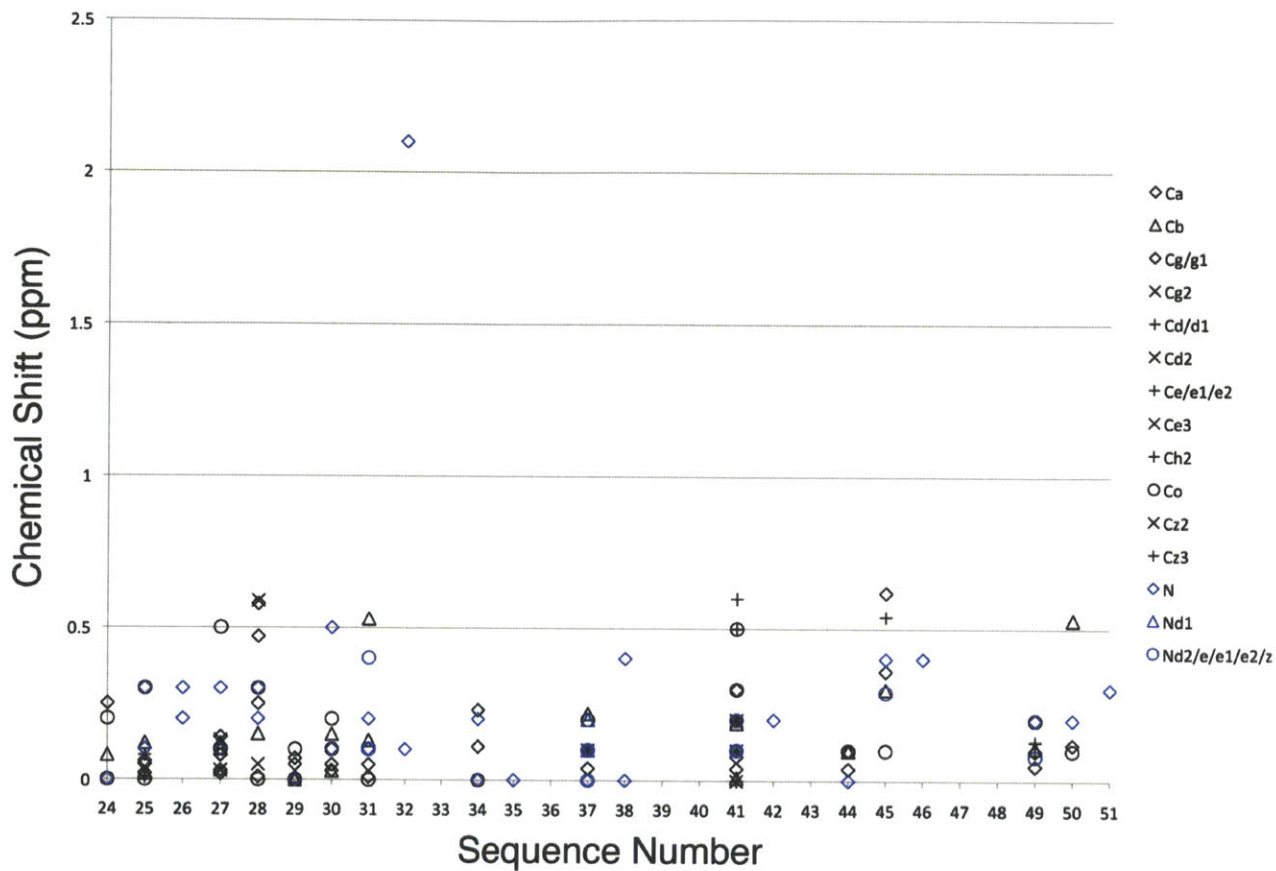


Figure 4.9. Chemical shift changes with addition of the inhibitor rimantadine are plotted against residue number for the S31N mutant of M2₁₈₋₆₀. Both sets of chemical shifts are displayed on the same chart in order to display the maximum changes in chemical shift. For example, the ¹⁵N of I32 shifts by 2.1 ppm for one set, and 0.1 ppm for the other—an average of only 1.1 ppm.

inequivalent helices. The predicted TALOS+ geometry of the two helices is also found to be distinct, particularly for the resistance residue N31. These structural features observed in lipid bilayers provide clues to the mechanism of resistance, and further structural investigation of drug resistant M2 could provide a starting point for the design of more potent or novel inhibitors.

Acknowledgement.

This work was supported by grants EB-001960 and EB-002026. We thank Rafal Pielak and Marcelo Berardi for thoughtful discussions.

4.6 References

- (1) Cady, S. D.; Schmidt-Rohr, K.; Wang, J.; Soto, C. S.; DeGrado, W. F.; Hong, M., Structure of the amantadine binding site of influenza M2 proton channels in lipid bilayers. *Nature* **2010**, *463* (7281), 689.
- (2) Jing, X.; Ma, C.; Ohigashi, Y.; Oliveira, F. A.; Jardetzky, T. S.; Pinto, L. H.; Lamb, R. A., Functional studies indicate amantadine binds to the pore of the influenza A virus M2 proton-selective ion channel. *Proc Natl Acad Sci U S A* **2008**, *105* (31), 10967-72.
- (3) Pielak, R. M.; Oxenoid, K.; Chou, J. J., Structural Investigation of Rimantadine Inhibition of the AM2-BM2 Chimera Channel of Influenza Viruses. *Structure* **2011**, *19* (11), 1655-63.
- (4) Stouffer, A. L.; Acharya, R.; Salom, D.; Levine, A. S.; Di Costanzo, L.; Soto, C. S.; Tereshko, V.; Nanda, V.; Stayrook, S.; DeGrado, W. F., Structural basis for the function and inhibition of an influenza virus proton channel. *Nature* **2008**, *451* (7178), 596-9.
- (5) Sharma, M.; Yi, M.; Dong, H.; Qin, H.; Peterson, E.; Busath, D. D.; Zhou, H. X.; Cross, T. A., Insight into the mechanism of the influenza A proton channel from a structure in a lipid bilayer. *Science* **2010**, *330* (6003), 509-12.
- (6) Yi, M.; Cross, T. A.; Zhou, H. X., A secondary gate as a mechanism for inhibition of the M2 proton channel by amantadine. *Journal of Physical Chemistry B* **2008**, *112* (27), 7977-7979.
- (7) Bright, R. A.; Shay, D. K.; Shu, B.; Cox, N. J.; Klimov, A. I., Adamantane resistance among influenza A viruses isolated early during the 2005-2006 influenza season in the United States. *JAMA* **2006**, *295* (8), 891-4.
- (8) Ma, C.; Polishchuk, A. L.; Ohigashi, Y.; Stouffer, A. L.; Schon, A.; Magavern, E.; Jing, X.; Lear, J. D.; Freire, E.; Lamb, R. A.; DeGrado, W. F.; Pinto, L. H., Identification of the functional core of the influenza A virus A/M2 proton-selective ion channel. *Proc Natl Acad Sci U S A* **2009**, *106* (30), 12283-8.
- (9) Pielak, R. M.; Schnell, J. R.; Chou, J. J., Mechanism of drug inhibition and drug resistance of influenza A M2 channel. *Proc Natl Acad Sci U S A* **2009**, *106* (18), 7379-84.
- (10) Schnell, J.; Chou, J., Structure and mechanism of the M2 proton channel of influenza A virus. *Nature* **2008**, *451* (7178), 591-595.
- (11) Hu, J.; Asbury, T.; Achuthan, S.; Li, C.; Bertram, R.; Quine, J. R.; Fu, R.; Cross, T. A., Backbone structure of the amantadine-blocked trans-membrane domain M2 proton channel from Influenza A virus. *Biophys J* **2007**, *92* (12), 4335-43.

- (12) Cady, S. D.; Schmidt-Rohr, K.; Wang, J.; Soto, C. S.; Degrado, W. F.; Hong, M., Structure of the amantadine binding site of influenza M2 proton channels in lipid bilayers. *Nature* **2009**, *463* (7281), 689-92.
- (13) Andreas, L. B.; Eddy, M. T.; Pielak, R. M.; Chou, J.; Griffin, R. G., Magic angle spinning NMR investigation of influenza A M2(18-60): support for an allosteric mechanism of inhibition. *J Am Chem Soc* **2010**, *132* (32), 10958-60.
- (14) Cady, S. D.; Mishanina, T. V.; Hong, M., Structure of amantadine-bound M2 transmembrane peptide of influenza A in lipid bilayers from magic-angle-spinning solid-state NMR: the role of Ser31 in amantadine binding. *J Mol Biol* **2009**, *385* (4), 1127-41.
- (15) Jaroniec, C. P.; Filip, C.; Griffin, R. G., 3D TEDOR NMR experiments for the simultaneous measurement of multiple carbon-nitrogen distances in uniformly (13)C,(15)N-labeled solids. *J Am Chem Soc* **2002**, *124* (36), 10728-42.
- (16) Hing, A. W.; Vega, S.; Schaefer, J., Transferred-Echo Double-Resonance Nmr. *Journal of Magnetic Resonance* **1992**, *96* (1), 205-209.
- (17) Bennett, A. E.; Ok, J. H.; Griffin, R. G.; Vega, S., Chemical-Shift Correlation Spectroscopy in Rotating Solids - Radio Frequency-Driven Dipolar Recoupling and Longitudinal Exchange. *Journal of Chemical Physics* **1992**, *96* (11), 8624-8627.
- (18) Bennett, A. E.; Rienstra, C. M.; Griffiths, J. M.; Zhen, W. G.; Lansbury, P. T.; Griffin, R. G., Homonuclear radio frequency-driven recoupling in rotating solids. *Journal of Chemical Physics* **1998**, *108* (22), 9463-9479.
- (19) Hu, J.; Fu, R.; Nishimura, K.; Zhang, L.; Zhou, H. X.; Busath, D. D.; Vijayvergiya, V.; Cross, T. A., Histidines, heart of the hydrogen ion channel from influenza A virus: Toward an understanding of conductance and proton selectivity. *Proceedings of the National Academy of Sciences of the United States of America* **2006**, *103* (18), 6865-6870.
- (20) Wang, C.; Lamb, R. A.; Pinto, L. H., Activation of the M2 ion channel of influenza virus: a role for the transmembrane domain histidine residue. *Biophys J* **1995**, *69* (4), 1363-71.
- (21) Wang, J. F.; Schnell, J. R.; Chou, J. J., Amantadine partition and localization in phospholipid membrane: a solution NMR study. *Biochemical and Biophysical Research Communications* **2004**, *324* (1), 212-217.
- (22) Astrahan, P.; Kass, I.; Cooper, M. A.; Arkin, I. T., A novel method of resistance for influenza against a channel-blocking antiviral drug. *Proteins-Structure Function and Bioinformatics* **2004**, *55* (2), 251-257.
- (23) Rosenberg, M. R.; Casarotto, M. G., Coexistence of two adamantane binding sites in the influenza A M2 ion channel. *Proceedings of the National Academy of Sciences of the United States of America* **2010**, *107* (31), 13866-13871.
- (24) Riedel, K.; Leppert, J.; Ohlenschlager, O.; Gorch, M.; Ramachandran, R., TEDOR with adiabatic inversion pulses: Resonance assignments of 13C/15N labelled RNAs. *J Biomol NMR* **2005**, *31* (1), 49-57.
- (25) Ladizhansky, V.; Jaroniec, C. P.; Diehl, A.; Oschkinat, H.; Griffin, R. G., Measurement of multiple psi torsion angles in uniformly C-13,N-15-labeled alpha-spectrin SH3 domain using 3D N-15-C-13-C-13-N-15 MAS dipolar-chemical shift correlation spectroscopy. *Journal of the American Chemical Society* **2003**, *125* (22), 6827-6833.
- (26) Rienstra, C. M.; Hohwy, M.; Mueller, L. J.; Jaroniec, C. P.; Reif, B.; Griffin, R. G., Determination of multiple torsion-angle constraints in U-(13)C,(15)N-labeled peptides: 3D (1)H-(15)N-(13)C-(1)H dipolar chemical shift NMR spectroscopy in rotating solids. *J Am Chem Soc* **2002**, *124* (40), 11908-22.
- (27) Sun, B. C.; Rienstra, C. M.; Costa, J. R.; Williamson, J. R.; Griffin, R. G., 3D 15N-13C-13C Chemical Shift Correlation Spectroscopy in Rotating Solids. *J Am Chem Soc* **1997**, *119* (36), 8540-8546.

- (28) Castellani, F.; van Rossum, B. J.; Diehl, A.; Rehbein, K.; Oschkinat, H., Determination of solid-state NMR structures of proteins by means of three-dimensional N-15-C-13-C-13 dipolar correlation spectroscopy and chemical shift analysis. *Biochemistry* **2003**, *42* (39), 11476-11483.
- (29) Raleigh, D. P.; Harbison, G. S.; Neiss, T. G.; Roberts, J. E.; Griffin, R. G., Homonuclear J-Couplings and Rotationally Induced Side-Band Enhancements in Nmr-Spectra of Rotating Solids. *Chemical Physics Letters* **1987**, *138* (4), 285-290.
- (30) Raleigh, D. P.; Levitt, M. H.; Griffin, R. G., Rotational Resonance in Solid-State Nmr. *Chemical Physics Letters* **1988**, *146* (1-2), 71-76.
- (31) Levitt, M. H.; Raleigh, D. P.; Cruzet, F.; Griffin, R. G., Theory and Simulations of Homonuclear Spin Pair Systems in Rotating Solids. *Journal of Chemical Physics* **1990**, *92* (11), 6347-6364.
- (32) Morcombe, C. R.; Zilm, K. W., Chemical shift referencing in MAS solid state NMR. *J Magn Reson* **2003**, *162* (2), 479-86.
- (33) Markley, J. L.; Bax, A.; Arata, Y.; Hilbers, C. W.; Kaptein, R.; Sykes, B. D.; Wright, P. E.; Wuthrich, K., Recommendations for the presentation of NMR structures of proteins and nucleic acids. IUPAC-IUBMB-IUPAB Inter-Union Task Group on the Standardization of Data Bases of Protein and Nucleic Acid Structures Determined by NMR Spectroscopy. *J Biomol NMR* **1998**, *12* (1), 1-23.
- (34) Harris, R. K.; Becker, E. D.; Cabral de Menezes, S. M.; Goodfellow, R.; Granger, P., NMR Nomenclature: Nuclear Spin Properties and Conventions for Chemical Shifts. IUPAC Recommendations 2001. *Solid State Nucl Magn Reson* **2002**, *22* (4), 458-483.
- (35) Thurber, K. R.; Tycko, R., Measurement of sample temperatures under magic-angle spinning from the chemical shift and spin-lattice relaxation rate of (79)Br in KBr powder. *Journal of Magnetic Resonance* **2009**, *196* (1), 84-87.
- (36) Delaglio, F.; Grzesiek, S.; Vuister, G. W.; Zhu, G.; Pfeifer, J.; Bax, A., NMRPipe: a multidimensional spectral processing system based on UNIX pipes. *J Biomol NMR* **1995**, *6* (3), 277-93.
- (37) Petkova, A. T.; Tycko, R., Rotational resonance in uniformly C-13-labeled solids: effects on high-resolution magic-angle spinning NMR spectra and applications in structural studies of biomolecular systems. *Journal of Magnetic Resonance* **2004**, *168* (1), 137-146.

Chapter 5: MAS NMR Structure of the Drug Resistant S31N M2 Proton Transporter from Influenza A in A Lipid Bilayer

To be submitted for publication: Loren B. Andreas, Marcel Reese, Matthew T. Eddy, Vladimir Gelev, Eric A. Miller, Lyndon Emsley, Guido Pintacuda, Robert G. Griffin

5.1 Introduction

Influenza A M2 is a 97 residue transmembrane protein that assembles as a tetramer and conducts protons at low pH in order to trigger membrane fusion in an endosome and unpacking of the viral genome. The N-terminus of the protein is positioned on the outside of infected cells, with at least the first 18 residues exposed.^{1, 2} A single pass alpha helix places the C-terminal domain on the cytoplasmic side of infected cells, a portion of which is responsible for stabilization of the protein.³

The M2 proton transporter is critical for viral replication, as evidenced by the therapeutic effect of aminoadamantyl inhibitors known to target M2 and to reduce proton conduction.³ There are now several excellent structures of the wild type (WT) protein in complex with aminoadamantyl inhibitors in the pore, placing the site of pharmacological binding between residues 27 and 34.⁴⁻⁸ However, resistance has developed in circulating strains of influenza, primarily due to a single point mutation S31N, which has precipitated a need for new inhibitors that target S31N M2 and motivated this report of the structure of S31N M2 in hydrated lipid bilayers.

Previous structural studies of M2 have been applied to several different constructs reconstituted in a variety of virus membrane mimetics. These constructs can be classified into three groups, the full length protein (FL), the conduction domain (CD) and the transmembrane domain (TM). The CD comprises approximately residues 18-60, which includes both the transmembrane residues (25-46) as well as an amphipathic helix (~47-59), which is known to stabilize the tetrameric assembly.^{3, 9} The CD lacks regions of the full-length protein that are thought to interact with other proteins of influenza, in particular M1. Transmembrane domain constructs from residue 22 to 46 contain a single membrane spanning helix that does not fully reproduce the conduction and drug inhibition of WT, but remains drug sensitive. Since the CD forms tetramers with conduction and drug sensitivity that is indistinguishable from the full protein, we have investigated a CD construct, M2₁₈₋₆₀.

Here we report the structure of the drug resistant S31N mutant of M2₁₈₋₆₀ in hydrated lipid bilayers. The structure shows marked deviation from 4-fold symmetry reported in previous

structures, instead revealing 2-fold symmetry in which 2 helices are displaced in the direction of the bilayer normal. The structure shows large differences in both helical packing and the orientation of side chains when compared with previously reported structures of WT M2 and from the two previously reported structures of S31N M2, which were solved in detergent micelles. The dimer of dimers structure reported here was determined in lipid bilayers that closely mimic the viral environment, and using a preparation that allowed pharmacological drug binding in WT M2,⁴ supporting the assertion that we have reconstituted a native state of the protein. The conduction pathway and the mechanism for drug resistance are discussed in light of the dimer of dimers structure.

5.2 Results and Discussion

A set of 70 intrahelical distance measurements, 41 interhelical distance measurements, 70 highly ambiguous distance measurements, and 92 TALOS restraints were used to calculate an atomic resolution structure of M2₁₈₋₆₀ with above 5 restraints per residue. The precision of the structure is characterized by an ensemble of 7 low energy structures with an RMSD of 0.8 for backbone heavy atoms, and 1.2 for all heavy atoms (*Figure 5.1*). The RMSD was calculated for the structured region of the protein, which extended from P25 to R45 and P25 to S50 for the two asymmetric helices, and corresponds to all observed residues. Part of the amphipathic helix was observed for only one set of resonances. The residues that are not observed can be assumed to undergo μ s to ms motion.

The structure is packed tightly together with a narrow pore, and displays a hydrophobic surface in the direction of lipids (*Figure 5.1*) as expected for membrane proteins. At the base, the hydrophilic residues of the amphipathic helix are positioned to interact with the hydrophilic head groups of the lipids. In *Figure 5.1 b*, the interior surface of the tetramer is drawn using the program HOLE.¹⁰ Consistent with the understanding that the conserved HxxxW sequence is responsible for ion selectivity and pH dependence, the narrowest part of the channel is found at H37 and W41. The surface is colored in red where less than one water molecule can fit in the channel, in green where no more than one water molecule can fit, and in blue where the pore diameter fits multiple water molecules.

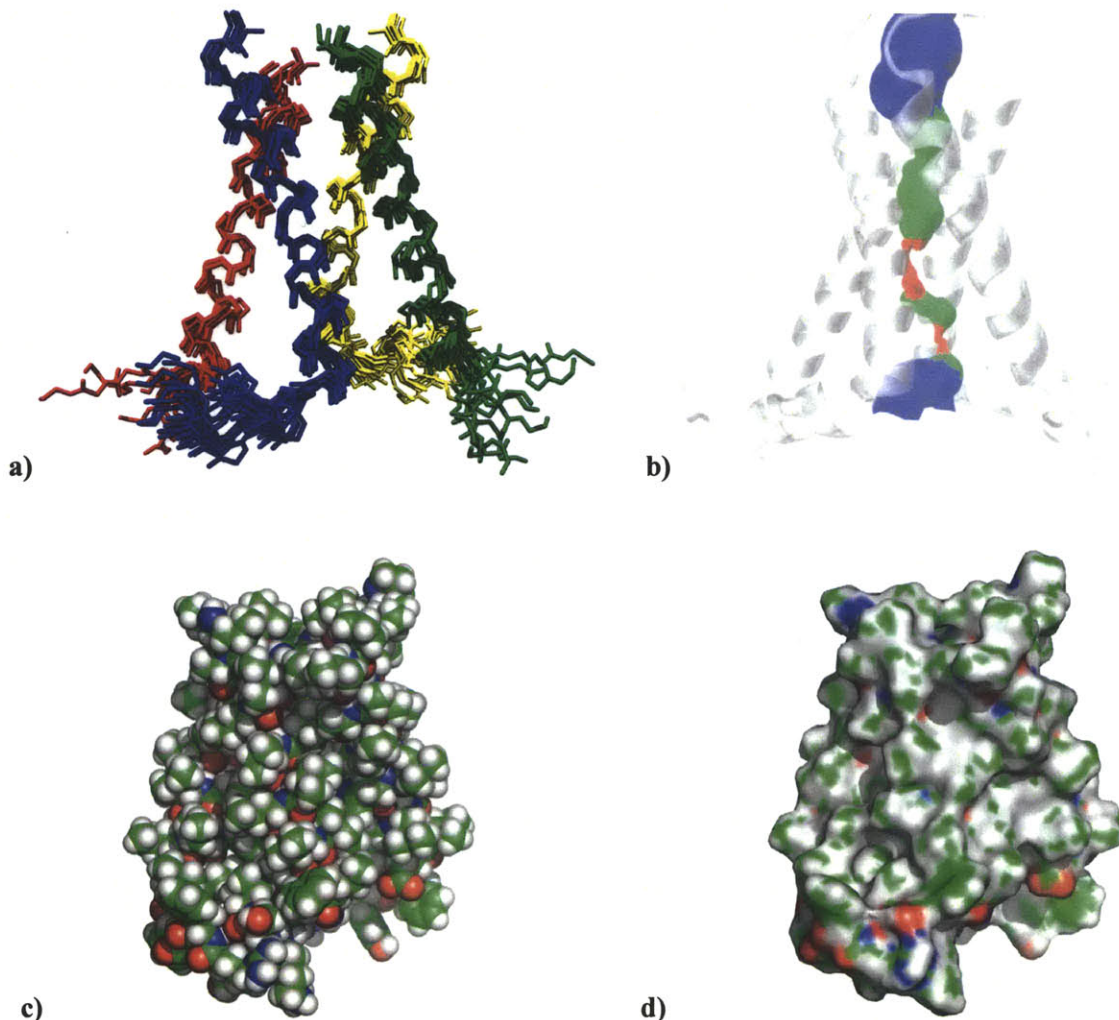


Figure 5.1. Dimer of dimers structure of M2. **(a)** An ensemble of 7 low energy structures. The backbone and all heavy atom r.m.s deviations are 0.8 and 1.2 Å, respectively. **(b)** the pore surface as calculated using the program HOLE, colored in red, green and blue, for pore widths of <1 water, 1 water, and >1 water, respectively. **(c)** sphere representation and **(d)** surface representation showing a hydrophobic exterior.

Two-fold symmetry:

The two fold symmetric structure raises interesting questions about the exact mechanism of proton conduction. Might the protons first bind to the more N-terminal H37 before continuing to the more C-terminal H37, and finally exiting at the C-terminal side? Notably, the M2 channel contains very few hydrophilic residues lining the pore, particularly toward the N terminus where a stretch of 6 hydrophobic residues from P25 to A30 span nearly two helical turns. The result that adjacent helices are out of register may improve the ability of the channel to form a hydrophilic pathway for proton conduction along the pore. On the other hand, the two fold symmetry might be a result of packing bulky W41 side chains on the inside of the tetramer. W41 side chains are found in two distinct secondary structures, with two helices in an 'indole in' conformation, and the

other two in and 'indole out' conformation, which in combination with the helix displacement allows the tetramer to pack into a tight bundle.

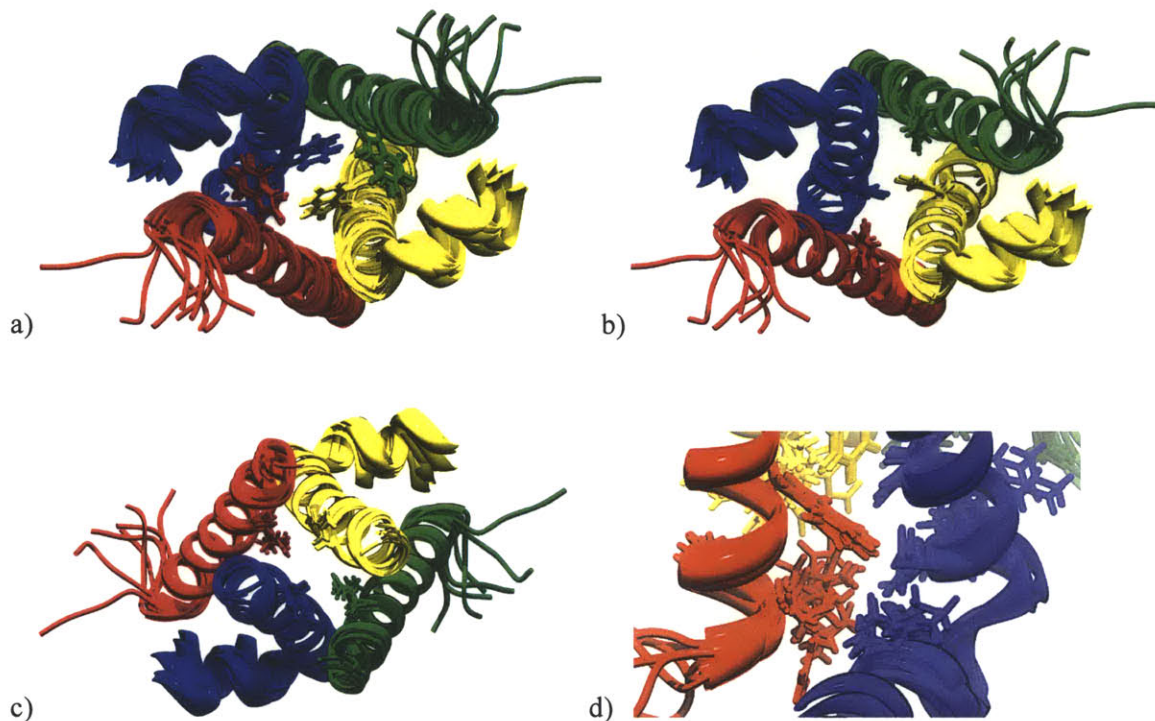


Figure 5.2. Side chain conformations of the S31N M2 tetramer. In **a)** W41 adopts an 'indole in' conformation for one helix and an 'indole out' conformation in the other. In **b)** two distinct orientations are evident for H37. In **c)** N31 points towards the pore (green and red helices) and toward a neighboring helix (blue and yellow helices). In **d)** is shown the location of drug association in the solution NMR structure, which is occupied by I51.

Drug Resistance:

The lipid structure has interesting implications for the resistance mechanism and the potential to overcome resistance with novel inhibitors. Despite the S31N mutation occurring near the pharmacological drug binding site, the precise influence of N31 on drug binding is unclear in the literature due to the substantial differences in reported structures that were solved for a variety of constructs under sample conditions that may not adequately mimic the viral membrane. There are two reported structures of the S31N mutant. The first of these was determined under conditions that did not bind drug in the pore. The other was solved with an inhibitor bound, and therefore may not represent a native state of the channel. While previous structures have pointed toward either helix packing⁵ or direct interaction⁶ to explain drug resistance, the two fold symmetric structure contains elements of both explanations. The side chain of N31 is found facing the pore in two helices, and facing an adjacent helix in the other two, with adjacent N31 side chains close enough to form polar contacts. N31 is well shielded from contact with the hydrophobic lipid

membrane. In contrast, drug bound structures of M2^{5,11} show position 31 in the interface between two helices, with the side chain pointing towards the lipids. This implies that two of the helices must rotate for the molecule to adopt the drug bound structure (see **Figure 5.3**). The larger hydrophilic N31 side chain would disfavor this motion. In addition, the direct interaction between the N31 side chain in the pore and the drug would also be unfavorable. While both effects could contribute to resistance, it is unclear which is more important. The simplest explanation is that in the drug bound state, N31 would point towards lipids, something that is much more favorable for Serine. For the design of a novel inhibitor, it will be useful to block the channel in the apo structure, without a helix rotation, and the structure presented herein should find use in these efforts. As evident in **Figure 5.1**, the largest pocket in the pore that might be targeted by an inhibitor is the pharmacological binding site of adamantane based drugs, near residue 31.

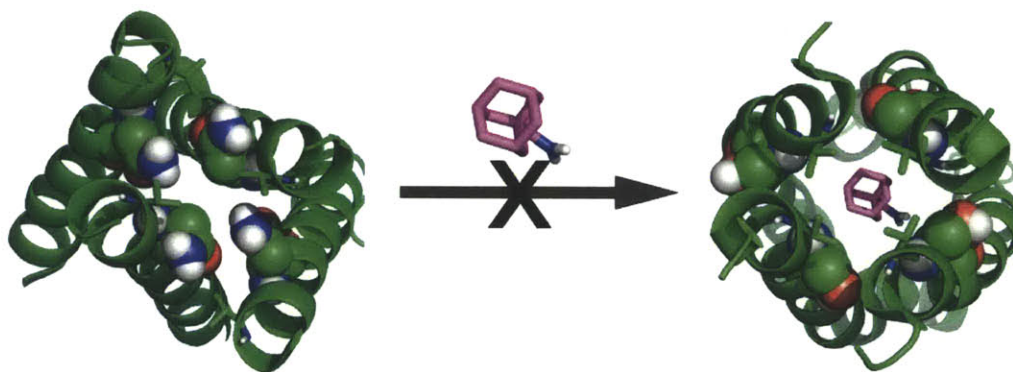


Figure 5.3. Explanation of drug resistance. **(left)** the S31N structure in lipids places N31 in the pore, or in the helix-helix interface. **(right)** the WT chimera structure with drug bound (pdb code 2LJC) places S31 in the helix-helix interface pointing out towards the (would be) lipid membrane. The increased hydrophilicity and size of the asparagine side chain compared with serine disfavors the drug bound conformation either by disrupting helical packing or by unfavorable association with lipids. Drug is shown in magenta, V27 is depicted as sticks, and residue 31 (serine or asparagine) is shown as spheres.

The explanation of drug resistance presented here also explains why small modification of aminoadamantyl inhibitors has failed to produce inhibitors against the S31N mutant. Clearly there is minimal or no contact between position 31 and amantadine or rimantadine in the drug bound conformation (**Figure 5.3 right**). Thus the interaction between the drug and the protein remains approximately the same, but the interaction between N31 and the hydrophobic membrane is unfavorable in the bound state, implying that a new drug would need to bind to a different conformation of the channel and requiring a complete redesign of the drug.

Heart of the channel: proton conduction

Regulation of the pH dependent proton conduction and selectivity is determined largely by the conserved HxxxW motif, with the rate of conduction tuned by the pKa of H37.^{12, 13} Previous explanations of the unusual pKa of H37 led to the proposal of imidazole-imidazolium dimerization in which the first two protons to enter the tetramer were shared in a low barrier hydrogen bond (LBHB).¹² An alternative explanation places H37 in a His-box conformation,¹⁴ with water as the hydrogen bonding partner.¹³ Although the present structure approximates a His-box conformation, it was solved at pH 7.8, above the first pKa of this construct, and therefore does not indicate if a LBHB occurs at lower pH. If the dimerization does occur, some rearrangement of the helices would be expected in order to bring the $\delta 1$ and $\epsilon 2$ nitrogens of adjacent H37s near enough to form a hydrogen bond (~ 5 Å in the structure). Alternatively, tuning of the H37 pKa could be accomplished with favorable cation-pi interactions. The two fold symmetric structure has a network of pi systems that could form favorable cation pi interactions between histadine and tryptophan, both within a helix, and between neighboring helices.

Previous structures of M2

M2 structures have been determined under a variety of sample conditions including both lipid bilayers, in detergent micelles, and crystallized out of detergents. Among the complete tetramer structures, these investigations have either been conducted in detergents, or have included a limited set of interhelical restraints, resulting in reported structures that show a high degree of conformational variability, which must be explained primarily from the difference in sample preparations. Surprisingly, none of the tetramer structures reported thus far are a dimer of dimers as was recently observed in lipids via peak doubling,¹⁵⁻¹⁷ except for a recent structure¹⁸ based on oriented sample NMR and molecular dynamics (MD) in which the deviation from four-fold symmetry was restricted to the side chain of H37.

In this oriented sample NMR structure, the helical tilt angle was determined experimentally, and a tetramer was assembled using molecular dynamics simulations. However, PISEMA is invariant with respect to translation and rotation about the bilayer normal. Since the four-fold symmetry of the backbone is primarily broken by translation in the S31N structure in lipids, this structure is in general agreement with the previously reported oriented sample measurements of WT M2, although there may be some differences due to the mutation. This highlights the importance of measuring inter-helical contacts between helices in the determination of structure. Ideally, orientation restraints based on PISEMA would also be included in structure determinations, because orientation restraints can provide long-range information that is complementary to

distance measurements. However, PISEMA data is not available for the S31N mutant, and we instead used an over determined set of distance restraints.

5.3 Methods

NMR spectroscopy

NMR spectra were recorded on several high field Bruker (Bruker Biospin, Billerica, MA) spectrometers operating at a ^1H frequency of 800, 900, and 1000 MHz, and using 3.2 mm efree probes at 800 and 900 MHz, and 1.3 mm probes at 800 MHz and 1000 MHz. Spectra were also recorded using a home built spectrometer designed by Dave Ruben and operating at a ^1H frequency of 750 MHz equipped with a Bruker 3.2 Efree probe. ^{13}C detected spectra were recorded with 3.2 mm Bruker E-free probes, and proton-detected spectra were recorded with Bruker 1.3 mm solenoid probes tuned to HCN or HCD. The sample temperature was maintained at 20 to 30 °C using Bruker cooling units (BCU II or BCU extreme) or on the 750 MHz instrument, a Kinetics Thermal System XR air-jet system (Stone Ridge, NY). Chemical shifts are reported on the DSS scale using adamantane as a secondary reference.

NMR spectra affording distance restraints

PAR

PAR spectra with 15 ms mixing were recorded at a ^1H frequency of 900 MHz and 20 kHz MAS. The ILFY reverse labeled sample was used, and primarily $\text{C}\alpha_i\text{-C}\alpha_{i+3}$ contacts were identified. A 4-fold molar excess of rimantadine was added to the sample, but had minimal impact (< 0.5 ppm) on the chemical shifts, indicating that the inhibitor does not induce the drug bound conformation in the S31N mutant.¹⁵ Recorded at MIT.

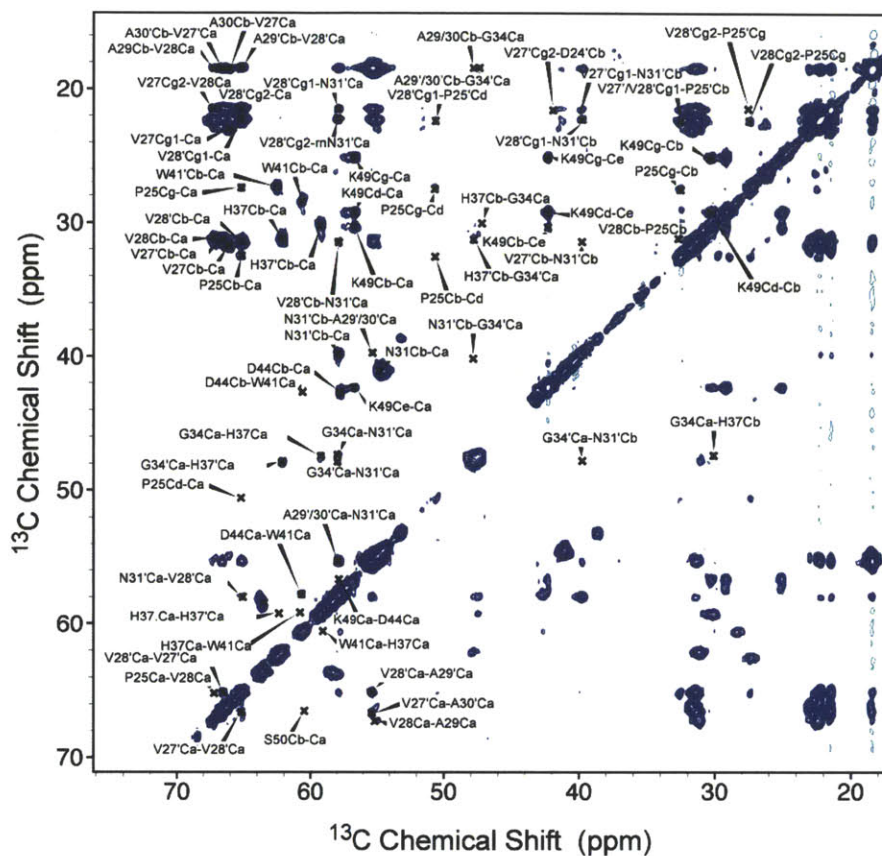


Figure 5.4. PAR spectrum with 15 ms mixing recorded at a ^1H frequency of 900 MHz and 20 kHz MAS. A four-fold molar excess of rimantadine drug was present in the sample.

PDS

PDS spectra with 400 ms mixing were recorded at 750 MHz spinning at 14.287 kHz. The ILFY reverse labeled sample was used. A 4-fold molar excess of rimantadine was added to the sample, as for the PAR spectrum. Primarily Ca-Ca contacts are shown in **Figure 5.5**. In addition, structurally important aromatic-aromatic,¹⁵ and aromatic-aliphatic contacts were present in the spectrum. Recorded at MIT.

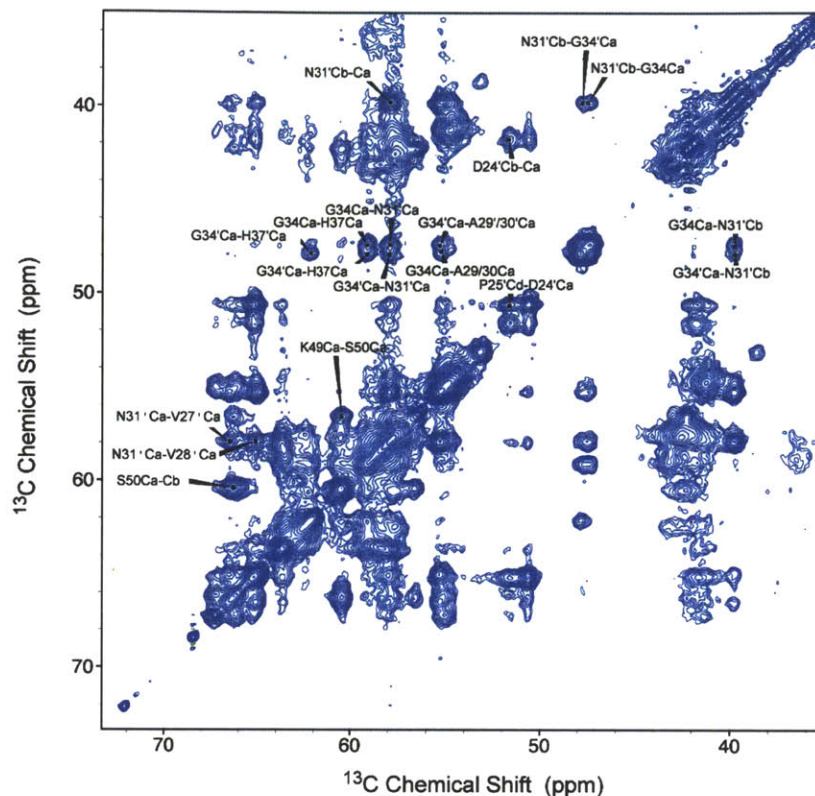


Figure 5.5. The Ca-Ca region of a PDSD spectra with 400 ms mixing were recorded at 750 MHz spinning at 14.287 kHz. A four-fold molar excess of rimantadine drug was present in the sample.

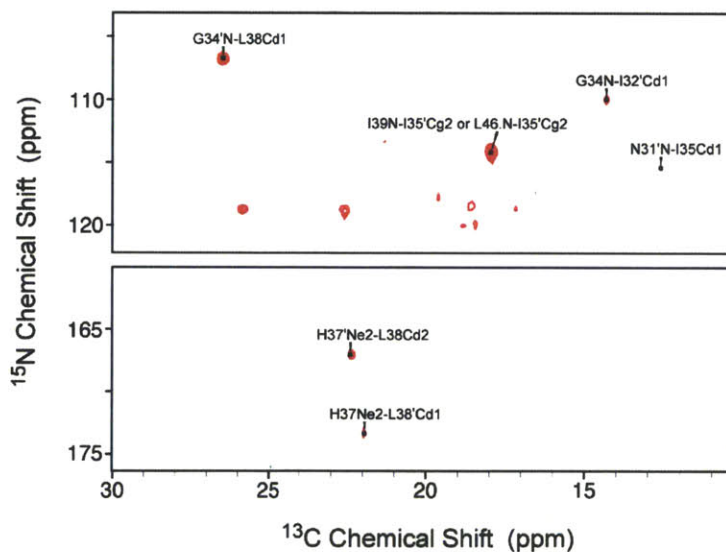


Figure 5.6. ^{15}N -aliphatic correlations from a ^{15}N - ^{13}C TEDOR spectrum of a 1:1 mixture of ^{15}N and 1,6- ^{13}C glucose labeled M2. 14.336 ms of TEDOR mixing was applied.

^{15}N - ^{13}C TEDOR

A sample with mixed ^{15}N and ^{13}C labeling was used with TEDOR to find interhelical contacts. A 1:1 mixture of U- ^{15}N M2 and 1,6- ^{13}C glucose labeled M2 was refolded, ensuring that mixed

tetramers were formed. 21 ms of ZF-TEDOR (7 μ s 15 N pi pulses, 100 kHz TPPM decoupling) was applied at a 1 H frequency of 800 MHz, and interhelical contacts were identified. Mixing times of 7.168 ms, 14.336 ms, and 21.504 ms were used, and the best intensity for most cross-peaks was found at 14.336 ms (**Figure 5.6**). Recorded at MIT.

13 C RFDR

RFDR spectra were recorded at a 1 H frequency of 900 MHz (1 H) and provided the most interhelical contacts. A 1,6- 13 C glucose sample was used, and broadband RFDR was applied for 8 ms or 19.2 ms and spinning at 20 kHz. 83 kHz 13 C pulses and empirically optimized TPPM 1 H decoupling of approximately 100 kHz were used during the recoupling period. Recorded at MIT.

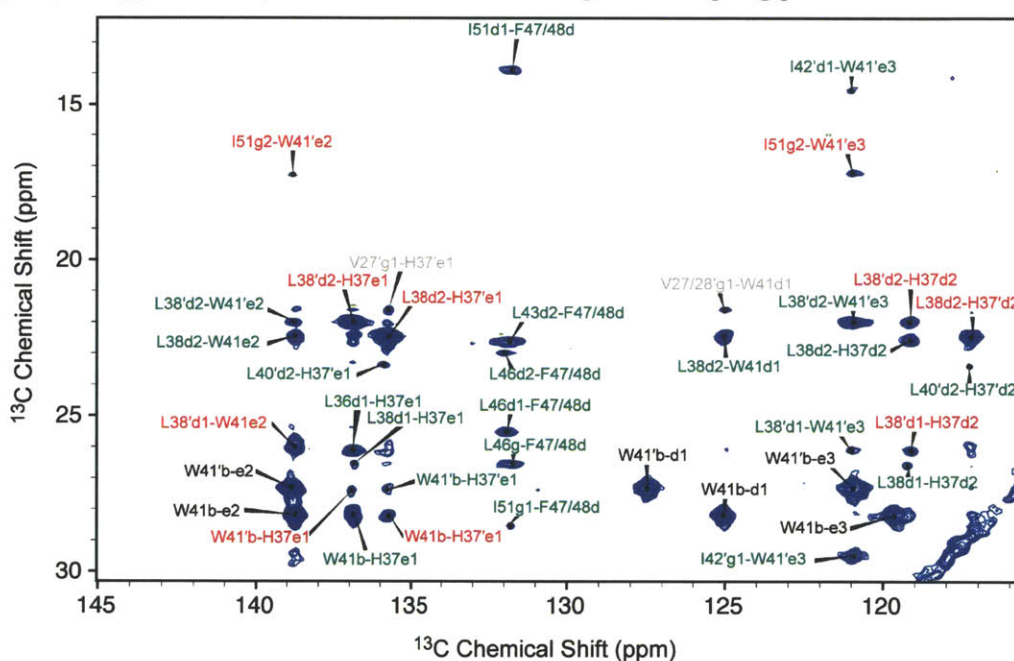


Figure 5.7. 13 C- 13 C RFDR spectrum of 1,6- 13 C Glucose labeled M2 showing inter-helical cross-peaks (red labels) inter-residue cross-peaks (green), and intra-residue cross-peaks (black). Grey labels indicate cross-peaks that can only be explained due to the presence of inter-tetramer contacts. An RFDR mixing time of 8 ms of was applied with approximately 100 kHz of proton decoupling, MAS of 20 kHz, and at a 1 H frequency of 900 MHz.

1 H RFDR (4D HCHHCH)

A 4 dimensional spectrum using 1 H- 1 H RFDR was recorded at 800 MHz (1 H) and provided intermolecular and intramolecular methyl-methyl distances. The sequence is similar to a recently reported 4D using DREAM mixing.¹⁹ Spinning was set to 60 kHz, and INEPT transfers were used for C-H and H-C. A mixing period of 8 ms of 1 H- 1 H RFDR was applied for the observation of long-range contacts, and 300 ms of water suppression²⁰ was used. Selected strips are displayed in

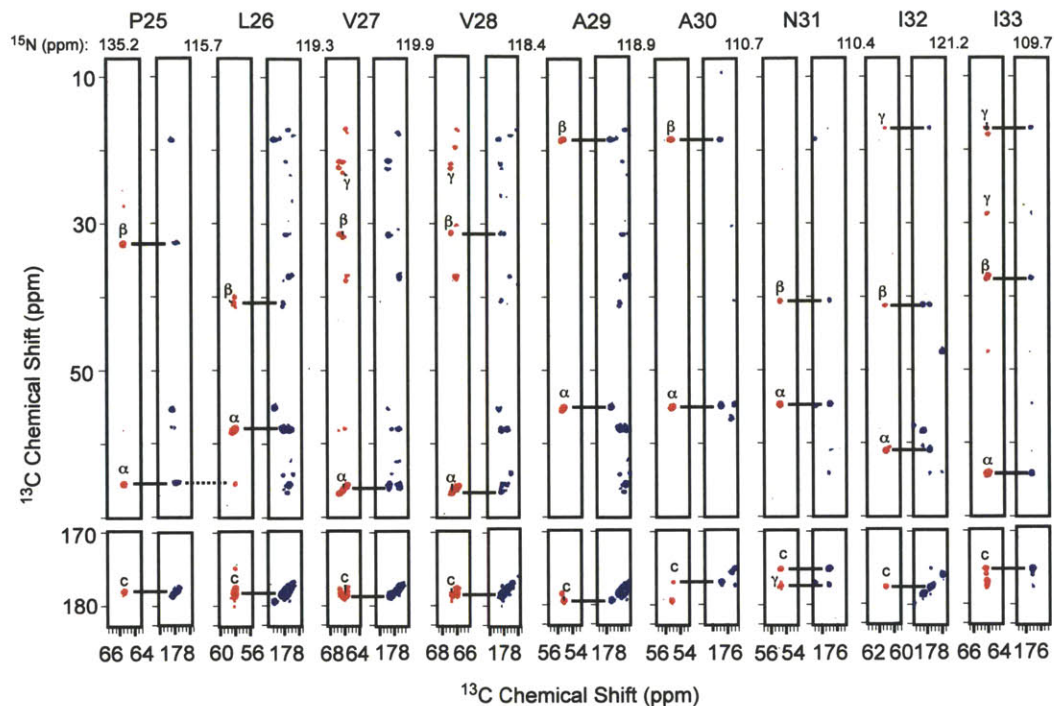


Figure 5.11. Selected strips from the 3D TEDOR-RFDR spectrum show the consecutive assignment of residues P25 to I33. 1.2 ms of TEDOR was applied and 4.8 ms of RFDR at a spinning frequency of 20 kHz. NCaCx transfer is shown in red, and NCoCx transfer in blue.

HN, (H)CaNH, (H)Ca(Co)NH

A 2D HN spectrum was recorded using an H-N CP transfer using 50 kHz on the ^{15}N channel ~4 to 10 kHz on the ^1H channel. A 3D (H)CaNH spectrum²¹ was recorded according to the recently published sequence using a H-Ca CP with a 35 to 50 kHz ramp on ^1H and 10 kHz on ^{13}C , Ca-N CP with 35 kHz on Ca and 25 kHz on ^{15}N , with a 10 percent ramp, and N-H CP with 50 kHz on ^{15}N and 4 to 10 kHz on ^1H . Selected strips from the spectrum are shown in **Figure 5.13**. A 3D (H)Ca(Co)NH spectrum was also recorded using similar parameters.²¹ The $\text{U-}^{13}\text{C}, ^{15}\text{N}, ^2\text{H}$ - [$^{12}\text{C}, ^{13}\text{C}^2\text{H}_2^1\text{Hd1-Ile}$, $^{12}\text{C}, ^{13}\text{Ca}, ^{13}\text{C}^1, ^{13}\text{C}^2\text{H}_2^1\text{Hd2-Leu}$, $^{12}\text{C}, ^{13}\text{C}^2\text{H}_2^1\text{Hg2-Val}$] sample was used. The spectra were recorded at 1000 MHz at the CRMN in Lyon, France.

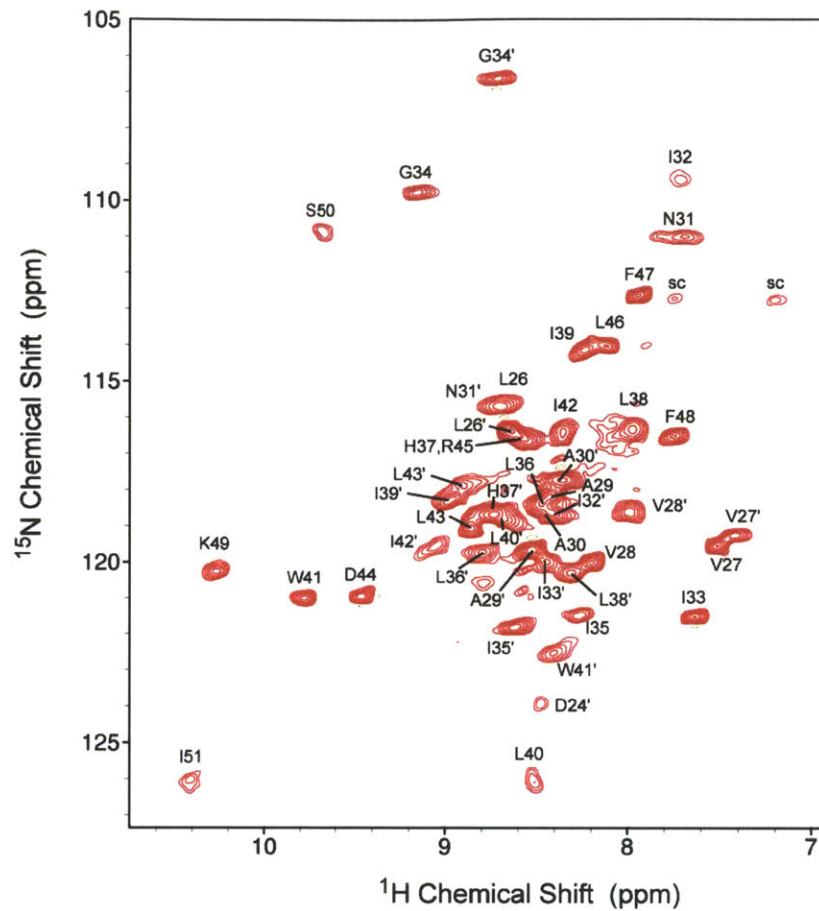


Figure 5.12. A cross polarization based HN spectrum showing the completed backbone amide assignments.

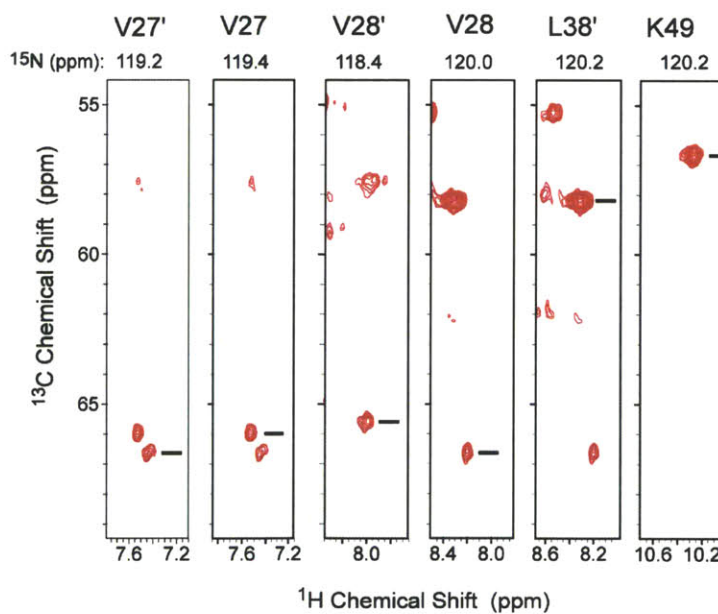


Figure 5.13. Selected strips from the HCaNH spectrum of ^2H M2.

Assignments

Backbone and side chain assignments were determined using TEDOR-RFDR 3D spectra to record NCACX and NCOCX connectivity, using an ILFY reverse labeled sample, and a uniformly labeled sample. Two sets of resonances were observed, due to the dimer of dimers structure observed previously for both WT and S31N M2.^{15,17} Inter and intra residue correlations in these spectra were sufficiently resolved to determine two continuous sets of assignments. One set of resonances extended from P25 to I51, while the other was observed from D24 to D44. The two sets of resonances were sufficiently separated for unambiguous assignment, except for the separation in the ¹⁵N dimension at L26, resulting in some ambiguity over which L26 spin system belonged with which V27 spin system. (H)CaNH and (H)Ca(Co)NH spectra were used to resolve this ambiguity, and to provide an additional independent check of the full assignments, according to an automated assignment protocol.²²

Conversion of peak volumes to distance restraints

For ¹³C-¹³C restraints, peak volumes of known distances ($\text{Ca}_i\text{-Ca}_{i+1}$ and $\text{Ca}_i\text{-Ca}_{i+3}$) and a distance dependence of r^{-3} were used to calibrate unknown distance restraints. For ¹³C-¹³C RFDR, $\text{Ca}_i\text{-Ca}_{i+1}$ peaks (3.8 Å distance) were used as calibration, and an upper distance limit was entered as 1.1 times the calculated distance plus one Angstrom. For non-aromatic sites, an additional Angstrom was added to account for differences in relaxation. We did not attempt to adjust the distance limits based on the site-specific degree of labeling. For ¹³C-¹³C PDS and PAR, $\text{Ca}_i\text{-Ca}_{i+1}$ peaks (5.3 Å distance) were used as calibration, and an upper distance limit was entered as 1.12 times the calculated distance plus one Angstrom. Several restraints from the 8 ms PAR spectrum were adjusted manually due to consistent violation. These restraints tended to involve carbonyl resonances, for which relaxation is expected to be different from the proton-bonded carbons used for calibration.

TALOS+ Predictions

TALOS+ predictions were made using all assigned residues both with and without the use of proton chemical shifts. A higher number of good predictions were made without the proton shifts, and we therefore excluded proton shifts in the predictions. This can be rationalized based on the sensitivity of the proton chemical shift to water accessibility,²³ which is atypically low in a membrane protein, and the slightly altered helical geometry²⁴ found in membrane proteins that may not be adequately represented in the TALOS+ database.

Introduction of helical hydrogen bonds

Based on the TALOS+ predictions, helical hydrogen bonds were entered for assigned residues except where the TM and AP helices meet. Residue i to $i+4$ C' to HN distances of 2.0 ± 0.2 Å, and C' to N distances of 3.0 ± 0.2 Å were entered from P25 to L43. For one set of resonances, these restraints continued between residues 47 and 52.

Highly ambiguous restraints

Highly ambiguous restraints were automatically identified in the RFDR spectra of 1,6-¹³C glucose labeled M2 using a cutoff of 0.25 ppm, the assignment tables, and the spectrum. Cross-peaks arising from sidebands or truncation artifacts were removed by manual inspection. The restraints were then filtered against a structure generated without these ambiguous restraints, but including all manually entered restraints. Restraints that violated by more than 3 Å were removed. The remaining restraints were entered directly into XPLOR as highly ambiguous restraints.

Treatment of intertetramer contacts

Contacts that do not fit the general channel architecture (A parallel tetramer with Histidine 37 facing inward) were excluded from the calculation, and may be due to intertetramer contacts that arise due to the high concentration of protein in the membrane. For example, Valine and Tryptophan are at opposite sides of the membrane, and cross-peaks that are seen between them most likely arise from contacts between adjacent tetramers, which are inserted in an antiparallel arrangement in the membrane. This arrangement is not surprising, given the wedge shape of M2 with a large C-terminal base, and is the arrangement observed in crystal structures of TM M2.

Structure calculations

Simulated annealing was performed using the program XPLOR-NIH. Due to the C2 symmetry, there are two different interfaces between each helix and its two neighbors. Each restraint was therefore entered as an ambiguous restraint to either of the neighboring helices. Since use of ambiguous restraints results in a rough energy landscape in which the protein is easily trapped in a local minimum satisfying one of the possibilities, these ambiguous restraints resulted in slow convergence if introduced too early. First, TALOS+ and hydrogen bonding restraints were introduced in a standard simulated annealing (SA) protocol, and once the structure converged, the four helices were aligned loosely in the membrane by applying four-fold symmetric restraints (upper bound 6 Å) from D44Cg-R45Cz, H37Ce1-H37Ce1, and V27Cg-V27Cg. Next, non-crystallographic restraints (NCS) were turned on to ensure C2 symmetry, and 10 structures were

calculated that satisfied these modeling restraints TALOS+ and hydrogen bond restraints. All restraints were included in the final annealing in which X structures were calculated from each of the Y lowest energy structures from the previous annealing. During annealing, a database-derived potential for side chain rotamers (Rama) was ramped from 0.02 to 0.2. Flat well harmonic potentials were used, with force constants were ramped from 25 to 100 kcal mol⁻¹ Å⁻² for distances (NOE), 20 to 100 kcal mol⁻¹ rad⁻² for TALOS based backbone dihedral restraints. Additional force constants used in the annealing were Van der Waals of 0.02 to 4.0 kcal mol⁻¹ Å⁻², improper of 0.1 to 1.0 kcal mol⁻¹ degree⁻², and bond angle of 0.4 to 1.0 kcal mol⁻¹ degree⁻². The temperature was reduced from 1000 to 20 K in steps of 20 K, and 4 picoseconds of Verlet dynamics at each temperature with 1.5 fs time steps. The mass of all atoms was set to 100 for the annealing.

M2 synthesis

M2 was synthesized, purified and refolded as described previously by overexpression in E. Coli BL21 DE3.¹⁵ Minimal media was prepared per liter with 3 to 4 g glucose, 1 g ammonium chloride, standard salts, and Centrum adult vitamins (1.5 mL of 2 pills in 40 mL, dissolved with shaking for 30 minutes). In addition, deuterated and ILV methyl labeled protein was produced as described below, and reconstituted in ²H-78 1,2-diphytanoyl-*sn*-glycero-3-phosphocholine (DPhPC). A description of the synthesis of ²H-78 DPhPC appears in Chapter 6.

Sample labeling

U-¹³C, ¹⁵N M2: Per liter, 3 g ¹³C glucose and 1 g ¹⁵N ammonium chloride (CIL), with another 0.5 to 1 g ¹³C glucose added at induction (150 μM IPTG, 18 °C) at an OD₆₀₀ of 0.7 to 0.9. The final OD₆₀₀ reached 3.5 to 4, after 18 hours of expression at 18 °C, and yielded up to 15 mg of pure protein.

U-¹³C, ¹⁵N-[¹²C, ¹⁴N-ILFY] M2: Per liter, 3 g ¹³C glucose and 1 g ¹⁵N ammonium chloride (CIL), with another 0.5 to 1 g ¹³C glucose added at induction. Cells were grown in 700 mL of media, with 300 mL of media used to dissolve the amino acids. When the OD₆₀₀ reached 0.7, the reserved 300 mL of media was added, along with 150 mg Isoleucine, 150 mg Leucine, 50 mg Phenylalanine, and 100 mg Tyrosine (Sigma-Aldrich). Expression of protein was induced with 150 μM IPTG at 18 °C as before. The final OD₆₀₀ reached 3.5 to 4.6, after 18 hours of expression at 18 °C, and yielded up to 15 mg of pure protein.

[1-¹³C]-GLUCOSE, [1,6-¹³C]-GLUCOSE M2: Preparation was identical to U-¹³C-¹⁵N M2 except that specifically isotopically labeled glucose was used. The labeling pattern resulting from [1-¹³C]-glucose and [1,6-¹³C]-glucose (Omicron Biochemicals) is the same, except that the [1,6-¹³C]-glucose results in double the labeling efficiency per site.

U-¹³C, ¹⁵N, ²H-[¹²C, ¹³C²H₂¹Hd1-Ile, ¹²C, ¹³Ca, ¹³C', ¹³C²H₂¹Hd2-Leu, ¹²C, ¹³C²H₂¹Hg2-Val] M2: An overnight culture in 50 mL of 90 % ²H M9, 10 % SOC media was grown from a fresh transformation in BL21-DE3 until an OD₆₀₀ of 2 to 3. Cells were then pelleted by centrifugation and transferred to 1L of ²H M9 media containing 3 g ²H-¹³C glucose, 1 g ¹⁵N ammonium chloride, salts, and Centrum as before, in 1 L of 99.8 % ²H D₂O. The doubling time was 2 hours. At an OD₆₀₀ of 0.65 to 0.75, ILV precursors were added: 75 mg alpha-keto butyric acid, sodium salt 4-¹³C 99 %, 3,3,4,4-²H₄, 98 % (CIL), and 350 mg of 2-(¹³C,²H₂)methyl-4-(²H₃)-acetolactate prepared as described previously.²⁵ Cells were harvested after 24 to 36 hours, and yielded up to 5 mg of pure protein. This labeling pattern results in methyl groups with isolated ¹³C¹H spin pairs in an otherwise ²H, ¹²C background at nearby sites. The protein was purified and refolded in ¹H buffers, resulting in complete exchange to ¹H at exchangeable sites such as the backbone amides.

U-¹³C, ¹⁵N, ²H-[¹³CH₃d1-I] M2: The same protocol as above was used, but the precursor was 75 mg of ¹³C₄, 98 %, 3,3-²H₂, 98 % alpha-ketobutyric acid, sodium salt.

U-¹³C, ¹⁵N, ²H-[¹³C²H₂¹Hd2-Leu, ¹³C²H₂¹Hg2-Val] The same protocol as above was used, but the precursor was 350 mg of of U-¹³C,2-(²H₂)methyl-4-(²H₃)-acetolactate.

5.4 Supporting Information

Seq	H	N	Co	Ca	Cb	Cg,	Cg2,	Cd,	Cd2	Ce,	Ce3	Cz,	Cz3
D24'	8.47	124.2	175.0	52.0	41.9	179.1	-	-	-	-	-	-	-
P25	-	135.2	177.9	65.4	32.7	27.5	-	50.7	-	-	-	-	-
P25'	-	136.2	177.5	65.3	32.6	27.3	-	50.7	-	-	-	-	-
L26	8.69	115.7	178.2	58.1	40.8	28.2	-	25.8	23.3	-	-	-	-
L26'	8.64	116.2	178.3	57.9	41.3	26.5	-	25.3	22.6	-	-	-	-
V27	7.51	119.3	178.6	66.1	31.9	21.6	23.1	-	-	-	-	-	-
V27'	7.43	119.1	177.7	66.6	31.5	22.4	21.6	-	-	-	-	-	-
V28	8.19	120.0	178.3	66.7	31.3	21.9	22.5	-	-	-	-	-	-
V28'	7.98	118.7	178.7	65.6	31.7	21.5	22.7	-	-	-	-	-	-
A29	8.44	118.4	179.4	55.2	18.5	-	-	-	-	-	-	-	-
A29'	8.53	119.9	178.6	55.4	18.4	-	-	-	-	-	-	-	-
A30	8.43	118.9	176.9	55.0	18.6	-	-	-	-	-	-	-	-
A30'	8.36	117.9	178.3	55.4	18.7	-	-	-	-	-	-	-	-
N31	7.69	110.8	175.1	54.7	40.6	177.5	-	-	-	-	-	-	-
N31'	8.73	115.6	177.5	58.0	39.9	174.8	-	-	-	-	-	-	-
I32	7.71	110.4	177.7	61.4	41.3	26.3	17.2	14.3	-	-	-	-	-
I32'	8.69	118.8	177.2	65.6	37.2	29.6	17.6	14.1	-	-	-	-	-
I33	7.62	121.3	175.3	64.3	37.6	28.9	17.2	14.6	-	-	-	-	-
I33'	8.46	120.2	177.7	66.0	37.1	30.2	19.6	13.6	-	-	-	-	-
G34	9.15	109.8	176.0	47.6	-	-	-	-	-	-	-	-	-
G34'	8.72	106.8	175.2	47.9	-	-	-	-	-	-	-	-	-
I35	8.27	121.4	176.9	64.1	37.1	28.8	17.7	12.7	-	-	-	-	-
I35'	8.62	121.9	177.2	66.1	37.6	30.7	18.0	14.2	-	-	-	-	-
L36	8.46	118.6	177.4	57.6	41.7	26.8	-	26.1	24.7	-	-	-	-
L36'	8.80	119.9	177.3	58.1	41.3	26.5	-	24.7	24.4	-	-	-	-
H37	8.60	116.5	175.6	59.3	30.3	136.3	-	-	119.1	136.9	-	-	-
H37'	8.74	118.9	177.3	62.3	31.3	135.8	-	-	117.2	135.7	-	-	-
L38	7.98	116.3	178.7	58.4	42.3	26.4	-	26.5	22.5	-	-	-	-
L38'	8.32	120.5	178.3	58.3	40.4	26.5	-	22.0	26.0	-	-	-	-
I39	8.29	114.3	175.9	60.4	37.2	30.2	19.7	13.5	-	-	-	-	-
I39'	8.98	118.7	177.4	65.5	37.3	29.6	17.2	13.9	-	-	-	-	-
L40	8.52	126.3	178.5	58.5	41.3	26.9	-	25.0	24.4	-	-	-	-
L40'	8.70	118.8	179.3	58.1	40.8	27.0	-	26.2	23.2	-	-	-	-
W41	9.78	121.1	178.6	60.7	28.2	111.8	124.4	125.1	129.3	138.7	119.7	114.0	121.7
W41'	8.40	122.7	177.8	62.6	27.4	111.1	123.8	127.5	130.9	138.8	121.0	114.9	120.9
I42	8.35	116.8	178.4	64.2	37.9	28.8	18.6	14.2	-	-	-	-	-
I42'	9.04	119.6	178.1	65.8	37.8	29.4	17.1	14.4	-	-	-	-	-
L43	8.86	119.3	179.9	57.7	41.7	26.5	-	23.2	22.6	-	-	-	-
L43'	8.91	117.9	177.6	58.1	41.3	*	-	*	*	-	-	-	-
D44	9.47	121.0	178.5	57.9	42.7	180.2	-	-	-	-	-	-	-
D44'	*	117.7	*	*	*	*	-	-	-	-	-	-	-
R45	8.57	116.7	178.5	57.8	29.5	25.9	-	42.8	-	-	-	159.6	-
L46	8.13	114.6	177.5	56.3	43.0	26.7	-	25.5	22.9	-	-	-	-
F47	7.95	112.6	175.6	58.4	41.5	-	-	131.8	-	-	-	-	-
F48	7.76	116.6	175.8	61.0	39.1	-	-	131.8	-	-	-	-	-
K49	10.27	120.3	175.6	56.7	30.4	25.2	-	29.3	-	42.5	-	-	-
S50	9.69	111.0	174.4	60.6	66.9	-	-	-	-	-	-	-	-
I51	10.41	126.2	176.0	65.8	38.2	28.5	17.2	13.8	-	-	-	-	-
Y52	-	118.0	-	-	-	-	-	-	-	-	-	-	-

Seq	Hd1	Hd2	He1	He2	Hg2	Nd1	Nd2	Ne	Ne1	Ne2	Nz
D24'	-	-	-	-	-	-	-	-	-	-	-
P25	-	-	-	-	-	-	-	-	-	-	-
P25'	-	-	-	-	-	-	-	-	-	-	-
L26	-	-	-	-	-	-	-	-	-	-	-
L26'	-	-	-	-	-	-	-	-	-	-	-
V27	-	-	-	-	1.16	-	-	-	-	-	-
V27'	-	-	-	-	1.11	-	-	-	-	-	-
V28	-	-	-	-	1.12	-	-	-	-	-	-
V28'	-	-	-	-	1.24	-	-	-	-	-	-
A29	-	-	-	-	-	-	-	-	-	-	-
A29'	-	-	-	-	-	-	-	-	-	-	-
A30	-	-	-	-	-	-	-	-	-	-	-
A30'	-	-	-	-	-	-	-	-	-	-	-
N31	-	-	-	-	-	-	112.9	-	-	-	-
N31'	-	-	-	-	-	-	115.3	-	-	-	-
I32	0.85	-	-	-	-	-	-	-	-	-	-
I32'	0.95	-	-	-	-	-	-	-	-	-	-
I33	1.00	-	-	-	-	-	-	-	-	-	-
I33'	0.86	-	-	-	-	-	-	-	-	-	-
G34	-	-	-	-	-	-	-	-	-	-	-
G34'	-	-	-	-	-	-	-	-	-	-	-
I35	1.11	-	-	-	-	-	-	-	-	-	-
I35'	0.99	-	-	-	-	-	-	-	-	-	-
L36	-	-	-	-	-	-	-	-	-	-	-
L36'	-	-	-	-	-	-	-	-	-	-	-
H37	-	-	-	14.84	-	251.1	-	-	-	173.4	-
H37'	-	-	-	12.17	-	251.6	-	-	-	167.0	-
L38	-	1.06	-	-	-	-	-	-	-	-	-
L38'	0.87	-	-	-	-	-	-	-	-	-	-
I39	1.05	-	-	-	-	-	-	-	-	-	-
I39'	0.93	-	-	-	-	-	-	-	-	-	-
L40	-	1.09	-	-	-	-	-	-	-	-	-
L40'	-	-	-	-	-	-	-	-	-	-	-
W41	-	-	10.79	-	-	-	-	-	128.8	-	-
W41'	-	-	11.21	-	-	-	-	-	129.9	-	-
I42	1.02	-	-	-	-	-	-	-	-	-	-
I42'	1.00	-	-	-	-	-	-	-	-	-	-
L43	-	-	-	-	-	-	-	-	-	-	-
L43'	-	-	-	-	-	-	-	-	-	-	-
D44	-	-	-	-	-	-	-	-	-	-	-
D44'	-	-	-	-	-	-	-	-	-	-	-
R45	-	-	-	-	-	-	-	84.47	-	-	-
L46	-	-	-	-	-	-	-	-	-	-	-
F47	-	-	-	-	-	-	-	-	-	-	-
F48	-	-	-	-	-	-	-	-	-	-	-
K49	-	-	-	-	-	-	-	-	-	-	32.2
S50	-	-	-	-	-	-	-	-	-	-	-
I51	0.92	-	-	-	-	-	-	-	-	-	-
Y52	-	-	-	-	-	-	-	-	-	-	-

Table 1. Assignments of S31N M2 determined from TEDOR-CC spectra, (H)CaNH, and HCa(Co)NH spectra, as well as TEDOR, RFDR, CH and NH spectra. In bold are stereo specifically assigned. Missing resonances are indicated by *. In addition, Nh1 and Nh2 of R45b were not observed.

Restraint Summary:

The tetramer structure was calculated with four copies of the sequence distinguished by adding multiples of 100 to the residue numbers of each molecule. Residue numbers 118-160 and 318-360 correspond to the first set of resonances, and residue numbers 218-260 and 418-460 correspond to the second set of assignments (designated with a prime in the assignment tables). The following restraints appear in XPLOR-NIH format. For angles, the four numbers indicate, energy constant, angle in degrees, range in degrees, and exponent. For distances, the three numbers indicate the distance, the lower range, and the upper range. For the PDS and PAR, numbers following an exclamation point indicate the measured peak height.

TALOS:

```
assign (resid 124 and name c) (resid 125 and name n)
(resid 125 and name ca) (resid 125 and name c) 1.0 -56.448 7.36 2
assign (resid 125 and name n) (resid 125 and name ca)
(resid 125 and name c) (resid 126 and name n) 1.0 -34.824 5.66 2
assign (resid 324 and name c) (resid 325 and name n)
(resid 325 and name ca) (resid 325 and name c) 1.0 -56.448 7.36 2
assign (resid 325 and name n) (resid 325 and name ca)
(resid 325 and name c) (resid 326 and name n) 1.0 -34.824 5.66 2

assign (resid 125 and name c) (resid 126 and name n)
(resid 126 and name ca) (resid 126 and name c) 1.0 -62.207 9.70 2
assign (resid 126 and name n) (resid 126 and name ca)
(resid 126 and name c) (resid 127 and name n) 1.0 -36.616 17.36 2
assign (resid 325 and name c) (resid 326 and name n)
(resid 326 and name ca) (resid 326 and name c) 1.0 -62.207 9.70 2
assign (resid 326 and name n) (resid 326 and name ca)
(resid 326 and name c) (resid 327 and name n) 1.0 -36.616 17.36 2

assign (resid 126 and name c) (resid 127 and name n)
(resid 127 and name ca) (resid 127 and name c) 1.0 -66.374 14.07 2
assign (resid 127 and name n) (resid 127 and name ca)
(resid 127 and name c) (resid 128 and name n) 1.0 -45.906 9.01 2
assign (resid 326 and name c) (resid 327 and name n)
(resid 327 and name ca) (resid 327 and name c) 1.0 -66.374 14.07 2
assign (resid 327 and name n) (resid 327 and name ca)
(resid 327 and name c) (resid 328 and name n) 1.0 -45.906 9.01 2

assign (resid 127 and name c) (resid 128 and name n)
(resid 128 and name ca) (resid 128 and name c) 1.0 -61.982 13.75 2
```

assign (resid 128 and name n) (resid 128 and name ca)
(resid 128 and name c) (resid 129 and name n) 1.0 -48.008 15.66 2
assign (resid 327 and name c) (resid 328 and name n)
(resid 328 and name ca) (resid 328 and name c) 1.0 -61.982 13.75 2
assign (resid 328 and name n) (resid 328 and name ca)
(resid 328 and name c) (resid 329 and name n) 1.0 -48.008 15.66 2

assign (resid 128 and name c) (resid 129 and name n)
(resid 129 and name ca) (resid 129 and name c) 1.0 -62.209 10.91 2
assign (resid 129 and name n) (resid 129 and name ca)
(resid 129 and name c) (resid 130 and name n) 1.0 -38.373 18.79 2
assign (resid 328 and name c) (resid 329 and name n)
(resid 329 and name ca) (resid 329 and name c) 1.0 -62.209 10.91 2
assign (resid 329 and name n) (resid 329 and name ca)
(resid 329 and name c) (resid 330 and name n) 1.0 -38.373 18.79 2

assign (resid 129 and name c) (resid 130 and name n)
(resid 130 and name ca) (resid 130 and name c) 1.0 -66.976 21.99 2
assign (resid 130 and name n) (resid 130 and name ca)
(resid 130 and name c) (resid 131 and name n) 1.0 -35.703 12.98 2
assign (resid 329 and name c) (resid 330 and name n)
(resid 330 and name ca) (resid 330 and name c) 1.0 -66.976 21.99 2
assign (resid 330 and name n) (resid 330 and name ca)
(resid 330 and name c) (resid 331 and name n) 1.0 -35.703 12.98 2

assign (resid 130 and name c) (resid 131 and name n)
(resid 131 and name ca) (resid 131 and name c) 1.0 -82.027 25.21 2
assign (resid 131 and name n) (resid 131 and name ca)
(resid 131 and name c) (resid 132 and name n) 1.0 -30.706 38.66 2
assign (resid 330 and name c) (resid 331 and name n)
(resid 331 and name ca) (resid 331 and name c) 1.0 -82.027 25.21 2
assign (resid 331 and name n) (resid 331 and name ca)
(resid 331 and name c) (resid 332 and name n) 1.0 -30.706 38.66 2

assign (resid 131 and name c) (resid 132 and name n)
(resid 132 and name ca) (resid 132 and name c) 1.0 -104.029 51.96 2
assign (resid 132 and name n) (resid 132 and name ca)
(resid 132 and name c) (resid 133 and name n) 1.0 -9.411 26.94 2
assign (resid 331 and name c) (resid 332 and name n)
(resid 332 and name ca) (resid 332 and name c) 1.0 -104.029 51.96 2
assign (resid 332 and name n) (resid 332 and name ca)

(resid 332 and name c) (resid 333 and name n) 1.0 -9.411 26.94 2

assign (resid 132 and name c) (resid 133 and name n)
(resid 133 and name ca) (resid 133 and name c) 1.0 -78.934 53.16 2
assign (resid 133 and name n) (resid 133 and name ca)
(resid 133 and name c) (resid 134 and name n) 1.0 -34.191 22.80 2
assign (resid 332 and name c) (resid 333 and name n)
(resid 333 and name ca) (resid 333 and name c) 1.0 -78.934 53.16 2
assign (resid 333 and name n) (resid 333 and name ca)
(resid 333 and name c) (resid 334 and name n) 1.0 -34.191 22.80 2

assign (resid 133 and name c) (resid 134 and name n)
(resid 134 and name ca) (resid 134 and name c) 1.0 -59.292 11.27 2
assign (resid 134 and name n) (resid 134 and name ca)
(resid 134 and name c) (resid 135 and name n) 1.0 -42.920 12.37 2
assign (resid 333 and name c) (resid 334 and name n)
(resid 334 and name ca) (resid 334 and name c) 1.0 -59.292 11.27 2
assign (resid 334 and name n) (resid 334 and name ca)
(resid 334 and name c) (resid 335 and name n) 1.0 -42.920 12.37 2

assign (resid 134 and name c) (resid 135 and name n)
(resid 135 and name ca) (resid 135 and name c) 1.0 -66.242 12.51 2
assign (resid 135 and name n) (resid 135 and name ca)
(resid 135 and name c) (resid 136 and name n) 1.0 -43.284 22.18 2
assign (resid 334 and name c) (resid 335 and name n)
(resid 335 and name ca) (resid 335 and name c) 1.0 -66.242 12.51 2
assign (resid 335 and name n) (resid 335 and name ca)
(resid 335 and name c) (resid 336 and name n) 1.0 -43.284 22.18 2

assign (resid 135 and name c) (resid 136 and name n)
(resid 136 and name ca) (resid 136 and name c) 1.0 -61.124 11.05 2
assign (resid 136 and name n) (resid 136 and name ca)
(resid 136 and name c) (resid 137 and name n) 1.0 -34.939 27.31 2
assign (resid 335 and name c) (resid 336 and name n)
(resid 336 and name ca) (resid 336 and name c) 1.0 -61.124 11.05 2
assign (resid 336 and name n) (resid 336 and name ca)
(resid 336 and name c) (resid 337 and name n) 1.0 -34.939 27.31 2

assign (resid 136 and name c) (resid 137 and name n)
(resid 137 and name ca) (resid 137 and name c) 1.0 -61.135 8.31 2
assign (resid 137 and name n) (resid 137 and name ca)

(resid 137 and name c) (resid 138 and name n) 1.0 -44.125 14.75 2
assign (resid 336 and name c) (resid 337 and name n)
(resid 337 and name ca) (resid 337 and name c) 1.0 -61.135 8.31 2
assign (resid 337 and name n) (resid 337 and name ca)
(resid 337 and name c) (resid 338 and name n) 1.0 -44.125 14.75 2

assign (resid 137 and name c) (resid 138 and name n)
(resid 138 and name ca) (resid 138 and name c) 1.0 -65.341 19.62 2
assign (resid 138 and name n) (resid 138 and name ca)
(resid 138 and name c) (resid 139 and name n) 1.0 -34.248 20.98 2
assign (resid 337 and name c) (resid 338 and name n)
(resid 338 and name ca) (resid 338 and name c) 1.0 -65.341 19.62 2
assign (resid 338 and name n) (resid 338 and name ca)
(resid 338 and name c) (resid 339 and name n) 1.0 -34.248 20.98 2

assign (resid 138 and name c) (resid 139 and name n)
(resid 139 and name ca) (resid 139 and name c) 1.0 -87.024 30.51 2
assign (resid 139 and name n) (resid 139 and name ca)
(resid 139 and name c) (resid 140 and name n) 1.0 -13.390 55.61 2
assign (resid 338 and name c) (resid 339 and name n)
(resid 339 and name ca) (resid 339 and name c) 1.0 -87.024 30.51 2
assign (resid 339 and name n) (resid 339 and name ca)
(resid 339 and name c) (resid 340 and name n) 1.0 -13.390 55.61 2

assign (resid 139 and name c) (resid 140 and name n)
(resid 140 and name ca) (resid 140 and name c) 1.0 -62.373 19.93 2
assign (resid 140 and name n) (resid 140 and name ca)
(resid 140 and name c) (resid 141 and name n) 1.0 -38.907 21.30 2
assign (resid 339 and name c) (resid 340 and name n)
(resid 340 and name ca) (resid 340 and name c) 1.0 -62.373 19.93 2
assign (resid 340 and name n) (resid 340 and name ca)
(resid 340 and name c) (resid 341 and name n) 1.0 -38.907 21.30 2

assign (resid 140 and name c) (resid 141 and name n)
(resid 141 and name ca) (resid 141 and name c) 1.0 -62.523 7.38 2
assign (resid 141 and name n) (resid 141 and name ca)
(resid 141 and name c) (resid 142 and name n) 1.0 -40.807 13.36 2
assign (resid 340 and name c) (resid 341 and name n)
(resid 341 and name ca) (resid 341 and name c) 1.0 -62.523 7.38 2
assign (resid 341 and name n) (resid 341 and name ca)
(resid 341 and name c) (resid 342 and name n) 1.0 -40.807 13.36 2

assign (resid 141 and name c) (resid 142 and name n)
(resid 142 and name ca) (resid 142 and name c) 1.0 -64.420 12.85 2
assign (resid 142 and name n) (resid 142 and name ca)
(resid 142 and name c) (resid 143 and name n) 1.0 -44.052 9.04 2
assign (resid 341 and name c) (resid 342 and name n)
(resid 342 and name ca) (resid 342 and name c) 1.0 -64.420 12.85 2
assign (resid 342 and name n) (resid 342 and name ca)
(resid 342 and name c) (resid 343 and name n) 1.0 -44.052 9.04 2

assign (resid 142 and name c) (resid 143 and name n)
(resid 143 and name ca) (resid 143 and name c) 1.0 -64.090 10.97 2
assign (resid 143 and name n) (resid 143 and name ca)
(resid 143 and name c) (resid 144 and name n) 1.0 -40.436 13.55 2
assign (resid 342 and name c) (resid 343 and name n)
(resid 343 and name ca) (resid 343 and name c) 1.0 -64.090 10.97 2
assign (resid 343 and name n) (resid 343 and name ca)
(resid 343 and name c) (resid 344 and name n) 1.0 -40.436 13.55 2

assign (resid 143 and name c) (resid 144 and name n)
(resid 144 and name ca) (resid 144 and name c) 1.0 -63.406 10.96 2
assign (resid 144 and name n) (resid 144 and name ca)
(resid 144 and name c) (resid 145 and name n) 1.0 -44.176 14.95 2
assign (resid 343 and name c) (resid 344 and name n)
(resid 344 and name ca) (resid 344 and name c) 1.0 -63.406 10.96 2
assign (resid 344 and name n) (resid 344 and name ca)
(resid 344 and name c) (resid 345 and name n) 1.0 -44.176 14.95 2

assign (resid 144 and name c) (resid 145 and name n)
(resid 145 and name ca) (resid 145 and name c) 1.0 -61.988 10.15 2
assign (resid 145 and name n) (resid 145 and name ca)
(resid 145 and name c) (resid 146 and name n) 1.0 -33.250 18.04 2
assign (resid 344 and name c) (resid 345 and name n)
(resid 345 and name ca) (resid 345 and name c) 1.0 -61.988 10.15 2
assign (resid 345 and name n) (resid 345 and name ca)
(resid 345 and name c) (resid 346 and name n) 1.0 -33.250 18.04 2

assign (resid 145 and name c) (resid 146 and name n)
(resid 146 and name ca) (resid 146 and name c) 1.0 -76.806 23.19 2
assign (resid 146 and name n) (resid 146 and name ca)
(resid 146 and name c) (resid 147 and name n) 1.0 -32.127 14.78 2

assign (resid 345 and name c) (resid 346 and name n)
(resid 346 and name ca) (resid 346 and name c) 1.0 -76.806 23.19 2
assign (resid 346 and name n) (resid 346 and name ca)
(resid 346 and name c) (resid 347 and name n) 1.0 -32.127 14.78 2

assign (resid 146 and name c) (resid 147 and name n)
(resid 147 and name ca) (resid 147 and name c) 1.0 -110.926 47.24 2
assign (resid 147 and name n) (resid 147 and name ca)
(resid 147 and name c) (resid 148 and name n) 1.0 -7.345 42.23 2
assign (resid 346 and name c) (resid 347 and name n)
(resid 347 and name ca) (resid 347 and name c) 1.0 -110.926 47.24 2
assign (resid 347 and name n) (resid 347 and name ca)
(resid 347 and name c) (resid 348 and name n) 1.0 -7.345 42.23 2

assign (resid 147 and name c) (resid 148 and name n)
(resid 148 and name ca) (resid 148 and name c) 1.0 -92.554 51.92 2
assign (resid 148 and name n) (resid 148 and name ca)
(resid 148 and name c) (resid 149 and name n) 1.0 -37.175 33.78 2
assign (resid 347 and name c) (resid 348 and name n)
(resid 348 and name ca) (resid 348 and name c) 1.0 -92.554 51.92 2
assign (resid 348 and name n) (resid 348 and name ca)
(resid 348 and name c) (resid 349 and name n) 1.0 -37.175 33.78 2

assign (resid 148 and name c) (resid 149 and name n)
(resid 149 and name ca) (resid 149 and name c) 1.0 -71.776 21.69 2
assign (resid 149 and name n) (resid 149 and name ca)
(resid 149 and name c) (resid 150 and name n) 1.0 -36.144 14.91 2
assign (resid 348 and name c) (resid 349 and name n)
(resid 349 and name ca) (resid 349 and name c) 1.0 -71.776 21.69 2
assign (resid 349 and name n) (resid 349 and name ca)
(resid 349 and name c) (resid 350 and name n) 1.0 -36.144 14.91 2

assign (resid 149 and name c) (resid 150 and name n)
(resid 150 and name ca) (resid 150 and name c) 1.0 -97.226 48.53 2
assign (resid 150 and name n) (resid 150 and name ca)
(resid 150 and name c) (resid 151 and name n) 1.0 -10.033 58.08 2
assign (resid 349 and name c) (resid 350 and name n)
(resid 350 and name ca) (resid 350 and name c) 1.0 -97.226 48.53 2
assign (resid 350 and name n) (resid 350 and name ca)
(resid 350 and name c) (resid 351 and name n) 1.0 -10.033 58.08 2

assign (resid 150 and name c) (resid 151 and name n)
(resid 151 and name ca) (resid 151 and name c) 1.0 -63.710 25.40 2
assign (resid 151 and name n) (resid 151 and name ca)
(resid 151 and name c) (resid 152 and name n) 1.0 -43.864 22.56 2
assign (resid 350 and name c) (resid 351 and name n)
(resid 351 and name ca) (resid 351 and name c) 1.0 -63.710 25.40 2
assign (resid 351 and name n) (resid 351 and name ca)
(resid 351 and name c) (resid 352 and name n) 1.0 -43.864 22.56 2

assign (resid 224 and name c) (resid 225 and name n)
(resid 225 and name ca) (resid 225 and name c) 1.0 -54.743 9.20 2
assign (resid 225 and name n) (resid 225 and name ca)
(resid 225 and name c) (resid 226 and name n) 1.0 -35.243 6.36 2
assign (resid 424 and name c) (resid 425 and name n)
(resid 425 and name ca) (resid 425 and name c) 1.0 -54.743 9.20 2
assign (resid 425 and name n) (resid 425 and name ca)
(resid 425 and name c) (resid 426 and name n) 1.0 -35.243 6.36 2

assign (resid 225 and name c) (resid 226 and name n)
(resid 226 and name ca) (resid 226 and name c) 1.0 -62.669 12.21 2
assign (resid 226 and name n) (resid 226 and name ca)
(resid 226 and name c) (resid 227 and name n) 1.0 -37.235 22.54 2
assign (resid 425 and name c) (resid 426 and name n)
(resid 426 and name ca) (resid 426 and name c) 1.0 -62.669 12.21 2
assign (resid 426 and name n) (resid 426 and name ca)
(resid 426 and name c) (resid 427 and name n) 1.0 -37.235 22.54 2

assign (resid 226 and name c) (resid 227 and name n)
(resid 227 and name ca) (resid 227 and name c) 1.0 -66.183 15.89 2
assign (resid 227 and name n) (resid 227 and name ca)
(resid 227 and name c) (resid 228 and name n) 1.0 -45.101 9.69 2
assign (resid 426 and name c) (resid 427 and name n)
(resid 427 and name ca) (resid 427 and name c) 1.0 -66.183 15.89 2
assign (resid 427 and name n) (resid 427 and name ca)
(resid 427 and name c) (resid 428 and name n) 1.0 -45.101 9.69 2

assign (resid 227 and name c) (resid 228 and name n)
(resid 228 and name ca) (resid 228 and name c) 1.0 -61.290 11.25 2
assign (resid 228 and name n) (resid 228 and name ca)
(resid 228 and name c) (resid 229 and name n) 1.0 -41.100 17.88 2
assign (resid 427 and name c) (resid 428 and name n)

(resid 428 and name ca) (resid 428 and name c) 1.0 -61.290 11.25 2
assign (resid 428 and name n) (resid 428 and name ca)
(resid 428 and name c) (resid 429 and name n) 1.0 -41.100 17.88 2

assign (resid 228 and name c) (resid 229 and name n)
(resid 229 and name ca) (resid 229 and name c) 1.0 -62.155 18.92 2
assign (resid 229 and name n) (resid 229 and name ca)
(resid 229 and name c) (resid 230 and name n) 1.0 -43.003 20.43 2
assign (resid 428 and name c) (resid 429 and name n)
(resid 429 and name ca) (resid 429 and name c) 1.0 -62.155 18.92 2
assign (resid 429 and name n) (resid 429 and name ca)
(resid 429 and name c) (resid 430 and name n) 1.0 -43.003 20.43 2

assign (resid 229 and name c) (resid 230 and name n)
(resid 230 and name ca) (resid 230 and name c) 1.0 -63.370 16.04 2
assign (resid 230 and name n) (resid 230 and name ca)
(resid 230 and name c) (resid 231 and name n) 1.0 -37.108 16.23 2
assign (resid 429 and name c) (resid 430 and name n)
(resid 430 and name ca) (resid 430 and name c) 1.0 -63.370 16.04 2
assign (resid 430 and name n) (resid 430 and name ca)
(resid 430 and name c) (resid 431 and name n) 1.0 -37.108 16.23 2

assign (resid 230 and name c) (resid 231 and name n)
(resid 231 and name ca) (resid 231 and name c) 1.0 -65.096 17.68 2
assign (resid 231 and name n) (resid 231 and name ca)
(resid 231 and name c) (resid 232 and name n) 1.0 -41.820 12.70 2
assign (resid 430 and name c) (resid 431 and name n)
(resid 431 and name ca) (resid 431 and name c) 1.0 -65.096 17.68 2
assign (resid 431 and name n) (resid 431 and name ca)
(resid 431 and name c) (resid 432 and name n) 1.0 -41.820 12.70 2

assign (resid 231 and name c) (resid 232 and name n)
(resid 232 and name ca) (resid 232 and name c) 1.0 -60.894 11.25 2
assign (resid 232 and name n) (resid 232 and name ca)
(resid 232 and name c) (resid 233 and name n) 1.0 -41.688 16.10 2
assign (resid 431 and name c) (resid 432 and name n)
(resid 432 and name ca) (resid 432 and name c) 1.0 -60.894 11.25 2
assign (resid 432 and name n) (resid 432 and name ca)
(resid 432 and name c) (resid 433 and name n) 1.0 -41.688 16.10 2

assign (resid 232 and name c) (resid 233 and name n)

(resid 233 and name ca) (resid 233 and name c) 1.0 -61.975 8.66 2
assign (resid 233 and name n) (resid 233 and name ca)
(resid 233 and name c) (resid 234 and name n) 1.0 -42.654 8.80 2
assign (resid 432 and name c) (resid 433 and name n)
(resid 433 and name ca) (resid 433 and name c) 1.0 -61.975 8.66 2
assign (resid 433 and name n) (resid 433 and name ca)
(resid 433 and name c) (resid 434 and name n) 1.0 -42.654 8.80 2

assign (resid 233 and name c) (resid 234 and name n)
(resid 234 and name ca) (resid 234 and name c) 1.0 -63.278 6.35 2
assign (resid 234 and name n) (resid 234 and name ca)
(resid 234 and name c) (resid 235 and name n) 1.0 -41.626 13.37 2
assign (resid 433 and name c) (resid 434 and name n)
(resid 434 and name ca) (resid 434 and name c) 1.0 -63.278 6.35 2
assign (resid 434 and name n) (resid 434 and name ca)
(resid 434 and name c) (resid 435 and name n) 1.0 -41.626 13.37 2

assign (resid 234 and name c) (resid 235 and name n)
(resid 235 and name ca) (resid 235 and name c) 1.0 -62.511 12.14 2
assign (resid 235 and name n) (resid 235 and name ca)
(resid 235 and name c) (resid 236 and name n) 1.0 -40.892 9.66 2
assign (resid 434 and name c) (resid 435 and name n)
(resid 435 and name ca) (resid 435 and name c) 1.0 -62.511 12.14 2
assign (resid 435 and name n) (resid 435 and name ca)
(resid 435 and name c) (resid 436 and name n) 1.0 -40.892 9.66 2

assign (resid 235 and name c) (resid 236 and name n)
(resid 236 and name ca) (resid 236 and name c) 1.0 -60.727 5.53 2
assign (resid 236 and name n) (resid 236 and name ca)
(resid 236 and name c) (resid 237 and name n) 1.0 -41.190 8.77 2
assign (resid 435 and name c) (resid 436 and name n)
(resid 436 and name ca) (resid 436 and name c) 1.0 -60.727 5.53 2
assign (resid 436 and name n) (resid 436 and name ca)
(resid 436 and name c) (resid 437 and name n) 1.0 -41.190 8.77 2

assign (resid 236 and name c) (resid 237 and name n)
(resid 237 and name ca) (resid 237 and name c) 1.0 -63.974 9.83 2
assign (resid 237 and name n) (resid 237 and name ca)
(resid 237 and name c) (resid 238 and name n) 1.0 -40.368 9.57 2
assign (resid 436 and name c) (resid 437 and name n)
(resid 437 and name ca) (resid 437 and name c) 1.0 -63.974 9.83 2

assign (resid 437 and name n) (resid 437 and name ca)
(resid 437 and name c) (resid 438 and name n) 1.0 -40.368 9.57 2

assign (resid 237 and name c) (resid 238 and name n)
(resid 238 and name ca) (resid 238 and name c) 1.0 -64.898 11.04 2
assign (resid 238 and name n) (resid 238 and name ca)
(resid 238 and name c) (resid 239 and name n) 1.0 -41.620 10.38 2
assign (resid 437 and name c) (resid 438 and name n)
(resid 438 and name ca) (resid 438 and name c) 1.0 -64.898 11.04 2
assign (resid 438 and name n) (resid 438 and name ca)
(resid 438 and name c) (resid 439 and name n) 1.0 -41.620 10.38 2

assign (resid 238 and name c) (resid 239 and name n)
(resid 239 and name ca) (resid 239 and name c) 1.0 -61.963 6.76 2
assign (resid 239 and name n) (resid 239 and name ca)
(resid 239 and name c) (resid 240 and name n) 1.0 -46.175 7.99 2
assign (resid 438 and name c) (resid 439 and name n)
(resid 439 and name ca) (resid 439 and name c) 1.0 -61.963 6.76 2
assign (resid 439 and name n) (resid 439 and name ca)
(resid 439 and name c) (resid 440 and name n) 1.0 -46.175 7.99 2

assign (resid 239 and name c) (resid 240 and name n)
(resid 240 and name ca) (resid 240 and name c) 1.0 -63.049 5.79 2
assign (resid 240 and name n) (resid 240 and name ca)
(resid 240 and name c) (resid 241 and name n) 1.0 -36.830 15.32 2
assign (resid 439 and name c) (resid 440 and name n)
(resid 440 and name ca) (resid 440 and name c) 1.0 -63.049 5.79 2
assign (resid 440 and name n) (resid 440 and name ca)
(resid 440 and name c) (resid 441 and name n) 1.0 -36.830 15.32 2

assign (resid 240 and name c) (resid 241 and name n)
(resid 241 and name ca) (resid 241 and name c) 1.0 -67.355 17.31 2
assign (resid 241 and name n) (resid 241 and name ca)
(resid 241 and name c) (resid 242 and name n) 1.0 -41.243 14.12 2
assign (resid 440 and name c) (resid 441 and name n)
(resid 441 and name ca) (resid 441 and name c) 1.0 -67.355 17.31 2
assign (resid 441 and name n) (resid 441 and name ca)
(resid 441 and name c) (resid 442 and name n) 1.0 -41.243 14.12 2

assign (resid 241 and name c) (resid 242 and name n)
(resid 242 and name ca) (resid 242 and name c) 1.0 -60.937 6.57 2

assign (resid 242 and name n) (resid 242 and name ca)
(resid 242 and name c) (resid 243 and name n) 1.0 -44.962 12.99 2
assign (resid 441 and name c) (resid 442 and name n)
(resid 442 and name ca) (resid 442 and name c) 1.0 -60.937 6.57 2
assign (resid 442 and name n) (resid 442 and name ca)
(resid 442 and name c) (resid 443 and name n) 1.0 -44.962 12.99 2

assign (resid 242 and name c) (resid 243 and name n)
(resid 243 and name ca) (resid 243 and name c) 1.0 -66.535 39.70 2
assign (resid 243 and name n) (resid 243 and name ca)
(resid 243 and name c) (resid 244 and name n) 1.0 -39.344 23.71 2
assign (resid 442 and name c) (resid 443 and name n)
(resid 443 and name ca) (resid 443 and name c) 1.0 -66.535 39.70 2
assign (resid 443 and name n) (resid 443 and name ca)
(resid 443 and name c) (resid 444 and name n) 1.0 -39.344 23.71 2

Hydrogen Bonds:

assign (segid AN1 and resid 125 and name O) (segid AN1 and resid 129 and name HN) 2.00 0.20 0.20
assign (segid AN2 and resid 225 and name O) (segid AN2 and resid 229 and name HN) 2.00 0.20 0.20
assign (segid AN3 and resid 325 and name O) (segid AN3 and resid 329 and name HN) 2.00 0.20 0.20
assign (segid AN4 and resid 425 and name O) (segid AN4 and resid 429 and name HN) 2.00 0.20 0.20
assign (segid AN1 and resid 125 and name O) (segid AN1 and resid 129 and name N) 3.00 0.20 0.20
assign (segid AN2 and resid 225 and name O) (segid AN2 and resid 229 and name N) 3.00 0.20 0.20
assign (segid AN3 and resid 325 and name O) (segid AN3 and resid 329 and name N) 3.00 0.20 0.20
assign (segid AN4 and resid 425 and name O) (segid AN4 and resid 429 and name N) 3.00 0.20 0.20
assign (segid AN1 and resid 126 and name O) (segid AN1 and resid 130 and name HN) 2.00 0.20 0.20
assign (segid AN2 and resid 226 and name O) (segid AN2 and resid 230 and name HN) 2.00 0.20 0.20
assign (segid AN3 and resid 326 and name O) (segid AN3 and resid 330 and name HN) 2.00 0.20 0.20
assign (segid AN4 and resid 426 and name O) (segid AN4 and resid 430 and name HN) 2.00 0.20 0.20
assign (segid AN1 and resid 126 and name O) (segid AN1 and resid 130 and name N) 3.00 0.20 0.20
assign (segid AN2 and resid 226 and name O) (segid AN2 and resid 230 and name N) 3.00 0.20 0.20
assign (segid AN3 and resid 326 and name O) (segid AN3 and resid 330 and name N) 3.00 0.20 0.20
assign (segid AN4 and resid 426 and name O) (segid AN4 and resid 430 and name N) 3.00 0.20 0.20
assign (segid AN1 and resid 127 and name O) (segid AN1 and resid 131 and name HN) 2.00 0.20 0.20
assign (segid AN2 and resid 227 and name O) (segid AN2 and resid 231 and name HN) 2.00 0.20 0.20
assign (segid AN3 and resid 327 and name O) (segid AN3 and resid 331 and name HN) 2.00 0.20 0.20
assign (segid AN4 and resid 427 and name O) (segid AN4 and resid 431 and name HN) 2.00 0.20 0.20
assign (segid AN1 and resid 127 and name O) (segid AN1 and resid 131 and name N) 3.00 0.20 0.20
assign (segid AN2 and resid 227 and name O) (segid AN2 and resid 231 and name N) 3.00 0.20 0.20
assign (segid AN3 and resid 327 and name O) (segid AN3 and resid 331 and name N) 3.00 0.20 0.20
assign (segid AN4 and resid 427 and name O) (segid AN4 and resid 431 and name N) 3.00 0.20 0.20

assign (segid AN4 and resid 443 and name O) (segid AN4 and resid 447 and name N) 3.00 0.20 0.20
 assign (segid AN1 and resid 147 and name O) (segid AN1 and resid 151 and name HN) 2.00 0.20 0.20
 assign (segid AN3 and resid 347 and name O) (segid AN3 and resid 351 and name HN) 2.00 0.20 0.20
 assign (segid AN1 and resid 147 and name O) (segid AN1 and resid 151 and name N) 3.00 0.20 0.20
 assign (segid AN3 and resid 347 and name O) (segid AN3 and resid 351 and name N) 3.00 0.20 0.20
 assign (segid AN1 and resid 148 and name O) (segid AN1 and resid 152 and name HN) 2.00 0.20 0.20
 assign (segid AN3 and resid 348 and name O) (segid AN3 and resid 352 and name HN) 2.00 0.20 0.20
 assign (segid AN1 and resid 148 and name O) (segid AN1 and resid 152 and name N) 3.00 0.20 0.20
 assign (segid AN3 and resid 348 and name O) (segid AN3 and resid 352 and name N) 3.00 0.20 0.20
 assign (segid AN1 and resid 149 and name O) (segid AN1 and resid 153 and name HN) 2.00 0.20 0.20
 assign (segid AN3 and resid 349 and name O) (segid AN3 and resid 353 and name HN) 2.00 0.20 0.20
 assign (segid AN1 and resid 149 and name O) (segid AN1 and resid 153 and name N) 3.00 0.20 0.20
 assign (segid AN3 and resid 349 and name O) (segid AN3 and resid 353 and name N) 3.00 0.20 0.20
 assign (segid AN1 and resid 150 and name O) (segid AN1 and resid 154 and name HN) 2.00 0.50 0.50
 assign (segid AN3 and resid 350 and name O) (segid AN3 and resid 354 and name HN) 2.00 0.50 0.50
 assign (segid AN1 and resid 150 and name O) (segid AN1 and resid 154 and name N) 3.00 0.50 0.50
 assign (segid AN3 and resid 350 and name O) (segid AN3 and resid 354 and name N) 3.00 0.50 0.50
 assign (segid AN1 and resid 151 and name O) (segid AN1 and resid 155 and name HN) 2.00 0.50 0.50
 assign (segid AN3 and resid 351 and name O) (segid AN3 and resid 355 and name HN) 2.00 0.50 0.50
 assign (segid AN1 and resid 151 and name O) (segid AN1 and resid 155 and name N) 3.00 0.50 0.50
 assign (segid AN3 and resid 351 and name O) (segid AN3 and resid 355 and name N) 3.00 0.50 0.50
 assign (segid AN1 and resid 152 and name O) (segid AN1 and resid 156 and name HN) 2.00 0.50 0.50
 assign (segid AN3 and resid 352 and name O) (segid AN3 and resid 356 and name HN) 2.00 0.50 0.50
 assign (segid AN1 and resid 152 and name O) (segid AN1 and resid 156 and name N) 3.00 0.50 0.50
 assign (segid AN3 and resid 352 and name O) (segid AN3 and resid 356 and name N) 3.00 0.50 0.50

¹⁵N-¹³C TEDOR:

assign (resid 234 and name N) (resid 138 and name Cd1 or resid 338 and name Cd1) 5.0 3.0 0.50
 assign (resid 237 and name Ne2) (resid 338 and name Cd2 or resid 138 and name Cd2) 5.0 3.0 0.50
 assign (resid 137 and name Ne2) (resid 438 and name Cd2 or resid 238 and name Cd2) 5.0 3.0 0.50
 assign (resid 137 and name Ne2) (resid 438 and name Cd1 or resid 238 and name Cd1) 5.0 3.0 0.50
 assign (resid 231 and name N) (resid 135 and name Cg2 or resid 335 and name Cg2) 5.0 3.0 0.50
 assign (resid 231 and name N) (resid 135 and name Cd1 or resid 335 and name Cd1) 5.0 3.0 0.50
 assign (resid 134 and name N) (resid 235 and name Cd1 or resid 435 and name Cd1) 5.0 3.0 0.50

assign (resid 231 and name Nd2)	(resid 135 and name Cg2)	5.0 3.0 0.50
(resid 135 and name Cg2)	OR (resid 231 and name N)	OR (resid 126 and name Cd1)
5.0 3.0 0.50	(resid 335 and name Cg2)	(resid 329 and name N)
OR (resid 231 and name Nd2)		OR (resid 126 and name Cd1)
(resid 335 and name Cg2)	assign (resid 126 and name Cd1)	(resid 136 and name N)
OR (resid 231 and name N)	(resid 129 and name N)	OR (resid 126 and name Cd1)

OR (resid 228 and name Cg1) (resid 336 and name N)	OR (resid 228 and name Cg1) (resid 330 and name N)	OR (resid 136 and name Cd2) (resid 432 and name N)
OR (resid 228 and name Cg1) (resid 239 and name N)	OR (resid 228 and name Cg1) (resid 227 and name N)	OR (resid 136 and name Cd2) (resid 240 and name N)
OR (resid 228 and name Cg1) (resid 439 and name N)	OR (resid 228 and name Cg1) (resid 427 and name N)	OR (resid 136 and name Cd2) (resid 440 and name N)
OR (resid 228 and name Cg1) (resid 228 and name N)	OR (resid 228 and name Cg1) (resid 337 and name N)	OR (resid 136 and name Cd2) (resid 237 and name N)
OR (resid 228 and name Cg1) (resid 428 and name N)	OR (resid 228 and name Cg1) (resid 337 and name N)	OR (resid 136 and name Cd2) (resid 437 and name N)
OR (resid 228 and name Cg1) (resid 232 and name N)	OR (resid 136 and name Cd2) (resid 136 and name N)	OR (resid 136 and name Cd2) (resid 130 and name N)
OR (resid 228 and name Cg1) (resid 432 and name N)	OR (resid 136 and name Cd2) (resid 336 and name N)	OR (resid 136 and name Cd2) (resid 330 and name N)
OR (resid 228 and name Cg1) (resid 240 and name N)	OR (resid 136 and name Cd2) (resid 239 and name N)	OR (resid 136 and name Cd2) (resid 227 and name N)
OR (resid 228 and name Cg1) (resid 440 and name N)	OR (resid 136 and name Cd2) (resid 439 and name N)	OR (resid 136 and name Cd2) (resid 427 and name N)
OR (resid 228 and name Cg1) (resid 237 and name N)	OR (resid 136 and name Cd2) (resid 228 and name N)	OR (resid 136 and name Cd2) (resid 337 and name N)
OR (resid 228 and name Cg1) (resid 437 and name N)	OR (resid 136 and name Cd2) (resid 428 and name N)	OR (resid 136 and name Cd2) (resid 337 and name N)
OR (resid 228 and name Cg1) (resid 130 and name N)	OR (resid 136 and name Cd2) (resid 232 and name N)	

PDS

assign (resid 231 and name Ca) (resid 227 and name Ca) 5.46273056504 4.91645750854 2.46305427862 ! 11998539

assign (resid 231 and name Ca) (resid 228 and name Ca) 5.02358001459 4.52122201313 2.34543890585 ! 15428288

assign (resid 231 and name Cb) (resid 234 and name Ca) 6.45493633883 5.80944270495 2.72879151119 ! 7272468

assign (resid 231 and name Cb or resid 431 and name Cb) (resid 134 and name Ca) 5.8 5.2 2.55 ! 9961517

assign (resid 231 and name Cb or resid 431 and name Cb) (resid 334 and name Ca) 5.8 5.2 2.55 ! 9961517

assign (resid 234 and name Ca) (resid 231 and name Ca) 5.59511355623 5.03560220061 2.49850971604 ! 11166858

assign (resid 234 and name Ca) (resid 231 and name Cb) 6.51200852951 5.86080767656 2.74407685463 ! 7082928

assign (resid 234 and name Ca) (resid 237 and name Ca) 5.70440224027 5.13396201624 2.52777992714 ! 10537250

assign (resid 234 and name Ca or resid 434 and name Ca) (resid 137 and name Ca) 5.76 5.18 2.5 ! 10222989

assign (resid 234 and name Ca or resid 434 and name Ca) (resid 337 and name Ca) 5.76 5.18 2.5 ! 10222989

assign (resid 134 and name Ca or resid 334 and name Ca) (resid 231 and name Ca) 5.0 4.5 2.3 ! 15276946

assign (resid 134 and name Ca or resid 334 and name Ca) (resid 431 and name Ca) 5.0 4.5 2.3 ! 15276946

assign (resid 134 and name Ca or resid 334 and name Ca) (resid 231 and name Cb) 5.485 4.9 2.469 ! 11849913

assign (resid 134 and name Ca or resid 334 and name Ca) (resid 431 and name Cb) 5.485 4.9 2.469 ! 11849913

assign (resid 134 and name Ca) (resid 137 and name Ca) 5.02451181722 4.5220606355 2.34568846562 ! 15419706
assign (resid 237 and name Cd2 or resid 437 and name Cd2) (resid 137 and name Cd2) 7.3 6.6 2.968 ! 4927182
assign (resid 237 and name Cd2 or resid 437 and name Cd2) (resid 337 and name Cd2) 7.3 6.6 2.968 ! 4927182
assign (resid 237 and name Cd2 or resid 437 and name Cd2) (resid 137 and name Ce1) 5.9 5.3 2.585 ! 9434372
assign (resid 237 and name Cd2 or resid 437 and name Cd2) (resid 337 and name Ce1) 5.9 5.3 2.585 ! 9434372
assign (resid 141 and name Ch2 or resid 341 and name Ch2) (resid 241 and name Cd1) 7.9 7.1 3.1 ! 3938815
assign (resid 141 and name Ch2 or resid 341 and name Ch2) (resid 441 and name Cd1) 7.9 7.1 3.1 ! 3938815
assign (resid 149 and name Ca) (resid 150 and name Ca) 5.01055051588 4.50949546429 2.34194928401 ! 15548961

¹³C-¹³C PAR

assign (resid 125 and name Ca) (resid 128 and name Ca) 5.92247536514 5.33022782863 2.41260293034 ! 1528787
assign (resid 325 and name Ca) (resid 328 and name Ca) 5.92247536514 5.33022782863 2.41260293034 ! 1528787
assign (resid 227 and name Ca) (resid 230 and name Ca) 4.8715154802 4.38436393218 2.16193257351 ! 2747037
assign (resid 427 and name Ca) (resid 430 and name Ca) 4.8715154802 4.38436393218 2.16193257351 ! 2747037
assign (resid 227 and name Cb) (resid 231 and name Cb) 6.38455345361 5.74609810825 2.52281577575 ! 1220296
assign (resid 427 and name Cb) (resid 431 and name Cb) 6.38455345361 5.74609810825 2.52281577575 ! 1220296
assign (resid 227 and name Cg1) (resid 231 and name Cb) 4.88887444479 4.39998700031 2.16607295785 ! 2717879
assign (resid 427 and name Cg1) (resid 431 and name Cb) 4.88887444479 4.39998700031 2.16607295785 ! 2717879
assign (resid 128 and name Cg2) (resid 125 and name Cg) 4.84782964214 4.36304667793 2.15628313097 ! 2787499
assign (resid 328 and name Cg2) (resid 325 and name Cg) 4.84782964214 4.36304667793 2.15628313097 ! 2787499
assign (resid 228 and name Cb) (resid 231 and name Ca) 5.31819105753 4.78637195178 2.26847167929 ! 2111373
assign (resid 428 and name Cb) (resid 431 and name Ca) 5.31819105753 4.78637195178 2.26847167929 ! 2111373
assign (resid 228 and name Cg2) (resid 231 and name Ca) 4.53652020236 4.08286818212 2.08203096447 ! 3401639
assign (resid 428 and name Cg2) (resid 431 and name Ca) 4.53652020236 4.08286818212 2.08203096447 ! 3401639
assign (resid 228 and name Cg2) (resid 231 and name Cb) 4.88887444479 4.39998700031 2.16607295785 ! 2717879
assign (resid 428 and name Cg2) (resid 431 and name Cb) 4.88887444479 4.39998700031 2.16607295785 ! 2717879
assign (resid 228 and name Cg1) (resid 231 and name Ca) 4.29499394132 3.86549454719 2.02442317667 ! 4008382
assign (resid 428 and name Cg1) (resid 431 and name Ca) 4.29499394132 3.86549454719 2.02442317667 ! 4008382
assign (resid 229 and name Cb) (resid 228 and name Ca) 3.50145506407 3.15130955766 1.83515175311 ! 7397945
assign (resid 429 and name Cb) (resid 428 and name Ca) 3.50145506407 3.15130955766 1.83515175311 ! 7397945
assign (resid 130 and name Cb) (resid 127 and name Ca) 3.94054080932 3.54648672839 1.93988056534 ! 5190262
assign (resid 330 and name Cb) (resid 327 and name Ca) 3.94054080932 3.54648672839 1.93988056534 ! 5190262
assign (resid 230 and name Cb) (resid 227 and name Ca) 3.46704483745 3.12034035371 1.82694437631 ! 7620411
assign (resid 430 and name Cb) (resid 427 and name Ca) 3.46704483745 3.12034035371 1.82694437631 ! 7620411
assign (resid 231 and name Cb) (resid 234 and name Ca) 6.39363051276 5.75426746148 2.52498079621 ! 1215106
assign (resid 431 and name Cb) (resid 434 and name Ca) 6.39363051276 5.75426746148 2.52498079621 ! 1215106
assign (resid 231 and name Ca) (resid 228 and name Ca) 5.42978515728 4.88680664155 2.29508861606 ! 1983850
assign (resid 431 and name Ca) (resid 428 and name Ca) 5.42978515728 4.88680664155 2.29508861606 ! 1983850
assign (resid 234 and name Ca) (resid 231 and name Ca) 5.80645457026 5.22580911323 2.38493015761 ! 1622272
assign (resid 434 and name Ca) (resid 431 and name Ca) 5.80645457026 5.22580911323 2.38493015761 ! 1622272
assign (resid 234 and name Ca) (resid 231 and name Cb) 6.32780089739 5.69502080765 2.50927940417 ! 1253425

assign (resid 434 and name Ca) (resid 431 and name Cb) 6.32780089739 5.69502080765 2.50927940417 ! 1253425
assign (resid 234 and name Ca) (resid 237 and name Ca) 4.69279000382 4.22351100344 2.11930375429 ! 3073006
assign (resid 434 and name Ca) (resid 437 and name Ca) 4.69279000382 4.22351100344 2.11930375429 ! 3073006
assign (resid 134 and name Ca) (resid 137 and name Cb) 5.61577879172 5.05420091255 2.33945100457 ! 1793192
assign (resid 334 and name Ca) (resid 337 and name Cb) 5.61577879172 5.05420091255 2.33945100457 ! 1793192
assign (resid 134 and name Ca or resid 334 and name Ca) (resid 231 and name Ca) 5.1 4.6 2.2 ! 2377041
assign (resid 134 and name Ca or resid 334 and name Ca) (resid 431 and name Ca) 5.1 4.6 2.2 ! 2377041
assign (resid 134 and name Ca) (resid 137 and name Ca) 5.44483960822 4.9003556474 2.29867933788 ! 1967440
assign (resid 334 and name Ca) (resid 337 and name Ca) 5.44483960822 4.9003556474 2.29867933788 ! 1967440
assign (resid 237 and name Cb) (resid 234 and name Ca) 5.57950690191 5.02155621172 2.33079959199 ! 1828392
assign (resid 437 and name Cb) (resid 434 and name Ca) 5.57950690191 5.02155621172 2.33079959199 ! 1828392
assign (resid 137 and name Cb) (resid 134 and name Ca) 6.31558729723 5.68402856751 2.50636626965 ! 1260711
assign (resid 337 and name Cb) (resid 334 and name Ca) 6.31558729723 5.68402856751 2.50636626965 ! 1260711
assign (resid 137 and name Ca or resid 337 and name Ca) (resid 237 and name Ca) 6.6577 5.99 2.587969 !107
assign (resid 137 and name Ca or resid 337 and name Ca) (resid 437 and name Ca) 6.6577 5.99 2.587969 !107
assign (resid 137 and name Ca) (resid 141 and name Ca) 6.69773477203 6.02796129483 2.59751441455 ! 1056995
assign (resid 337 and name Ca) (resid 341 and name Ca) 6.69773477203 6.02796129483 2.59751441455 ! 1056995
assign (resid 141 and name Ca) (resid 137 and name Ca) 6.15486271112 5.53937644001 2.46803094408 ! 1362077
assign (resid 341 and name Ca) (resid 337 and name Ca) 6.15486271112 5.53937644001 2.46803094408 ! 1362077
assign (resid 144 and name Cb) (resid 141 and name Ca) 6.22908754252 5.60617878827 2.48573472635 ! 1313964
assign (resid 344 and name Cb) (resid 341 and name Ca) 6.22908754252 5.60617878827 2.48573472635 ! 1313964
assign (resid 144 and name Ca) (resid 141 and name Ca) 5.40620246122 4.8655822151 2.28946377451 ! 2009925
assign (resid 344 and name Ca) (resid 341 and name Ca) 5.40620246122 4.8655822151 2.28946377451 ! 2009925
assign (resid 149 and name Ca) (resid 144 and name Ca) 5.80311305026 5.22280174523 2.38413315287 ! 1625076
assign (resid 349 and name Ca) (resid 344 and name Ca) 5.80311305026 5.22280174523 2.38413315287 ! 1625076

8 ms ¹³C-¹³C RFDR

assign (resid 127 and name Cg2)

(resid 131 and name Cg)

6.44260056343 5.89834050709 1.05636588472 ! 4802294

OR (resid 240 and name Cd2)

(resid 237 and name C)

assign (resid 232 and name Cg1) (resid 231 and name C) 5.17593091077 4.75833781969 0.755175942214 ! 13144601

assign (resid 132 and name Cd1) (resid 131 and name Cg) 6.95878652738 6.36290787464 1.17910508549 ! 3453300

assign (resid 132 and name Cd1) (resid 131 and name C) 8.69803445342 7.92823100808 1.59266514967 ! 1401259

assign (resid 132 and name Cg2) (resid 131 and name Cg) 5.14951034311 4.8345593088 0.511112660906 ! 42397664

assign (resid 233 and name Cg2) (resid 231 and name C) 5.40313872322 5.0628248509 0.571420663915 ! 30340590

assign (resid 136 and name Cd2) (resid 136 and name C) 7.37292619297 6.73563357367 1.27757961814 ! 2714738

assign (resid 237 and name Ce1 or resid 437 and name Ce1) (resid 137 and name Ce1)

5.17300584037 4.65570525633 0.992261389152 ! 5794468

assign (resid 237 and name Ce1 or resid 437 and name Ce1) (resid 141 and name Ce2)

5.32563892814 4.79307503533 1.02855463328 ! 5202472

assign (resid 137 and name Ca) (resid 137 and name Cd2) 4.68942958988 4.22048663089 0.877276157779 ! 8384610
 assign (resid 137 and name Ce1 or resid 337 and name Ce1) (resid 241 and name Ce2)
 5.61103964719 5.04993568247 1.09641749395 ! 4295008
 assign (resid 238 and name Cd1 or resid 438 and name Cd1) (resid 137 and name Cd2)
 5.29466564312 4.76519907881 1.02118977543 ! 5315847
 assign (resid 238 and name Cd1) (resid 241 and name Ce3) 5.88653675349 5.29788307814 1.16192546395 ! 3608752
 assign (resid 238 and name Cd1 or resid 438 and name Cd1) (resid 141 and name Ce2)
 4.78507916923 4.30657125231 0.900019807826 ! 7764896
 assign (resid 238 and name Cd2) (resid 237 and name C) 5.74987981166 5.37489183049 0.65386909731 ! 20249738
 !the above was violating by 0.6 A. Added 1 A
 assign (resid 238 and name Cd2 or resid 438 and name Cd2) (resid 137 and name Cd2)
 4.73294061467 4.2596465532 0.887622251591 ! 8094822
 assign (resid 238 and name Cd2 or resid 438 and name Cd2) (resid 137 and name Ce1)
 3.88368808665 3.59531927798 0.447905186115 ! 62998988
 !to the above, added 1 angstrom due to violation of 0.3 A
 assign (resid 238 and name Cd2) (resid 241 and name Ce2) 5.41460709779 4.87314638801 1.04970957123 ! 4894230
 assign (resid 238 and name Cd2) (resid 241 and name Ce3) 4.2730618446 3.8457556602 0.778271830189 ! 12008753
 assign (resid 238 and name Cd2) (resid 242 and name Ca) 5.15687423615 4.64118681254 0.988425600603 ! 5862190
 assign (resid 138 and name Ca) (resid 137 and name Ce1) 4.53744237114 4.18369813403 0.603355515999 ! 25773416
 assign (resid 138 and name Cd1) (resid 137 and name Cd2) 6.34013912226 5.70612521003 1.26978347657 ! 2765049
 assign (resid 138 and name Cd1) (resid 137 and name Ce1) 6.16439923792 5.54795931413 1.22799587587 ! 3057040
 assign (resid 138 and name Cd2 or resid 338 and name Cd2) (resid 237 and name Cd2) 4.170 3.75 0.753 ! 13209886
 assign (resid 138 and name Cd2 or resid 338 and name Cd2) (resid 237 and name Ce1) 3.321 2.989 0.5519 ! 33667580
 assign (resid 138 and name Cd2) (resid 137 and name Cd2) 4.90110645887 4.41099581298 0.927608889 ! 7092464
 assign (resid 138 and name Cd2) (resid 141 and name Cd1) 4.83986037181 4.35587433463 0.9130457354 ! 7437282
 assign (resid 138 and name Cd2) (resid 141 and name Ce2) 4.845190777 4.36067170012 0.914313204629 ! 7406395
 assign (resid 241 and name Cb) (resid 237 and name Ce1) 6.10484249512 5.49435824561 1.21383441562 ! 3165290
 assign (resid 241 and name Cb) (resid 137 and name Ce1 or resid 337 and name Ce1) 6.3 5.7 1.3 ! 2877499
 assign (resid 141 and name Cb or resid 341 and name Cb) (resid 237 and name Ce1) 5.4203 4.8782 1.0510 ! 4875288
 assign (resid 141 and name Cb) (resid 137 and name Ce1) 4.24971865 3.82474679276 0.772721264695 ! 12269398
 assign (resid 242 and name Ca) (resid 241 and name Ce3) 5.59303373447 5.03373036102 1.09213603051 ! 4345719
 assign (resid 242 and name Cd1) (resid 241 and name Ce3) 6.50361245235 5.85325120712 1.30865432406 ! 2525905
 assign (resid 242 and name Cg1) (resid 241 and name Ce3) 5.12421728858 4.61179555972 0.980660399 ! 6002552
 assign (resid 142 and name Cd1 or resid 342 and name Cd1) (resid 237 and name C) 7.57783 6.9200 1.3263 ! 2426406
 assign (resid 143 and name Cd2) (resid 147 and name Cd1 or resid 147 and name Cd2) 4.5589 4.1030 0.846 ! 9341229
 assign (resid 144 and name Ca) (resid 148 and name Cd1 or resid 148 and name Cd2) 4.979 4.48 0.9461 ! 6682772
 assign (resid 145 and name Ca) (resid 141 and name Ce2) 6.0003916412 5.40035247708 1.18899798994 ! 3367817
 assign (resid 146 and name Ca) (resid 147 and name Cd1 or resid 147 and name Cd2) 5.215 4.693 1.002 ! 5622391
 assign (resid 146 and name Cd1) (resid 147 and name Cd1 or resid 147 and name Cd2) 5.156 4.641 0.9883 ! 5862649
 assign (resid 146 and name Cd2) (resid 147 and name Cd1 or resid 147 and name Cd2) 5.977 5.380 1.183 ! 3413707
 assign (resid 146 and name Cg) (resid 147 and name Cd1 or resid 147 and name Cd2) 5.47 4.921.0646 ! 4690752

assign (resid 151 and name Cd1)
 (resid 147 and name Cd1)
 5.62114610679 5.05903149611 1.09882061775
 OR (resid 151 and name Cd1)
 (resid 147 and name Cd2)
 OR (resid 151 and name Cd1)
 (resid 148 and name Cd1)
 OR (resid 151 and name Cd1)
 (resid 148 and name Cd2)
 assign (resid 151 and name Cg1)
 (resid 147 and name Cd1)
 6.45223657043 5.80701291339 1.29643811687
 OR (resid 151 and name Cg1)
 (resid 147 and name Cd2)
 OR (resid 151 and name Cg1)
 (resid 148 and name Cd1)
 OR (resid 151 and name Cg1)
 (resid 148 and name Cd2)
 assign (resid 151 and name Cg2 or resid 351 and name Cg2) (resid 241 and name Ce2)
 6.67272041139 6.00544837025 1.3488649791 ! 2306675
 assign (resid 151 and name Cg2 or resid 351 and name Cg2) (resid 241 and name Ce3)
 6.00404601515 5.40364141364 1.18986693053 ! 3360444
 assign (resid 151 and name Cg2) (resid 144 and name Cg) 6.77610298748 6.19849268873 1.13566641562 ! 3864911
 assign (resid 237 and name C) (resid 237 and name Ce1) 5.86678665008 5.28010798507 1.15722926515 ! 3652865
 assign (resid 237 and name C or resid 437 and name C) (resid 137 and name Ce1)
 5.77548451238 4.74793606114 1.0166288675 ! 5387714
 !To the above, added 0.5 angstrom to dist because was violating slightly, and transfer to Co is efficient
 assign (resid 237 and name C or resid 437 and name C) (resid 137 and name Cd2) 6.99475653993 6.29528088594
 1.4254390431 ! 1954546
 assign (resid 137 and name C) (resid 137 and name Cd2) 5.23431915878 4.7108872429 1.00684052966 ! 5546382
 assign (resid 137 and name C) (resid 137 and name Ce1) 6.08052133904 5.47246920514 1.20805130746 ! 3210966
 assign (resid 240 and name Cd2) (resid 237 and name Ce1) 6.10867261897 5.49780535707 1.21474514619 ! 3158176
 assign (resid 240 and name Cd2) (resid 237 and name Cd2) 6.70310338141 6.03279304327 1.35608947128 ! 2270005
 assign (resid 136 and name Cd1) (resid 137 and name Ce1) 4.3 3.8 0.8 ! 11700000
 OR (resid 238 and name Cd1) (resid 137 and name Ce1)
 OR (resid 438 and name Cd1) (resid 137 and name Ce1)
 OR (resid 240 and name Cd1) (resid 137 and name Ce1)
 OR (resid 440 and name Cd1) (resid 137 and name Ce1)

19.2 ms ¹³C-¹³C RFDR

assign

(resid 127 and name CB) ! V27.Cb 31.775ppm
(resid 132 and name CG1) ! I32.Cg1 26.361ppm
4.04279 3.5 3 ! intensity= 5496962
OR (resid 127 and name CB)
(resid 332 and name CG1)
OR (resid 127 and name CB) ! V27.Cb 31.775ppm
(resid 236 and name CG) ! L36"Cg 26.361ppm
OR (resid 127 and name CB)
(resid 436 and name CG)
OR (resid 127 and name CB) ! V27.Cb 31.775ppm
(resid 136 and name CD1) ! L36.Cd1 26.361ppm
OR (resid 127 and name CB)
(resid 336 and name CD1)
OR (resid 127 and name CB) ! V27.Cb 31.775ppm
(resid 238 and name CD1) ! L38"Cd1 26.361ppm
OR (resid 127 and name CB)
(resid 438 and name CD1)
OR (resid 127 and name CB) ! V27.Cb 31.775ppm
(resid 238 and name CG) ! L38"Cg 26.361ppm
OR (resid 127 and name CB)
(resid 438 and name CG)
OR (resid 127 and name CB) ! V27.Cb 31.775ppm
(resid 138 and name CD1) ! L38.Cd1 26.361ppm
OR (resid 127 and name CB)
(resid 338 and name CD1)
OR (resid 127 and name CB) ! V27.Cb 31.775ppm
(resid 138 and name CG) ! L38.Cg 26.361ppm
OR (resid 127 and name CB)
(resid 338 and name CG)
OR (resid 127 and name CB) ! V27.Cb 31.775ppm
(resid 240 and name CD1) ! L40"Cd1 26.361ppm
OR (resid 127 and name CB)
(resid 440 and name CD1)
OR (resid 127 and name CB) ! V27.Cb 31.775ppm
(resid 143 and name CG) ! L43.Cg 26.361ppm
OR (resid 127 and name CB)
(resid 343 and name CG)
OR (resid 228 and name CB) ! V28"Cb 31.775ppm

(resid 132 and name CG1) ! I32.Cg1 26.361ppm
OR (resid 228 and name CB)
(resid 332 and name CG1)
OR (resid 228 and name CB) ! nV28"Cb 31.775ppm
(resid 236 and name CG) ! L36"Cg 26.361ppm
OR (resid 228 and name CB)
(resid 436 and name CG)
OR (resid 228 and name CB) ! V28"Cb 31.775ppm
(resid 136 and name CD1) ! L36.Cd1 26.361ppm
OR (resid 228 and name CB)
(resid 336 and name CD1)
OR (resid 228 and name CB) ! nV28"Cb 31.775ppm
(resid 238 and name CD1) ! L38"Cd1 26.361ppm
OR (resid 228 and name CB)
(resid 438 and name CD1)
OR (resid 228 and name CB) ! nV28"Cb 31.775ppm
(resid 238 and name CG) ! L38"Cg 26.361ppm
OR (resid 228 and name CB)
(resid 438 and name CG)
OR (resid 228 and name CB) ! V28"Cb 31.775ppm
(resid 138 and name CD1) ! L38.Cd1 26.361ppm
OR (resid 228 and name CB)
(resid 338 and name CD1)
OR (resid 228 and name CB) ! V28"Cb 31.775ppm
(resid 138 and name CG) ! L38.Cg 26.361ppm
OR (resid 228 and name CB)
(resid 338 and name CG)
OR (resid 228 and name CB) ! nV28"Cb 31.775ppm
(resid 240 and name CD1) ! L40"Cd1 26.361ppm
OR (resid 228 and name CB)
(resid 440 and name CD1)
OR (resid 228 and name CB) ! V28"Cb 31.775ppm
(resid 143 and name CG) ! L43.Cg 26.361ppm
OR (resid 228 and name CB)
(resid 343 and name CG)

assign

(resid 227 and name CG1) ! V27"Cg1 21.567ppm
(resid 132 and name CG2) ! I32.Cg2 17.053ppm
4.28344 3.5 3 ! intensity= 3885566
OR (resid 227 and name CG1)

(resid 332 and name CG2)
 OR (resid 227 and name CG1) ! V27"Cg1
 21.567ppm
 (resid 133 and name CG2) ! I33.Cg2 17.053ppm
 OR (resid 227 and name CG1)
 (resid 333 and name CG2)
 OR (resid 227 and name CG1) ! V27"Cg1
 21.567ppm
 (resid 239 and name CG2) ! I39"Cg2 17.053ppm
 OR (resid 227 and name CG1)
 (resid 439 and name CG2)
 OR (resid 227 and name CG1) ! V27"Cg1
 21.567ppm
 (resid 242 and name CG2) ! I42"Cg2 17.053ppm
 OR (resid 227 and name CG1)
 (resid 442 and name CG2)
 OR (resid 227 and name CG1) ! V27"Cg1
 21.567ppm
 (resid 151 and name CG2) ! I51.Cg2 17.053ppm
 OR (resid 227 and name CG1)
 (resid 351 and name CG2)
 OR (resid 127 and name CG1) ! V27.Cg1
 21.567ppm
 (resid 132 and name CG2) ! I32.Cg2 17.053ppm
 OR (resid 127 and name CG1)
 (resid 332 and name CG2)
 OR (resid 127 and name CG1) ! V27.Cg1
 21.567ppm
 (resid 133 and name CG2) ! I33.Cg2 17.053ppm
 OR (resid 127 and name CG1)
 (resid 333 and name CG2)
 OR (resid 127 and name CG1) ! V27.Cg1
 21.567ppm
 (resid 239 and name CG2) ! I39"Cg2 17.053ppm
 OR (resid 127 and name CG1)

 (resid 439 and name CG2)
 OR (resid 127 and name CG1) ! V27.Cg1
 21.567ppm
 (resid 242 and name CG2) ! I42"Cg2 17.053ppm
 OR (resid 127 and name CG1)

(resid 442 and name CG2)
 OR (resid 127 and name CG1) ! V27.Cg1
 21.567ppm
 (resid 151 and name CG2) ! I51.Cg2 17.053ppm
 OR (resid 127 and name CG1)
 (resid 351 and name CG2)
 OR (resid 228 and name CG2) ! V28"Cg2
 21.567ppm
 (resid 132 and name CG2) ! I32.Cg2 17.053ppm
 OR (resid 228 and name CG2)
 (resid 332 and name CG2)
 OR (resid 228 and name CG2) ! V28"Cg2
 21.567ppm
 (resid 133 and name CG2) ! I33.Cg2 17.053ppm
 OR (resid 228 and name CG2)
 (resid 333 and name CG2)
 OR (resid 228 and name CG2) ! V28"Cg2
 21.567ppm
 (resid 239 and name CG2) ! I39"Cg2 17.053ppm
 OR (resid 228 and name CG2)
 (resid 439 and name CG2)
 OR (resid 228 and name CG2) ! V28"Cg2
 21.567ppm
 (resid 242 and name CG2) ! I42"Cg2 17.053ppm
 OR (resid 228 and name CG2)
 (resid 442 and name CG2)
 OR (resid 228 and name CG2) ! V28"Cg2
 21.567ppm
 (resid 151 and name CG2) ! I51.Cg2 17.053ppm
 OR (resid 228 and name CG2)
 (resid 351 and name CG2)

 assign
 (resid 132 and name CG1) ! I32.Cg1 26.403ppm
 (resid 127 and name CB) ! V27.Cb 31.655ppm
 4.24388 3.5 3 ! intensity= 4108001
 OR (resid 132 and name CG1)
 (resid 327 and name CB)
 OR (resid 132 and name CG1) ! I32.Cg1 26.403ppm
 (resid 228 and name CB) ! V28"Cb 31.655ppm
 OR (resid 132 and name CG1)

(resid 428 and name CB)
 OR (resid 236 and name CG) ! L36"Cg 26.403ppm

 (resid 127 and name CB) ! V27.Cb 31.655ppm
 OR (resid 236 and name CG)
 (resid 327 and name CB)
 OR (resid 236 and name CG) ! nL36"Cg 26.403ppm
 (resid 228 and name CB) ! V28"Cb 31.655ppm
 OR (resid 236 and name CG)
 (resid 428 and name CB)
 OR (resid 238 and name CG) ! L38"Cg 26.403ppm
 (resid 127 and name CB) ! V27.Cb 31.655ppm
 OR (resid 238 and name CG)
 (resid 327 and name CB)
 OR (resid 238 and name CG) ! nL38"Cg 26.403ppm
 (resid 228 and name CB) ! V28"Cb 31.655ppm
 OR (resid 238 and name CG)
 (resid 428 and name CB)
 OR (resid 138 and name CD1) ! L38.Cd1
 26.403ppm
 (resid 127 and name CB) ! V27.Cb 31.655ppm
 OR (resid 138 and name CD1)
 (resid 327 and name CB)
 OR (resid 138 and name CD1) ! L38.Cd1
 26.403ppm
 (resid 228 and name CB) ! V28"Cb 31.655ppm
 OR (resid 138 and name CD1)
 (resid 428 and name CB)
 OR (resid 138 and name CG) ! L38.Cg 26.403ppm
 (resid 127 and name CB) ! V27.Cb 31.655ppm
 OR (resid 138 and name CG)
 (resid 327 and name CB)
 OR (resid 138 and name CG) ! L38.Cg 26.403ppm
 (resid 228 and name CB) ! V28"Cb 31.655ppm
 OR (resid 138 and name CG)
 (resid 428 and name CB)
 OR (resid 240 and name CD1) ! L40"Cd1
 26.403ppm
 (resid 127 and name CB) ! V27.Cb 31.655ppm
 OR (resid 240 and name CD1)
 (resid 327 and name CB)

OR (resid 240 and name CD1) ! nL40"Cd1
 26.403ppm
 (resid 228 and name CB) ! V28"Cb 31.655ppm
 OR (resid 240 and name CD1)
 (resid 428 and name CB)
 OR (resid 143 and name CG) ! L43.Cg 26.403ppm
 (resid 127 and name CB) ! V27.Cb 31.655ppm
 OR (resid 143 and name CG)
 (resid 327 and name CB)
 OR (resid 143 and name CG) ! L43.Cg 26.403ppm
 (resid 228 and name CB) ! V28"Cb 31.655ppm
 OR (resid 143 and name CG)
 (resid 428 and name CB)

 assign
 (resid 227 and name CG1) ! V27"Cg1 21.543ppm
 (resid 133 and name CG1) ! I33.Cg1 28.785ppm
 4.3453 3.5 3 ! intensity= 3565248
 OR (resid 227 and name CG1)
 (resid 333 and name CG1)
 OR (resid 227 and name CG1) ! V27"Cg1
 21.543ppm
 (resid 135 and name CG1) ! I35.Cg1 28.785ppm
 OR (resid 227 and name CG1)
 (resid 335 and name CG1)
 OR (resid 227 and name CG1) ! V27"Cg1
 21.543ppm
 (resid 142 and name CG1) ! I42.Cg1 28.785ppm
 OR (resid 227 and name CG1)
 (resid 342 and name CG1)
 OR (resid 227 and name CG1) ! V27"Cg1
 21.543ppm
 (resid 151 and name CG1) ! I51.Cg1 28.785ppm
 OR (resid 227 and name CG1)
 (resid 351 and name CG1)
 OR (resid 127 and name CG1) ! V27.Cg1
 21.543ppm
 (resid 133 and name CG1) ! I33.Cg1 28.785ppm
 OR (resid 127 and name CG1)
 (resid 333 and name CG1)

OR (resid 127 and name CG1) ! V27.Cg1
 21.543ppm
 (resid 135 and name CG1) ! I35.Cg1 28.785ppm
 OR (resid 127 and name CG1)
 (resid 335 and name CG1)
 OR (resid 127 and name CG1) ! V27.Cg1
 21.543ppm
 (resid 142 and name CG1) ! I42.Cg1 28.785ppm
 OR (resid 127 and name CG1)
 (resid 342 and name CG1)
 OR (resid 127 and name CG1) ! V27.Cg1
 21.543ppm
 (resid 151 and name CG1) ! I51.Cg1 28.785ppm
 OR (resid 127 and name CG1)
 (resid 351 and name CG1)

 OR (resid 228 and name CG2) ! V28"Cg2
 21.543ppm
 (resid 133 and name CG1) ! I33.Cg1 28.785ppm
 OR (resid 228 and name CG2)
 (resid 333 and name CG1)
 OR (resid 228 and name CG2) ! V28"Cg2
 21.543ppm
 (resid 135 and name CG1) ! I35.Cg1 28.785ppm
 OR (resid 228 and name CG2)
 (resid 335 and name CG1)
 OR (resid 228 and name CG2) ! V28"Cg2
 21.543ppm
 (resid 142 and name CG1) ! I42.Cg1 28.785ppm
 OR (resid 228 and name CG2)
 (resid 342 and name CG1)
 OR (resid 228 and name CG2) ! V28"Cg2
 21.543ppm
 (resid 151 and name CG1) ! I51.Cg1 28.785ppm
 OR (resid 228 and name CG2)
 (resid 351 and name CG1)

 assign
 (resid 227 and name CG1) ! V27"Cg1 21.560ppm
 (resid 133 and name C) ! I33.Co 175.442ppm

4.73764 3.5 3 ! intensity= 2122446
 OR (resid 227 and name CG1)
 (resid 333 and name C)
 OR (resid 227 and name CG1) ! V27"Cg1
 21.560ppm
 (resid 137 and name C) ! H37.Co 175.442ppm
 OR (resid 227 and name CG1)
 (resid 337 and name C)
 OR (resid 227 and name CG1) ! V27"Cg1
 21.560ppm
 (resid 147 and name C) ! F47.Co 175.442ppm
 OR (resid 227 and name CG1)
 (resid 347 and name C)
 OR (resid 227 and name CG1) ! V27"Cg1
 21.560ppm
 (resid 149 and name C) ! K49.Co 175.442ppm
 OR (resid 227 and name CG1)
 (resid 349 and name C)
 OR (resid 127 and name CG1) ! V27.Cg1
 21.560ppm
 (resid 133 and name C) ! I33.Co 175.442ppm
 OR (resid 127 and name CG1)
 (resid 333 and name C)
 OR (resid 127 and name CG1) ! V27.Cg1
 21.560ppm
 (resid 137 and name C) ! H37.Co 175.442ppm
 OR (resid 127 and name CG1)
 (resid 337 and name C)
 OR (resid 127 and name CG1) ! V27.Cg1
 21.560ppm
 (resid 147 and name C) ! F47.Co 175.442ppm
 OR (resid 127 and name CG1)
 (resid 347 and name C)
 OR (resid 127 and name CG1) ! V27.Cg1
 21.560ppm
 (resid 149 and name C) ! K49.Co 175.442ppm
 OR (resid 127 and name CG1)
 (resid 349 and name C)
 OR (resid 228 and name CG2) ! V28"Cg2
 21.560ppm
 (resid 133 and name C) ! I33.Co 175.442ppm

OR (resid 228 and name CG2)
 (resid 333 and name C)
 OR (resid 228 and name CG2) ! V28"Ca 21.560ppm
 (resid 137 and name C) ! H37.Co 175.442ppm
 OR (resid 228 and name CG2)
 (resid 337 and name C)
 OR (resid 228 and name CG2) ! V28"Ca 21.560ppm
 (resid 147 and name C) ! F47.Co 175.442ppm
 OR (resid 228 and name CG2)
 (resid 347 and name C)
 OR (resid 228 and name CG2) ! V28"Ca 21.560ppm
 (resid 149 and name C) ! K49.Co 175.442ppm
 OR (resid 228 and name CG2)
 (resid 349 and name C)

assign

(resid 230 and name CB) ! nA30"Cb 18.546ppm
 (resid 228 and name CA) ! V28"Ca 65.486ppm
 3.63324 3.5 3 ! intensity= 10433915
 OR (resid 230 and name CB)
 (resid 428 and name CA)
 OR (resid 230 and name CB) ! nA30"Cb 18.546ppm
 (resid 232 and name CA) ! I32"Ca 65.486ppm
 OR (resid 230 and name CB)
 (resid 432 and name CA)
 OR (resid 230 and name CB) ! nA30"Cb 18.546ppm
 (resid 239 and name CA) ! I39"Ca 65.486ppm
 OR (resid 230 and name CB)
 (resid 439 and name CA)
 OR (resid 230 and name CB) ! nA30"Cb 18.546ppm
 (resid 242 and name CA) ! I42"Ca 65.486ppm
 OR (resid 230 and name CB)
 (resid 442 and name CA)
 OR (resid 130 and name CB) ! A30.Cb 18.546ppm
 (resid 228 and name CA) ! V28"Ca 65.486ppm
 OR (resid 130 and name CB)
 (resid 428 and name CA)
 OR (resid 130 and name CB) ! A30.Cb 18.546ppm

(resid 232 and name CA) ! I32"Ca 65.486ppm
 OR (resid 130 and name CB)
 (resid 432 and name CA)
 OR (resid 130 and name CB) ! A30.Cb 18.546ppm
 (resid 239 and name CA) ! I39"Ca 65.486ppm
 OR (resid 130 and name CB)
 (resid 439 and name CA)
 OR (resid 130 and name CB) ! A30.Cb 18.546ppm
 (resid 242 and name CA) ! I42"Ca 65.486ppm
 OR (resid 130 and name CB)
 (resid 442 and name CA)
 OR (resid 142 and name CG2) ! I42.Cg2 18.546ppm
 (resid 228 and name CA) ! V28"Ca 65.486ppm
 OR (resid 142 and name CG2)
 (resid 428 and name CA)
 OR (resid 142 and name CG2) ! I42.Cg2 18.546ppm
 (resid 232 and name CA) ! I32"Ca 65.486ppm
 OR (resid 142 and name CG2)
 (resid 432 and name CA)
 OR (resid 142 and name CG2) ! I42.Cg2 18.546ppm
 (resid 239 and name CA) ! I39"Ca 65.486ppm
 OR (resid 142 and name CG2)
 (resid 439 and name CA)
 OR (resid 142 and name CG2) ! I42.Cg2 18.546ppm
 (resid 242 and name CA) ! I42"Ca 65.486ppm
 OR (resid 142 and name CG2)
 (resid 442 and name CA)

assign

(resid 131 and name CB) ! N31.Cb 40.645ppm
 (resid 133 and name C) ! I33.Co 175.028ppm
 3.5488 3.5 3 ! intensity= 12014871
 OR (resid 131 and name CB)
 (resid 333 and name C)
 OR (resid 131 and name CB) ! N31.Cb 40.645ppm
 (resid 137 and name C) ! H37.Co 175.028ppm
 OR (resid 131 and name CB)
 (resid 337 and name C)
 OR (resid 131 and name CB) ! N31.Cb 40.645ppm
 (resid 147 and name C) ! F47.Co 175.028ppm
 OR (resid 131 and name CB)

(resid 347 and name C)
 OR (resid 131 and name CB) ! N31.Cb 40.645ppm
 (resid 149 and name C) ! K49.Co 175.028ppm
 OR (resid 131 and name CB)
 (resid 349 and name C)
 OR (resid 238 and name CB) ! L38"Cb 40.645ppm
 (resid 133 and name C) ! I33.Co 175.028ppm
 OR (resid 238 and name CB)
 (resid 333 and name C)
 OR (resid 238 and name CB) ! L38"Cb 40.645ppm
 (resid 137 and name C) ! H37.Co 175.028ppm
 OR (resid 238 and name CB)
 (resid 337 and name C)
 OR (resid 238 and name CB) ! L38"Cb 40.645ppm
 (resid 147 and name C) ! F47.Co 175.028ppm
 OR (resid 238 and name CB)
 (resid 347 and name C)
 OR (resid 238 and name CB) ! L38"Cb 40.645ppm
 (resid 149 and name C) ! K49.Co 175.028ppm
 OR (resid 238 and name CB)
 (resid 349 and name C)
 OR (resid 240 and name CB) ! L40"Cb 40.645ppm
 (resid 133 and name C) ! I33.Co 175.028ppm
 OR (resid 240 and name CB)
 (resid 333 and name C)
 OR (resid 240 and name CB) ! L40"Cb 40.645ppm
 (resid 137 and name C) ! H37.Co 175.028ppm
 OR (resid 240 and name CB)
 (resid 337 and name C)
 OR (resid 240 and name CB) ! L40"Cb 40.645ppm
 (resid 147 and name C) ! F47.Co 175.028ppm
 OR (resid 240 and name CB)
 (resid 347 and name C)
 OR (resid 240 and name CB) ! L40"Cb 40.645ppm
 (resid 149 and name C) ! K49.Co 175.028ppm
 OR (resid 240 and name CB)
 (resid 349 and name C)

assign

(resid 227 and name CG2) ! V27"Cg2 22.433ppm
 (resid 237 and name CE1) ! H37"Ce1 135.674ppm

2.86909 3.5 3 ! intensity= 43027776
 OR (resid 227 and name CG2)
 (resid 437 and name CE1)
 OR (resid 227 and name CG2) ! nV27"Cg2
 22.433ppm
 (resid 237 and name CG) ! H37"Cg 135.674ppm
 OR (resid 227 and name CG2)
 (resid 437 and name CG)
 OR (resid 228 and name CG1) ! V28"Cg1
 22.433ppm
 (resid 237 and name CE1) ! H37"Ce1 135.674ppm
 OR (resid 228 and name CG1)
 (resid 437 and name CE1)
 OR (resid 228 and name CG1) ! nV28"Cg1
 22.433ppm
 (resid 237 and name CG) ! H37"Cg 135.674ppm
 OR (resid 228 and name CG1)
 (resid 437 and name CG)
 OR (resid 128 and name CG1) ! V28.Cg1
 22.433ppm
 (resid 237 and name CE1) ! H37"Ce1 135.674ppm
 OR (resid 128 and name CG1)
 (resid 437 and name CE1)
 OR (resid 128 and name CG1) ! V28.Cg1
 22.433ppm
 (resid 237 and name CG) ! H37"Cg 135.674ppm
 OR (resid 128 and name CG1)
 (resid 437 and name CG)
 OR (resid 138 and name CD2) ! L38.Cd2
 22.433ppm
 (resid 237 and name CE1) ! H37"Ce1 135.674ppm
 OR (resid 138 and name CD2)
 (resid 437 and name CE1)
 OR (resid 138 and name CD2) ! L38.Cd2
 22.433ppm
 (resid 237 and name CG) ! H37"Cg 135.674ppm
 OR (resid 138 and name CD2)
 (resid 437 and name CG)
 OR (resid 143 and name CD2) ! L43.Cd2
 22.433ppm
 (resid 237 and name CE1) ! H37"Ce1 135.674ppm

OR (resid 143 and name CD2)
(resid 437 and name CE1)
OR (resid 143 and name CD2) ! L43.Cd2
22.433ppm
(resid 237 and name CG) ! H37"Cg 135.674ppm
OR (resid 143 and name CD2)
(resid 437 and name CG)

assign

(resid 227 and name CG2) ! V27"Cg2 22.583ppm
(resid 239 and name CD1) ! I39"Cd1 13.822ppm
4.62741 3.5 3 ! intensity= 2444473
OR (resid 227 and name CG2)
(resid 439 and name CD1)
OR (resid 227 and name CG2) ! V27"Cg2
22.587ppm
(resid 151 and name CD1) ! I51.Cd1 13.815ppm
OR (resid 227 and name CG2)
(resid 351 and name CD1)
OR (resid 228 and name CG1) ! V28"Cg1
22.584ppm
(resid 239 and name CD1) ! I39"Cd1 13.823ppm
OR (resid 228 and name CG1)
(resid 439 and name CD1)
OR (resid 228 and name CG1) ! V28"Cg1
22.587ppm
(resid 151 and name CD1) ! I51.Cd1 13.824ppm
OR (resid 228 and name CG1)
(resid 351 and name CD1)
OR (resid 128 and name CG1) ! V28.Cg1
22.588ppm
(resid 239 and name CD1) ! I39"Cd1 13.817ppm
OR (resid 128 and name CG1)
(resid 439 and name CD1)
OR (resid 128 and name CG1) ! V28.Cg1
22.595ppm
(resid 151 and name CD1) ! I51.Cd1 13.818ppm
OR (resid 128 and name CG1)
(resid 351 and name CD1)
OR (resid 138 and name CD2) ! L38.Cd2
22.581ppm

(resid 239 and name CD1) ! I39"Cd1 13.822ppm
OR (resid 138 and name CD2)
(resid 439 and name CD1)
OR (resid 138 and name CD2) ! L38.Cd2
22.589ppm
(resid 151 and name CD1) ! I51.Cd1 13.822ppm
OR (resid 138 and name CD2)
(resid 351 and name CD1)
OR (resid 143 and name CD2) ! L43.Cd2
22.591ppm
(resid 239 and name CD1) ! I39"Cd1 13.824ppm
OR (resid 143 and name CD2)
(resid 439 and name CD1)
OR (resid 143 and name CD2) ! L43.Cd2
22.583ppm
(resid 151 and name CD1) ! I51.Cd1 13.821ppm
OR (resid 143 and name CD2)
(resid 351 and name CD1)

assign

(resid 127 and name CA) ! V27.Ca 66.010ppm
(resid 143 and name C) ! L43.Co 180.162ppm
4.56098 3.5 3 ! intensity= 2666014
OR (resid 127 and name CA)
(resid 343 and name C)
OR (resid 127 and name CA) ! V27.Ca 66.010ppm
(resid 144 and name CG) ! D44.Cg 180.162ppm
OR (resid 127 and name CA)
(resid 344 and name CG)
OR (resid 233 and name CA) ! I33"Ca 66.010ppm
(resid 143 and name C) ! L43.Co 180.162ppm
OR (resid 233 and name CA)
(resid 343 and name C)
OR (resid 233 and name CA) ! I33"Ca 66.010ppm
(resid 144 and name CG) ! D44.Cg 180.162ppm
OR (resid 233 and name CA)
(resid 344 and name CG)
OR (resid 235 and name CA) ! I35"Ca 66.010ppm
(resid 143 and name C) ! L43.Co 180.162ppm
OR (resid 235 and name CA)
(resid 343 and name C)

OR (resid 235 and name CA) ! I35"Ca 66.010ppm
 (resid 144 and name CG) ! D44.Cg 180.162ppm
 OR (resid 235 and name CA)
 (resid 344 and name CG)

OR (resid 242 and name CA) ! I42"Ca 66.010ppm
 (resid 143 and name C) ! L43.Co 180.162ppm
 OR (resid 242 and name CA)
 (resid 343 and name C)

OR (resid 242 and name CA) ! I42"Ca 66.010ppm
 (resid 144 and name CG) ! D44.Cg 180.162ppm
 OR (resid 242 and name CA)
 (resid 344 and name CG)

OR (resid 151 and name CA) ! I51.Ca 66.010ppm
 (resid 143 and name C) ! L43.Co 180.162ppm
 OR (resid 151 and name CA)
 (resid 343 and name C)

OR (resid 151 and name CA) ! I51.Ca 66.010ppm
 (resid 144 and name CG) ! D44.Cg 180.162ppm
 OR (resid 151 and name CA)
 (resid 344 and name CG)

assign

(resid 132 and name CG2) ! I32.Cg2 17.185ppm
 (resid 143 and name C) ! L43.Co 180.137ppm
 4.06708 3.5 3 ! intensity= 5302941
 OR (resid 132 and name CG2)
 (resid 343 and name C)

OR (resid 132 and name CG2) ! I32.Cg2 17.185ppm
 (resid 144 and name CG) ! D44.Cg 180.137ppm
 OR (resid 132 and name CG2)
 (resid 344 and name CG)

OR (resid 133 and name CG2) ! I33.Cg2 17.185ppm
 (resid 143 and name C) ! L43.Co 180.137ppm
 OR (resid 133 and name CG2)
 (resid 343 and name C)

OR (resid 133 and name CG2) ! I33.Cg2 17.185ppm
 (resid 144 and name CG) ! D44.Cg 180.137ppm
 OR (resid 133 and name CG2)
 (resid 344 and name CG)

OR (resid 239 and name CG2) ! I39"Cg2
 17.185ppm
 (resid 143 and name C) ! L43.Co 180.137ppm
 OR (resid 239 and name CG2)
 (resid 343 and name C)

OR (resid 239 and name CG2) ! I39"Cg2
 17.185ppm
 (resid 144 and name CG) ! D44.Cg 180.137ppm
 OR (resid 239 and name CG2)
 (resid 344 and name CG)

OR (resid 242 and name CG2) ! I42"Cg2
 17.185ppm
 (resid 143 and name C) ! L43.Co 180.137ppm
 OR (resid 242 and name CG2)
 (resid 343 and name C)

OR (resid 242 and name CG2) ! I42"Cg2
 17.185ppm
 (resid 144 and name CG) ! D44.Cg 180.137ppm
 OR (resid 242 and name CG2)
 (resid 344 and name CG)

OR (resid 151 and name CG2) ! I51.Cg2 17.185ppm
 (resid 143 and name C) ! L43.Co 180.137ppm
 OR (resid 151 and name CG2)
 (resid 343 and name C)

OR (resid 151 and name CG2) ! I51.Cg2 17.185ppm
 (resid 144 and name CG) ! D44.Cg 180.137ppm
 OR (resid 151 and name CG2)
 (resid 344 and name CG)

assign

(resid 237 and name CE1) ! H37"Ce1 135.731ppm
 (resid 227 and name CG2) ! V27"Cg2 22.378ppm
 3.06269 3.5 3 ! intensity= 29079942
 OR (resid 237 and name CE1)
 (resid 427 and name CG2)

OR (resid 237 and name CE1) ! H37"Ce1
 135.731ppm
 (resid 228 and name CG1) ! V28"Cg1 22.378ppm
 OR (resid 237 and name CE1)
 (resid 428 and name CG1)

OR (resid 237 and name CE1) ! H37"Ce1
 135.731ppm
 (resid 128 and name CG1) ! V28.Cg1 22.378ppm
 OR (resid 237 and name CE1)
 (resid 328 and name CG1)
 OR (resid 237 and name CE1) ! H37"Ce1
 135.731ppm
 (resid 138 and name CD2) ! L38.Cd2 22.378ppm
 OR (resid 237 and name CE1)
 (resid 338 and name CD2)
 OR (resid 237 and name CE1) ! H37"Ce1
 135.731ppm
 (resid 143 and name CD2) ! L43.Cd2 22.378ppm
 OR (resid 237 and name CE1)
 (resid 343 and name CD2)
 OR (resid 237 and name CG) ! nH37"Cg
 135.731ppm
 (resid 227 and name CG2) ! V27"Cg2 22.378ppm
 OR (resid 237 and name CG)
 (resid 427 and name CG2)
 OR (resid 237 and name CG) ! nH37"Cg
 135.731ppm
 (resid 228 and name CG1) ! V28"Cg1 22.378ppm
 OR (resid 237 and name CG)
 (resid 428 and name CG1)
 OR (resid 237 and name CG) ! H37"Cg 135.731ppm
 (resid 128 and name CG1) ! V28.Cg1 22.378ppm
 OR (resid 237 and name CG)
 (resid 328 and name CG1)
 OR (resid 237 and name CG) ! H37"Cg 135.731ppm
 (resid 138 and name CD2) ! L38.Cd2 22.378ppm
 OR (resid 237 and name CG)
 (resid 338 and name CD2)
 OR (resid 237 and name CG) ! H37"Cg 135.731ppm
 (resid 143 and name CD2) ! L43.Cd2 22.378ppm
 OR (resid 237 and name CG)
 (resid 343 and name CD2)
 assign
 (resid 140 and name CD1) ! L40.Cd1 25.040ppm
 (resid 132 and name CG2) ! I32.Cg2 17.107ppm

4.09496 3.5 3 ! intensity= 5089915
 OR (resid 140 and name CD1)
 (resid 332 and name CG2)
 OR (resid 140 and name CD1) ! L40.Cd1
 25.040ppm
 (resid 133 and name CG2) ! I33.Cg2 17.107ppm
 OR (resid 140 and name CD1)
 (resid 333 and name CG2)
 OR (resid 140 and name CD1) ! L40.Cd1
 25.040ppm
 (resid 239 and name CG2) ! I39"Cg2 17.107ppm
 OR (resid 140 and name CD1)
 (resid 439 and name CG2)
 OR (resid 140 and name CD1) ! L40.Cd1
 25.040ppm
 (resid 242 and name CG2) ! I42"Cg2 17.107ppm
 OR (resid 140 and name CD1)
 (resid 442 and name CG2)
 OR (resid 140 and name CD1) ! L40.Cd1
 25.040ppm
 (resid 151 and name CG2) ! I51.Cg2 17.107ppm
 OR (resid 140 and name CD1)
 (resid 351 and name CG2)
 OR (resid 149 and name CG) ! K49.Cg 25.040ppm
 (resid 132 and name CG2) ! I32.Cg2 17.107ppm
 OR (resid 149 and name CG)
 (resid 332 and name CG2)
 OR (resid 149 and name CG) ! K49.Cg 25.040ppm
 (resid 133 and name CG2) ! I33.Cg2 17.107ppm
 OR (resid 149 and name CG)
 (resid 333 and name CG2)
 OR (resid 149 and name CG) ! K49.Cg 25.040ppm
 (resid 239 and name CG2) ! I39"Cg2 17.107ppm
 OR (resid 149 and name CG)
 (resid 439 and name CG2)
 OR (resid 149 and name CG) ! K49.Cg 25.040ppm
 (resid 242 and name CG2) ! I42"Cg2 17.107ppm
 OR (resid 149 and name CG)
 (resid 442 and name CG2)
 OR (resid 149 and name CG) ! K49.Cg 25.040ppm
 (resid 151 and name CG2) ! I51.Cg2 17.107ppm

OR (resid 149 and name CG)
 (resid 351 and name CG2)

assign
 (resid 143 and name C) ! L43.Co 180.201ppm
 (resid 132 and name CG2) ! I32.Cg2 17.120ppm
 4.44227 3.5 3 ! intensity= 3123070

OR (resid 143 and name C)
 (resid 332 and name CG2)

OR (resid 143 and name C) ! L43.Co 180.201ppm
 (resid 133 and name CG2) ! I33.Cg2 17.120ppm

OR (resid 143 and name C)
 (resid 333 and name CG2)

OR (resid 143 and name C) ! L43.Co 180.201ppm
 (resid 239 and name CG2) ! I39.Cg2 17.120ppm

OR (resid 143 and name C)
 (resid 439 and name CG2)

OR (resid 143 and name C) ! L43.Co 180.201ppm
 (resid 242 and name CG2) ! I42.Cg2 17.120ppm

OR (resid 143 and name C)
 (resid 442 and name CG2)

OR (resid 143 and name C) ! L43.Co 180.201ppm
 (resid 151 and name CG2) ! I51.Cg2 17.120ppm

OR (resid 143 and name C)
 (resid 351 and name CG2)

OR (resid 144 and name CG) ! D44.Cg 180.201ppm
 (resid 132 and name CG2) ! I32.Cg2 17.120ppm

OR (resid 144 and name CG)
 (resid 332 and name CG2)

OR (resid 144 and name CG) ! D44.Cg 180.201ppm
 (resid 133 and name CG2) ! I33.Cg2 17.120ppm

OR (resid 144 and name CG)
 (resid 333 and name CG2)

OR (resid 144 and name CG) ! D44.Cg 180.201ppm
 (resid 239 and name CG2) ! I39.Cg2 17.120ppm

OR (resid 144 and name CG)
 (resid 439 and name CG2)

OR (resid 144 and name CG) ! D44.Cg 180.201ppm
 (resid 242 and name CG2) ! I42.Cg2 17.120ppm

OR (resid 144 and name CG)
 (resid 442 and name CG2)

OR (resid 144 and name CG) ! D44.Cg 180.201ppm
 (resid 151 and name CG2) ! I51.Cg2 17.120ppm

OR (resid 144 and name CG)
 (resid 351 and name CG2)

assign
 (resid 227 and name CG1) ! V27.Cg1 21.553ppm
 (resid 133 and name CA) ! I33.Ca 64.189ppm
 4.20552 3.5 3 ! intensity= 4338010

OR (resid 227 and name CG1)
 (resid 333 and name CA)

OR (resid 227 and name CG1) ! V27.Cg1
 21.553ppm
 (resid 135 and name CA) ! I35.Ca 64.189ppm

OR (resid 227 and name CG1)
 (resid 335 and name CA)

OR (resid 227 and name CG1) ! V27.Cg1
 21.553ppm
 (resid 142 and name CA) ! I42.Ca 64.189ppm

OR (resid 227 and name CG1)
 (resid 342 and name CA)

OR (resid 127 and name CG1) ! V27.Cg1
 21.553ppm
 (resid 133 and name CA) ! I33.Ca 64.189ppm

OR (resid 127 and name CG1)
 (resid 333 and name CA)

OR (resid 127 and name CG1) ! V27.Cg1
 21.553ppm
 (resid 135 and name CA) ! I35.Ca 64.189ppm

OR (resid 127 and name CG1)
 (resid 335 and name CA)

OR (resid 127 and name CG1) ! V27.Cg1
 21.553ppm
 (resid 142 and name CA) ! I42.Ca 64.189ppm

OR (resid 127 and name CG1)
 (resid 342 and name CA)

OR (resid 228 and name CG2) ! V28.Cg2
 21.553ppm
 (resid 133 and name CA) ! I33.Ca 64.189ppm

OR (resid 228 and name CG2)
 (resid 333 and name CA)

OR (resid 228 and name CG2) ! V28"Cg2
21.553ppm
(resid 135 and name CA) ! I35.Ca 64.189ppm
OR (resid 228 and name CG2)
(resid 335 and name CA)
OR (resid 228 and name CG2) ! V28"Cg2
21.553ppm
(resid 142 and name CA) ! I42.Ca 64.189ppm
OR (resid 228 and name CG2)
(resid 342 and name CA)

assign

(resid 133 and name CA) ! I33.Ca 64.221ppm
(resid 227 and name CG1) ! V27"Cg1 21.498ppm
4.53703 3.5 3 ! intensity= 2751586
OR (resid 133 and name CA)
(resid 427 and name CG1)
OR (resid 133 and name CA) ! I33.Ca 64.221ppm
(resid 127 and name CG1) ! V27.Cg1 21.498ppm
OR (resid 133 and name CA)
(resid 327 and name CG1)
OR (resid 133 and name CA) ! I33.Ca 64.221ppm
(resid 228 and name CG2) ! V28"Cg2 21.498ppm
OR (resid 133 and name CA)
(resid 428 and name CG2)
OR (resid 135 and name CA) ! I35.Ca 64.221ppm
(resid 227 and name CG1) ! V27"Cg1 21.498ppm
OR (resid 135 and name CA)
(resid 427 and name CG1)
OR (resid 135 and name CA) ! I35.Ca 64.221ppm
(resid 127 and name CG1) ! V27.Cg1 21.498ppm
OR (resid 135 and name CA)
(resid 327 and name CG1)
OR (resid 135 and name CA) ! I35.Ca 64.221ppm
(resid 228 and name CG2) ! V28"Cg2 21.498ppm
OR (resid 135 and name CA)
(resid 428 and name CG2)
OR (resid 142 and name CA) ! I42.Ca 64.221ppm
(resid 227 and name CG1) ! V27"Cg1 21.498ppm
OR (resid 142 and name CA)
(resid 427 and name CG1)

OR (resid 142 and name CA) ! I42.Ca 64.221ppm
(resid 127 and name CG1) ! V27.Cg1 21.498ppm
OR (resid 142 and name CA)
(resid 327 and name CG1)
OR (resid 142 and name CA) ! I42.Ca 64.221ppm
(resid 228 and name CG2) ! V28"Cg2 21.498ppm
OR (resid 142 and name CA)
(resid 428 and name CG2)

assign

(resid 128 and name CG2) ! V28.Cg2 21.977ppm
(resid 133 and name C) ! I33.Co 175.440ppm
4.09578 3.5 3 ! intensity= 5083873
OR (resid 128 and name CG2)
(resid 333 and name C)
OR (resid 128 and name CG2) ! V28.Cg2
21.977ppm
(resid 137 and name C) ! H37.Co 175.440ppm
OR (resid 128 and name CG2)
(resid 337 and name C)
OR (resid 128 and name CG2) ! V28.Cg2
21.977ppm
(resid 147 and name C) ! F47.Co 175.440ppm
OR (resid 128 and name CG2)
(resid 347 and name C)
OR (resid 128 and name CG2) ! V28.Cg2
21.977ppm
(resid 149 and name C) ! K49.Co 175.440ppm
OR (resid 128 and name CG2)
(resid 349 and name C)
OR (resid 238 and name CD2) ! L38"Cd2
21.977ppm
(resid 133 and name C) ! I33.Co 175.440ppm
OR (resid 238 and name CD2)
(resid 333 and name C)
OR (resid 238 and name CD2) ! L38"Cd2
21.977ppm
(resid 137 and name C) ! H37.Co 175.440ppm
OR (resid 238 and name CD2)
(resid 337 and name C)

OR (resid 238 and name CD2) ! L38"Cd2
21.977ppm
(resid 147 and name C) ! F47.Co 175.440ppm
OR (resid 238 and name CD2)
(resid 347 and name C)
OR (resid 238 and name CD2) ! L38"Cd2
21.977ppm
(resid 149 and name C) ! K49.Co 175.440ppm
OR (resid 238 and name CD2)
(resid 349 and name C)

assign

(resid 233 and name CG2) ! I33"Cg2 19.670ppm
(resid 133 and name C) ! I33.Co 175.471ppm
3.61799 3.5 3 ! intensity= 10700557
OR (resid 233 and name CG2)
(resid 333 and name C)
OR (resid 233 and name CG2) ! I33"Cg2
19.670ppm
(resid 137 and name C) ! H37.Co 175.471ppm
OR (resid 233 and name CG2)
(resid 337 and name C)
OR (resid 233 and name CG2) ! I33"Cg2
19.670ppm
(resid 147 and name C) ! F47.Co 175.471ppm
OR (resid 233 and name CG2)
(resid 347 and name C)
OR (resid 233 and name CG2) ! I33"Cg2
19.670ppm
(resid 149 and name C) ! K49.Co 175.471ppm
OR (resid 233 and name CG2)
(resid 349 and name C)
OR (resid 139 and name CG2) ! I39.Cg2 19.670ppm
(resid 133 and name C) ! I33.Co 175.471ppm
OR (resid 139 and name CG2)
(resid 333 and name C)
OR (resid 139 and name CG2) ! I39.Cg2 19.670ppm
(resid 137 and name C) ! H37.Co 175.471ppm
OR (resid 139 and name CG2)
(resid 337 and name C)
OR (resid 139 and name CG2) ! I39.Cg2 19.670ppm

(resid 147 and name C) ! F47.Co 175.471ppm
OR (resid 139 and name CG2)
(resid 347 and name C)
OR (resid 139 and name CG2) ! I39.Cg2 19.670ppm
(resid 149 and name C) ! K49.Co 175.471ppm
OR (resid 139 and name CG2)
(resid 349 and name C)

assign

(resid 133 and name C) ! I33.Co 175.504ppm
(resid 128 and name CG2) ! V28.Cg2 21.901ppm
4.43865 3.5 3 ! intensity= 3138396
OR (resid 133 and name C)
(resid 328 and name CG2)
OR (resid 133 and name C) ! I33.Co 175.504ppm
(resid 238 and name CD2) ! L38"Cd2 21.901ppm
OR (resid 133 and name C)
(resid 438 and name CD2)
OR (resid 137 and name C) ! H37.Co 175.504ppm
(resid 128 and name CG2) ! V28.Cg2 21.901ppm
OR (resid 137 and name C)
(resid 328 and name CG2)
OR (resid 137 and name C) ! H37.Co 175.504ppm
(resid 238 and name CD2) ! L38"Cd2 21.901ppm
OR (resid 137 and name C)
(resid 438 and name CD2)
OR (resid 147 and name C) ! F47.Co 175.504ppm
(resid 128 and name CG2) ! V28.Cg2 21.901ppm
OR (resid 147 and name C)
(resid 328 and name CG2)
OR (resid 147 and name C) ! F47.Co 175.504ppm
(resid 238 and name CD2) ! L38"Cd2 21.901ppm
OR (resid 147 and name C)
(resid 438 and name CD2)
OR (resid 149 and name C) ! K49.Co 175.504ppm
(resid 128 and name CG2) ! V28.Cg2 21.901ppm
OR (resid 149 and name C)
(resid 328 and name CG2)
OR (resid 149 and name C) ! K49.Co 175.504ppm
(resid 238 and name CD2) ! L38"Cd2 21.901ppm
OR (resid 149 and name C)

(resid 438 and name CD2)

assign

(resid 235 and name CG2) ! I35"Cg2 17.990ppm

(resid 133 and name C) ! I33.Co 175.426ppm

3.54835 3.5 3 ! intensity= 12024085

OR (resid 235 and name CG2)

(resid 333 and name C)

OR (resid 235 and name CG2) ! I35"Cg2

17.990ppm

(resid 137 and name C) ! H37.Co 175.426ppm

OR (resid 235 and name CG2)

(resid 337 and name C)

OR (resid 235 and name CG2) ! I35"Cg2

17.990ppm

(resid 147 and name C) ! F47.Co 175.426ppm

OR (resid 235 and name CG2)

(resid 347 and name C)

OR (resid 235 and name CG2) ! I35"Cg2

17.990ppm

(resid 149 and name C) ! K49.Co 175.426ppm

OR (resid 235 and name CG2)

(resid 349 and name C)

OR (resid 135 and name CG2) ! I35.Cg2 17.990ppm

(resid 133 and name C) ! I33.Co 175.426ppm

OR (resid 135 and name CG2)

(resid 333 and name C)

OR (resid 135 and name CG2) ! I35.Cg2 17.990ppm

(resid 137 and name C) ! H37.Co 175.426ppm

OR (resid 135 and name CG2)

(resid 337 and name C)

OR (resid 135 and name CG2) ! I35.Cg2 17.990ppm

(resid 147 and name C) ! F47.Co 175.426ppm

OR (resid 135 and name CG2)

(resid 347 and name C)

OR (resid 135 and name CG2) ! I35.Cg2 17.990ppm

(resid 149 and name C) ! K49.Co 175.426ppm

OR (resid 135 and name CG2)

(resid 349 and name C)

assign

(resid 227 and name CG1) ! V27"Cg1 21.544ppm

(resid 132 and name CA) ! I32.Ca 61.129ppm

4.74338 3.5 3 ! intensity= 2107103

OR (resid 227 and name CG1)

(resid 332 and name CA)

OR (resid 227 and name CG1) ! V27"Cg1

21.544ppm

(resid 148 and name CA) ! F48.Ca 61.129ppm

OR (resid 227 and name CG1)

(resid 348 and name CA)

OR (resid 127 and name CG1) ! V27.Cg1

21.544ppm

(resid 132 and name CA) ! I32.Ca 61.129ppm

OR (resid 127 and name CG1)

(resid 332 and name CA)

OR (resid 127 and name CG1) ! V27.Cg1

21.544ppm

(resid 148 and name CA) ! F48.Ca 61.129ppm

OR (resid 127 and name CG1)

(resid 348 and name CA)

OR (resid 228 and name CG2) ! V28"Cg2

21.544ppm

(resid 132 and name CA) ! I32.Ca 61.129ppm

OR (resid 228 and name CG2)

(resid 332 and name CA)

OR (resid 228 and name CG2) ! V28"Cg2

21.544ppm

(resid 148 and name CA) ! F48.Ca 61.129ppm

OR (resid 228 and name CG2)

(resid 348 and name CA)

assign

(resid 228 and name CA) ! V28"Ca 65.615ppm

(resid 130 and name CB) ! A30.Cb 18.548ppm

4.29307 3.5 3 ! intensity= 3833582

OR (resid 228 and name CA)

(resid 330 and name CB)

OR (resid 228 and name CA) ! V28"Ca 65.624ppm

(resid 142 and name CG2) ! I42.Cg2 18.567ppm

OR (resid 228 and name CA)

(resid 342 and name CG2)

OR (resid 232 and name CA) ! I32"Ca 65.615ppm
 (resid 130 and name CB) ! A30.Cb 18.565ppm
 OR (resid 232 and name CA)
 (resid 330 and name CB)
 OR (resid 232 and name CA) ! I32"Ca 65.620ppm
 (resid 142 and name CG2) ! I42.Cg2 18.557ppm
 OR (resid 232 and name CA)
 (resid 342 and name CG2)
 OR (resid 239 and name CA) ! I39"Ca 65.614ppm
 (resid 130 and name CB) ! A30.Cb 18.548ppm
 OR (resid 239 and name CA)
 (resid 330 and name CB)
 OR (resid 239 and name CA) ! I39"Ca 65.621ppm
 (resid 142 and name CG2) ! I42.Cg2 18.556ppm
 OR (resid 239 and name CA)
 (resid 342 and name CG2)

assign
 (resid 128 and name CG2) ! V28.Cg2 21.917ppm
 (resid 230 and name CB) ! A30"Cb 18.447ppm
 3.78646 3.5 3 ! intensity= 8143485
 OR (resid 128 and name CG2)
 (resid 430 and name CB)
 OR (resid 128 and name CG2) ! V28.Cg2
 21.917ppm
 (resid 130 and name CB) ! A30.Cb 18.447ppm
 OR (resid 128 and name CG2)
 (resid 330 and name CB)
 OR (resid 128 and name CG2) ! V28.Cg2
 21.917ppm
 (resid 142 and name CG2) ! I42.Cg2 18.447ppm
 OR (resid 128 and name CG2)
 (resid 342 and name CG2)
 OR (resid 238 and name CD2) ! nL38"Cd2
 21.917ppm
 (resid 230 and name CB) ! A30"Cb 18.447ppm
 OR (resid 238 and name CD2)
 (resid 430 and name CB)
 OR (resid 238 and name CD2) ! L38"Cd2
 21.917ppm
 (resid 130 and name CB) ! A30.Cb 18.447ppm

OR (resid 238 and name CD2)
 (resid 330 and name CB)
 OR (resid 238 and name CD2) ! L38"Cd2
 21.917ppm
 (resid 142 and name CG2) ! I42.Cg2 18.447ppm
 OR (resid 238 and name CD2)
 (resid 342 and name CG2)

assign
 (resid 128 and name CG2) ! V28.Cg2 21.901ppm
 (resid 133 and name CA) ! I33.Ca 64.286ppm
 5.12213 3.5 3 ! intensity= 1328943

OR (resid 128 and name CG2)
 (resid 333 and name CA)
 OR (resid 128 and name CG2) ! V28.Cg2
 21.901ppm
 (resid 135 and name CA) ! I35.Ca 64.286ppm
 OR (resid 128 and name CG2)
 (resid 335 and name CA)
 OR (resid 128 and name CG2) ! V28.Cg2
 21.901ppm
 (resid 142 and name CA) ! I42.Ca 64.286ppm
 OR (resid 128 and name CG2)
 (resid 342 and name CA)
 OR (resid 238 and name CD2) ! L38"Cd2
 21.901ppm
 (resid 133 and name CA) ! I33.Ca 64.286ppm
 OR (resid 238 and name CD2)
 (resid 333 and name CA)
 OR (resid 238 and name CD2) ! L38"Cd2
 21.901ppm
 (resid 135 and name CA) ! I35.Ca 64.286ppm
 OR (resid 238 and name CD2)
 (resid 335 and name CA)
 OR (resid 238 and name CD2) ! L38"Cd2
 21.901ppm
 (resid 142 and name CA) ! I42.Ca 64.286ppm
 OR (resid 238 and name CD2)
 (resid 342 and name CA)

assign

(resid 230 and name CB) ! A30"Cb 18.538ppm
(resid 128 and name CG2) ! V28.Cg2 21.792ppm
3.75393 3.5 3 ! intensity= 8576250
OR (resid 230 and name CB)
(resid 328 and name CG2)
OR (resid 230 and name CB) ! nA30"Cb 18.538ppm
(resid 238 and name CD2) ! L38"Cd2 21.792ppm
OR (resid 230 and name CB)
(resid 438 and name CD2)
OR (resid 130 and name CB) ! A30.Cb 18.538ppm
(resid 128 and name CG2) ! V28.Cg2 21.792ppm
OR (resid 130 and name CB)
(resid 328 and name CG2)
OR (resid 130 and name CB) ! A30.Cb 18.538ppm
(resid 238 and name CD2) ! L38"Cd2 21.792ppm
OR (resid 130 and name CB)
(resid 438 and name CD2)
OR (resid 142 and name CG2) ! I42.Cg2 18.538ppm
(resid 128 and name CG2) ! V28.Cg2 21.792ppm
OR (resid 142 and name CG2)
(resid 328 and name CG2)
OR (resid 142 and name CG2) ! I42.Cg2 18.538ppm
(resid 238 and name CD2) ! L38"Cd2 21.792ppm
OR (resid 142 and name CG2)
(resid 438 and name CD2)

!added -0.5 Angstrom to the below restraint because it was violating by 0.282

assign

(resid 230 and name CB) ! nA30"Cb 18.548ppm
(resid 236 and name CD2) ! L36"Cd2 24.285ppm
4.06457 3.5 3.5 ! intensity= 5322563
OR (resid 230 and name CB)
(resid 436 and name CD2)
OR (resid 230 and name CB) ! A30"Cb 18.548ppm
(resid 140 and name CD2) ! L40.Cd2 24.285ppm
OR (resid 230 and name CB)
(resid 340 and name CD2)
OR (resid 130 and name CB) ! A30.Cb 18.548ppm
(resid 236 and name CD2) ! L36"Cd2 24.285ppm

OR (resid 130 and name CB)

(resid 436 and name CD2)

OR (resid 130 and name CB) ! A30.Cb 18.548ppm

(resid 140 and name CD2) ! L40.Cd2 24.285ppm

OR (resid 130 and name CB)

(resid 340 and name CD2)

OR (resid 142 and name CG2) ! I42.Cg2 18.548ppm

(resid 236 and name CD2) ! L36"Cd2 24.285ppm

OR (resid 142 and name CG2)

(resid 436 and name CD2)

OR (resid 142 and name CG2) ! I42.Cg2 18.548ppm

(resid 140 and name CD2) ! L40.Cd2 24.285ppm

OR (resid 142 and name CG2)

(resid 340 and name CD2)

assign

(resid 136 and name CD1) ! L36.Cd1 26.107ppm

(resid 230 and name CB) ! A30"Cb 18.599ppm

4.15818 3.5 3 ! intensity= 4642932

OR (resid 136 and name CD1)

(resid 430 and name CB)

OR (resid 136 and name CD1) ! L36.Cd1
26.107ppm

(resid 130 and name CB) ! A30.Cb 18.599ppm

OR (resid 136 and name CD1)

(resid 330 and name CB)

OR (resid 136 and name CD1) ! L36.Cd1
26.107ppm

(resid 142 and name CG2) ! I42.Cg2 18.599ppm

OR (resid 136 and name CD1)

(resid 342 and name CG2)

OR (resid 238 and name CD1) ! nL38"Cd1
26.107ppm

(resid 230 and name CB) ! A30"Cb 18.599ppm

OR (resid 238 and name CD1)

(resid 430 and name CB)

OR (resid 238 and name CD1) ! L38"Cd1
26.107ppm

(resid 130 and name CB) ! A30.Cb 18.599ppm

OR (resid 238 and name CD1)

(resid 330 and name CB)

OR (resid 238 and name CD1) ! L38"Cd1
26.107ppm
(resid 142 and name CG2) ! I42.Cg2 18.599ppm
OR (resid 238 and name CD1)
(resid 342 and name CG2)

assign

(resid 137 and name C) ! H37.Co 175.602ppm
(resid 233 and name CG2) ! I33"Cg2 19.618ppm
3.82767 3.5 3 ! intensity= 7631373
OR (resid 137 and name C)
(resid 433 and name CG2)
OR (resid 137 and name C) ! H37.Co 175.593ppm
(resid 139 and name CG2) ! I39.Cg2 19.625ppm
OR (resid 137 and name C)
(resid 339 and name CG2)
OR (resid 147 and name C) ! F47.Co 175.609ppm
(resid 233 and name CG2) ! I33"Cg2 19.625ppm
OR (resid 147 and name C)
(resid 433 and name CG2)
OR (resid 147 and name C) ! F47.Co 175.598ppm
(resid 139 and name CG2) ! I39.Cg2 19.616ppm
OR (resid 147 and name C)
(resid 339 and name CG2)
OR (resid 149 and name C) ! K49.Co 175.590ppm
(resid 233 and name CG2) ! I33"Cg2 19.621ppm
OR (resid 149 and name C)
(resid 433 and name CG2)
OR (resid 149 and name C) ! K49.Co 175.592ppm
(resid 139 and name CG2) ! I39.Cg2 19.630ppm
OR (resid 149 and name C)
(resid 339 and name CG2)

assign

(resid 137 and name C) ! H37.Co 175.594ppm
(resid 235 and name CG2) ! I35"Cg2 17.948ppm
3.92341 3.5 3 ! intensity= 6580094
OR (resid 137 and name C)
(resid 435 and name CG2)
OR (resid 137 and name C) ! H37.Co 175.594ppm
(resid 135 and name CG2) ! I35.Cg2 17.976ppm

OR (resid 137 and name C)
(resid 335 and name CG2)
OR (resid 147 and name C) ! F47.Co 175.633ppm
(resid 235 and name CG2) ! I35"Cg2 17.948ppm
OR (resid 147 and name C)
(resid 435 and name CG2)
OR (resid 147 and name C) ! F47.Co 175.633ppm
(resid 135 and name CG2) ! I35.Cg2 17.976ppm
OR (resid 147 and name C)
(resid 335 and name CG2)
OR (resid 149 and name C) ! K49.Co 175.611ppm
(resid 235 and name CG2) ! I35"Cg2 17.948ppm
OR (resid 149 and name C)
(resid 435 and name CG2)
OR (resid 149 and name C) ! K49.Co 175.611ppm
(resid 135 and name CG2) ! I35.Cg2 17.976ppm
OR (resid 149 and name C)
(resid 335 and name CG2)

assign

(resid 140 and name CD1) ! L40.Cd1 25.081ppm
(resid 133 and name CA) ! I33.Ca 64.199ppm
4.77952 3.5 3 ! intensity= 2013281
OR (resid 140 and name CD1)
(resid 333 and name CA)
OR (resid 140 and name CD1) ! L40.Cd1
25.081ppm
(resid 135 and name CA) ! I35.Ca 64.199ppm
OR (resid 140 and name CD1)
(resid 335 and name CA)
OR (resid 140 and name CD1) ! L40.Cd1
25.081ppm
(resid 142 and name CA) ! I42.Ca 64.199ppm
OR (resid 140 and name CD1)
(resid 342 and name CA)
OR (resid 149 and name CG) ! K49.Cg 25.081ppm
(resid 133 and name CA) ! I33.Ca 64.199ppm
OR (resid 149 and name CG)
(resid 333 and name CA)
OR (resid 149 and name CG) ! K49.Cg 25.081ppm
(resid 135 and name CA) ! I35.Ca 64.199ppm

OR (resid 149 and name CG)
 (resid 335 and name CA)
OR (resid 149 and name CG) ! K49.Cg 25.081ppm
 (resid 142 and name CA) ! I42.Ca 64.199ppm
OR (resid 149 and name CG)
 (resid 342 and name CA)

assign

 (resid 227 and name CG2) ! V27"Cg2 22.437ppm
 (resid 237 and name CD2) ! H37"Cd2
117.172ppm
3.43279 3.5 3 ! intensity= 14666466
OR (resid 227 and name CG2)
 (resid 437 and name CD2)
OR (resid 228 and name CG1) ! V28"Cg1
22.437ppm
 (resid 237 and name CD2) ! H37"Cd2
117.172ppm
OR (resid 228 and name CG1)
 (resid 437 and name CD2)
OR (resid 128 and name CG1) ! V28.Cg1 22.437ppm
 (resid 237 and name CD2) ! H37"Cd2
117.172ppm
OR (resid 128 and name CG1)
 (resid 437 and name CD2)
OR (resid 138 and name CD2) ! L38.Cd2
22.437ppm
 (resid 237 and name CD2) ! H37"Cd2
117.172ppm
OR (resid 138 and name CD2)
 (resid 437 and name CD2)
OR (resid 143 and name CD2) ! L43.Cd2
22.437ppm
 (resid 237 and name CD2) ! H37"Cd2
117.172ppm
OR (resid 143 and name CD2)
 (resid 437 and name CD2)

assign

 (resid 227 and name CG2) ! nV27"Cg2
22.460ppm

 (resid 241 and name CB) ! W41"Cb 27.455ppm
4.04185 3.5 3 ! intensity= 5504620
OR (resid 227 and name CG2)
 (resid 441 and name CB)
OR (resid 228 and name CG1) ! nV28"Cg1
22.460ppm
 (resid 241 and name CB) ! W41"Cb 27.455ppm
OR (resid 228 and name CG1)
 (resid 441 and name CB)
OR (resid 128 and name CG1) ! V28.Cg1
22.460ppm
 (resid 241 and name CB) ! W41"Cb 27.455ppm
OR (resid 128 and name CG1)
 (resid 441 and name CB)
OR (resid 138 and name CD2) ! L38.Cd2
22.460ppm
 (resid 241 and name CB) ! W41"Cb 27.455ppm
OR (resid 138 and name CD2)
 (resid 441 and name CB)
OR (resid 143 and name CD2) ! L43.Cd2
22.460ppm
 (resid 241 and name CB) ! W41"Cb 27.455ppm
OR (resid 143 and name CD2)
 (resid 441 and name CB)

assign

 (resid 231 and name CA) ! N31"Ca 58.102ppm
 (resid 135 and name CD1) ! I35.Cd1 12.636ppm
4.49693 3.5 3 ! intensity= 2902122
OR (resid 231 and name CA)
 (resid 335 and name CD1)
OR (resid 236 and name CA) ! L36"Ca 58.102ppm
 (resid 135 and name CD1) ! I35.Cd1 12.636ppm
OR (resid 236 and name CA)
 (resid 335 and name CD1)
OR (resid 240 and name CA) ! L40"Ca 58.102ppm
 (resid 135 and name CD1) ! I35.Cd1 12.636ppm
OR (resid 240 and name CA)
 (resid 335 and name CD1)
OR (resid 243 and name CA) ! L43"Ca 58.102ppm
 (resid 135 and name CD1) ! I35.Cd1 12.636ppm

OR (resid 243 and name CA)
 (resid 335 and name CD1)
OR (resid 144 and name CA) ! D44.Ca 58.102ppm
 (resid 135 and name CD1) ! I35.Cd1 12.636ppm
OR (resid 144 and name CA)
 (resid 335 and name CD1)

assign

 (resid 135 and name CD1) ! I35.Cd1 12.673ppm
 (resid 231 and name CA) ! N31"Ca 58.074ppm
4.5954 3.5 3 ! intensity= 2548412
OR (resid 135 and name CD1)
 (resid 431 and name CA)
OR (resid 135 and name CD1) ! I35.Cd1 12.673ppm
 (resid 236 and name CA) ! L36"Ca 58.074ppm
OR (resid 135 and name CD1)
 (resid 436 and name CA)
OR (resid 135 and name CD1) ! I35.Cd1 12.673ppm
 (resid 240 and name CA) ! L40"Ca 58.074ppm
OR (resid 135 and name CD1)
 (resid 440 and name CA)
OR (resid 135 and name CD1) ! I35.Cd1 12.673ppm
 (resid 243 and name CA) ! L43"Ca 58.074ppm
OR (resid 135 and name CD1)
 (resid 443 and name CA)
OR (resid 135 and name CD1) ! I35.Cd1 12.673ppm
 (resid 144 and name CA) ! D44.Ca 58.074ppm
OR (resid 135 and name CD1)
 (resid 344 and name CA)

assign

 (resid 237 and name CD2) ! H37"Cd2
117.230ppm
 (resid 227 and name CG2) ! V27"Cg2 22.375ppm
3.63582 3.5 3 ! intensity= 10389578
OR (resid 237 and name CD2)
 (resid 427 and name CG2)
OR (resid 237 and name CD2) ! H37"Cd2
117.230ppm
 (resid 228 and name CG1) ! V28"Cg1 22.375ppm
OR (resid 237 and name CD2)

 (resid 428 and name CG1)
OR (resid 237 and name CD2) ! H37"Cd2
117.230ppm
 (resid 128 and name CG1) ! V28.Cg1 22.375ppm
OR (resid 237 and name CD2)
 (resid 328 and name CG1)
OR (resid 237 and name CD2) ! H37"Cd2
117.230ppm
 (resid 138 and name CD2) ! L38.Cd2 22.375ppm
OR (resid 237 and name CD2)
 (resid 338 and name CD2)
OR (resid 237 and name CD2) ! H37"Cd2
117.230ppm
 (resid 143 and name CD2) ! L43.Cd2 22.375ppm
OR (resid 237 and name CD2)
 (resid 343 and name CD2)

assign

 (resid 144 and name CG) ! D44.Cg 180.178ppm
 (resid 127 and name CA) ! V27.Ca 65.969ppm
4.76241 3.5 3 ! intensity= 2057080
OR (resid 144 and name CG)
 (resid 327 and name CA)
OR (resid 144 and name CG) ! D44.Cg 180.178ppm
 (resid 233 and name CA) ! I33"Ca 65.969ppm
OR (resid 144 and name CG)
 (resid 433 and name CA)
OR (resid 144 and name CG) ! D44.Cg 180.178ppm
 (resid 235 and name CA) ! I35"Ca 65.969ppm
OR (resid 144 and name CG)
 (resid 435 and name CA)
OR (resid 144 and name CG) ! D44.Cg 180.178ppm
 (resid 242 and name CA) ! I42"Ca 65.969ppm
OR (resid 144 and name CG)
 (resid 442 and name CA)
OR (resid 144 and name CG) ! D44.Cg 180.178ppm
 (resid 151 and name CA) ! I51.Ca 65.969ppm
OR (resid 144 and name CG)
 (resid 351 and name CA)

assign

(resid 131 and name CA) ! N31.Ca 54.776ppm
 (resid 133 and name C) ! I33.Co 175.078ppm
 3.7094 3.5 3 ! intensity= 9212728
 OR (resid 131 and name CA)
 (resid 333 and name C)
 OR (resid 131 and name CA) ! N31.Ca 54.776ppm
 (resid 137 and name C) ! H37.Co 175.078ppm
 OR (resid 131 and name CA)
 (resid 337 and name C)
 OR (resid 131 and name CA) ! N31.Ca 54.776ppm
 (resid 147 and name C) ! F47.Co 175.078ppm
 OR (resid 131 and name CA)
 (resid 347 and name C)
 OR (resid 131 and name CA) ! N31.Ca 54.776ppm
 (resid 149 and name C) ! K49.Co 175.078ppm
 OR (resid 131 and name CA)
 (resid 349 and name C)

assign

(resid 133 and name C) ! I33.Co 175.557ppm
 (resid 139 and name CD1) ! I39.Cd1 13.443ppm
 4.76107 3.5 3 ! intensity= 2060556
 OR (resid 133 and name C)
 (resid 339 and name CD1)
 OR (resid 137 and name C) ! H37.Co 175.557ppm
 (resid 139 and name CD1) ! I39.Cd1 13.443ppm
 OR (resid 137 and name C)
 (resid 339 and name CD1)
 OR (resid 147 and name C) ! F47.Co 175.557ppm
 (resid 139 and name CD1) ! I39.Cd1 13.443ppm
 OR (resid 147 and name C)
 (resid 339 and name CD1)
 OR (resid 149 and name C) ! K49.Co 175.557ppm
 (resid 139 and name CD1) ! I39.Cd1 13.443ppm
 OR (resid 149 and name C)
 (resid 339 and name CD1)

assign

(resid 139 and name CD1) ! I39.Cd1 13.496ppm
 (resid 133 and name C) ! I33.Co 175.410ppm
 4.57011 3.5 3 ! intensity= 2634207

OR (resid 139 and name CD1)
 (resid 333 and name C)
 OR (resid 139 and name CD1) ! I39.Cd1 13.496ppm
 (resid 137 and name C) ! H37.Co 175.410ppm
 OR (resid 139 and name CD1)
 (resid 337 and name C)
 OR (resid 139 and name CD1) ! I39.Cd1 13.496ppm
 (resid 147 and name C) ! F47.Co 175.410ppm
 OR (resid 139 and name CD1)
 (resid 347 and name C)
 OR (resid 139 and name CD1) ! I39.Cd1 13.496ppm
 (resid 149 and name C) ! K49.Co 175.410ppm
 OR (resid 139 and name CD1)
 (resid 349 and name C)

assign

(resid 227 and name CG1) ! V27"Cg1 21.550ppm
 (resid 135 and name CD1) ! I35.Cd1 12.664ppm
 4.22654 3.5 3 ! intensity= 4210174
 OR (resid 227 and name CG1)
 (resid 335 and name CD1)
 OR (resid 127 and name CG1) ! V27.Cg1
 21.550ppm
 (resid 135 and name CD1) ! I35.Cd1 12.664ppm
 OR (resid 127 and name CG1)
 (resid 335 and name CD1)
 OR (resid 228 and name CG2) ! V28"Cg2
 21.550ppm
 (resid 135 and name CD1) ! I35.Cd1 12.664ppm
 OR (resid 228 and name CG2)
 (resid 335 and name CD1)

assign

(resid 228 and name CA) ! nV28"Ca 65.624ppm
 (resid 230 and name CB) ! A30"Cb 18.708ppm
 4.41011 3.5 3 ! intensity= 3262225
 OR (resid 228 and name CA)
 (resid 430 and name CB)
 OR (resid 232 and name CA) ! nI32"Ca 65.625ppm
 (resid 230 and name CB) ! A30"Cb 18.709ppm
 OR (resid 232 and name CA)

(resid 430 and name CB)
OR (resid 239 and name CA) ! nI39"Ca 65.613ppm
(resid 230 and name CB) ! A30"Cb 18.708ppm
OR (resid 239 and name CA)
(resid 430 and name CB)

assign

(resid 230 and name CB) ! A30"Cb 18.735ppm
(resid 135 and name CD1) ! I35.Cd1 12.662ppm
4.12477 3.5 3 ! intensity= 4873214
OR (resid 230 and name CB)
(resid 335 and name CD1)
OR (resid 130 and name CB) ! A30.Cb 18.735ppm
(resid 135 and name CD1) ! I35.Cd1 12.662ppm
OR (resid 130 and name CB)
(resid 335 and name CD1)
OR (resid 142 and name CG2) ! I42.Cg2 18.735ppm
(resid 135 and name CD1) ! I35.Cd1 12.662ppm
OR (resid 142 and name CG2)
(resid 335 and name CD1)

assign

(resid 132 and name CA) ! I32.Ca 61.173ppm
(resid 230 and name CB) ! A30"Cb 18.504ppm
4.3524 3.5 3 ! intensity= 3530497
OR (resid 132 and name CA)
(resid 430 and name CB)
OR (resid 132 and name CA) ! I32.Ca 61.173ppm
(resid 130 and name CB) ! A30.Cb 18.504ppm
OR (resid 132 and name CA)
(resid 330 and name CB)
OR (resid 132 and name CA) ! I32.Ca 61.173ppm
(resid 142 and name CG2) ! I42.Cg2 18.504ppm
OR (resid 132 and name CA)
(resid 342 and name CG2)

assign

(resid 133 and name CG1) ! I33.Cg1 28.811ppm
(resid 231 and name CB) ! N31"Cb 39.924ppm
4.68792 3.5 3 ! intensity= 2261156
OR (resid 133 and name CG1)

(resid 431 and name CB)
OR (resid 135 and name CG1) ! I35.Cg1 28.811ppm
(resid 231 and name CB) ! N31"Cb 39.924ppm
OR (resid 135 and name CG1)
(resid 431 and name CB)
OR (resid 142 and name CG1) ! I42.Cg1 28.811ppm
(resid 231 and name CB) ! N31"Cb 39.924ppm
OR (resid 142 and name CG1)
(resid 431 and name CB)

assign

(resid 133 and name C) ! I33.Co 175.065ppm
(resid 131 and name CB) ! N31.Cb 40.609ppm
3.81015 3.5 3 ! intensity= 7844394
OR (resid 133 and name C)
(resid 331 and name CB)
OR (resid 133 and name C) ! I33.Co 175.065ppm
(resid 238 and name CB) ! L38"Cb 40.609ppm
OR (resid 133 and name C)
(resid 438 and name CB)
OR (resid 133 and name C) ! I33.Co 175.065ppm
(resid 240 and name CB) ! L40"Cb 40.609ppm
OR (resid 133 and name C)
(resid 440 and name CB)

assign

(resid 135 and name CD1) ! I35.Cd1 12.807ppm
(resid 227 and name CG1) ! V27"Cg1 21.503ppm
4.48878 3.5 3 ! intensity= 2933867
OR (resid 135 and name CD1)
(resid 427 and name CG1)
OR (resid 135 and name CD1) ! I35.Cd1 12.807ppm
(resid 127 and name CG1) ! V27.Cg1 21.503ppm
OR (resid 135 and name CD1)
(resid 327 and name CG1)
OR (resid 135 and name CD1) ! I35.Cd1 12.807ppm
(resid 228 and name CG2) ! V28"Cg2 21.503ppm
OR (resid 135 and name CD1)
(resid 428 and name CG2)

assign

(resid 135 and name CD1) ! I35.Cd1 12.650ppm
(resid 230 and name CB) ! A30.Cb 18.646ppm
4.32191 3.5 3 ! intensity= 3682625
OR (resid 135 and name CD1)
(resid 430 and name CB)
OR (resid 135 and name CD1) ! I35.Cd1 12.650ppm
(resid 130 and name CB) ! A30.Cb 18.646ppm
OR (resid 135 and name CD1)
(resid 330 and name CB)
OR (resid 135 and name CD1) ! I35.Cd1 12.650ppm
(resid 142 and name CG2) ! I42.Cg2 18.646ppm
OR (resid 135 and name CD1)
(resid 342 and name CG2)

assign

(resid 241 and name CB) ! W41.Cb 27.561ppm
(resid 133 and name CA) ! I33.Ca 64.195ppm
4.53115 3.5 3 ! intensity= 2773074
OR (resid 241 and name CB)
(resid 333 and name CA)
OR (resid 241 and name CB) ! W41.Cb 27.561ppm
(resid 135 and name CA) ! I35.Ca 64.195ppm
OR (resid 241 and name CB)
(resid 335 and name CA)
OR (resid 241 and name CB) ! W41.Cb 27.561ppm
(resid 142 and name CA) ! I42.Ca 64.195ppm
OR (resid 241 and name CB)
(resid 342 and name CA)

assign

(resid 128 and name CG2) ! V28.Cg2 21.959ppm
(resid 137 and name CE1) ! H37.Ce1 136.814ppm
2.66212 3.5 3 ! intensity= 67428160
OR (resid 128 and name CG2)
(resid 337 and name CE1)
OR (resid 238 and name CD2) ! L38.Cd2
21.959ppm
(resid 137 and name CE1) ! H37.Ce1 136.814ppm
OR (resid 238 and name CD2)
(resid 337 and name CE1)

assign

(resid 128 and name CG2) ! V28.Cg2 21.938ppm
(resid 137 and name CG) ! H37.Cg 136.279ppm
4.45498 3.5 3 ! intensity= 3069973
OR (resid 128 and name CG2)
(resid 337 and name CG)
OR (resid 238 and name CD2) ! L38.Cd2
21.963ppm
(resid 137 and name CG) ! H37.Cg 136.279ppm
OR (resid 238 and name CD2)
(resid 337 and name CG)

assign

(resid 128 and name CG2) ! V28.Cg2 21.978ppm
(resid 141 and name CB) ! W41.Cb 28.066ppm
4.06404 3.5 3 ! intensity= 5326724
OR (resid 128 and name CG2)
(resid 341 and name CB)
OR (resid 238 and name CD2) ! L38.Cd2
21.978ppm
(resid 141 and name CB) ! W41.Cb 28.066ppm
OR (resid 238 and name CD2)
(resid 341 and name CB)

assign

(resid 128 and name CG2) ! V28.Cg2 21.949ppm
(resid 141 and name CE3) ! W41.Ce3 119.690ppm
4.51793 3.5 3 ! intensity= 2822126
OR (resid 128 and name CG2)
(resid 341 and name CE3)
OR (resid 238 and name CD2) ! L38.Cd2
21.949ppm
(resid 141 and name CE3) ! W41.Ce3 119.690ppm
OR (resid 238 and name CD2)
(resid 341 and name CE3)

assign

(resid 130 and name CB) ! A30.Cb 18.588ppm
(resid 132 and name CA) ! I32.Ca 61.094ppm
4.09377 3.5 3 ! intensity= 5098825
OR (resid 130 and name CB)

(resid 332 and name CA)
OR (resid 142 and name CG2) ! I42.Cg2 18.567ppm
(resid 132 and name CA) ! I32.Ca 61.094ppm
OR (resid 142 and name CG2)
(resid 332 and name CA)

assign

(resid 133 and name C) ! I33.Co 175.397ppm
(resid 235 and name CG2) ! I35.Cg2 17.948ppm
4.07904 3.5 3 ! intensity= 5210303
OR (resid 133 and name C)
(resid 435 and name CG2)
OR (resid 133 and name C) ! I33.Co 175.397ppm
(resid 135 and name CG2) ! I35.Cg2 17.976ppm
OR (resid 133 and name C)
(resid 335 and name CG2)

assign

(resid 136 and name CD1) ! L36.Cd1 26.084ppm
(resid 141 and name CE3) ! W41.Ce3 119.697ppm
4.80509 3.5 3 ! intensity= 1949854
OR (resid 136 and name CD1)
(resid 341 and name CE3)
OR (resid 238 and name CD1) ! L38.Cd1
26.047ppm
(resid 141 and name CE3) ! W41.Ce3 119.697ppm
OR (resid 238 and name CD1)
(resid 341 and name CE3)

assign

(resid 136 and name CD1) ! L36.Cd1 26.084ppm
(resid 144 and name CB) ! D44.Cb 42.724ppm
5.1814 3.5 3 ! intensity= 1240306
OR (resid 136 and name CD1)
(resid 344 and name CB)
OR (resid 238 and name CD1) ! L38.Cd1
26.047ppm
(resid 144 and name CB) ! D44.Cb 42.724ppm
OR (resid 238 and name CD1)
(resid 344 and name CB)

assign

(resid 237 and name CE1) ! H37.Ce1 135.743ppm
(resid 137 and name CE1) ! H37.Ce1 136.848ppm
4.23693 3.5 3 ! intensity= 4148629
OR (resid 237 and name CE1)
(resid 337 and name CE1)
OR (resid 237 and name CG) ! H37.Cg 135.727ppm
(resid 137 and name CE1) ! H37.Ce1 136.856ppm
OR (resid 237 and name CG)
(resid 337 and name CE1)

assign

(resid 237 and name CE1) ! H37.Ce1 135.747ppm
(resid 141 and name CB) ! W41.Cb 28.076ppm
4.07 3.5 3 ! intensity= 5280154
OR (resid 237 and name CE1)
(resid 341 and name CB)
OR (resid 237 and name CG) ! H37.Cg 135.747ppm
(resid 141 and name CB) ! W41.Cb 28.076ppm
OR (resid 237 and name CG)
(resid 341 and name CB)

assign

(resid 237 and name CE1) ! H37.Ce1 135.689ppm
(resid 141 and name CD1) ! W41.Cd1
124.991ppm
4.73158 3.5 3 ! intensity= 2138809
OR (resid 237 and name CE1)
(resid 341 and name CD1)
OR (resid 237 and name CG) ! H37.Cg 135.689ppm
(resid 141 and name CD1) ! W41.Cd1
124.991ppm
OR (resid 237 and name CG)
(resid 341 and name CD1)

assign

(resid 137 and name CE1) ! H37.Ce1 136.865ppm
(resid 128 and name CG2) ! V28.Cg2 21.911ppm
2.78593 3.5 3 ! intensity= 51332104
OR (resid 137 and name CE1)

(resid 328 and name CG2)
OR (resid 137 and name CE1) ! H37.Ce1
136.865ppm
(resid 238 and name CD2) ! L38"Cd2 21.911ppm
OR (resid 137 and name CE1)
(resid 438 and name CD2)

assign

(resid 137 and name CE1) ! H37.Ce1 136.812ppm
(resid 237 and name CE1) ! H37"Ce1 135.680ppm
4.28217 3.5 3 ! intensity= 3892469
OR (resid 137 and name CE1)
(resid 437 and name CE1)
OR (resid 137 and name CE1) ! H37.Ce1
136.804ppm
(resid 237 and name CG) ! H37"Cg 135.664ppm
OR (resid 137 and name CE1)
(resid 437 and name CG)

assign

(resid 239 and name CD1) ! I39"Cd1 13.782ppm
(resid 140 and name CD1) ! L40.Cd1 24.971ppm
4.54216 3.5 3 ! intensity= 2732966
OR (resid 239 and name CD1)
(resid 340 and name CD1)
OR (resid 151 and name CD1) ! I51.Cd1 13.782ppm
(resid 140 and name CD1) ! L40.Cd1 24.971ppm
OR (resid 151 and name CD1)
(resid 340 and name CD1)

assign

(resid 241 and name CB) ! nW41"Cb 27.492ppm
(resid 236 and name CD2) ! L36"Cd2 24.262ppm
3.66693 3.5 3 ! intensity= 9871712
OR (resid 241 and name CB)
(resid 436 and name CD2)
OR (resid 241 and name CB) ! W41"Cb 27.492ppm
(resid 140 and name CD2) ! L40.Cd2 24.262ppm
OR (resid 241 and name CB)
(resid 340 and name CD2)

assign

(resid 141 and name CB) ! W41.Cb 28.122ppm
(resid 237 and name CE1) ! H37"Ce1 135.658ppm
4.03247 3.5 3 ! intensity= 5581908
OR (resid 141 and name CB)
(resid 437 and name CE1)
OR (resid 141 and name CB) ! W41.Cb 28.122ppm
(resid 237 and name CG) ! H37"Cg 135.658ppm
OR (resid 141 and name CB)
(resid 437 and name CG)

assign

(resid 141 and name CE3) ! W41.Ce3 119.697ppm
(resid 128 and name CG2) ! V28.Cg2 21.890ppm
4.84161 3.5 3 ! intensity= 1863247
OR (resid 141 and name CE3)
(resid 328 and name CG2)
OR (resid 141 and name CE3) ! W41.Ce3
119.704ppm
(resid 238 and name CD2) ! L38"Cd2 21.879ppm
OR (resid 141 and name CE3)
(resid 438 and name CD2)

assign

(resid 230 and name CB) ! A30"Cb 18.756ppm
(resid 132 and name CA) ! I32.Ca 61.094ppm
4.56036 3.5 3 ! intensity= 2668180
OR (resid 230 and name CB)
(resid 332 and name CA)

!to the below, added 1.0 A was violating by 0.3A

assign

(resid 232 and name CG2) ! I32"Cg2 17.603ppm
(resid 135 and name CD1) ! I35.Cd1 12.679ppm
4.5043 3.5 4.0 ! intensity= 2873742
OR (resid 232 and name CG2)
(resid 335 and name CD1)

assign

(resid 137 and name CE1) ! H37.Ce1 136.968ppm
(resid 241 and name CB) ! W41"Cb 27.518ppm
4.7182 3.5 3 ! intensity= 2175471

OR (resid 137 and name CE1) (resid 437 and name CD2)
 (resid 441 and name CB)

assign
 (resid 241 and name CB) ! W41"Cb 27.327ppm
 (resid 137 and name CE1) ! H37.Ce1 136.848ppm
 (resid 237 and name CD2) ! H37"Cd2 4.42948 3.5 3 ! intensity= 3177570
 117.188ppm OR (resid 241 and name CB)
 4.75059 3.5 3 ! intensity= 2087989 (resid 337 and name CE1)
 OR (resid 137 and name CG)

1H-1H RFDR

The methyl constraints were entered to the methyl carbon due to three fold hopping of methyl ¹H.

assign (resid 232 and name Cd1) (resid 133 and name Cd1 or resid 333 and name Cd1) 6.5 4.0 0.50
 assign (resid 432 and name Cd1) (resid 133 and name Cd1 or resid 333 and name Cd1) 6.5 4.0 0.50
 assign (resid 238 and name Cd2) (resid 133 and name Cd1 or resid 333 and name Cd1) 6.5 4.0 0.50
 assign (resid 438 and name Cd2) (resid 133 and name Cd1 or resid 333 and name Cd1) 6.5 4.0 0.50
 assign (resid 139 and name Cd1) (resid 233 and name Cd1 or resid 433 and name Cd1) 6.5 4.0 0.50
 assign (resid 339 and name Cd1) (resid 233 and name Cd1 or resid 433 and name Cd1) 6.5 4.0 0.50
 assign (resid 239 and name Cd1) (resid 242 and name Cd1) 6.5 4.0 0.50
 assign (resid 439 and name Cd1) (resid 442 and name Cd1) 6.5 4.0 0.50
 assign (resid 140 and name Cd2) (resid 151 and name Cd1) 6.5 4.0 0.50
 assign (resid 340 and name Cd2) (resid 351 and name Cd1) 6.5 4.0 0.50
 assign (resid 135 and name Cd1) (resid 139 and name Cd1) 6.5 4.0 0.50
 assign (resid 335 and name Cd1) (resid 339 and name Cd1) 6.5 4.0 0.50

Acknowledgement.

This work was supported by grants EB-001960 and EB-002026. We thank Rafal Pielak and Marcelo Berardi for thoughtful discussions.

5.5 References

- (1) Zebedee, S. L.; Richardson, C. D.; Lamb, R. A., Characterization of the Influenza Virus-M2 Integral Membrane-Protein and Expression at the Infected-Cell Surface from Cloned Cdna. *Journal of Virology* **1985**, *56* (2), 502-511.
- (2) Lamb, R. A.; Zebedee, S. L.; Richardson, C. D., Influenza Virus-M2 Protein Is an Integral Membrane-Protein Expressed on the Infected-Cell Surface. *Cell* **1985**, *40* (3), 627-633.

- (3) Tobler, K.; Kelly, M. L.; Pinto, L. H.; Lamb, R. A., Effect of cytoplasmic tail truncations on the activity of the M-2 ion channel of influenza A virus. *Journal of Virology* **1999**, *73* (12), 9695-9701.
- (4) Andreas, L. B.; Barnes, A. B.; Corzilius, B.; Chou, J. J.; Miller, E. A.; Caporini, M.; Rosay, M.; Griffin, R. G., Dynamic nuclear polarization study of inhibitor binding to the m218-60 proton transporter from influenza a. *Biochemistry* **2013**, *52* (16), 2774-82.
- (5) Pielak, R. M.; Oxenoid, K.; Chou, J. J., Structural Investigation of Rimantadine Inhibition of the AM2-BM2 Chimera Channel of Influenza Viruses. *Structure* **2011**, *19* (11), 1655-1663.
- (6) Stouffer, A. L.; Acharya, R.; Salom, D.; Levine, A. S.; Di Costanzo, L.; Soto, C. S.; Tereshko, V.; Nanda, V.; Stayrook, S.; DeGrado, W. F., Structural basis for the function and inhibition of an influenza virus proton channel. *Nature* **2008**, *451* (7178), 596-9.
- (7) Cady, S. D.; Schmidt-Rohr, K.; Wang, J.; Soto, C. S.; DeGrado, W. F.; Hong, M., Structure of the amantadine binding site of influenza M2 proton channels in lipid bilayers. *Nature* **2010**, *463* (7281), 689.
- (8) Cady, S. D.; Wang, J.; Wu, Y.; DeGrado, W. F.; Hong, M., Specific binding of adamantane drugs and direction of their polar amines in the pore of the influenza M2 transmembrane domain in lipid bilayers and dodecylphosphocholine micelles determined by NMR spectroscopy. *J Am Chem Soc* **2011**, *133* (12), 4274-84.
- (9) Schnell, J.; Chou, J., Structure and mechanism of the M2 proton channel of influenza A virus. *Nature* **2008**, *451* (7178), 591-595.
- (10) Smart, O. S.; Goodfellow, J. M.; Wallace, B. A., The pore dimensions of gramicidin A. *Biophys J* **1993**, *65* (6), 2455-60.
- (11) Pielak, R. M.; Schnell, J. R.; Chou, J. J., Mechanism of drug inhibition and drug resistance of influenza A M2 channel. *Proc Natl Acad Sci U S A* **2009**, *106* (18), 7379-84.
- (12) Hu, J.; Fu, R.; Nishimura, K.; Zhang, L.; Zhou, H. X.; Busath, D. D.; Vijayvergiya, V.; Cross, T. A., Histidines, heart of the hydrogen ion channel from influenza A virus: toward an understanding of conductance and proton selectivity. *Proc Natl Acad Sci U S A* **2006**, *103* (18), 6865-70.
- (13) Hu, F.; Schmidt-Rohr, K.; Hong, M., NMR detection of pH-dependent histidine-water proton exchange reveals the conduction mechanism of a transmembrane proton channel. *J Am Chem Soc* **2012**, *134* (8), 3703-13.
- (14) Acharya, R.; Carnevale, V.; Fiorin, G.; Levine, B. G.; Polishchuk, A. L.; Balannik, V.; Samish, I.; Lamb, R. A.; Pinto, L. H.; DeGrado, W. F.; Klein, M. L., Structure and mechanism of proton transport through the transmembrane tetrameric M2 protein bundle of the influenza A virus. *Proc Natl Acad Sci U S A* **2010**, *107* (34), 15075-80.
- (15) Andreas, L. B.; Eddy, M. T.; Chou, J. J.; Griffin, R. G., Magic-Angle-Spinning NMR of the Drug Resistant S31N M2 Proton Transporter from Influenza A. *Journal of the American Chemical Society* **2012**, *134* (17), 7215-7218.
- (16) Andreas, L. B.; Eddy, M. T.; Pielak, R. M.; Chou, J.; Griffin, R. G., Magic Angle Spinning NMR Investigation of Influenza A M2(18-60): Support for an Allosteric Mechanism of Inhibition. *Journal of the American Chemical Society* **2010**, *132* (32), 10958-10960.
- (17) Can, T. V.; Sharma, M.; Hung, I.; Gor'kov, P. L.; Brey, W. W.; Cross, T. A., Magic angle spinning and oriented sample solid-state NMR structural restraints combine for influenza a M2 protein functional insights. *J Am Chem Soc* **2012**, *134* (22), 9022-5.
- (18) Sharma, M.; Yi, M.; Dong, H.; Qin, H.; Peterson, E.; Busath, D. D.; Zhou, H. X.; Cross, T. A., Insight into the mechanism of the influenza A proton channel from a structure in a lipid bilayer. *Science* **2010**, *330* (6003), 509-12.
- (19) Huber, M.; Hiller, S.; Schanda, P.; Ernst, M.; Bockmann, A.; Verel, R.; Meier, B. H., A proton-detected 4D solid-state NMR experiment for protein structure determination. *Chemphyschem* **2011**, *12* (5), 915-8.

- (20) Zhou, D. H.; Rienstra, C. M., High-performance solvent suppression for proton detected solid-state NMR. *Journal of Magnetic Resonance* **2008**, *192* (1), 167-172.
- (21) Knight, M. J.; Webber, A. L.; Pell, A. J.; Guerry, P.; Barbet-Massin, E.; Bertini, I.; Felli, I. C.; Gonnelli, L.; Pierattelli, R.; Emsley, L.; Lesage, A.; Herrmann, T.; Pintacuda, G., Fast resonance assignment and fold determination of human superoxide dismutase by high-resolution proton-detected solid-state MAS NMR spectroscopy. *Angew Chem Int Ed Engl* **2011**, *50* (49), 11697-701.
- (22) Guerry, P.; Herrmann, T., Advances in automated NMR protein structure determination. *Quarterly Reviews of Biophysics* **2011**, *44* (3), 257-309.
- (23) Walsh, S. T. R.; Cheng, R. P.; Wright, W. W.; Alonso, D. O. V.; Daggett, V.; Vanderkooi, J. M.; DeGrado, W. F., The hydration of amides in helices; a comprehensive picture from molecular dynamics, IR, and NMR. *Protein Science* **2003**, *12* (3), 520-531.
- (24) Olivella, M.; Deupi, X.; Govaerts, C.; Pardo, L., Influence of the environment in the conformation of alpha-helices studied by protein database search and molecular dynamics simulations. *Biophysical Journal* **2002**, *82* (6), 3207-3213.
- (25) Gans, P.; Hamelin, O.; Sounier, R.; Ayala, I.; Dura, M. A.; Amero, C. D.; Noirclerc-Savoie, M.; Franzetti, B.; Plevin, M. J.; Boisbouvier, J., Stereospecific isotopic labeling of methyl groups for NMR spectroscopic studies of high-molecular-weight proteins. *Angew Chem Int Ed Engl* **2010**, *49* (11), 1958-62.

Chapter 6: Synthesis and physical properties of Deuterated 1,2-Diphytanoyl-*sn*-glycero-3-phosphocholine Lipid

This project received major contribution from Ta-Chung Ong, who recorded and analyzed deuterium spectra, and from Vladimir Gelev, who helped with lipid synthesis.

6.1 Introduction

MAS NMR of sizeable biological molecules requires control of isotopic labeling in order to introduce NMR active nuclei into the protein of interest. For proteins, this typically involves ^{15}N and ^{13}C labeling. Additional labeling of oxygen with ^{17}O may become another important strategy for structure determination, but currently the high cost and low sensitivity have limited research in this area. In contrast, ^1H is a naturally abundant, an NMR active nucleus with a high magnetic moment ideal for NMR and nearly all biological solution NMR measurements are detected on ^1H for this reason. In the solid state, however, the strong ^1H - ^1H dipole couplings result in broad lines for highly ^1H dense samples, even with high MAS rates (>60 kHz). Nevertheless, it is possible to retain the high sensitivity of ^1H with high resolution (<0.05 ppm FWHM) by perdeuteration of the protein and introduction of select sites with ^1H at 100% labeling. This motivates the synthesis of deuterated lipids and precursors for the introduction of ^1H at select sites on the protein in a perdeuterated background. In addition, dynamic nuclear polarization studies require a low proton concentration in order to reach high signal enhancement factors, which can be achieved for membrane protein samples by deuterating the lipid.

1,2-Diphytanoyl-*sn*-glycero-3-phosphocholine Lipid (DPhPC) forms a favorable membrane for the study of membrane proteins. Notably, the gel to liquid crystalline phase transition that characterizes most lipids has not been detected in DPhPC, and the acyl chains probably remain in a disordered state or a glass as the temperature is decreased.¹ Given that most membrane proteins are functional in the liquid crystalline phase, the absence of gel phase makes DPhPC an ideal candidate for temperature dependent membrane protein studies. Among others, DPhPC has been used in the study of gramicidin,^{2,3} alamethicin,⁴ rhodopsin,^{5,6} VDAC,⁷ and M2.⁸

The chemical structure of DPhPC is shown in *Figure 6.1*. Unlike other saturated straight-chain lipids like 1,2-dimyristoyl-*sn*-glycero-3-phosphocholine (DMPC) and 1,2-dipalmitoyl-*sn*-glycero-3-phosphocholine (DPPC), DPhPC has four additional methyl groups on each acyl chain. The lipid is found naturally in the membranes of halobacteria,⁹ and is known to form very stable

bilayers. The bilayers also experience low ion leakage, making them suitable for electrophysiological ion-conducting studies.¹⁰ A unique and important property of DPhPC bilayers is that they are phase stable at liquid crystalline phase for an extended temperature range from -120 °C to 120 °C according to DSC studies.¹

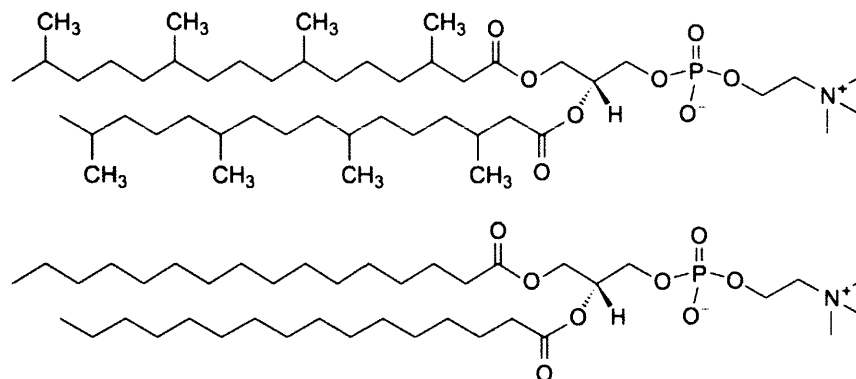


Figure 6.1 Protonated DPhPC (top) and DPPC (bottom). The only structural difference is the addition of the four methyl groups in DPhPC.

Recent advancements in solid-state NMR have created a new need to synthesize more deuterated lipids such as DPhPC. Dynamic nuclear polarization (DNP),^{11, 12} which improves NMR signal-to-noise by one to two orders of magnitude, is optimal at low proton concentration. Deuterating the proton-rich acyl chains (39 protons per chain for DPhPC) effectively decreases overall sample proton concentration and is expected to improve DNP efficiency by a factor of two.¹³ In general, deuteration has the advantage of reducing heteronuclear dipolar coupling between ¹³C and ¹H, leading to sharper line width and better resolution. It also eliminates unwanted lipid signals in ¹H-¹³C cross-polarization experiments when one only wishes to observe the protein. While fully protonated DPhPC is commercially available, the chain-deuterated version is not.

²H NMR spectra can be used as a sensitive probe of molecular motions that take place over a broad range of timescales¹⁴ spanning $\sim 10^3$ s⁻¹ to $\sim 10^8$ s⁻¹, and has been used extensively in the study of membrane dynamics.^{15, 16} Due to the unusual behavior of DPhPC and its utility for spectroscopic studies of membrane proteins, we synthesized alkyl deuterated (d79) DPhPC and undertook a careful analysis of the temperature the dependent ²H spectra in order to better understand the lipid's dynamic properties at ambient temperatures and at cryogenic temperatures that are used for DNP.

6.2 Results and Discussion

The temperature dependent ^2H spectra for pure DPhPC and DPhPC incorporated with M2 at 1:1 wt ratio are shown in **Figure 6.2** and compared with DPPC. Three distinct temperature regimes can be identified for DPhPC. For the spectral line shapes at 180 K and below, the inner two peaks are separated by 36 kHz that is indicative of methyl groups undergoing fast 3-site hops ($> 10^6 \text{ s}^{-1}$).¹⁷ The outer two peaks are separated by 120 kHz, which is the expected splitting for rigid C-D ($< 10^4 \text{ s}^{-1}$). The overlap of these two sets of powder patterns suggest that at these temperatures the acyl chains only have slow motions at these temperatures, while the methyl groups retain fast local motions. At temperatures between 180 K and 220 K, an isotropic component begins to emerge and the intensity of the powder pattern is reduced, as shown in **Figure 6.3**. This is indicative of motion on an intermediate timescale (microseconds to milliseconds). Above 220 K, the isotropic component dominates the spectrum, and a significant broad component is also seen at the base of the sharp resonance. The incorporation of M2 into DPhPC increased the transition temperature slightly by 7 degrees, which suggests that the pure lipids are more mobile.

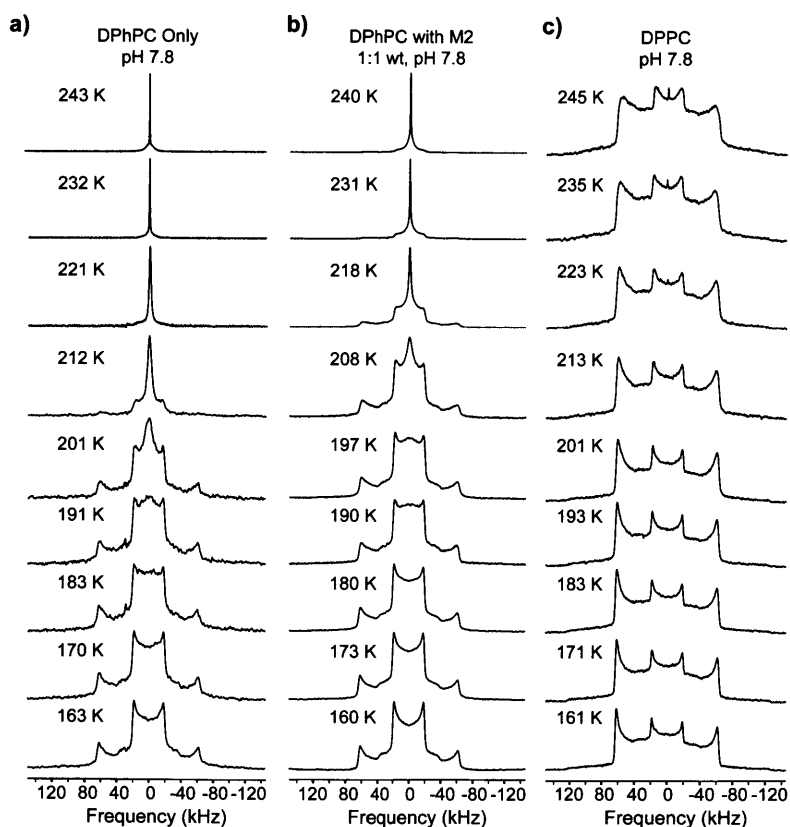


Figure 6.2. Temperature dependent ^2H spectra of DPhPC, DPhPC:M2, and DPPC.

The observation of a sharp isotropic peak at higher temperature was unexpected. As shown in *Figure 6.2 c*), DPPC ^2H spectra are gel phase powder patterns for the same temperature range. The comparison shows that the additional four methyl groups in DPhPC appeared to have led to major motional difference respective to DPPC. The isotropic peak suggests that the acyl chains undergo fast randomized motions similar to an isotropic liquid, which is surprising given that the acyl chains are tethered at one end to the phosphocholine bilayer. In addition, recent MD simulation work by Shinoda et al. comparing DPhPC and DPPC shows that the methyl groups of DPhPC inhibit gauche-trans isomerization in the acyl chains, reducing the rate of acyl chain motions in DPhPC compared with DPPC.¹⁸ Clearly this effect must be small enough that the local chain motions are still fast limit, and the difference between the spectra of DPPC and DPhPC must be explained by a difference in population; in DPPC, the trans conformation is highly favored, whereas in DPhPC, there is no single highly favorable state.

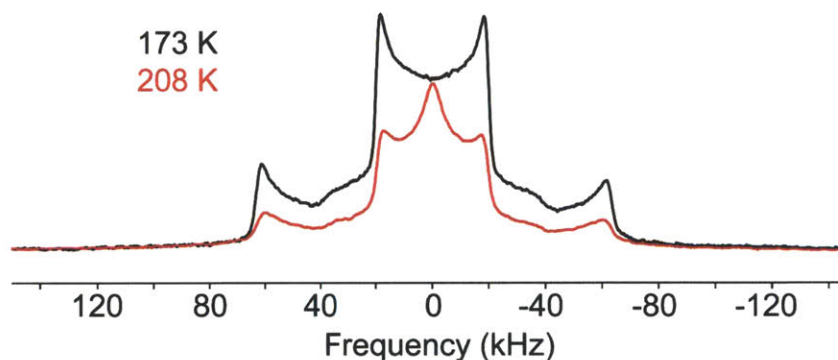


Figure 6.3. The ^2H spectrum of DPhPC at 173 K overlapped with that of 208 K on an absolute scale. The isotropic peak emerges while the powder pattern is reduced by 50%.

The fact that we see fast DPhPC acyl chain motions suggests that DPhPC might undergo a phase transition as the temperature is reduced. This does not appear to be the case. In a previous report, no transition was observed by DSC,¹ a sensitive method. A DSC of the deuterated DPhPC in 60% glycerol, *Figure 6.4*, shows no lipid phase transition (the glass transition near 160 K is from the 60:40 glycerol:water¹⁹). A low intensity glass transition might be observed between 180 and 200 K, in agreement with the ^2H spectra of *Figure 6.2*. However, the intensity of this feature in the DSC trace is too low to be certain. Instead of a phase transition, molecular motion appears to reduce gradually with temperature, with no detectable phase transition and probably leaving the acyl chains in a glassy state. The ^2H NMR spectra (*Figure 6.2*) also support this gradual transition, with spectral changes occurring well over 30 degrees.

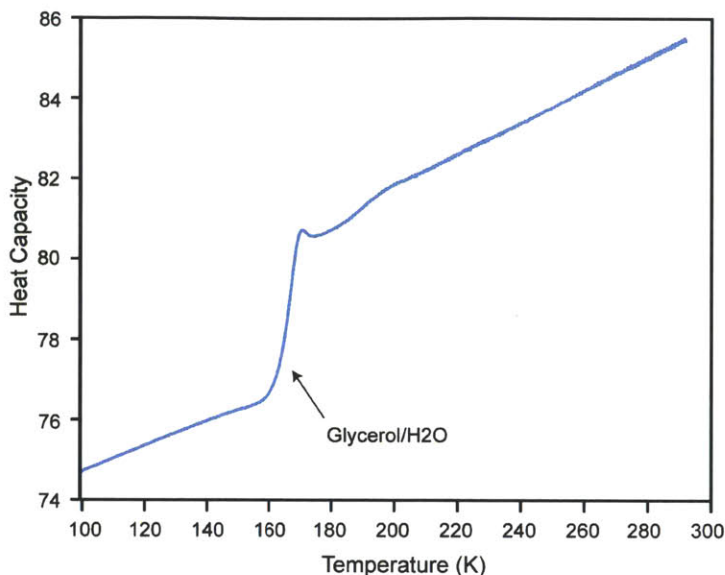


Figure 6.4. Differential scanning calorimetry (DSC) trace of ²H DPhPC in 60:40 glycerol:water (vol). The trace was recorded with a heating rate of 20 °C per minute, and the temperature calibrated with cyclohexane. Approximately 30 to 40 percent of the sample weight was estimated to be lipid.

Since the entire DPhPC molecule does not undergo isotropic tumbling as in liquids, the most likely explanation for a narrow peak is multiple local motions that in aggregate provide motional averaging that completely removes orientation dependence. A ²H NMR study by Hsieh and Wu showed that well-hydrated deuterated DMPC headgroup exhibits similar ²H spectra as the ones we observed for DPhPC acyl chain.²⁰ At first glance, this may not seem like a good comparison, because the phosphocholine is hydrophilic, carrying positive and negative charge, while the acyl chain is hydrophobic. Nonetheless, choline also has multiple methyl groups that equally favor all three of the positions about the C-N bond, resulting in multi-axis averaging. Hsieh and Wu argued that motions in the headgroup constantly reorient the headgroup methyl groups along the C-N bond, thereby eliminating orientation dependence and the powder pattern is averaged into an isotropic peak. In the same way, it is not farfetched to argue that motions in the acyl chain must be having a similar effect on the DPhPC acyl chain deuterons. We observed that the methyl groups have localized fast motions at lower temperature (< 160 K) at which the acyl chain motions are frozen. As the temperature increases and acyl chain motion returns, and aggregate acyl chain motion averages the angular dependence of the deuterons, collapsing the powder pattern into the observed isotropic component. Some residual angular dependence (most likely from deuterium nearest the glycerol group) is evident at the base of the isotropic peak, as shown in **Figure 6.5**. However, even these broader components of the spectrum are significantly narrowed to less than 10 to 20 kHz. Further elucidation of the lipid side chain motion could be provided

with specifically deuterated DPhPC and examination of the motional characteristic of specific acyl chain deuterons.

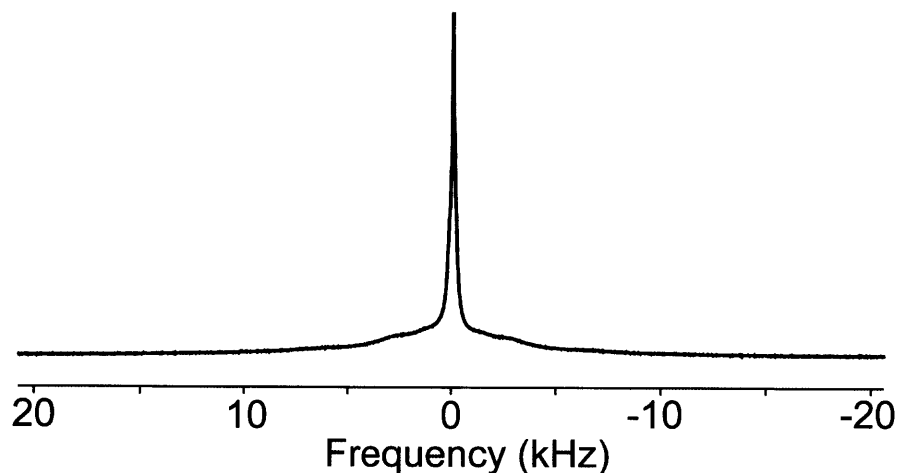


Figure 6.5. The ^2H NMR spectrum of chain deuterated DPhPC at 290 K. At this temperature, acyl chain motion constantly reorients the deuterons (particularly in the methyl groups) resulting in an isotropic peak. Sites with a non-isotropic average have residual angular dependence and therefore appear as a ~ 10 kHz broad feature underneath the sharp peak.

6.3 Methods

NMR Spectroscopy

Solid state ^2H NMR experiments were performed on a custom-built spectrometer (Courtesy of Dr. D. Ruben) operating at 60.8 MHz for ^2H using a single-channel probe with 4.0 mm coil. Spectra were obtained with a quadrupolar echo sequence with a $\pi/2$ pulse of $2.0 \mu\text{s}$ and a delay of $30 \mu\text{s}$ between the two pulses. For cryogenic temperature experiments, cold N_2 gas was cooled by a custom designed heat exchanger²¹ with temperature modulated by a Lakeshore temperature controller before transfer to the probe. The magnet bore was protected from the cold probe by a custom designed dewar.²² Temperature inside the probe was monitored by Neoptix fiber optics temperature sensors.

Solid state ^{31}P NMR experiments were performed on a custom-built spectrometer (Courtesy of Dr. D. Ruben) operating at 153 MHz for ^{31}P using a Varian probe with a 4.0 mm coil.

Differential Scanning Calorimetry

DSC traces were recorded on a Perkin Elmer calorimeter with a cryofill LN₂ cooler. A trace of an empty pan was subtracted from the sample trace, and the temperature was calibrated using the known transitions of cyclohexane at 280 K and 186 K.^{23,24}

Synthesis of DPhPC

Dideuterophytol

Dideuterophytol was synthesized using Raney-nickel hydrogenation of phytol purchased from Sigma-Aldrich. The procedure has been described in the literature²⁵ and is briefly reproduced here. To an 85 mL solution of 20% phytol in ethanol was added 4 mL of Raney Ni Slurry, which was purged with N₂ in a round bottomed flask. The flask was left for 24 hrs under a stream of D₂ at 1 atm pressure, and the product was separated from the catalyst by filtration and rotary evaporation.

Phytanic Acid

Phytanic Acid was synthesized from Dideuterophytol by oxidation with chromium trioxide as previously described.²⁶ This procedure is described briefly here. To 5 g of dideuterophytol in 300 mL 2:1 acetone/acetic acid solvent mixture was added 0.8 g of chromium trioxide in 5 mL of water. The chromium trioxide was added dropwise at room temperature, with stirring for over 1 hr. 250 mL of water was then added, and excess sodium bisulfate was used to destroy excess oxidant. Extraction in diethyl ether and purification on silica followed the previously described protocol. The product was verified with ¹H and ¹³C NMR.

²H Phytanic Acid

Perdeuteration of phytanic acid was performed using a simple method of hydrogenation conditions at an elevated temperature of 195 °C with palladium on charcoal (Pd/C) catalyst (Sigma-Aldrich).²⁷ 4 to 5 grams of Pd/C (10% Pd) and 25g of phytanic acid were heated to 195 °C and 1 atm. of D₂ with stirring in a 250 mL round bottom flask. A continual flow of D₂ gas was generated from D₂O using a Parker-Balston hydrogen generator with a flow rate exceeding 30 cubic centimeters per minute. The reaction was tracked by the loss of proton NMR signal using benzene as an internal standard, and reached 97-98% deuteration after 16 days.

DPhPC

Coupling of phytanic acid to GPC was performed by FBReagents (Cambridge MA) using DCC and DMAP, and purified with silica gel chromatography. The ^1H NMR spectrum of DPhPC in deuterated chloroform is shown in **Figure 6.6 a**. The choline methyl ($9\ ^1\text{H}$) at 3.2 ppm and the choline and glycerol methylene and methine groups ($9\ ^1\text{H}$) around 4 ppm are the major signals expected. In addition, residual signal from the deuterated acyl chains ($\sim 3\%$ of $78\ ^1\text{H}$) appears between 0 and 3 ppm. The remaining signal intensity between 0 and 3 ppm and at 5.2 ppm arises from impurity. With this analysis, the purity by NMR is above 85%. In **Figure 6.6 b**, a thin layer chromatogram shows a single spot with the same retention time as commercial protonated DPhPC (Avanti). The running condition for the TLC was 65:24:4 chloroform:methanol:4M Ammonium Hydroxide.

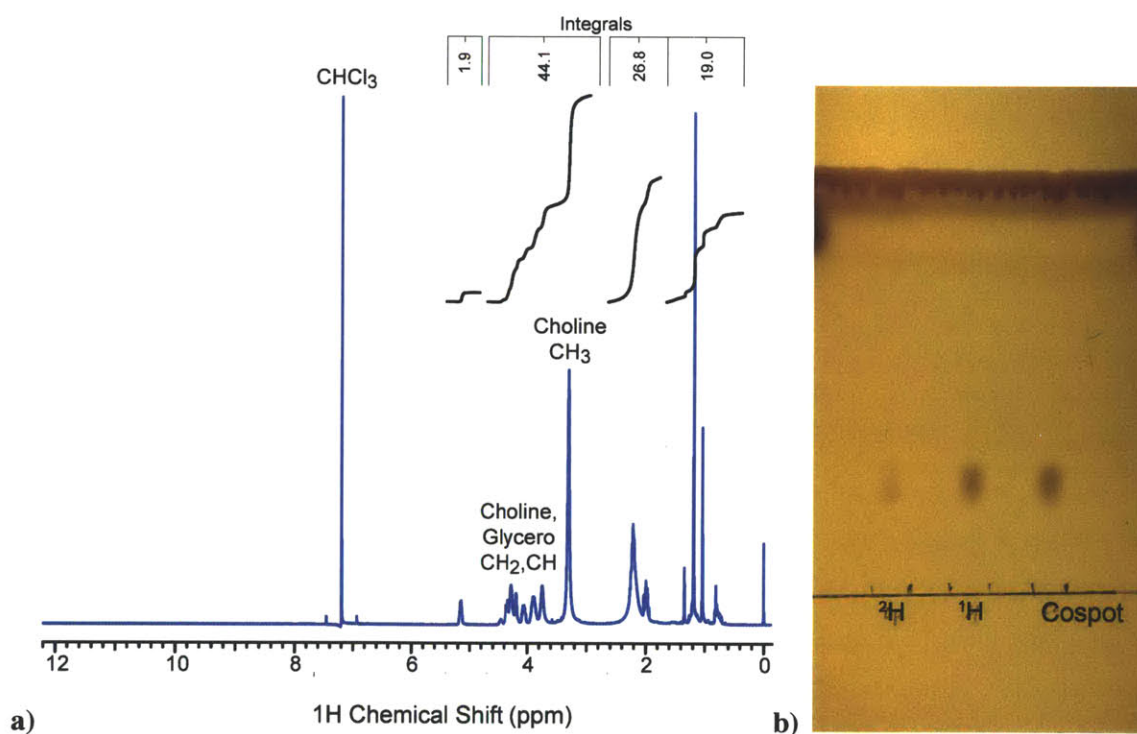


Figure 6.6. Proton spectrum (a) of acyl chain deuterated (d_{78}) DPhPC demonstrating a purity by NMR of above 85%. In (b), a thin layer chromatogram shows a single spot with the same retention time as commercial protonated DPhPC.

Sample Preparation

Lipid bilayer

Lipid bilayer samples were prepared by a simple dialysis procedure. Lipid was dissolved in octyl glucoside detergent, in glutamate buffer at pH 7.8, and the detergent was removed by dialysis

against glutamate buffer using a 3.5 kD dialysis cassette (Pearce). After several days, the sample was centrifuged and transferred to a glass capillary sample tube.

In order to confirm the presence of bilayers, a ^{31}P spectrum was recorded at a ^{31}P frequency of 153 MHz (*Figure 6.7*). The spectrum exhibits the expected axial powder pattern of liquid crystalline lipids in a bilayer, which results from the uniaxial rotational diffusion about the bilayer normal. In addition, there is a small component evident as a narrowed peak in the middle of the spectrum. This component could occur due to lipid in a high-curvature phase, such as a hexagonal phase, where lateral diffusion about a curved surface results in additional averaging.

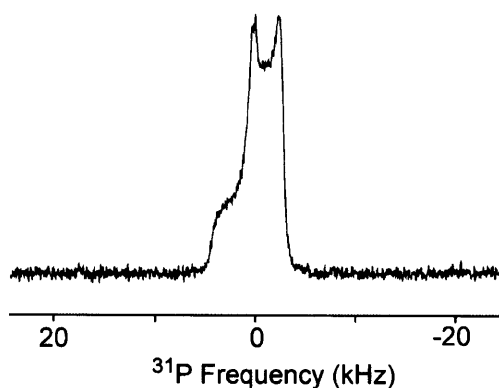


Figure 6.7. Phosphorus spectrum of alkyl chain deuterated (d78) DPhPC. The spectrum is dominated by an axial powder pattern typical of bilayers. In addition, a small narrowed component is present, which may come from a small amount of the sample in a hexagonal phase or another phase with high curvature.

Lipid bilayer with M2 Embedded

Lipid bilayer samples with M2 embedded were prepared using a detergent dialysis procedure as described previously⁸ and the ^{13}C and ^{15}N shifts of M2 were verified as identical to previously recorded spectra in commercial protonated DPhPC (*Figure 6.8*). In *Figure 6.8* the additional peaks in the ^2H lipids sample are due to differences in protein labeling – FY amino acids were reverse labeled in the commercial lipid sample. This is further evidence of the high purity of the deuterated lipids, which was sufficient for the reconstitution of a membrane protein.

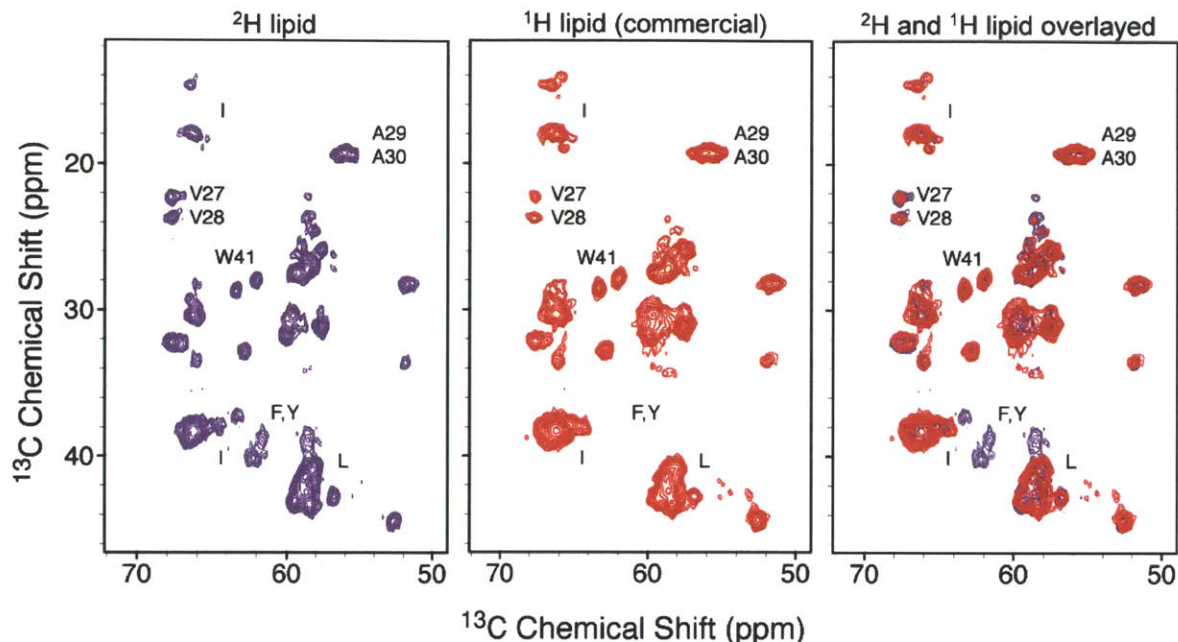


Figure 6.8. Comparison of $M2_{18-60}$ spectra in ^2H DPhPC and in commercial ether linked DPhPC. Proton driven spin diffusion PDSF spectra (15 ms mixing) are shown in purple and red for the ^2H and commercial lipids, respectively. Spectra were recorded at magnetic fields corresponding to ^1H frequencies of 700 (commercial) and 750 MHz (^2H) and spinning at 12.5 kHz and 13.4 kHz, respectively. The protein was $\text{U-}^{13}\text{C-}^{15}\text{N}$ labeled for the ^2H lipids sample, and $\text{U-}^{13}\text{C-}^{15}\text{N-}[^{12}\text{C-}^{14}\text{N-FY}]$ labeled for the commercial lipids sample.

Acknowledgement.

This work was supported by grants EB-001960 and EB-002026. We thank Professor Vladimir Gelev for intimate involvement in this work. Without his help, this project would not have moved forward.

6.4 References

- (1) Lindsey, H.; Petersen, N. O.; Chan, S. I., Physicochemical Characterization of 1,2-Diphytanoyl-Sn-Glycero-3-Phosphocholine in Model Membrane Systems. *Biochimica Et Biophysica Acta* **1979**, *555* (1), 147-167.
- (2) Koeppe, R. E., 2nd; Anderson, O. S., Engineering the gramicidin channel. *Annu Rev Biophys Biomol Struct* **1996**, *25*, 231-58.
- (3) Durkin, J. T.; Koeppe, R. E., 2nd; Andersen, O. S., Energetics of gramicidin hybrid channel formation as a test for structural equivalence. Side-chain substitutions in the native sequence. *J Mol Biol* **1990**, *211* (1), 221-34.
- (4) Taylor, R. J.; Delevie, R., Reversed Alamethicin Conductance in Lipid Bilayers. *Biophys J* **1991**, *59* (4), 873-879.
- (5) Mollevanger, L. C. P. J.; Kentgens, A. P. M.; Pardo, J. A.; Courtin, J. M. L.; Veeman, W. S.; Lugtenburg, J.; Degrip, W. J., High-Resolution Solid-State C-13-Nmr Study of Carbons C-

5 and C-12 of the Chromophore of Bovine Rhodopsin - Evidence for a 6-S-Cis Conformation with Negative-Charge Perturbation near C-12. *European Journal of Biochemistry* **1987**, *163* (1), 9-14.

(6) Baldwin, P. A.; Hubbell, W. L., Effects of Lipid Environment on the Light-Induced Conformational-Changes of Rhodopsin .2. Roles of Lipid Chain-Length, Unsaturation, and Phase State. *Biochemistry-Us* **1985**, *24* (11), 2633-2639.

(7) Eddy, M. T.; Ong, T. C.; Clark, L.; Tejjido, O.; van der Wel, P. C. A.; Garces, R.; Wagner, G.; Rostovtseva, T. K.; Griffin, R. G., Lipid Dynamics and Protein-Lipid Interactions in 2D Crystals Formed with the beta-Barrel Integral Membrane Protein VDAC1. *J. Am. Chem. Soc.* **2012**, *134* (14), 6375-6387.

(8) Andreas, L. B.; Eddy, M. T.; Pielak, R. M.; Chou, J.; Griffin, R. G., Magic Angle Spinning NMR Investigation of Influenza A M2(18-60): Support for an Allosteric Mechanism of Inhibition. *Journal of the American Chemical Society* **2010**, *132* (32), 10958-10960.

(9) Kates, M.; Yengoyan, L. S.; Sastry, P. S., A Diether Analog of Phosphatidyl Glycerophosphate in Halobacterium Cutirubrum. *Biochim Biophys Acta* **1965**, *98* (2), 252-268.

(10) Gutknecht, J., Proton Hydroxide Conductance and Permeability through Phospholipid-Bilayer Membranes. *P. Natl. Acad. Sci. USA* **1987**, *84* (18), 6443-6446.

(11) Mak-Jurkauskas, M. L.; Bajaj, V. S.; Hornstein, M. K.; Belenky, M.; Griffin, R. G.; Herzfeld, J., Energy transformations early in the bacteriorhodopsin photocycle revealed by DNP-enhanced solid-state NMR. *P. Natl. Acad. Sci. USA* **2008**, *105* (3), 883-888.

(12) Andreas, L. B.; Barnes, A. B.; Corzilius, B.; Chou, J. J.; Miller, E. A.; Caporini, M.; Rosay, M.; Griffin, R. G., Dynamic Nuclear Polarization Study of Inhibitor Binding to the M2(18-60) Proton Transporter from Influenza A. *Biochemistry-Us* **2013**, *52* (16), 2774-2782.

(13) Rosay, M. M. Sensitivity-enhanced nuclear magnetic resonance of biological solids. Massachusetts Institute of Technology, Cambridge, MA, 2001.

(14) Long, J. R.; Ebelhauser, R.; Griffin, R. G., H-2 NMR line shapes and spin-lattice relaxation in Ba(ClO₃)₂·(H₂O)-H-2. *Journal of Physical Chemistry A* **1997**, *101* (6), 988-994.

(15) Franzin, C. M.; Macdonald, P. M., Detection and quantification of asymmetric lipid vesicle fusion using deuterium NMR. *Biochemistry* **1997**, *36* (9), 2360-2370.

(16) Thurmond, R. L.; Lindblom, G.; Brown, M. F., Curvature, Order, and Dynamics of Lipid Hexagonal Phases Studied by Deuterium Nmr-Spectroscopy. *Biochemistry* **1993**, *32* (20), 5394-5410.

(17) Beshah, K.; Olejniczak, E. T.; Griffin, R. G., Deuterium Nmr-Study of Methyl-Group Dynamics in L-Alanine. *Journal of Chemical Physics* **1987**, *86* (9), 4730-4736.

(18) Shinoda, W.; Mikami, M.; Baba, T.; Hato, M., Molecular dynamics study on the effect of chain branching on the physical properties of lipid bilayers: Structural stability. *J Phys Chem B* **2003**, *107* (50), 14030-14035.

(19) Murata, K.; Tanaka, H., Liquid-liquid transition without macroscopic phase separation in a water-glycerol mixture. *Nat Mater* **2012**, *11* (5), 436-43.

(20) Hsieh, C. H.; Wu, W. G., Solvent Effect on Phosphatidylcholine Headgroup Dynamics as Revealed by the Energetics and Dynamics of 2 Gel-State Bilayer Headgroup Structures at Subzero Temperatures. *Biophys J* **1995**, *69* (1), 4-12.

(21) Allen, P. J.; Creuzet, F.; de Groot, H. J. M.; Griffin, R. G., Apparatus for Low-Temperature Magic-Angle Spinning Nmr. *J. Magn. Reson.* **1991**, *92* (3), 614-617.

(22) Barnes, A. B. High-resolution high-frequency dynamic nuclear polarization for biomolecular solid state NMR. Massachusetts Institute of Technology, Cambridge, MA, 2011.

(23) Mayer, J.; Urban, S.; Habrylo, S.; Holderna, K.; Natkaniec, I.; Wurflinger, A.; Zajac, W., Neutron-Scattering Studies of C₆H₁₂ and C₆D₁₂ Cyclohexane under High-Pressure. *Physica Status Solidi B-Basic Research* **1991**, *166* (2), 381-394.

- (24) Price, D. M., Temperature calibration of differential scanning calorimeters. *Journal of Thermal Analysis* **1995**, *45* (6), 1285-1296.
- (25) Jellum, E.; Eldjarn, L.; Try, K., Conversion of Phytol into Dihydrophytol and Phytanic Acid. *Acta Chemica Scandinavica* **1966**, *20* (9), 2535-&.
- (26) Sita, L. R., Convenient Highly Stereoselective Syntheses of (3r,7r,11r) and (3s,7r,11r)-3,7,11,15-Tetramethylhexadecanoic Acid (Phytanic Acid) and the Corresponding 3,7,11,15-Tetramethylhexadecan-1-Ols. *Journal of Organic Chemistry* **1993**, *58* (19), 5285-5287.
- (27) Hsiao, C. Y. Y.; Ottaway, C. A.; Wetlaufe.Db, Preparation of Fully Deuterated Fatty-Acids by Simple Method. *Lipids* **1974**, *9* (11), 913-915.

Chapter 7: ^2H -DNP-enhanced ^2H - ^{13}C solid-state NMR correlation spectroscopy

Adapted from Maly, T; Andreas, LB; Smith, AA; Griffin, RG; PCCP, 2010, 12:5872-5878.

7.1 Introduction

In recent years magic angle spinning NMR (MAS-NMR) spectroscopy has emerged as a valuable method to determine atomic-resolution structures of biomolecular macromolecules such as globular proteins, membrane proteins and amyloid fibrils ^{1, 2}. However, in contrast to solution-state NMR, the majority of MAS-NMR experiments rely on recording homo- and heteronuclear ^{13}C and ^{15}N correlation spectra because direct ^1H detection is often compromised by the strong ^1H - ^1H dipolar interactions present in the solid state. Under typical experimental conditions, these strong couplings result in broad, unresolved ^1H resonances. Techniques such as ultrafast sample spinning ^{3, 4}, windowed homonuclear decoupling techniques ^{5, 6}, and dilution of the ^1H - ^1H dipolar bath by deuteration can be used to narrow ^1H lines in MAS-NMR experiments and are currently under investigation ⁷⁻¹⁰. Successful implementation of these techniques would bring the resolving power of a third nucleus to MAS-NMR protein investigations.

Another approach to access a third nucleus is to observe deuterons (^2H) because their reduced homonuclear dipolar coupling that can be attenuated under moderate MAS frequencies (~ 5 kHz). Deuterons contain similar information on the chemical environment as protons, and can therefore be directly employed to obtain structural information.

Recently it was shown that spectra of deuterated proteins exhibit high-resolution MAS-NMR and the method is therefore of great interest for the structural biology community ^{8, 11}. Furthermore, deuteration can also result in additional benefits in both the resolution and sensitivity of more conventional ^{13}C and ^{15}N MAS-NMR experiments. For example, the resolution of 3D or 4D ^{13}C spectra of deuterated proteins is no longer limited by the ^1H decoupling power and resulting rf heating. In addition, cross-polarization (CP) enhancements are increased and neither ^1H nor ^{13}C longitudinal relaxation times are significantly increased ¹². However, the ^2H quadrupole coupling ($e^2qQ/h \sim 200$ kHz) often reduces the sensitivity and resolution of directly observed ^2H spectra in solids. At the same time, the relaxation and lineshape properties of the deuterium nucleus are particularly sensitive to the local dynamics and can provide valuable information ⁸.

To overcome the difficulties associated with the deuterium quadrupole coupling, techniques such as rotor-synchronized pulse sequences or indirect detection through for example ^{13}C can be used. Furthermore, in hetero-nuclear correlation experiments (e.g. ^2H - ^{13}C), MAS narrows the first order ^2H quadrupole interaction and the resolution can be further improved if a ^2H double-quantum (^2H -DQ) excitation and reconversion scheme is employed ^{11, 13, 14}.

NMR signal intensities of solids and liquids can be enhanced by several orders of magnitude with dynamic nuclear polarization (DNP) ^{15, 16} and in the last decade high-frequency DNP has emerged as a valuable method for a variety of applications, spanning particle physics ^{17, 18}, pharmaceutical applications ^{19, 20} and structural and mechanistic studies of biologically relevant molecules ^{15, 21, 22}.

In a DNP experiment, the large thermal polarization of a paramagnetic polarizing agent is transferred to surrounding nuclei by microwave irradiation of the sample at the electron paramagnetic resonance (EPR) transition. DNP enhancements are measured by taking the ratio of signal intensity in spectra with and without microwaves, leaving all other experimental parameters unchanged. Currently, the largest signal enhancements in solids at high magnetic fields (>5 T) are observed in experiments that exploit the cross-effect (CE) as the dominant DNP mechanism ^{21, 22}.

Depending on the inhomogeneous breadth of the EPR spectrum (Δ) and the homogeneous linewidth (δ), DNP can either occur through the solid-effect (SE) if the nuclear Larmor frequency ω_{01} is larger than the EPR linewidth ($\omega_{01} > \Delta, \delta$), or through the much more efficient cross-effect (CE) if $\Delta > \omega_{01} > \delta$ ^{15, 23}. In the classical description of the CE the underlying mechanism is a two-step process involving two electrons with Larmor frequencies ω_{0S1} and ω_{0S2} , and a nucleus with a frequency ω_{0I} . Initially, the *allowed* EPR transition of one electron is irradiated and nuclear polarization is generated in a subsequent three-spin flip-flop process through transitions such as $|\alpha_{1S}\beta_{2S}\beta_I\rangle \leftrightarrow |\beta_{1S}\alpha_{2S}\alpha_I\rangle$ or $|\beta_{1S}\alpha_{2S}\beta_I\rangle \leftrightarrow |\alpha_{1S}\beta_{2S}\alpha_I\rangle$ ^{24, 25}. The maximum DNP enhancement is achieved when the difference between the electron Larmor frequencies of two electron spin packets satisfy the matching condition $|\omega_{0S1} - \omega_{0S2}| = \omega_{0I}$, with ω_{0I} the nuclear Larmor frequency. The DNP-enhanced nuclear polarization then disperses throughout the bulk via spin-diffusion. ²⁶

Here we demonstrate that the combination of sample deuteration and DNP yields resolved ^2H , ^{13}C correlation spectra with a signal enhancement of $\epsilon = 700$. To our knowledge, ^2H -DNP has been reported only for the preparation of polarized targets ²⁷⁻²⁹ and in dissolution DNP ³⁰, focusing on the polarization of small alcohol molecules. In this study, we demonstrate that high-field ^2H -DNP can be used to enhance MAS-NMR spectra of biologically relevant molecules. Although the technique is initially demonstrated using a single amino acid residue, the concept has tremendous

potential for structural investigations of biologically relevant macromolecules in the solid state at high magnetic fields. Given sufficient sensitivity, the resolving power of ^2H , ^{13}C and ^{15}N , 3D and 4D experiments have the potential to extend MAS-NMR to the application of larger biological systems.

7.2 Results and Discussion

Polarizing Agents and DNP-Enhancement Profiles

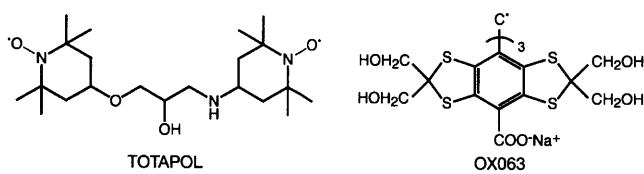


Figure 7.1. Molecular structures of the two polarizing agents TOTAPOL and OX063.

The molecular structures of the two polarizing agents TOTAPOL (1-(TEMPO-4-oxy)-3-(TEMPO-4-amino)-propan-2-ol) and OX063 (methyl-tris[8-carboxy-2,2,6,6-tetrakis[(2-hydroxyethyl)-benzo[1,2-d:4,5-d]bis[1,3]dithiol-4-yl]]) are shown in **Figure 7.1** and both are soluble in aqueous media at high concentration.

The 140 GHz (5 T) EPR spectra of TOTAPOL and OX063 are shown in **Figure 7.2** (top). While the EPR spectrum of TOTAPOL shows a large anisotropy of the g -tensor and additional features due to the large ^{14}N hyperfine interaction with the electron spin 31 , the EPR spectrum of OX063 appears almost symmetric at high-magnetic fields because no significantly large hyperfine couplings are present and the g -tensor anisotropy is small³². With an inhomogeneous breadth of $\Delta \approx 600$ MHz and 55 MHz for TOTAPOL and OX063, respectively, and a ^2H nuclear Larmor frequency at 5 T of 32 MHz, we see that both radicals satisfy the conditions ($\Delta > \omega_{01} > \delta$) for CE DNP for ^2H .

The field swept DNP enhancement profile is closely related to the high-field EPR spectrum recorded at the same magnetic field strengths as shown in **Figure 7.2**. Typically high-field DNP experiments are performed using a fixed-frequency microwave source and the DNP process needs to be optimized with respect to the magnetic field to find the best irradiation frequency.

In addition to determining the optimum field position for DNP, the enhancement profile also reveals much information about the nature of the underlying DNP process. Since both enhancement profiles of TOTAPOL and OX063 do not show resolved features at frequencies

corresponding to $\omega_{0S} \pm \omega_{0I}$, it can be directly concluded that the underlying DNP mechanism observed in experiments reported here is the CE^{18, 23, 25, 33-35}.

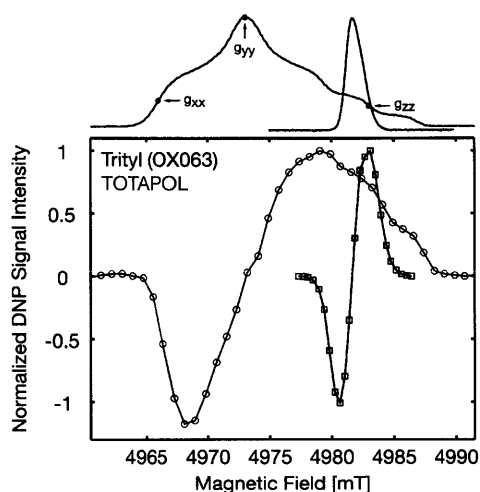


Figure 7.2. Trityl EPR spectra and ^2H enhancement profiles. Top: Two-pulse echo-detected 140 GHz EPR spectra of 1 mM TOTAPOL and OX063 in glycerol/ H_2O (60/40), $T = 20$ K. Bottom: Direct detected ^2H -DNP enhancement profiles of 20 mM TOTAPOL and 40 mM Trityl (OX063) in d_8 -glycerol/ D_2O (60/40) using a rotor-synchronized quadrupole-echo sequence. $T = 90$ K, $t_p(\pi/2) = 3$ μs , $\tau = 166$ μs , $\omega_r/2\pi = 6$ kHz. For comparison the DNP enhancement profiles are normalized to maximum intensity.

The DNP enhancement profile for TOTAPOL resembles the shape typically observed for TEMPO based (bi)-radicals³⁸⁻⁴⁰. For ^2H -DNP the maximum negative enhancement is obtained at the low-field side of the profile corresponding to 4968.6 mT (DNP(-)), while the maximum positive enhancement is observed at 4979.1 mT (DNP(+)). This is in contrast to ^1H -DNP, where the overall extremum ^1H enhancement is observed at the high-field side (DNP(+)) of the DNP enhancement profile^{36, 37}. Note that the ^2H -DNP enhancement profile for TOTAPOL shows a pronounced asymmetry. This feature is similar to direct ^{13}C -DNP using TOTAPOL and the two enhancement profiles for ^2H and ^{13}C DNP coincide with the maximum absolute enhancement observed on the low-field side (DNP(-)). This seems to be an inherent feature of TEMPO based polarizing agents, when low- γ nuclei such as ^{13}C and ^2H are polarized. In contrast to ^1H -DNP the maximum absolute enhancement is observed on the high-field side (DNP(+)).

For ^1H DNP, the TEMPO based biradical TOTAPOL currently yields the largest enhancements in DNP-enhanced MAS-NMR experiments^{36, 37}. However, with an inhomogeneous breadth of $\Delta \approx 600$ MHz at 5 T, TOTAPOL is not optimized for polarizing low- γ nuclei such as ^2H , ^{13}C or ^{15}N and polarizing agents with narrower EPR spectra are preferable. At present only two radicals are known for DNP applications that have a narrow EPR spectrum at high magnetic fields, the stable trityl radical and its derivatives^{38, 39} and BDPA⁴⁰. Here we choose the trityl radical OX063

(see *Figure 7.1*) as the polarizing agent, because of its great solubility in aqueous media ⁴¹. The 140 GHz EPR spectrum of OX063 is shown in *Figure 7.2* (top). The spectrum is essentially symmetric with a spectral breadth of $\Delta \approx 55$ MHz (FWHH) as determined from the EPR spectrum. As a consequence the enhancement profile of OX063 for direct ²H-DNP shown in *Figure 7.2* is symmetric with the maximum positive enhancement occurring at 4983.0 mT (DNP(+)) and the maximum negative enhancement occurring at 4980.7 mT (DNP(-)).

A direct comparison of these two enhancement profiles can be used to illustrate another important fact for high-field DNP. At 5 T the separation between the optimum field positions for ¹H-DNP using TOTAPOL (DNP(+)) and ²H-DNP (or ¹³C) is approximately 4 mT, corresponding to ~ 112 MHz electron Larmor frequency. The separation is 14 mT between DNP(-) for TOTAPOL and DNP(+) for OX063, corresponding to 400 MHz for electrons. To be able to study different polarizing agents and to cover the complete field range, the DNP spectrometer has to be either equipped with a sweep coil or the gyrotron needs to be tunable over a range of > 0.5 GHz ⁴²⁻⁴⁴. Note that the sweep/tuning range will increase at higher fields.

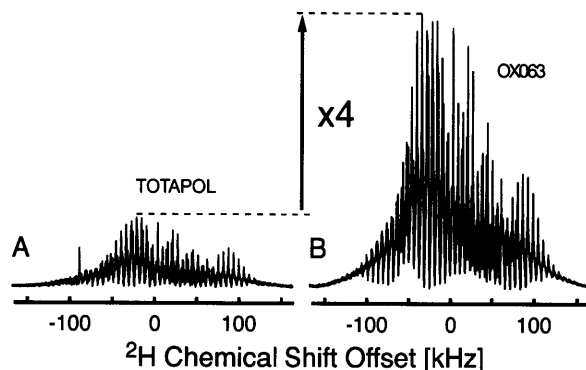


Figure 7.3. Comparison of the steady-state ²H signal intensity for TOTAPOL (A) and OX063 (B). Both spectra are recorded back-to-back under identical experimental conditions. Due to the insufficient excitation bandwidth of 83 kHz, the magnitude spectrum is shown. T = 90 K, $\omega_r/2\pi = 5.882$ kHz. The spectra are recorded using a rotor-synchronized quadrupole echo sequence.

A comparison of the ²H-DNP performance for TOTAPOL and OX063 is shown in *Figure 7.3* and approximately a factor of 4 larger enhancement is observed for OX063 under similar experimental conditions. This improvement is due to the much narrower EPR spectrum of OX063 ($\Delta(\text{TOTAPOL})/\Delta(\text{OX063}) \approx 11$) allowing a larger fraction of the electron spins to be excited by the microwave radiation. Note that at the same electron concentration TEMPO based biradicals give a factor of 4 larger enhancements compared to monomeric TEMPO ²¹, and we therefore expect that further improvements could be made using biradicals based on OX063. Due to the

much better performance of OX063 over TOTAPOL, the following DNP experiments were all performed using OX063 as the polarizing agent.

Bulk-Polarization Build-up and Maximum Enhancement

During the DNP process, the high thermal electron polarization is transferred to the surrounding nuclei resulting in a bulk-polarization build-up curve that can be modeled by an exponential process with a characteristic bulk-polarization build-up time constant τ_B . In **Figure 7.4** a ^{13}C -detected bulk-polarization build-up curve for ^2H DNP using OX063 as the polarizing agent is shown. Here the DNP-enhanced ^2H polarization is transferred to the proline ^{13}C nuclei for detection via a subsequent cross-polarization (CP) step⁴⁵. This allows an accurate determination of the signal enhancement, because the ^{13}C spectrum is much narrower compared to the direct detected ^2H spectrum. At a temperature of 90 K, the steady state polarization is reached after approximately 100 s of microwave irradiation and a build-up time constant of $\tau_B(^2\text{H}) = 21$ s was obtained.

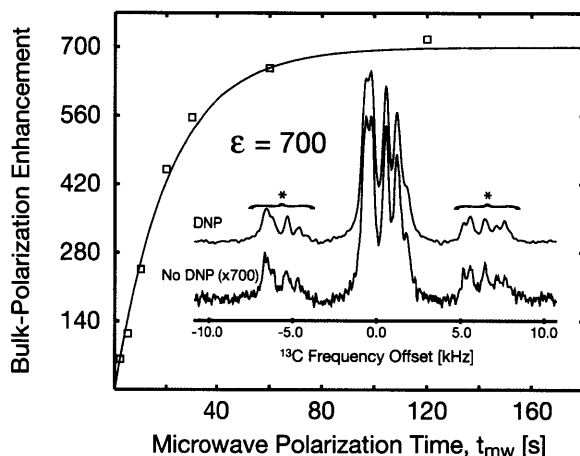


Figure 7.4. ^2H bulk-polarization build-up curve showing an enhancement of 700. The build-up curve was recorded at a magnetic field position corresponding to DNP(+) using OX063. The ^2H polarization is detected indirectly from the total ^{13}C signal of U- $[\text{}^2\text{H}_7, \text{}^{13}\text{C}_5]$ -proline through a ramped cross-polarization step (1.5 ms), 16 scans averaged. The inset shows the mw-on and off signal. The DNP enhanced spectrum was recorded at a field position corresponding to DNP(+) with a DNP buildup time of $t_{\text{mw}} = 120$ s. For the mw-on signal 32 transients were averaged while for the mw-off signal in total 1280 transients were averaged. $T = 90$ K, $\omega_r/2\pi = 5.882$ kHz. Spinning side bands are marked by asterisks.

The absolute enhancement is obtained from the microwave on and off spectra, recorded under identical experimental conditions (see **Figure 7.4**, inset). For the off signal, 40 times more scans were averaged to provide sufficient signal-to-noise due to the small ^2H signal intensity without DNP enhancement and a steady-state ^2H DNP enhancement of $\epsilon = 700$ was observed. Theoretically, the maximum enhancement that can be achieved in a DNP experiment is given by

the ratio of the gyromagnetic ratios of the electron and the nucleus that is polarized, here ^2H ($\gamma(e^-)/\gamma(^2\text{H})$). This gives a theoretical maximum enhancement of 4300 for ^2H -DNP.

In **Figure 7.5** two direct ^{13}C -DNP enhanced spectra of proline are shown, one spectrum taken without decoupling (A) and one with 83 kHz high-power ^2H TPPM decoupling (B) ⁴⁶. As expected, no significant difference in resolution was detected between the two acquisition schemes. Therefore, the following experiments were all performed without decoupling of the (residual) ^1H or ^2H nuclei.

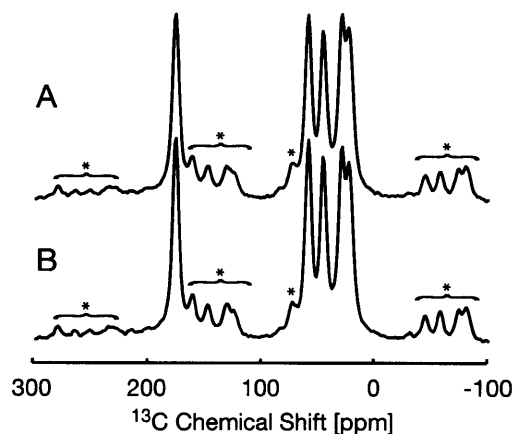


Figure 7.5. Direct ^{13}C DNP-enhanced MAS-NMR spectra of U- $[^2\text{H}_7, ^{13}\text{C}_5]$ -proline taken (A) without decoupling and (B) with 83 kHz of TPPM ^2H decoupling. The temperature was 90 K, magic angle spinning was $\omega_r/2\pi = 5.5$ kHz, and 4 scans were recorded.

^2H -DNP Enhanced ^2H - ^{13}C Correlation Spectroscopy

Depending on the experimental conditions the electron polarization can be either used to polarize ^{13}C nuclei directly ($e^- \rightarrow ^{13}\text{C}$) or indirectly ($e^- \rightarrow ^2\text{H} \rightarrow ^{13}\text{C}$). In the second case the electron polarization is first transferred to the ^2H nuclei via DNP and then transferred to the ^{13}C nuclei by a subsequent CP step ⁴⁷. In **Figure 7.6** two ^2H -DNP-enhanced ^{13}C detected MAS-NMR spectra of U- $[^2\text{H}_7, ^{13}\text{C}_5]$ -proline recorded at 90 K are shown. The top spectrum in **Figure 7.6** is a direct ^{13}C -DNP enhanced spectrum of proline and all five proline ^{13}C resonances are visible in the spectrum. The second spectrum shown in **Figure 7.6** (bottom) is an indirect polarized ^{13}C spectrum of proline.

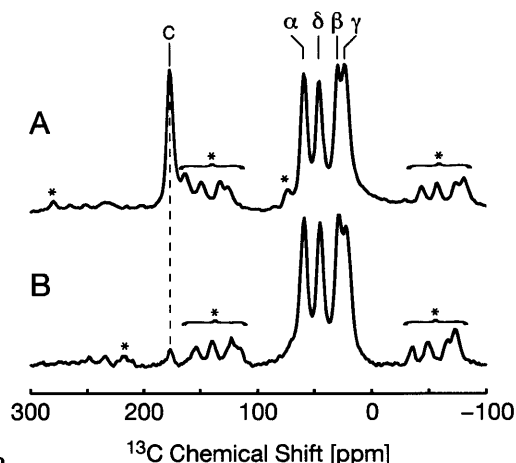


Figure 7.6. Direct and ^2H -CP ^{13}C MAS-NMR spectra of U-117, ^{13}C -protein taken at 90 K. A: Direct ^{13}C DNP-enhanced MAS-NMR spectrum, $\omega_R/2\pi = 5.5$ kHz, 4 scans, $t_{\text{mw}} = 60$ s. B: ^2H DNP-enhanced ^{13}C MAS-NMR spectrum. The polarization is transferred from ^2H to ^{13}C by a cross-polarization step (1.5 ms), $\omega_R/2\pi = 5.0$ kHz, 64 scans, $t_{\text{mw}} = 20$ s. Spinning side bands are marked by asterisks. The sensitivity of the two spectra are 7.9 and 1.3 S/N \cdot seconds $^{1/2}$ for A and B, respectively. The main source of sensitivity difference is due to inefficiency in the CP step in which the ^2H spin lock of ~ 83 kHz covers less than half of the ~ 200 kHz broad ^2H spectrum.

Due to the short contact time of the CP process (1.5 ms), predominantly one-bond polarization transfer from ^2H to ^{13}C is observed. The ^{13}C signal intensity for the carbonyl atom is attenuated due to the lack of a directly bonded deuterium, whereas nuclei that do possess a directly bonded deuterium (α - γ) yield intense lines.

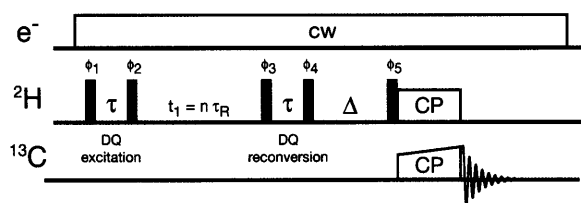


Figure 7.7. Pulse sequence to record a ^2H double-quantum, ^{13}C correlation spectrum. Double quantum coherences are generated using a two-pulse sequence. The t_1 evolution time is rotor-synchronized.

The pulse sequence used for DNP-enhanced ^2H double-quantum (DQ) filtered ^{13}C correlation spectroscopy is shown in **Figure 7.7**. Double quantum coherences are excited using a two-pulse scheme⁴⁸, consisting of a DQ excitation and reconversion period (characterized by τ) separated by a rotor-synchronized t_1 evolution period given by $n \cdot \tau_R$ with n the number of rotor cycles and τ_R the rotor period. Finally the ^2H magnetization is transferred to ^{13}C by a CP step⁴⁷. For ^2H -DNP-enhanced measurements, the sample is irradiated by continuous wave (CW) microwave radiation, on-resonant with the DNP transition.

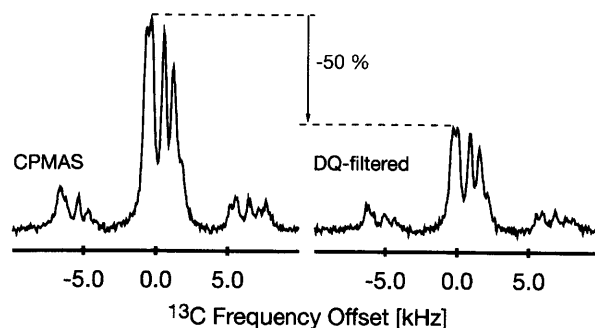


Figure 7.8. Determination of the DQ efficiency for U-[$^2\text{H}_7$, $^{13}\text{C}_5$]-proline from DNP enhanced spectra. Top: ^{13}C CPMAS spectrum. Bottom: ^2H double-quantum filtered ^{13}C CPMAS spectrum with $t_1 = 0$. Experimental conditions: $T = 90\text{ K}$, $\tau = 1\ \mu\text{s}$, $\Delta = 3\ \mu\text{s}$, $\omega_R/2\pi = 5.882\text{ kHz}$, $t_{\text{mw}} = 20\text{ s}$.

The DQ efficiency is determined by comparing the signal intensity obtained from a ^{13}C CPMAS experiment with the signal intensity obtained from a ^2H double-quantum filtered ^{13}C CPMAS experiment as shown in **Figure 7.8**. From this comparison a ^2H double-quantum efficiency of $\sim 50\%$ is observed.

A two-dimensional ^2H -DNP enhanced ^2H , ^{13}C correlation spectrum of proline is shown in **Figure 7.9**. Here a ^2H double-quantum filter is used before the polarization is transferred to ^{13}C through a 1.5 ms CP step. A double-quantum excitation and reconversion time of $1\ \mu\text{s}$ was used, followed by a z-filter of $3\ \mu\text{s}$ length. The pulse sequence used here is similar to the one previously reported for DQ-filtered ^2H , ^{13}C correlation spectroscopy in perdeuterated proteins ¹¹. The two-dimensional spectrum shows 4 resolved cross-peaks, corresponding to correlations between the ^{13}C proline atoms and the covalently attached ^2H nuclei.

Spectral Linewidths

Under the current experimental conditions linewidths of approximately 10 ppm and 8 ppm were observed for ^2H and ^{13}C , respectively. These linewidths are larger than those observed previously for perdeuterated proteins ^{8,11}. However, the source of the increased linewidth is not of a general nature. In particular the main contribution arises from the fact that proline is a small molecule embedded in a frozen (90 K) glassy solvent matrix (DMSO/water). DNP samples are typically prepared in a glass-forming solvent, which serves as a cryoprotectant to ensure that the polarizing agent is homogeneously dispersed throughout the sample and protects proteins from cold degradation caused by thermal cycling of the sample. This is known to induce conformational distributions, which in turn can cause inhomogeneous broadening ⁴⁹. However, this factor becomes unimportant for larger systems such as bio-macromolecules or (nano) crystals. For

example in contributions by Barnes et al. and Debelouchina et al. (same issue) ^{13}C linewidths of 1-2 ppm are observed for the membrane protein bacteriorhodopsin (bR) and GNNQQNY nano-crystals.

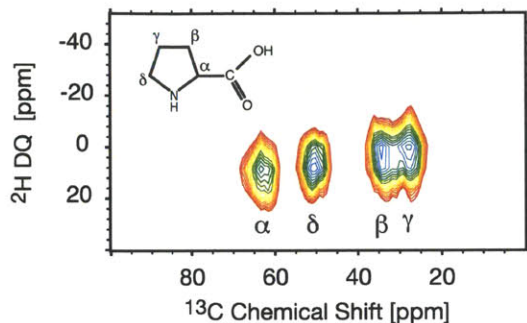


Figure 7.9. Two-dimensional DNP-enhanced ^2H -DQ- ^{13}C correlation spectrum of U- $[^2\text{H}_7, ^{13}\text{C}_5]$ -proline recorded at 90 K, $\omega_{\text{R}}/2\pi = 5.882$ kHz, sampling time in the indirect dimension $\Delta t_1 = 170$ μs , DQ excitation and reconversion time $\tau = 1$ μs , $\Delta = 3$ μs , $t_{\text{mw}} = 25$ s, 64 scans per t_1 point, ~ 10 hrs of total acquisition time.

The paramagnetic polarizing agent has only minor effects on the linewidth. For example in DNP-enhanced MAS-NMR experiments on amyloid nano crystals GNNQQNY⁵⁰ or the membrane protein bacteriorhodopsin (bR) the radical does not penetrate into the protein or nano-crystals. In the case of bR even electron concentrations of up to 100 mM did not show any effect on the linewidth of the retinal, which is buried inside the protein⁵¹. The last factor is of a technical nature. All experiments described here are performed at a magnetic field strength of 5 T (212 MHz for ^1H), which is rather low for contemporary MAS-NMR spectroscopy and second order quadrupole effects could have a contribution to the observed linewidth. In addition, it is rather difficult to accurately set the magic angle at cryogenic temperatures for this particular probe, since it is not equipped with a cryogenic sample-eject system¹⁶ or a Hall effect sensor⁵². Although a misadjusted magic angle has only minor effects on the linewidth for double-quantum filtered ^2H experiments^{11,14} it nevertheless adds a small contribution to the line broadening. There is also the possibility that small inhomogeneities in the magnetic field at the sample caused additional line broadening.

Sensitivity Gain Through DNP

Acquisition of a ^2H dimension offers several advantages over a ^1H dimension. The deuterium spin system has a lower gyromagnetic ratio, and therefore does not suffer from the homogenous broadening observed for high concentrations of protons in solids. Spins of interest can be perdeuterated without deuteration of solvents, crystallization agents and cofactors. Comparable

sensitivity should also be achievable with deuterium detection. For example, methyl-methyl contacts are often important for determination of protein structure, and in cases where a CD₂H labeling is used to reduce proton couplings, perdeuteration (~97%) is employed⁸. At 3% protonation, methyl groups are ~9% CD₂H spin systems to first order, with minimal (~0.3%) CDH₂ and CH₃ labeling. This avoids broadening in the ¹³C dimension due to the shift in the isotropic resonance between CH and CD which results in different isotropic shifts for CH₃, CH₂D, CHD₂ and CD₃ groups. Since 10% labeling is often found to be necessary for optimized relaxation characteristics of amide protons⁸, perdeuteration will be used as a point of comparison, but may need to be adjusted to by a factor of ~3 if higher protonation is found to be optimal.

In a perdeuterated sample (~97%) ²H NMR should have a factor of ~8.6 higher sensitivity compared to ¹H detection, and a factor of ~2.5 was experimentally observed, as reported by Agarwal et al.¹¹. If CH or CH₂ groups are of primary interest, or if a higher proton concentration is found to be optimal, this analysis needs to be adjusted. This gain in sensitivity is mainly due to the short longitudinal relaxation of the ²H nuclei, a direct consequence of the large quadrupolar coupling. Therefore, at room temperature the recycle delay in the NMR experiment can be short. Furthermore, sample heating is not an issue due to the much lower decoupling power needed for deuterium. Nevertheless recycling delays between 1.25 and 3 s were reported for previous work on biological samples¹¹.

This advantage no longer exists at 90 K because the DNP build-up time constant is 21 s. Therefore, to run the DNP experiment at the optimum recycling rate one needs to wait 21*1.25 s between shots = 26 s and the sensitivity for low temperature ²H MAS-NMR spectroscopy would be decreased by a factor of 3 to 5 depending on the actual recycling delay used in the experiment compared to experiments performed at 300K. However, with DNP a signal enhancement of $\epsilon = 700$ is demonstrated, and therefore the overall sensitivity of a low-temperature ²H-DNP enhanced MAS-NMR experiment is a factor of 140 to 240 larger than at room temperature. This does not include the additional factor of ~3 in sensitivity due to the lower temperature (300 K/90 K).

To compare the overall efficiency of ²H-DNP with ¹H-DNP the degree of nuclear polarization can be compared. In the case of ²H-DNP this is 16 % of the theoretical maximum, and for ¹H-DNP typically 27 % (175/660) is observed at a magnetic field of 5 T^{21, 37}. Therefore, overall ¹H-DNP currently performs more efficiently than ²H-DNP. However, with further advances in polarizing agents, and despite a bulk-polarization build-up time of ~5 s for ¹H-DNP⁵³ and 21 s for ²H DNP, we expect both methods to be competitive on a sensitivity basis. However, ²H MAS-NMR spectroscopy offers structural information due to the reduced homonuclear dipolar coupling that

are difficult to obtain directly from ^1H nuclei. Note that this comparison does not include the efficiency of the CP transfer.

7.3 Methods

Sample Preparation

Field swept DNP enhancement profiles are recorded using a solution of 20 mM TOTAPOL or 40 mM OX063 in d_8 -glycerol/ D_2O (60/40). Direct ^2H signal detection was performed using a rotor-synchronized quadrupole-echo sequence.

For DNP experiments on proline, a 1.25 M solution of U- $^{13}\text{C}_5$, D_7]-proline in d_8 -glycerol/ D_2O (60/40) was prepared with 40 mM OX063 as the polarizing agent. Note that the high proline concentration is only necessary for recording the off-signal (no mw) in a reasonable amount of time. Isotopically labeled proline (U- $^{13}\text{C}_5$, 97-99 %; U- D_7 , 97-99 %; ^{15}N , 97-99 %) was purchased from Cambridge Isotope Laboratories (Andover MA, USA). All solvent mixtures are given in weight ratios.

DNP Spectroscopy

All DNP experiments were performed on a custom-designed DNP NMR spectrometer operating at a magnetic field of 5 T corresponding to a Larmor frequency of 211 MHz (^1H) and 140 GHz (e^-), respectively. A custom-designed cryogenic MAS-NMR probe was used for radio-frequency (rf) irradiation (^{13}C and ^2H) with a commercial 2.5 mm spinning module (Revolution NMR Inc.). Typically 50 kHz rf field-strength was obtained on the ^{13}C channel, while the ^2H field-strength was 83 kHz. ^2H - ^{13}C cross-polarization was performed using a 50 kHz field on both channels for a duration of 1500 μs . All spectra are recorded without high-power ^1H or ^2H decoupling (see *Figure 7.5*).

High-power microwave radiation was generated using a gyrotron oscillator operating at 139.662 GHz^{54,55}, capable of producing high-power (>10 W) millimeter waves. The DNP sample (~6 μL) was placed in a 2.5 mm sapphire rotor and a microwave power of 2.5 W was estimated at the position of the sample. The 5 T superconducting magnet is equipped with a superconducting sweep coil to sweep the magnetic field over a range of 750 G. For accurate field measurements, the spectrometer is equipped with a field/frequency lock system⁵⁶.

EPR Spectroscopy

EPR experiments were performed on a previously described custom-designed high-field EPR spectrometer operating at a microwave frequency of 139.504 GHz^{57, 58}. The sample (~ 250 nL, 1 mM) was placed in a Suprasil quartz tube with an outer diameter of 0.55 mm. EPR spectra were recorded with a two-pulse echo sequence ($\pi/2$ - τ - π - τ -echo) by integrating the echo intensity while sweeping the magnetic field ($t_p(\pi/2) = 60$ ns, $\tau = 300$ ns). For accurate field measurements, the spectrometer is equipped with a field/frequency lock system⁵⁶.

7.4 Conclusions

We have demonstrated the application of direct ^2H -DNP for two-dimensional ^2H , ^{13}C MAS-NMR correlation spectroscopy. A steady-state signal enhancement of $\epsilon = 700$ was observed with a bulk-polarization build-up constant of $\tau_B = 21$ s. Under these conditions the sensitivity of a ^2H MAS-NMR experiment can be increased by two orders of magnitude, compared to ^2H experiments performed at room temperature. We believe that the combination of perdeuteration and ^2H -DNP could have a large impact on protein assignment and structure determination, as the deuteron can be used as an additional nucleus to gain structural information about the system under study. We present this approach as a method that may be widely applicable, requiring no optimization of isotopic labeling or isotopic labeling of cofactors and solvent. Furthermore, we expect that technical improvements in hardware and sample preparation for low-temperature MAS-NMR spectroscopy can be expected to vastly improve linewidths in future biological application of this approach. We are currently exploring these improvements.

Acknowledgements

This research was supported by the National Institutes of Health through grants EB002084 and EB002026. TM and LBA acknowledge receipt of a postdoctoral fellowship of the Deutsche Forschungs Gemeinschaft and a graduate research fellowship of the National Science Foundation, respectively. The symmetric trityl radical OX063 was a gift of Nycomed Innovation (now GE Healthcare, Malmo, Sweden). The authors are grateful to Albert Smith, Alexander Barnes, Bjorn Corzilius, and Ta-Chung Ong for many fruitful discussions.

7.5 References

- (1) McDermott, A., Structure and Dynamics of Membrane Proteins by Magic Angle Spinning Solid-State NMR. *Annu. Rev. Biophys.* **2009**, *38* (1), 385-403.
- (2) Grey, C. P.; Tycko, R., Solid-state NMR in biological and materials physics. *Physics Today* **2009**, *62* (9), 44-49.
- (3) Zhou, D.; Shah, G.; Cormos, M.; Mullen, C.; Sandoz, D.; Rienstra, C., Proton-detected solid-state NMR spectroscopy of fully protonated proteins at 40 kHz magic-angle spinning. *J. Am. Chem. Soc.* **2007**, *129* (38), 11791-801.
- (4) .
- (5) Vinogradov, E.; Madhu, P. K.; Vega, S., Proton spectroscopy in solid state nuclear magnetic resonance with windowed phase modulated Lee-Goldburg decoupling sequences. *Chem. Phys. Lett.* **2002**, *354* (3-4), 193-202.
- (6) Lesage, A.; Sakellariou, D.; Hediger, S.; Elena, B.; Charmont, P.; Steuernagel, S.; Emsley, L., Experimental aspects of proton NMR spectroscopy in solids using phase-modulated homonuclear dipolar decoupling. *J. Magn. Reson.* **2003**, *163* (1), 105-13.
- (7) Agarwal, V.; Reif, B., Residual methyl protonation in perdeuterated proteins for multi-dimensional correlation experiments in MAS solid-state NMR spectroscopy. *J. Magn. Reson.* **2008**, *194* (1), 16-24.
- (8) Hologne, M.; Chevelkov, V.; Reif, B., Deuterated peptides and proteins in MAS solid-state NMR. *Prog. NMR. Spec.* **2006**, *48* (4), 211-232.
- (9) Agarwal, V.; Diehl, A.; Skrynnikov, N.; Reif, B., High Resolution ¹H Detected ¹H,¹³C Correlation Spectra in MAS Solid-State NMR using Deuterated Proteins with Selective ¹H,²H Isotopic Labeling of Methyl Groups. *J. Am. Chem. Soc.* **2006**, *128* (39), 12620-12621.
- (10) Morcombe, C. R.; Paulson, E. K.; Gaponenko, V.; Byrd, R. A.; Zilm, K. W., ¹H-¹⁵N correlation spectroscopy of nanocrystalline proteins. *J. Biomol. NMR* **2005**, *31* (3), 217-30.
- (11) Agarwal, V.; Faelber, K.; Schmieder, P.; Reif, B., High-Resolution Double-Quantum Deuterium Magic Angle Spinning Solid-State NMR Spectroscopy of Perdeuterated Proteins. *J. Am. Chem. Soc.* **2009**, *131* (1), 2-3.
- (12) Morcombe, C. R.; Gaponenko, V.; Byrd, R. A.; Zilm, K. W., ¹³C CPMAS spectroscopy of deuterated proteins: CP dynamics, line shapes, and T1 relaxation. *J. Am. Chem. Soc.* **2005**, *127* (1), 397-404.
- (13) Vega, S.; Shattuck, T. W.; Pines, A., Fourier-Transform Double-Quantum NMR in Solids. *Phys. Rev. Lett.* **1976**, *37* (1), 43.
- (14) Hoffman, A.; Schnell, I., Two-Dimensional Double-Quantum ²H NMR Spectroscopy in the Solid State under OMAS Conditions: Correlating ²H Chemical Shifts with Quasistatic Line Shapes. *ChemPhysChem* **2004**, *5* (7), 966-974.
- (15) Maly, T.; Debelouchina, G. T.; Bajaj, V. S.; Hu, K.-N.; Joo, C.-G.; MakJurkauskas, M. L.; Sirigiri, J. R.; van der Wel, P. C. A.; Herzfeld, J.; Temkin, R. J.; Griffin, R. G., Dynamic nuclear polarization at high magnetic fields. *J. Chem. Phys.* **2008**, *128* (5), 052211-19.
- (16) Barnes, A.; Mak-Jurkauskas, M. L.; Matsuki, Y.; Bajaj, V. S.; van der Wel, P. C. A.; DeRocher, R.; Bryant, J.; Sirigiri, J. R.; Temkin, R. J.; Lugtenburg, J.; Herzfeld, J.; Griffin, R. G., Cryogenic sampe exchange NMR probe for magic angle spinning dynamic nuclear polarization. *J. Magn. Reson.* **2009**, *198*, 261-270.
- (17) Goertz, S. T., The dynamic nuclear polarization process. *Nucl. Instrum. Methods Phys. Res., Sect. A* **2004**, *526* (1-2), 28-42.
- (18) Wind, R. A.; Duijvestijn, M. J.; van der Lugt, C.; Manenschijn, A.; Vriend, J., Applications of dynamic nuclear polarization in ¹³C NMR in solids. *Prog. NMR. Spec.* **1985**, *17*, 33-67.
- (19) Gallagher, F. A.; Kettunen, M. I.; Day, S. E.; Hu, D.-E.; Ardenkjaer-Larsen, J. H.; Zandt, R. i. t.; Jensen, P. R.; Karlsson, M.; Golman, K.; Lerche, M. H.; Brindle, K. M., Magnetic resonance imaging of pH in vivo using hyperpolarized ¹³C-labelled bicarbonate. *Nature* **2008**, *453* (7197), 940-943.

- (20) Day, I. J.; Mitchell, J. C.; Snowden, M. J.; Davis, A. L., Investigation of the Potential of the Dissolution Dynamic Nuclear Polarization Method for General Sensitivity Enhancement in Small-Molecule NMR Spectroscopy. *Appl. Magn. Reson.* **2008**, *34* (3), 453-460.
- (21) Hu, K.; Yu, H.; Swager, T.; Griffin, R., Dynamic nuclear polarization with biradicals. *J. Am. Chem. Soc.* **2004**, *126* (35), 10844-5.
- (22) Farrar, C. T.; Hall, D. A.; Gerfen, G. J.; Inati, S. J.; Griffin, R. G., Mechanism of dynamic nuclear polarization in high magnetic fields. *J. Chem. Phys.* **2001**, *114* (11), 4922-4933.
- (23) Atsarkin, V. A., Dynamic Polarization of Nuclei in Solid Dielectrics. *Sov. Phys. Usp. (english translation)* **1978**, *21* (9), 725-743.
- (24) Wollan, D. S., Dynamic nuclear polarization with an inhomogeneously broadened ESR line. II. Experiment. *Phys. Rev. B* **1976**, *13* (9), 3686.
- (25) Wollan, D. S., Dynamic nuclear polarization with an inhomogeneously broadened ESR line. I. Theory. *Phys. Rev. B* **1976**, *13*, 3671.
- (26) Bloembergen, N., On the interaction of nuclear spins in a crystalline lattice. *Physica* **1949**, *15* (3-4), 386-426.
- (27) Borghini, M.; Scheffler, K., A butanol polarized deuteron target I. Polarization at 25 kOe. *Nuc. Inst. and Methods* **1971**, *95* (1), 93-98.
- (28) Borghini, M.; Masaike, A.; Scheffler, K.; Udo, F., A butanol polarized deuteron target: II. Polarization at 50 kOe. *Nuc. Inst. and Methods* **1971**, *97* (3), 577-579.
- (29) Goertz, S. T.; Harmsen, J.; Heckmann, J.; He, C.; Meyer, W.; Radtke, E.; Reicherz, G., Highest polarizations in deuterated compounds. *Nucl. Instrum. Methods Phys. Res., Sect. A* **2004**, *526* (1-2), 43-52.
- (30) Reynolds, S.; Patel, H., Monitoring the Solid-State Polarization of ^{13}C , ^{15}N , ^2H , ^{29}Si and ^{31}P . *Appl. Magn. Reson.* **2008**, *34* (3), 495-508.
- (31) Grinberg, O. Y.; Dubinskii, A. A.; Lebedev, Y. S., Electron Paramagnetic Resonance of Free Radicals in the Two-millimeter Wavelength Range. *Russ. Chem. Rev.* **1983**, *52* (9), 850-865.
- (32) Wolber, J.; Ellner, F.; Fridlund, B.; Gram, A.; Johannesson, H.; Hansson, G.; Hansson, L. H.; Lerche, M. H.; Mansson, S.; Servin, R.; Thaning, M.; Golman, K.; Ardenkjaer-Larsen, J. H., Generating highly polarized nuclear spins in solution using dynamic nuclear polarization. *Nucl. Instrum. Methods Phys. Res., Sect. A* **2004**, *526* (1-2), 173-181.
- (33) Jeffries, C. D., Dynamic Orientation of Nuclei by Forbidden Transitions in Paramagnetic Resonance. *Physical Review Phys. Rev. PR* **1960**, *117* (4), 1056.
- (34) Abragam, A.; Goldman, M., *Nuclear magnetism : order and disorder*. Clarendon Press Oxford University Press: Oxford New York, 1982; p xix, 626 p.
- (35) Abragam, A.; Goldman, M., Principles of dynamic nuclear polarisation. *Rep. Prog. Phys.* **1978**, *41* (3), 395-467.
- (36) Hu, K.-N.; Song, C.; Yu, H.-h.; Swager, T. M.; Griffin, R. G., High-frequency dynamic nuclear polarization using biradicals: A multifrequency EPR lineshape analysis. *J. Chem. Phys.* **2008**, *128* (5), 052302-17.
- (37) Song, C.; Hu, K.; Joo, C.; Swager, T.; Griffin, R., TOTAPOL: a biradical polarizing agent for dynamic nuclear polarization experiments in aqueous media. *J. Am. Chem. Soc.* **2006**, *128* (35), 11385-90.
- (38) Reddy, T.; Iwama, T.; Halpern, H.; Rawal, V., General synthesis of persistent trityl radicals for EPR imaging of biological systems. *J. Org. Chem.* **2002**, *67* (14), 4635-9.
- (39) Bowman, M.; Mailer, C.; Halpern, H., The solution conformation of triarylmethyl radicals. *J. Magn. Reson.* **2005**, *172* (2), 254-67.
- (40) Koelsch, C. F., Syntheses with Triarylvinylmagnesium Bromides. α,γ -Bisdiphenylene- β -phenylallyl, a Stable Free Radical. *J. Am. Chem. Soc.* **1957**, *79* (16), 4439-4441.

- (41) Ardenkjær-Larsen, J.; Fridlund, B.; Gram, A.; Hansson, G.; Hansson, L.; Lerche, M.; Servin, R.; Thaning, M.; Golman, K., Increase in signal-to-noise ratio of > 10,000 times in liquid-state NMR. *Proc. Nat. Aca. Sci. USA* **2003**, *100* (18), 10158-63.
- (42) Glyavin, M.; Khizhnyak, V.; Luchinin, A.; Idehara, T.; Saito, T., The Design of the 394.6 Ghz Continuously Tunable Coaxial Gyrotron for DNP Spectroscopy. *International Journal of Infrared and Millimeter Waves* **2008**, *29* (7), 641-648.
- (43) Hornstein, M. K.; Bajaj, V. S.; Griffin, R. G.; Kreischer, K. E.; Mastovsky, I.; Shapiro, M. A.; Sirigiri, J. R.; Temkin, R. J., Second harmonic operation at 460 GHz and broadband continuous frequency tuning of a gyrotron oscillator. *IEEE Transactions on Electron Devices* **2005**, *52* (5), 798-807.
- (44) Torrezan, A. C.; Han, S.-T.; Mastovsky, I.; Shapiro, M.; Sirigiri, J. R.; Temkin, R. J.; Barnes, A.; Griffin, R. G., Coninuous Wave Operation of a Frequency Tunable 460 GHz Second-Harmonic Gyrotron for Enhanced Nuclear Magnetic Resonance. *IEEE Transactions on Plasma Science* **accepted for publication**.
- (45) Pines, A.; Gibby, M. G.; Waugh, J. S., Proton Enhanced Nuclear Induction Spectroscopy. A Method for High Resolution NMR of Dilute Spins in Solids. *J. Chem. Phys.* **1972**, *56* (4), 1776-1777.
- (46) Bennett, A. E.; Rienstra, C. M.; Auger, M.; Lakshmi, K. V.; Griffin, R. G., Heteronuclear decoupling in rotating solids. *J. Chem. Phys.* **1995**, *103* (16), 6951-6958.
- (47) Pines, A.; Gibby, M. G.; Waugh, J. S., Proton-enhanced NMR of dilute spins in solids. *J. Chem. Phys.* **1973**, *59* (2), 569-590.
- (48) Chandrakumar, N.; Fircks, G. v.; Harald G_nther, The 2D QUADSHIFT experiment: Separation of deuterium chemical shifts and quadrupolar couplings by two-dimensional solid-state MAS NMR spectroscopy. *Magn. Reson. Chem.* **1994**, *32* (7), 433-435.
- (49) Warncke, K.; Babcock, G. T.; McCracken, J., Static Conformational Distributions in the Solid State: Analysis and Application to Angular Dispersion in Side Chain Orientations in Model Tyrosine in Aqueous Glass. *J. Phys. Chem.* **1996**, *100* (11), 4654-4661.
- (50) van der Wel, P.; Hu, K.; Lewandowski, J.; Griffin, R., Dynamic nuclear polarization of amyloidogenic peptide nanocrystals: GNNQQNY, a core segment of the yeast prion protein Sup35p. *J Am Chem Soc* **2006**, *128* (33), 10840-6.
- (51) Barnes, A., *Personal communication* **2010**.
- (52) Mamone, S.; Dorsch, A.; Johannessen, O. G.; Naik, M. V.; Madhu, P. K.; Levitt, M. H., A Hall effect angle detector for solid-state NMR. *J. Magn. Reson.* **2008**, *190* (1), 135-141.
- (53) Maly, T.; Miller, A.-F.; Griffin, R. G., *In-situ* High-Field Dynamic Nuclear Polarization - Direct and Indirect Polarization of ¹³C nuclei. *ChemPhysChem* **2010**.
- (54) Becerra, L.; Gerfen, G.; Temkin, R.; Singel, D.; Griffin, R., Dynamic nuclear polarization with a cyclotron resonance maser at 5 T. *Phys. Rev. Lett.* **1993**, *71* (21), 3561-3564.
- (55) Granatstein, V. L.; Parker, R. K.; Armstrong, C. M., Vacuum electronics at the dawn of the twenty-first century. *Proc. IEEE* **1999**, *87* (5), 702-716.
- (56) Maly, T.; Bryant, J.; Ruben, D.; Griffin, R., A field-sweep/field-lock system for superconducting magnets--Application to high-field EPR. *J. Magn. Reson.* **2006**, *183* (2), 303-7.
- (57) Bennati, M.; Farrar, C.; Bryant, J.; Inati, S.; Weis, V.; Gerfen, G.; Riggs-Gelasco, P.; Stubbe, J.; Griffin, R., Pulsed electron-nuclear double resonance (ENDOR) at 140 GHz. *J. Magn. Reson.* **1999**, *138* (2), 232-43.
- (58) Becerra, L. R.; Gerfen, G. J.; Bellew, B. F.; Bryant, J. A.; Hall, D. A.; Inati, S. J.; Weber, R. T.; Un, S.; Prisner, T. F.; McDermott, A. E.; Fishbein, K. W.; Kreischer, K.; Temkin, R. J.; Singel, D. J.; Griffin, R. G., A Spectrometer for Dynamic Nuclear Polarization and Electron Paramagnetic Resonance at High Frequencies. *J. Magn. Reson.* **1995**, *A117* (1), 28-40.

Chapter 8: Paramagnetic Signal Quenching in MAS-DNP of Homogeneous Solutions

Adapted from Corzilius, B; Andreas, LB; Smith, AA; Zhe Ni, Q, Griffin, RG; J. Mag. Res. Submitted

8.1 Introduction

Dynamic nuclear polarization (DNP) is a technique to enhance the polarization of nuclear spins by several orders of magnitude and relies on the transfer of the high polarization present in the electron Zeeman reservoir to the nuclear Zeeman reservoir. Accordingly, DNP accelerates otherwise time-consuming experiments or allows observation of spins that are undetectable by conventional magic angle spinning (MAS) nuclear magnetic resonance (NMR)¹⁻⁷ and is rapidly becoming a standard technique in chemistry, biochemistry, structural biology, and material sciences⁸⁻¹¹. An essential requirement is that the samples contain electron spins in the form of paramagnetic centers from which the relatively high Boltzmann polarization (~660 times larger than ¹H) can be transferred to the nuclear spins via microwave driven mechanisms reviewed briefly below. In biochemical applications these paramagnets can in principle be endogenous (protein free radicals¹²), but are usually exogenous additions to the sample¹³. In the latter case the paramagnetic polarizing agent (PA) is co-dissolved in a cryoprotecting glass forming solvent together with the target molecule and both are randomly distributed in the frozen solution. If the sample is *heterogeneous* the target molecule is in a spatially separate phase (*e.g.*, nanocrystals, amyloid fibrils or membrane protein dispersed in the cryoprotectant) from the polarizing agent. Thus, in a heterogeneous sample, the enhanced polarization is transferred to the molecule of interest by efficient ¹H-¹H spin diffusion across phase boundaries, an example being amyloidiogenic nanocrystals such as GNNQQNY,^{14, 15} and a polarization gradient can be observed¹⁴. More recently, heterogeneous samples were further exploited by Emsley and coworkers in applications to microcrystalline analytes dispersed in an organic solvent¹⁶. In addition, Lesage *et al.*¹⁷ and Kobayashi, *et al.*¹⁸ recently demonstrated that it is possible to enhance the NMR signals at a surface and of small ligands bound to a catalytically active surface or mesoporous material using DNP by wetting the surface with a solution containing the polarizing agent. In contrast, in a *homogeneous* solution of small molecules¹⁹ or proteins,²⁰ which is the case considered here, the distance bridged via spin diffusion is short and a uniform polarization enhancement of all spins in the solvent and of the target molecule is possible²¹.

Because polarizing agents must be present within the sample, nuclear spins are subject to interactions with these paramagnetic species. These interactions can manifest themselves as shifts of the nuclear Larmor frequencies due to hyperfine interaction with the electron spin as well as a general shortening of the typical relaxation times encountered in solid state NMR. The former can generally be neglected in MAS DNP, since nuclei subject to strong paramagnetic (first-order) shifts are either filtered by the limited NMR excitation bandwidth or are broadened beyond detection at temperatures around 80 K. Additionally, polarizing agents typically do not induce significant pseudocontact (second-order) shifts due to EPR properties required for efficient DNP. However, nuclei detectable in MAS DNP are subject to reduced relaxation times by incoherent electron-nuclear interactions. These reduced T_1 and T_2 's can be beneficial (*e.g.*, shorter T_{1n} 's that allow for accelerated acquisition of NMR spectra) or detrimental (*e.g.*, enhanced transverse relaxation that broadens resonances and leads to reduced signal intensities). We observed both of these effects in early experiments using the monoradical TEMPO²², especially when the $[e^-] > 40$ - 60 mM²³. Importantly, observation of these intensity losses with monoradicals stimulated us to develop biradical polarizing agents that function at significantly lower electron concentrations²⁴⁻²⁷. However, until now we have not performed a systemic investigation of the intensity losses comparing the addition of mono and biradical polarizing agents during MAS experiments. Therefore, it is important to investigate these effects using model systems for both *homogeneous* and *heterogeneous* samples in order to optimize a variety of DNP parameters, sample preparation methods, design of new polarizing agents, and further the development of DNP as a generally applicable technique.

In this paper we report paramagnetic induced intensity losses and enhancements using four polarizing agents - TOTAPOL, 4-amino-TEMPO, trityl (OX063), and Gd-DOTA -- in MAS DNP experiments. We find that all four polarizing agents result in substantial improvements in sensitivity, with enhancements from 11 to 139, and sensitivity enhancements of 15 to 226. The polarizing agent TOTAPOL stands out because it results in the largest gain in sensitivity and does so at a concentration of only 5 to 10 mM that has minimal impact on the resolution while substantially reducing T_B , the build-up time.

An outline of the paper is as follows. In Section 2 we present a brief review of DNP mechanisms and relaxation theory along with a discussion of the polarizing agents chosen for this study. Section 3 describes the instrumentation, sample preparation, and details of data acquisition. In Section 4, we discuss the results in the context of contemporary DNP MAS spectroscopy, along with measurements of T_1 , T_2 , and T_{10} . We also include in Section 4 a discussion of enhancement factors, signal quenching, and overall sensitivity enhancement.

8.2 Background and Theory

Mechanisms of DNP

In a MAS DNP experiment using continuous microwave irradiation, the electron-to-nuclear polarization transfer occurs *via* two different mechanisms: solid effect (SE) and cross effect (CE) which we briefly review.

SE DNP²⁸⁻³⁵ relies on formally forbidden excitation of electron-nuclear zero or double quantum transitions. These transitions become partially allowed under the influence of non-secular electron nuclear dipole coupling. In order to achieve a net-enhancement of nuclear polarization, either the zero or double quantum transition is directly and selectively excited by irradiation with microwaves of appropriate frequency, derived by the SE matching condition

$$\omega_{\text{mw}} = \omega_{0S} \pm \omega_{0I}, \quad (8.1)$$

where ω_{mw} is the microwave frequency and ω_{0S} and ω_{0I} are the electron and nuclear Larmor frequencies, respectively. This selectivity can only be achieved efficiently if the overall breadth of the polarizing agent's EPR line – consisting of both the homogeneous linewidth δ and inhomogeneous breadth Δ – is smaller than the nuclear Larmor frequency: $\delta, \Delta < \omega_{0I}$. This prerequisite makes paramagnets with a narrow EPR line like trityl,³⁶ BDPA^{37,38} or Gd-DOTA³⁹ ideal polarizing agents for SE DNP.⁴⁰

In contrast the CE DNP^{24, 41-49} relies on three-spin flip-flop-flips between two electron spins and one nuclear spin. The flip-flop-flip process is efficient if the net energy involved is vanishing, a condition that is satisfied when the difference in the Larmor frequency of the two electron spins $\omega_{0S,1}$ and $\omega_{0S,2}$ matches the nuclear Larmor frequency:

$$\omega_{0S,1} - \omega_{0S,2} = \pm \omega_{0I} \quad (8.2)$$

In contrast to the SE, where the coherent transfer has to be extrinsically stimulated by application of a microwave field, the coherent electron-nuclear transfer during CE DNP is intrinsically excited by the dipole coupling between the electron spins. As a result, magnetization is exchanged between the electron and nuclear spins even in the absence of microwave irradiation. However, without extrinsic stimulation, no net polarization is transferred from the electrons to the nuclei because the differential polarization of the two electron spins equals the absolute polarization of the nuclear spin within the three spin system, and transfer rates leading to positive and negative polarization enhancement that cancel one another. Upon selective (partial) saturation

of one of the two electron spins, this equilibrium is perturbed and net polarization enhancement is generated on the nuclear spin. Given the two electron spins are of equal or similar nature (*e.g.*, two equal monoradicals are interacting in the glassy matrix or two similar radical moieties are tethered in a symmetric biradical) the inhomogeneous breadth of the polarizing agent's EPR line has to exceed the nuclear Larmor frequency to satisfy 2 while its homogeneous linewidth has to be smaller, so that one electron spin can be selectively saturated: $\delta < \omega_{0I} < \Delta$. This condition is met in the case of nitroxide radicals, whose EPR spectra are broadened by the *g*-anisotropy of the electron and of the ^{14}N hyperfine interaction. In this case MAS introduces a further complication because spin transitions shift in/out of resonance with the microwave frequency as several level crossings occur during the rotor period.^{49,50}

Electron-nuclear interactions during MAS DNP

During MAS nuclear spins are subject to coupling with the electron spins of the polarizing agent. Nuclei and unpaired electron(s) within a short distance of one another are strongly coupled leading to paramagnetic shifts and broadening, which effectively reduces the number of nuclear spins detectable by NMR. Concurrently, nuclear spins detectable by NMR exhibit enhanced paramagnetic relaxation. The shortening of T_2 and $T_{1\rho}$, even while only minimally impacting resolution in inhomogeneously broadened spectra, leads to a faster decay of magnetization during polarization transfer experiments that can reduce the efficiency of homo- and heteronuclear mixing experiments. Therefore it is crucial to understand the concentration dependent impacts on relaxation times induced by polarizing agents commonly used for MAS DNP.

The existing theory of paramagnetic enhanced relaxation of nuclear spins is mainly based on concepts derived by Solomon and Bloembergen and Morgan⁵¹⁻⁵⁴ that invoke incoherent interactions between the dipole moments of electron and nuclear spins. Given the two spins maintain fixed positions within a rigid lattice on average, the paramagnetic induced nuclear spin relaxation rate for spin "i" $\tilde{\Gamma}_{ik}$ of a single relaxation mode k scales as

$$\tilde{\Gamma}_{ik} \propto \left[\frac{\gamma_S^2 \gamma_I^2 (3\cos^2\theta - 1)^2}{r^6} \right] \times \frac{\tau_{ck}}{1 - \omega_k^2 \tau_{ck}^2}, \quad (8.3)$$

where the first term results from the dipole interaction between the spins, defined by the electron and nuclear gyromagnetic ratios γ_S and γ_I , respectively, the distance between the two spins r , and θ , being the angle between their orientation vector and the external magnetic field. The second factor in 3 describes the relaxation dispersion of the particular mode k with its characteristic

correlation time τ_{ck} and frequency ω_k . Note that typically several relaxation modes occur in parallel, but as long as these are independent, their rates are additive to the final observed relaxation rate.

Some of the models mentioned above are derived under conditions typically satisfied in liquids (*e.g.* fast isotropic motional averaging due to molecular tumbling). At the other extreme are models that apply to a rigid lattice in which it is assumed that local field fluctuations caused by electron flips are the dominant source of paramagnetic relaxation^{51,55}. In particular, Blumberg has shown that internuclear spin-diffusion plays an important role in longitudinal relaxation in solids doped with paramagnets⁵⁵. However, these models do not account for electron-electron interaction or fluctuations in the local field at the nucleus caused by dynamics of nuclei in the local field gradient of the electron spin or by MAS. Accordingly, they are not generally applicable to paramagnetic relaxation effects of nuclei in dielectric or rotating solids. An analytic or numerical derivation of relaxation in DNP samples would need to consider static and dynamic interactions of secular and non-secular nature between electrons, between electrons and nuclei, as well as between nuclei, all of which span a wide range of magnitude and time-scale. In the absence of a model to treat these effects, we can rely on empirical relaxation data for different DNP polarizing agents.

Properties of the polarizing agents

We studied the paramagnetic relaxation effects induced by varying concentrations of TOTAPOL, 4-amino-TEMPO, trityl OX063, and Gd-DOTA in MAS DNP experiments. Each of these paramagnets (see *Figure 8.1* for their chemical structures) is representative of a certain group of polarizing agents active under different DNP mechanisms. Nitroxide-based polarizing agents enable CE DNP with TOTAPOL being an example of a biradical that allows for a relatively strong intramolecular e⁻-e⁻ dipolar coupling at low e⁻ concentrations²⁶. In contrast, the monoradical 4-amino-TEMPO requires high concentrations in order to provide the required intermolecular coupling and efficient CE⁵⁶. Trityl OX063³⁶ is a radical with a narrow EPR line that is commonly used for SE DNP^{40, 57}, and Gd-DOTA³⁹ represents the group of recently introduced high-spin polarizing agents also supporting the SE⁵⁸. In the following sections we report the major differences between these polarizing agents and their respective DNP mechanisms, together with the expected effects on nuclear spin relaxation.

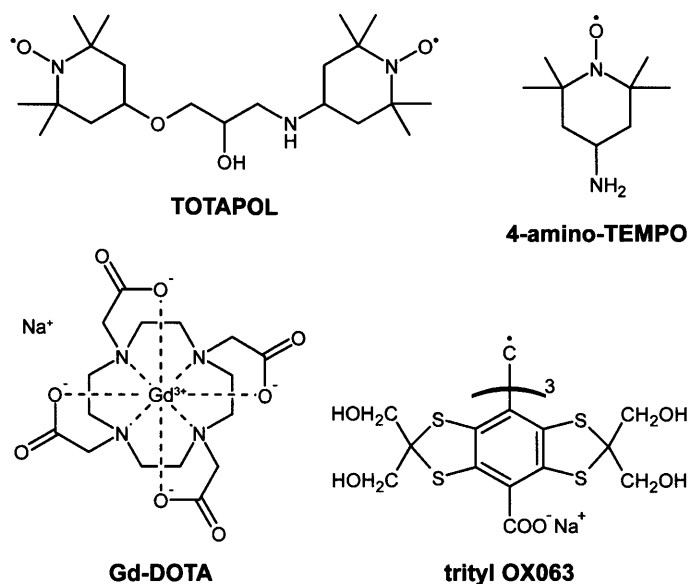


Figure 8.1. Polarizing agents investigated in this study.

TOTAPOL (1-(TEMPO-4-oxy)-3-(TEMPO-4-amino)propan-2-ol) was introduced by Song *et al.* as an efficient biradical polarizing agent for CE DNP^{24, 26, 27, 41, 44-49}. Due to the fact that the CE relies on efficient cross-relaxation (CR) between one electron spin and an electron-nuclear spin pair (*vide supra*), one expects a pronounced effect on the paramagnetically induced nuclear T_1 . Note that the same CR mechanism allowing for CE DNP also leads to efficient paramagnetic relaxation by providing a coherent pathway for nuclear magnetization to the bath *via* the energy difference of the two electron spins. The e^-e^- dipole coupling is ~ 23 MHz²⁷.

4-Amino-2,2,6,6-tetramethylpiperidine-1-oxyl (4-amino-TEMPO, TEMPAMINE) is a stable, water-soluble, nitroxide radical that exhibits a very similar EPR spectrum to TOTAPOL at 140 GHz^{24, 26, 48, 56}. Therefore, the CE is also the active DNP mechanism; however, the two electron spins are located on separate molecules and the crucial e^-e^- dipole coupling is intermolecular rather than intramolecular. Obviously, the strength of the dipole coupling and hence the efficiency of CR depends strongly on the molecular concentration of the radical in the cryoprotecting matrix, which at 40 mM is ~ 2 MHz²⁷

The stable trityl radical OX063 exhibits a narrow EPR line of ~ 50 MHz width at 140 GHz^{36, 48}, due to a small g -anisotropy. The chance of energy matching an electron-electron-proton triplet is small so CR is quenched at high field, and in this case ^1H DNP can be driven by the SE. Paramagnetically enhanced spin-lattice relaxation is caused by local magnetic field fluctuations by random spin flips of the electron spin or by dynamic motion of the nucleus in the local magnetic field gradient of the electron spin.

Gd-DOTA is an extremely stable Gd(III) complex formed by the macrocyclic chelating derivative 1,4,7,10-tetraazacyclododecane-*N,N',N'',N'''*-tetraacetate (DOTA) and exhibits a high-spin state of $S = 7/2$ due to the $4f^7$ electronic structure of Gd^{3+} , which potentially leads to strong paramagnetic relaxation effects^{39, 59, 60}. The electron spin of Gd^{3+} generally experiences a significant zero-field splitting (*i.e.*, electron quadrupole interaction) in the ligand field, with an axially symmetric tensor described by the single constant $D = 570$ MHz⁶¹. This interaction leads to a dispersion of the full EPR spectrum over almost 7 GHz. However, because of the half-integer spin state, the central EPR transition ($m_s = -1/2 \rightarrow +1/2$) is not influenced by zero-field splitting to first order and exhibits a full width at half maximum (FWHM) of only ~29 MHz at the magnetic field of interest (5 T)⁵⁸. In a previous study we have shown that this narrow transition can be exploited for SE DNP, whereas no signs of CE DNP have been observed⁵⁸. The absence of CE DNP does not, however, automatically indicate that CR is inactive as well. For example, for a very broad EPR line (*i.e.* the inhomogeneous width greatly exceeding the nuclear Larmor frequency), positive and negative CE conditions cancel each other, leading to negligible CE DNP enhancement; CR might still be active and might lead to efficient relaxation of nuclear polarization toward thermal equilibrium. Nevertheless, we expect CR to be less efficient with Gd-DOTA due to the fact that the probability of finding two dipolar coupled Gd^{3+} sites in the correct orientation and spin states to fulfill the CE matching condition 2 is small, especially in low concentration solutions investigated in this study.

For a further discussion of DNP and its mechanisms, we refer the reader to excellent work on DNP as such by Abragam and Goldman,⁸ and reviews about MAS DNP by Maly *et al.*,¹⁰ and Barnes *et al.*⁹. Hu has recently published an excellent review focusing on polarizing agents and the related DNP mechanisms⁴⁷.

Transverse paramagnetic relaxation

Existing theories of transverse relaxation are either based on assumptions of fast isotropic averaging of spin-spin interactions or on spin-spin interactions in a rigid lattice⁵¹⁻⁵⁵. The former are not generally applicable to glasses at typical MAS DNP temperatures where the nuclear spins experience static spin-spin interactions. Relaxation behavior of low- γ nuclei (*e.g.*, ^{13}C) is further expected to be influenced not only directly by couplings to paramagnetic centers, but also indirectly by coupling to a pool of highly abundant 1H spins, which is most often the case in biological systems. Although low- γ nuclei are normally decoupled during NMR experiments from 1H by strong rf irradiation, the efficiency of decoupling is typically finite.

8.3 Methods

Instrumentation

All DNP NMR experiments were performed on a custom-built NMR spectrometer operating at 212 MHz (^1H frequency), courtesy of D. Ruben. A custom-built MAS NMR probe allowed for MAS at cryogenic temperatures ($T \geq 80$ K) and features a triple resonance rf circuit (^1H , ^{13}C , ^{15}N) and efficient microwave coupling to the sample using overmoded corrugated waveguides (similar to a design published by Barnes *et al.*⁶²). The probe has a cryogenic sample exchange system that allows efficient screening of multiple samples. A detailed description of the probe will be published elsewhere. Microwaves were generated with a gyrotron oscillator operating at 139.65 GHz with a maximum output power of ~ 13 W⁶³⁻⁶⁵. Because the gyrotron operates at a fixed frequency, the magnetic field was swept to the optimal matching condition for each polarizing agent with a cryogenic sweep coil. Optimal DNP fields were determined in previous studies^{40, 58}, being 4.9798 T for TOTAPOL and 4-amino-TEMPO, 4.9891 T for trityl, and 5.0178 T for Gd-DOTA. Due to their relatively narrow DNP matching conditions, trityl and especially Gd-DOTA require careful adjustment of the magnetic field in order to optimize the enhancement. EPR spectra were recorded on a custom-built pulsed EPR spectrometer operating at 140 GHz. A detailed description of that instrument was published recently⁶⁶.

Sample preparation

All samples were prepared by dissolving an appropriate amount of polarizing agent in a mixture of d_8 -glycerol/ $\text{D}_2\text{O}/\text{H}_2\text{O}$ with a volume ratio of 60:30:10 to which 1 M ^{13}C -urea was added to provide the required ^{13}C for detection of the non-DNP-enhanced signal (off-signal) in 16–128 scans at sufficient S/N for accurate determination of enhancement factors. Samples with varying polarizing agent concentrations were prepared by diluting the most concentrated solution with undoped solvent mixture. All isotope labeled compounds were purchased from Cambridge Isotope Laboratories, Inc. (Andover, MA) and were used without further purification. TOTAPOL was acquired from Dynupol, Inc (Cambridge, MA). We found that TOTAPOL when properly purified and dried is soluble to a maximum concentration of ~ 50 mM in 60/40 (v/v) glycerol/water mixtures. In contrast to previous reports⁶⁷ we have never been able to achieve concentrations of 200 mM. 4-Amino-TEMPO from Sigma-Aldrich (St. Louis, MO) was used without further purification. Trityl OX063 was from Oxford Instruments and Gd-DOTA ($\text{Na}(\text{Gd}[\text{DOTA}])\cdot 4\text{H}_2\text{O}$) was provided by C. Luchinat and I. Bertini (CERM, Florence, Italy).

Spectra comparing the intensity of static and MAS experiments were obtained from samples composed of d_8 -glycerol/ D_2O/H_2O with a volume ratio of 60:30:10 containing 2- ^{13}C -glycerol. Since the static ^{13}C powder pattern of ^{13}C -urea is 18 kHz in breadth, we used 2- ^{13}C -glycerol which has line of ~ 5 kHz. The samples were doped with 20 mM electrons, either 10 mM TOTAPOL or 20 mM trityl.

Data acquisition and analysis

Samples for DNP NMR studies were contained in a 4 mm OD sapphire MAS rotor from Insaco (Quakertown, PA). The axial sample dimension was restricted by the length of Vespel spacers to the central ~ 4 mm inside the 8 mm long coil volume. All experiments have been performed using a MAS frequency of $\omega_r/2\pi = 5$ kHz at a temperature of 84 K. Approximately 8 W's of microwave power (measured at the probe input) were used for all DNP experiments, and signal intensities were detected on ^{13}C after a cross-polarization (CP) step from 1H with 2 ms contact time and $\omega_1/2\pi = 83$ kHz. Polarization on 1H and ^{13}C was first saturated with a 16-pulse train applied to both channels ($\omega_1/2\pi = 50$ kHz) after which polarization built up during a microwave irradiation period. The length of this period was varied for determination of the longitudinal DNP build-up time constant T_B (or the longitudinal relaxation time constant T_1° in the case of the undoped samples). All other experiments were performed using a fixed recovery period of $1.26 \times T_B$ (or T_1°), thus allowing for optimal sensitivity in a given experimental time. T_2 was determined by measuring the decay of polarization during a rotor-synchronized Hahn-Echo sequence. Two-pulse phase modulation (TPPM)⁶⁸ was used for 1H decoupling with an rf field strength corresponding to $\omega_1/2\pi = 83$ kHz during T_2 evolution and acquisition. 1H $T_{1\rho}$ was measured by a spin-lock experiment before the CP sequence, whereas ^{13}C $T_{1\rho}$ was determined by measuring the magnetization decay during a ^{13}C spin-lock after the CP transfer step. In the latter case no 1H decoupling field was applied since application of typical decoupling fields avoiding Hartmann-Hahn matching resulted in significant shortening of ^{13}C $T_{1\rho}$. All spin-lock pulses were limited to a maximum duration of 20 ms to prevent extensive energy dissipation in the rf circuit and potential arcing. A timing diagram containing all pulses is shown in **Figure 8.2**. Relaxation or build-up time constants were determined by least-square fitting the signal amplitude (after Fourier transform of the FID/echo) with an exponential function.

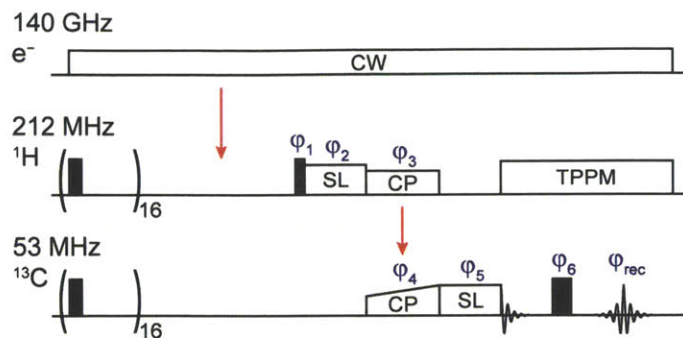


Figure 8.2. Pulse sequence used for relaxation time measurements. The ^1H and ^{13}C spin-lock pulses as well as the Hahn-echo sequence were only used for the respective $T_{1\rho}$ and T_2 experiments; the pulses not needed for certain experiments having been disabled accordingly. The pathway of polarization transfer has been marked by red arrows. The saturation pulses were phase alternated between 0 and 90° phase angle. A phase cycle of $\varphi_1 = x\bar{x}$, $\varphi_2 = yy\bar{y}\bar{y}$, $\varphi_3 = y$, $\varphi_4 = xx\bar{y}y\bar{x}\bar{y}\bar{y}$, $\varphi_5 = xx\bar{y}y$, $\varphi_6 = xx\bar{y}y$, and $\varphi_{\text{rec}} = y\bar{y}\bar{x}\bar{y}\bar{y}\bar{x}\bar{x}$ was used in order to suppress unwanted coherences and artifacts due to experimental imperfections.

EPR experiments were performed on the same sample solutions used for DNP NMR experiments at a temperature of 80 K. Due to a more complicated and time consuming sample changing procedure -- the EPR probe has to be removed from the cryostat, warmed up completely to ambient temperature, and dried to avoid build-up of humidity before returning it into the cold cryostat -- the sample space was limited to 3 samples of each polarizing agent. For each compound the smallest, the largest, and an intermediate concentration was chosen. For determination of T_{1S} a saturation recovery experiment was performed using a long continuous wave (cw) irradiation period followed by a recovery period of varying time during which longitudinal magnetization is built-up and read-out using a Hahn echo sequence $\pi/2 - \tau - \pi - \tau$. Although being theoretically inferior to inversion recovery in terms of sensitivity, saturation recovery minimizes effects of spectral diffusion interfering with longitudinal relaxation due to the incomplete excitation of inhomogeneously broadened spectra. The resulting polarization build-up curve can be fitted using a monoexponential, directly yielding the longitudinal relaxation time constant T_{1S} . The transverse relaxation time constant T_{2S} was determined using a Hahn echo experiment with a pulse sequence $\pi/2 - \tau - \pi - \tau$ that varies the time τ during which transverse relaxation is occurring. However, in systems with large electron spin concentration and therefore significant electronic spin-spin couplings the transverse magnetization not only decays due to T_{2S} but also evolves under these couplings; thus care has to be taken to sufficiently refocus these couplings. Otherwise a combination of transverse relaxation and interelectronic spin evolution results in a shortening of the measured echo decay time constant, described by the phase-memory time T_m . In order to determine the actual T_{2S} , we measured T_m for various

microwave field strengths and respective pulse lengths and extrapolated the decay time constant to infinite pulse length (see Fig. S10). This extrapolated value represents the echo decay time constant for an infinitely selective (soft) excitation of a single spin packet and therefore T_{2S} . All data recorded and analyzed is compiled in Tables S1-S5 in the supporting information.

8.4 Results and Discussion

In **Figure 8.3** we show the signal intensities in MAS NMR spectra from an undoped sample of ^{13}C -urea in glycerol/water and spectra enhanced by each of the four PA's with respect to the non-enhanced (off-) signal. The enhanced signal spectra were recorded using the PA concentration yielding the largest enhancement. As can be seen in **Figure 8.9** these concentrations also led to the maximum sensitivity for each polarizing agent.

The signal at 175 ppm in **Figure 8.3** is the carbonyl group of urea used to measure all of the relaxation, quenching, and enhancement parameters in the text. Signals from 120-150 ppm arise from Vespel and Kel-F used in the rotor and stator assembly, and as expected are not altered by the presence of the polarizing agent. The urea spectrum is inhomogeneously broadened, as expected from a small molecule resident in a glass, and high electron concentrations of ~ 60 mM are needed in order to observe noticeable changes in the linewidth.

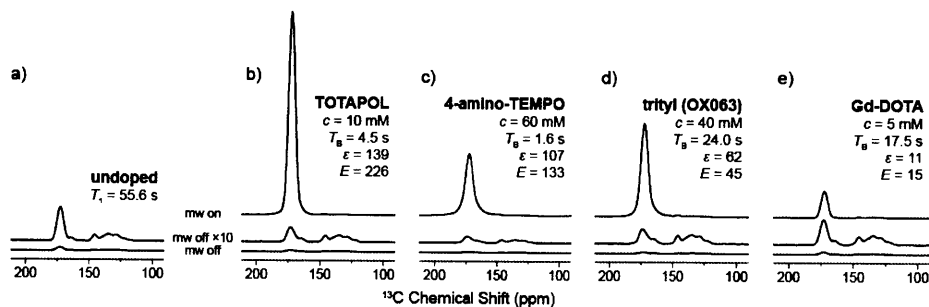


Figure 8.3. DNP enhanced ^{13}C - ^1H CP spectra of ^{13}C -urea in 60/30/10 (vol.-%) d_8 -glycerol/ $\text{D}_2\text{O}/\text{H}_2\text{O}$ for (a) signal of the undoped sample at equilibrium and (b-e) for each polarizing agent as labeled at the optimal concentration, for maximum enhancement and sensitivity. Off-signals are shown at the same scale and multiplied by a factor of 10. Spectra were recorded with a recycle delay of $1.26 \times T_B$ and were scaled in order to correct for variations in spectrometer sensitivity as described in supporting information. $\omega_r/2\pi = 5$ kHz, $T = 84$ K.

Evident in **Figure 8.3** is a paramagnet induced reduction in the off signal intensity. In order to explore the physical basis for this signal quenching, we determined the equilibrium signal intensity of a 20 mM trityl sample and a 10 mM TOTAPOL sample under both spinning and static conditions (**Figure 8.4**). We anticipated that for TOTAPOL, MAS would result in additional quenching due to CE depolarization of the nuclear spins. This is caused by an equalized polarization across the EPR spectrum (electron electron nuclear level crossings) under

MAS^{49, 50}. In the case of trityl, CE condition is not met for ¹H and this mechanism is not active. Interestingly, additional signal loss was observed for *both* TOTAPOL and trityl under MAS, accompanied by a reduction in the nuclear T1, pointing to the importance of another mechanism of quenching.

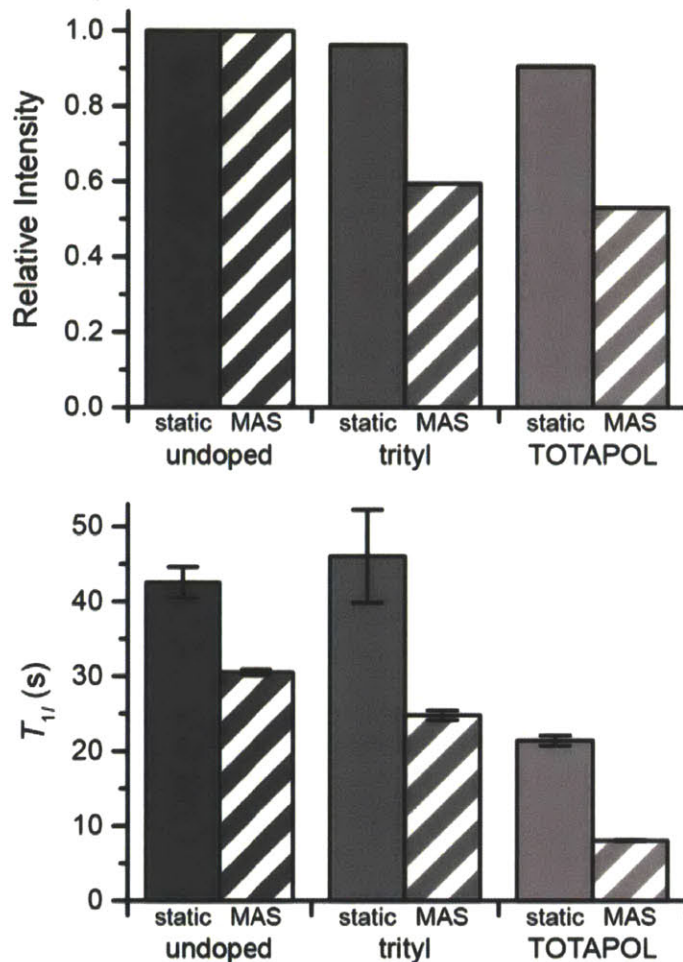


Figure 8.4. Equilibrium signal intensity (top) and T1 (bottom) are compared for a 20 mM trityl sample and a 10 mM TOTAPOL sample under static and MAS conditions. The spinning frequency was set to 4975 Hz, and spectra were recorded at 380 MHz. The sample was 30/30/30/10 D8 glycerol/ 2-¹³C, D8 glycerol/ D₂O / H₂O.

Determination of paramagnet induced relaxation rates

In order to separate relaxation effects induced by paramagnetic polarizing agents from those intrinsic to the sample *sans* polarizing agent, we calculate the paramagnetic relaxation rate by subtracting the intrinsic relaxation rate of the undoped sample from the measured overall relaxation rate:

$$\begin{aligned}\tilde{\Gamma}_B &= \Gamma_B - \Gamma_1^\circ = \frac{1}{T_B} - \frac{1}{T_1^\circ}, \\ \tilde{\Gamma}_2 &= \Gamma_2 - \Gamma_2^\circ = \frac{1}{T_2} - \frac{1}{T_2^\circ},\end{aligned}\tag{8.4}$$

where $\tilde{\Gamma}_i$, Γ_i , and Γ_i° denote the paramagnetically induced relaxation rate constant, the observed overall relaxation rate constant, and the relaxation rate constant intrinsic to the undoped sample, respectively. The same nomenclature is applied to relaxation time constants T_i , and T_i° . For DNP samples, we use the subscript 'B' to describe the longitudinal DNP build-up rate and time constant. $T_{1\rho}^\circ$ greatly exceeded our maximum spin-locking time and was not measured. Accordingly we conclude $\Gamma_{1\rho} \gg \Gamma_{1\rho}^\circ$ in all cases and estimate

$$\tilde{\Gamma}_{1\rho} = \Gamma_{1\rho} - \Gamma_{1\rho}^\circ \approx \Gamma_{1\rho} = \frac{1}{T_{1\rho}}\tag{8.5}$$

without significant error. Further details on the determination of $T_{1\rho}$ are provided in the appropriate section below. All paramagnetic induced relaxation rates are plotted in *Figure 8.5*.

T₁ relaxation and build-up of polarization

Electron spin concentration dependent build-up time and rate constants are shown in *Figure 8.5*. For the undoped sample, the ¹H T_1° was measure as ~54.6 s.¹ Clearly all the paramagnetic samples show a significant reduction of T_B with respect to T_1 as is expected. Interestingly, TOTAPOL shows the largest reduction of T_B of all the polarizing agents. Even at [e⁻] =4 mM (2 mM molecular concentration), T_B is reduced by a factor of ~3 with respect to T_1 . With spin concentrations of 10–20 mM commonly used for MAS DNP, T_B is reduced ~12–30 fold, and at 80 mM it is ~65 fold. This pronounced effect is attributed to the efficient nuclear CR, which also is responsible for CE DNP. Although 4-amino-TEMPO exhibits an EPR spectrum essentially identical to TOTAPOL with a comparable T_{1S} (see *Figure 8.6*), it leads to a significantly smaller effect on the polarization build-up time constant at low concentrations. This is due to the fact that CR induced by 4-amino-TEMPO relies on intermolecular couplings between nitroxide moieties

¹ We measured $T_1^\circ = 61.6$ s for the 4-amino-TEMPO and 5 mM trityl samples prepared from the second stem solution. All build-up time constants are scaled to $T_1^\circ = 61.6$ s using the relation $1/T_{B,a} - 1/T_{B,b} = 1/T_{1,a}^\circ - 1/T_{1,b}^\circ$.

which are weaker particularly at low molecular concentrations. Even at the largest concentration investigated the average radical-radical distance at 60 mM is $\sim 30 \text{ \AA}$, which corresponds to dipolar coupling of only $\sim 2 \text{ MHz}$ compared with the intramolecular coupling of $\sim 25 \text{ MHz}$ present in TOTAPOL²⁶. Trityl induces only a relatively minor reduction of T_B even at a higher concentration, because the narrow linewidth of trityl does not mediate efficient energy conserving CR. Longitudinal paramagnetic relaxation relies mostly on a fluctuating dipole field at the nuclei caused by electron spin flips or motion. The long T_{1S} (see *Figure 8.6*) and rigidity of the glassy matrix also translates into inefficient longitudinal paramagnetic relaxation efficiency.

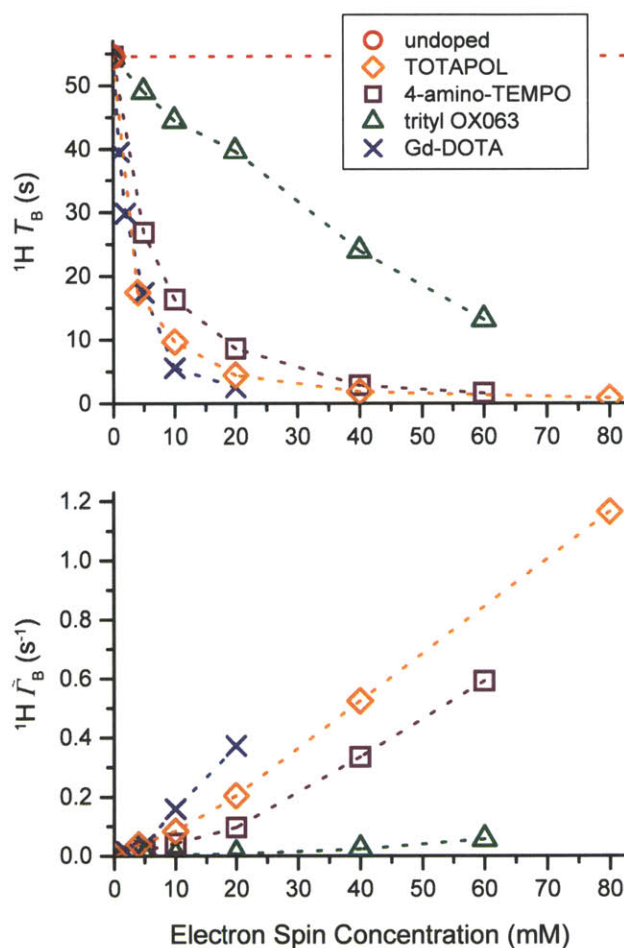


Figure 8.5. ${}^1\text{H}$ DNP build-up time constant T_B (top) and paramagnetically enhanced buildup rate constant \tilde{r}_B according to eq. 8.4 (bottom) as a function of electron spin concentration of various polarizing agents. \tilde{r}_B includes PRE as well as DNP effects (for details see text).

Although CR is expected to be inefficient for Gd-DOTA, there is a strong reduction in T_B . At $[e^-] > 10 \text{ mM}$ Gd-DOTA induces relaxation rates larger than TOTAPOL. Thus, the $S = 7/2$ spin state, subject to significant static zero-field splitting in conjunction with the short T_{1S} of the high-spin

system (see **Figure 8.6**), leads to a significant decrease of T_B . This is the case even though cross-relaxation and the CE do not seem to be active with this polarizing agent and SE is the dominant DNP mechanism. Note that we measured a bi-exponential behavior of electron spin-lattice relaxation for Gd-DOTA and give a fast and a slow relaxation time constant in **Figure 8.6** as well as Table S5. This behavior was reported previously by Goldfarb and coworkers⁶⁹.

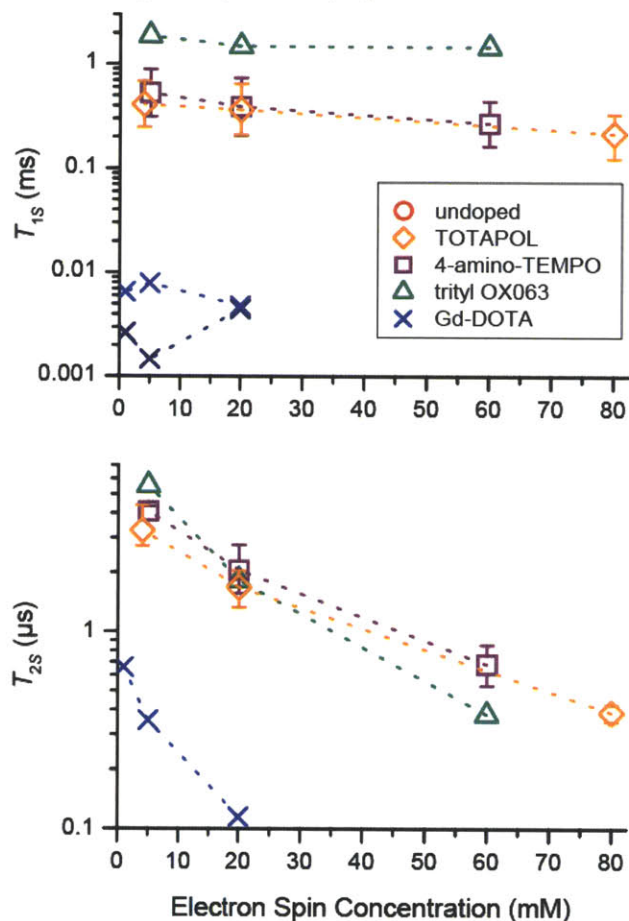


Figure 8.6. Electron spin longitudinal relaxation time constant T_{1s} (top) and transverse relaxation time constant T_{2s} (bottom) as a function of electron spin concentration of various polarizing agents measured at 140 GHz EPR frequency. Data of trityl and Gd-DOTA have been measured at the maximum of the EPR line. TOTAPOL and 4-amino-TEMPO was measured at four different field positions (4980, 4986, 4994, and 4998 mT; for a figure showing the field position with respect to the EPR spectrum see SI, Fig. S9); data points represent the average (mean) value, error bars indicate the maximum and minimum value. If no error bar is given, the difference between the minimum and maximum value is smaller than the data symbol.

Generally a short T_B is beneficial since it allows for rapid recycling of the NMR experiment and therefore higher sensitivity⁷⁰, and the sensitivity increase due to a shorter of T_B with respect to T_1° is expressed as

$$\kappa^\circ = \sqrt{\frac{T_1^\circ}{T_B}}. \quad (8.6)$$

This factor κ° is not to be confused with the decrease of T_B with respect to T_1 (*i.e.*, the longitudinal relaxation time without microwave irradiation) within one sample by excitation of SE DNP as was described in our earlier publications^{40, 57}. Here, we focus on the effects by paramagnetic relaxation and compare T_B under DNP conditions with T_1° of a different sample not containing a polarizing agent.

At the same time, the more efficient longitudinal relaxation competes with polarization build-up by DNP and leads to smaller observed enhancement. It is important to distinguish between polarizing agents that mediate the CE and those that operate solely by the SE. While for the SE paramagnetically accelerated nuclear spin-lattice relaxation always prevents development of large DNP enhancements,^{40, 57} the same is not true for the CE. In the latter case the major part of the strong reduction of T_B is due to CR and indicates an efficient DNP process and leads to large enhancement factors. Clearly, the enhancement factor alone understates the sensitivity gain of CE DNP radicals such as TOTAPOL when compared with SE DNP and κ° should always be taken into account when considering DNP efficiency.

T_2 and homogeneous linewidth

The paramagnetic effects on the nuclear T_2 do not show as strong a dependence on the nature of the paramagnet as is observed for T_1 (see **Figure 8.7**). Because the intrinsic T_2° might be significantly different in other samples of biological interest and since relaxation rates are additive, the paramagnet-induced transverse relaxation rates \tilde{T}_2 are also reported as a more intrinsic measure of paramagnetic effects. The high-spin Gd-DOTA shows a slightly stronger influence compared to the $S = 1/2$ radicals, especially at lower concentrations. For the $S = 1/2$ monoradicals, \tilde{T}_2 fall within a narrow region so that differences between the polarizing agents can be neglected. The TOTAPOL biradical exhibits about only half of the reduction in T_2 compared to the monoradicals at similar electron spin concentration, indicating that the molecular concentration plays the dominant role in dephasing of nuclear coherence and the biradical character can more or less be neglected. For all PA's \tilde{T}_2 shows a strong approximately linear increase with higher polarizing agent concentration. The similarity of transverse relaxation rates induced by different polarizing agents with different electronic spin relaxation properties

indicates that a mechanism independent of electronic spin-flips is governing the paramagnetic T_2 , pointing to modulation due to MAS or dynamic motion of the nuclei within the magnetic field gradient of the electron spin as the cause of transverse relaxation; however, the exact nature cannot be determined using the presently available data.

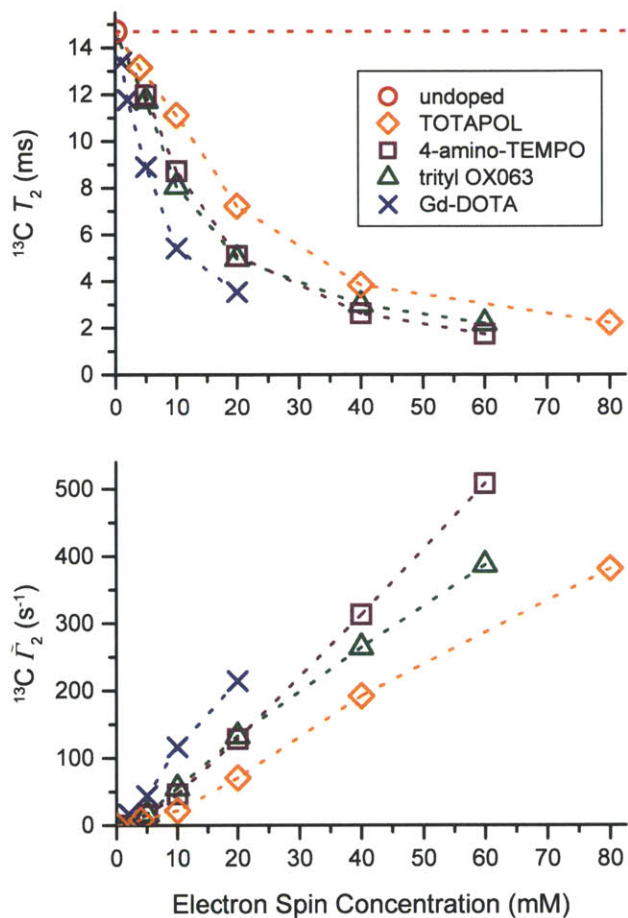


Figure 8.7. ^{13}C transverse relaxation time constant T_2 (top) and the related rate constant \tilde{T}_2 according to eq. 8.4 as a function of electron spin concentration of various polarizing agents.

Quantitatively, the $^{13}\text{C} T_2$ of the paramagnetically doped samples is reduced to about 50% of that of the undoped sample at around 10 mM polarizing agent concentration. This is an important consideration when optimizing sample conditions since a short T_2 not only leads to faster magnetization decay during transverse mixing and therefore lower sensitivity, but also leads to increased homogeneous broadening and reduced resolution. Recall that the homogeneous full width at half maximum (FWHM) is $\delta / 2\pi = 1 / \pi T_2$ (in units of radians). For the undoped sample, we measured $T_2 = 15.6$ ms corresponding to a homogeneous line width of 20 Hz, or ~ 0.4 ppm at the ^{13}C frequency of 53.3 MHz. For a polarizing agent concentration of $c_{\text{PA}} = 10$ mM,

the average $T_2 \sim 7.5$ ms, yielding $\delta/2\pi = 42$ Hz (~ 0.8 ppm). If the concentration is increased to 20 mM, the average $T_2 \sim 4.5$ ms, resulting in a homogeneous line width of 70.7 Hz (~ 1.3 ppm), which can potentially lead to significant line broadening. Note that the homogeneous line widths in ppm decrease linearly with increasing magnetic field; therefore, the effects in this study conducted at $B_0 = 5$ T are larger than at 17.4 T where the observed homogeneous line width for 10 mM polarizing agent concentration would correspond to only ~ 0.2 ppm, assuming a similar T_2 . Since spectral broadening at cryogenic temperatures has been empirically found to be dominated by inhomogeneity⁷¹, the additional broadening by shortening of T_2 will most likely be a minor effect, especially at high field. This is experimentally supported by a previous study performed at 9 T (380 MHz ^1H , 95.6 MHz ^{13}C), where it was possible to resolve cross peaks with a width of ~ 1 ppm of the active site of bacteriorhodopsin (bR) using DNP, even when [TOTAPOL] = 20 mM²¹. However, in the case of bR, the biradical was sterically excluded from the active site by distance of ≥ 20 Å. In contrast, Akbey *et al.* described an example where TOTAPOL was presumably binding to the unfolded $\alpha\text{S-SH3}$ domain, leading to a significantly increased linewidth of the protein resonances, especially if ^{13}C was directly polarized and detected during a Bloch decay instead of using a “filtering” ^1H - ^{13}C CP step²⁰. Thus, a bulky biradical polarizing agent which is sterically separated from the NMR sites of interest is requisite for maintaining resolution, and concurrently achieving large ϵ .

$T_{1\rho}$ relaxation

$T_{1\rho}$ measurements are shown in **Figure 8.8** for ^1H and ^{13}C in spin-lock fields of 50 kHz. $T_{1\rho}$ was not determined precisely for the undoped sample but we ascertain that it is >20 ms because of the absence of detectable decay. Both ^1H and ^{13}C show a very similar behavior at $\omega_{1l}/2\pi = 50$ kHz spin-locking fields. Increasing the spin-lock field strength to 100 kHz (see Fig. S7) leads to a two-fold decrease of $\tilde{T}_{1\rho}$ for all polarizing agents and concentrations investigated, indicating linear relaxation dispersion in that field regime. Gd-DOTA shows a very high $\tilde{T}_{1\rho}$ even at low concentrations most probably due to the high-spin properties, whereas the biradical character of TOTAPOL leads to low $\tilde{T}_{1\rho}$ even at high electron spin concentrations. It is noteworthy that 4-amino-TEMPO and trityl show similar $\tilde{T}_{1\rho}$'s at their respective concentrations. This differs from the T_B behavior, where we observed a more pronounced reduction by 4-amino-TEMPO. Clearly, previous arguments we made in order to explain the differences in T_B behavior do not apply to $T_{1\rho}$

relaxation; in this case, the spin-locking frequency is much smaller than the linewidth of either polarizing agent. Longitudinal relaxation, on the other hand, requires energy matching on the order of the nuclear Zeeman frequency $\omega_{0l} = \gamma_l B_0$, in which case all previous arguments about greatly different inhomogeneous EPR line widths and differences in cross-relaxation have to be considered.

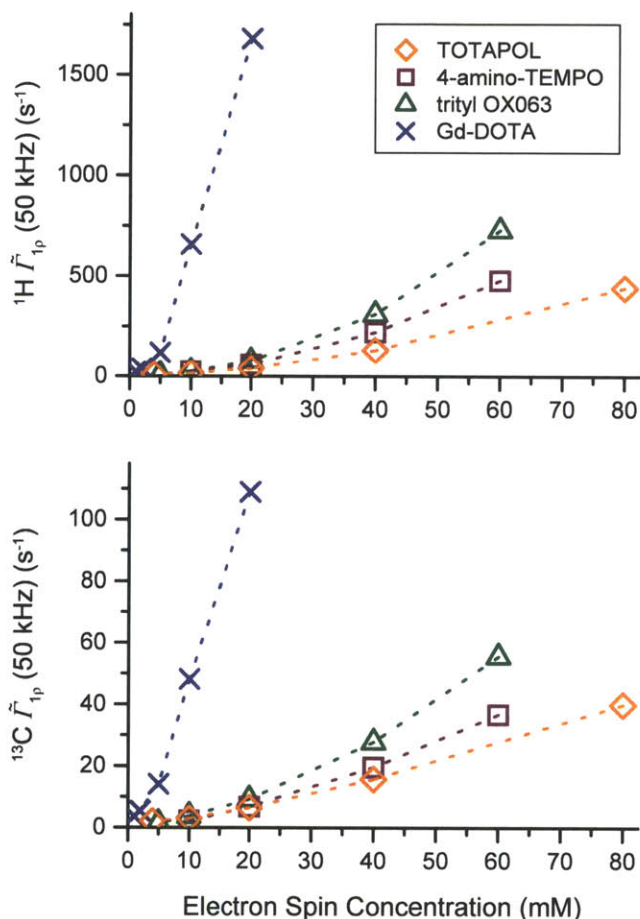


Figure 8.8. ^1H (top) and ^{13}C (bottom) $\tilde{\Gamma}_{1\rho}$ at a spin-lock field of $\omega_{\text{SL}}/2\pi = 50$ kHz as a function of electron spin concentration of various polarizing agents.

A quantitative comparison of $\tilde{\Gamma}_{1\rho}$ shows that the relaxation rates uniformly differ by a factor of ~ 16 between ^1H and ^{13}C at the same spin-locking field strength for all polarizing agents and concentrations. This behavior indicates that a direct paramagnetic effect is responsible for transverse relaxation in the rotating frame, which scales as γ_l^2 following 3. Therefore, relayed effects where paramagnetic enhanced relaxation of ^1H induces relaxation of ^{13}C can be neglected. This is further supported by the observation that a spin-locking field of 50 kHz applied to ^{13}C

sufficiently attenuated ^1H - ^{13}C interactions while the application of additional ^1H decoupling fields during the ^{13}C spin-lock lead to shortening of $T_{1\rho}$ in all cases.

DNP enhancement factor

An important measure of the efficiency of DNP is the enhancement factor ϵ , which is determined as the amplitude ratio between the DNP-enhanced and the non-enhanced signal (on- vs. off-signal). Measured enhancement factors are shown in **Figure 8.9** (top). Here the efficiency of TOTAPOL biradical as a CE polarizing agent is quite obvious because it yields very high ϵ even at low $[\text{e}^-]$ (<20mM). Trityl shows slightly larger enhancements than 4-amino-TEMPO for concentrations <40 mM. At higher concentrations, the larger intermolecular electron-electron dipole couplings improve the CE efficiency, thus causing the CE with 4-amino-TEMPO to yield much larger ϵ than trityl. However, the DNP enhancements at high radical concentration are accompanied by compromised nuclear coherence times (*vide supra*) and reduced off-signal amplitudes (*vide infra*), a fact that greatly emphasizes the advantage of biradical polarizing agents. Gd-DOTA shows the smallest enhancements with $\epsilon \approx 11$, and we therefore do not expect general applicability of this polarizing agent in typical MAS DNP experiments commonly performed today. However, paramagnetic metal ions might lead to novel applications of DNP, such as investigation of metal centers in enzymes or catalysts in which the benefits of specific localization of the electron spin near the site of interest may be more important than achieving the largest overall enhancement.

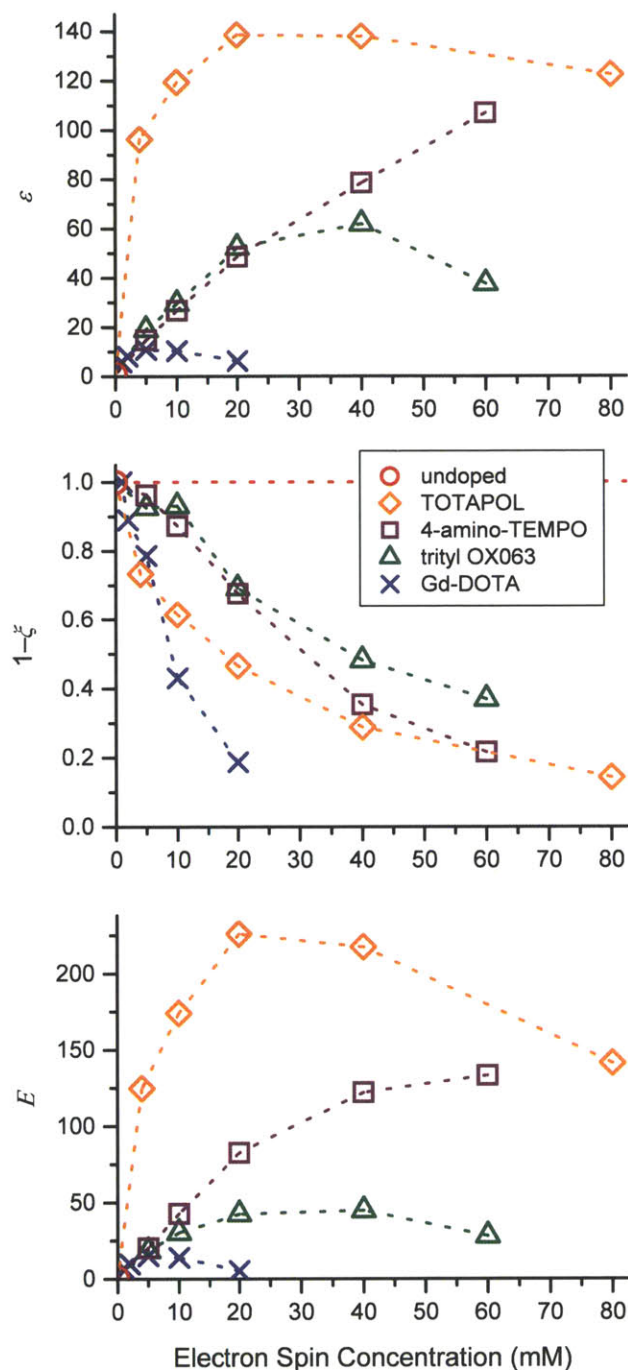


Figure 8.9. Characterization of sensitivity gain by DNP. ^1H DNP enhancement ε (top), relative off-signal intensity not affected by paramagnetic bleaching $1-\xi$ following eq. 8.7 (middle), and effective DNP sensitivity gain E according to eq. 8.10 (bottom) as a function of electron spin concentration of various polarizing agents.

If absolute enhancement factors are of interest, the superiority of the CE is somewhat exaggerated due to significantly different power dependencies between CE and SE. Enhancements were measured using a moderate microwave power of 8 W which we have recently shown that the

enhancement is still not saturated ⁷². The SE is also far from that condition due to the low transition moment of the electron-nuclear double-quantum transition. In a previous study we observed signal enhancement factors of up to 92 using trityl under similar conditions but higher microwave power ⁴⁰; We have observed Gd-DOTA enhancement factors of ~20 at the highest microwave power available (data not shown).

Signal quenching

Although the enhancement factor ε is an easily comparable and a convenient measure for DNP efficiency, it does not incorporate the reduction in the polarization build-up time constant leading to an additional increase of sensitivity due to faster signal accumulation. Concurrently, a certain amount of the signal amplitude is attenuated (quenched) by interactions with the polarizing agent. Accordingly, we introduce the quenching factor

$$\xi = 1 - \frac{I}{I^{\circ}}, \quad (8.7)$$

where I is the off-signal amplitude of the doped sample and I° is that of the undoped sample. In **Figure 8.10** (middle) we plotted $(1-\xi)$ for various concentrations of the four PA's. We measured the amplitude rather than the area of the peak since amplitude is the most significant measure of signal/noise and hence sensitivity.

In a CPMAS experiment this quenching can have several causes: (i) NMR signals of certain nuclei are shifted outside the excitation or detection bandwidth by paramagnetic shifts, (ii) the amplitude of the NMR signal of the detected nucleus is decreased due to homogeneous broadening by transverse paramagnetic relaxation, (iii) spin-locked coherence of the abundant (proton) spins is decaying during the CP contact time by enhanced $T_{1\rho}$ relaxation, or (iv) level crossings due to MAS along with cross effect deplete polarization. We cannot distinguish among these signal quenching mechanisms by a simple CPMAS experiment. Nevertheless, the overall signal quenching we observe fits a simple model, which is qualitatively very similar to a treatment introduced by Lange *et al.* ⁶⁷. We assume a certain volume around the polarizing agent inside of which all NMR signals are quenched, whereas outside this volume there is no signal reduction. This approximation allows us to semi-quantitatively compare the quenching effects of different polarizing agents. The model is simplified in that quenching is expected to be a continuous process with larger effects closer to the electron spin due to larger paramagnetic shift and increased relaxation broadening. Since the paramagnetic interactions are highly non-linear in nature (couplings scale with r^{-3} and relaxation scales with r^{-6}), it is valid to assume a steep increase in signal quenching as the distance between the nuclear and the electron spin is reduced,

justifying the validity of the simplicity of the model. The model does not take into account depolarization due to CR and electronic level crossings during sample rotation^{49, 50}. Following a simple mathematical model⁷³, we introduce a void volume V of arbitrary shape around a PA inside of which no signal is observed. If we assume a random uncorrelated distribution of polarizing agent, and allow void volumes to overlap, the signal quenching can be described as

$$\xi = 1 - e^{-nV} = 1 - e^{-N_A c_{PA} V}, \quad (8.8)$$

where n is the number density of polarizing agent molecules, N_A is Avogadro's constant and c_{PA} is the polarizing agent concentration. Due to the binary nature of this model (spins are either outside of any void volume or inside a volume created by one or many voids), it does not account for enhanced effects due to couplings of one nuclear spin to two or more electron spins or effects relayed by another nuclear spin. Also effective concentration changes due to polarizing agent molecules are neglected. This is a valid simplification because the maximum effective volume any polarizing agent occupies in the sample is expected to be less than 5 % even for the samples containing 60 mM of polarizing agent. In **Figure 8.10** we show the empirical signal quenching factor induced by various concentrations of the four PA's together with an exponential fit using the model. Signal quenching by all polarizing agents except TOTAPOL follow an exponential reduction within margin of error (see Fig. S8). The effective void volumes are 29 and 41 nm³ for trityl and 4-amino-TEMPO, respectively, which correspond to similar quenching radii of 1.9 and 2.1 nm, respectively for a spherical volume. For the $S = 7/2$ Gd-DOTA, the void volume is 133 nm³, corresponding to 3.2 nm quenching radius. Signal quenching induced by TOTAPOL shows an initially steep concentration dependence at low concentration after which there is a leveling effect at higher concentrations. Even though the exponential fit is of poor quality, we can extract a void volume of 105 nm³ around each TOTAPOL molecule, yielding to a quenching radius of 2.9 nm. This behavior might be caused if TOTAPOL molecules have a propensity to self associate at higher concentrations, thus increasing overlap of void volume. More likely it is caused by the fact that TOTAPOL is a biradical in which the strong electron-electron dipole couplings mediate efficient CR even at low concentrations. 4-amino-TEMPO at concentrations of 40 mM and higher seem to show a similar effect, where the signal quenching is slightly more pronounced compared to trityl at the same concentration. Although the significance of that difference in quenching factor is too small to certainly determine CR as the clear cause of the effect, it is in agreement with depolarization due CR and electronic level crossings during MAS. Secular dipole interactions have an orientation dependence proportional to $(3\cos^2\theta - 1)$, where θ is the angle between the vector connecting the electron and nuclear spin and the external magnetic field direction, and this should be incorporated into our model for the void volume. However, if

we neglecting this orientation dependence and approximate it as a spherical shape, we can derive a characteristic quenching distance (*Figure 8.10*). Again this distance is understood not to be a hard quenching barrier. Spins within a shorter distance to the electron spin may still be detectable, but they experience a higher than average signal attenuation, whereas spins with a longer distance exhibit a relatively low attenuation.

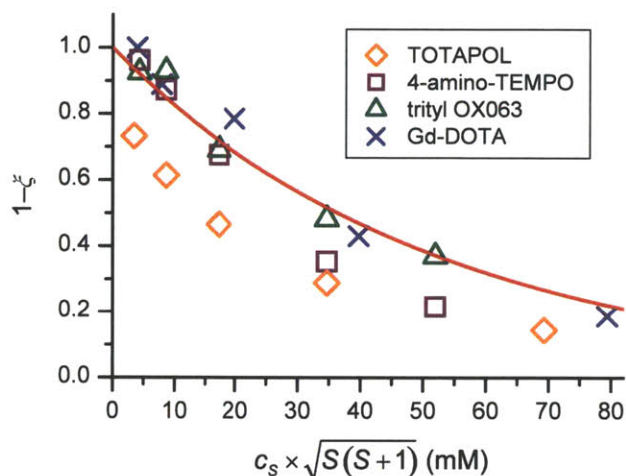


Figure 8.10. Relative off-signal intensity not affected by paramagnetic quenching ($1-\xi$) as a function of the electron spin concentration c_s normalized to the absolute magnetization of each electron spin. The red line indicates an exponential fit according to eq. 8.9.

In addition, we include the electron spin quantum number of the polarizing agent to show that in the case of all monomeric radicals the void volume around each radical molecule is proportional to the absolute magnetic moment of the electron spin, which is proportional to $\sqrt{S(S+1)}$ as can be seen in *Figure 8.10*. Here, we fitted a single exponential function following

$$\xi = 1 - e^{-N_A c_s \sqrt{S(S+1)} V} \quad (8.9)$$

to the experimental data of all samples plotted against $c_s \sqrt{S(S+1)}$, where c_s is the concentration of electron spins. Except for the two highest concentration samples of 4-amino-TEMPO and all concentrations of TOTAPOL (which have been excluded from the fit) there is semi-quantitative agreement between all data points and the fitting function. Therefore we can conclude that signal bleaching can be described by a single parameter for trityl, Gd-DOTA, and for concentration of <40 mM of 4-amino-TEMPO. This parameter is $32 \text{ nm}^3 \times \sqrt{S(S+1)}$, which corresponds to 28 nm^3 void volume for $S = 1/2$ and 127 nm^3 for $S = 7/2$. These values closely match the values obtained by separate fits of each polarizing agent of 29 and 133 nm^3 for

trityl and Gd-DOTA, respectively. The slight discrepancy of the separate-fit value of 4-amino-TEMPO might be caused by an onset of efficient CR as has already been discussed above. As can be clearly seen in *Figure 8.10*, this model does not apply to TOTAPOL, most probably because the efficient electron-nuclear CR allows for a different mechanism of signal quenching^{49,50}.

Overall sensitivity enhancement

We can combine the DNP enhancement factor, quenching factor and the shortening of T_B into a single DNP sensitivity gain factor (*Figure 8.9*) given by

$$E = \varepsilon(1 - \xi)\kappa^\circ = \varepsilon \frac{I}{I^\circ} \sqrt{\frac{T_1^\circ}{T_B}}. \quad (8.10)$$

E represents the practical sensitivity gain one observes when performing DNP as compared to a MAS NMR experiment performed at the same (cryogenic) temperature without DNP and where no paramagnet has been added to the cryoprotecting solution. The time needed to achieve a specific S/N ratio with DNP is reduced accordingly by a factor of E^2 . Note that 10 does not account for increased Boltzmann polarization nor does it include differences in nuclear T_1 at cryogenic temperature; both would be necessary for comparison of sensitivity to ‘typical’ MAS NMR near ambient temperatures. In such a comparison, E would increase by a factor of ~ 3.5 due to Boltzmann polarization, but decrease by a factor of about 5 due to nuclear T_1 differences for all polarizing agents and respective concentrations. However, since significant changes in the inhomogeneous linewidth, probe performance, and noise levels are in the rf coil and transmission line accompany the reduction in temperature, we do not report absolute changes in sensitivity compared with room temperature experiments.

In this representation the improved performance of biradicals like TOTAPOL becomes even clearer. As illustrated in *Figure 8.3*, a maximum sensitivity gain of a factor of 226 was achieved with ~ 10 mM TOTAPOL (20 mM electron spins). For 4-amino-TEMPO concentrations of 40 mM or higher are required to just reach an E of 120-130. However, as has been shown in the preceding sections, paramagnetic relaxation effects at these concentrations are severe and would negatively impact more sophisticated MAS NMR experiments. Polarizing agents operating on the SE were found to exhibit $E < 50$ in this study. However, as higher microwave field strengths become available, sensitivity is expected to greatly increase due to its strong effect on both ε and κ° . Furthermore, there might be future applications, where doping with biradicals and/or application of the CE is inappropriate, for example, in inorganic solids, or where the simplicity of

a two-spin mechanism is preferred. In these cases the SE using polarizing agents like trityl or Gd-DOTA will be the method of choice.

Electron Decoupling

The intensity loss that we observe during MAS with all of the polarizing agents amounts to ~50%, and can in principle be partially recovered by decoupling electrons during data acquisition. Since the electron-nuclear Hamiltonian is identical to the heteronuclear Hamiltonian - $I_z S_z$ -- this is an approach similar to that used to decouple ^1H from $^{13}\text{C}/^{15}\text{N}$, etc. in MAS experiments. However, the electron relaxation times are short and could require the experiments to be performed at temperatures to lengthen T_{1s} . In addition, it will be necessary to develop decoupling sequences that are effective for lines which are wide compared to γB_{1s} . For example at 5 T the trityl line has a width of ~50 MHz due to a small g-anisotropy, and is one of the narrowest EPR lines exhibited by a polarizing agent. There are also strongly dipole and hyperfine coupled nuclei whose resonance frequencies could lie outside this linewidth. The instrumentation to perform the experiments will require amplifiers with a bandwidth sufficient to polarize the nuclei, for example at the solid effect condition, and then switch on resonance with the EPR spectrum for decoupling. The pulse forming and phase control would optimally be performed at low frequencies and mixed to the appropriate microwave frequency. Since the blind volume surrounding the paramagnetic center contains several hundred nuclei it is possible to achieve a significant sensitivity gain with this approach.

8.5 Supporting Information

Synopsis

For determination of the bleaching factor, assessment of the spectrometer stability and sensitivity over an extended period of time is of crucial importance. Table S1 lists the experimental date and the MAS stator temperature for each sample.

Table S1. Overview of date and temperature of experiments.

Polarizing agent	conc. (mM)	date	temp. (K)
Undoped 1	–	03/21/2011	78
TOTAPOL	5	03/22/2011	80
TOTAPOL	10	03/23/2011	79
TOTAPOL	20	03/23/2011	79
TOTAPOL	40	03/23/2011	79
TOTAPOL	2	03/24/2011	79
trityl OX063	40	03/24/2011	81
trityl OX063	10	03/24/2011	81
trityl OX063	20	03/25/2011	81
trityl OX063	60	03/26/2011	81
trityl OX063	5	03/27/2011	81
Gd-DOTA	10	03/27/2011	81
Gd-DOTA	2	03/28/2011	81
Gd-DOTA	5	03/28/2011	81
Gd-DOTA	20	03/28/2011	82
Gd-DOTA	1	03/29/2011	81
Undoped 2 ^a	–	03/31/2011	78
4-amino-TEMPO	10	06/07/2011	83
4-amino-TEMPO	5	06/08/2011	84
4-amino-TEMPO	40	06/08/2011	85
4-amino-TEMPO	60	06/08/2011	85
4-amino-TEMPO	20	06/09/2011	84

^aSample “Undoped 2” was measured because “Trityl 5 mM” and all TEMPAMINE samples were prepared from different stem solution (“Undoped 2”) than all other samples.

Many parameters were kept consistent during the experimental period, for example, retuning of the probe’s rf channels was not necessary due to practically identical dielectric properties of all samples and therefore identical Q of the resonant circuit. Nevertheless, inherent drifts or fluctuations in sensitivity might still be present. To account for these influences, we correct the collected data (NMR signal amplitude of ^{13}C -urea) by calibration to an internal standard.

Choice of internal standard

We used the NMR signal of the Vespel spacers as internal standard for NMR signal amplitude measurements. The spacer signal is well separated from the urea and glycerol signals, so it is well suited to serve as internal amplitude standard. Before amplitude determination the frequency domain spectrum was broadened by application of sinebell apodization function with a time constant of 2 ms in order to minimize noise.

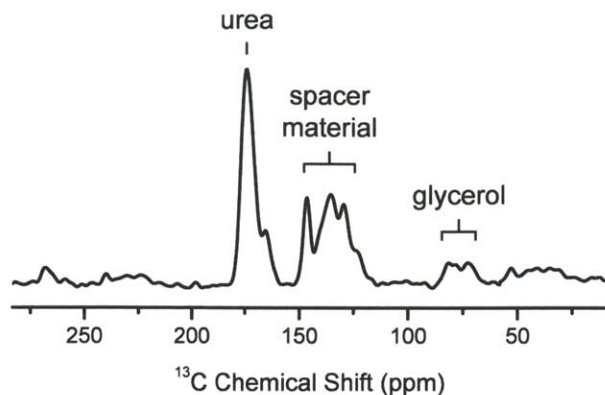


Figure S1. ^{13}C CP-MAS spectrum of the sample containing 10 mM trityl. The signal arising from the spacer material is used for internal standard correction.

Determination of internal standard signal amplitude of undoped samples

The internal standard amplitudes of samples “Undoped 1” and “Undoped 2” were determined by fitting the polarization buildup curve with a monoexponential function and dividing the preexponential factor by a factor of 10 (see Fig. S2). This division was necessary because “Undoped 1” and “Undoped 2” sample buildup curves were measured using a receiver gain 20 dB higher compared to the DNP enhanced signal measurements. The linearity of the receiver gain on the signal amplitude was confirmed by experiment (not shown).

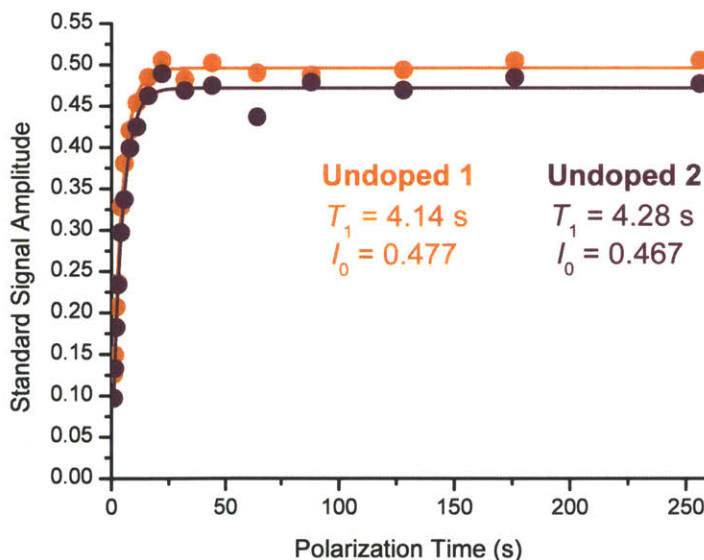


Figure S2. Determination of signal amplitude I_0 and relaxation time T_1 of the standard signal of the undoped samples.

Determination of urea signal amplitude of doped samples

Urea signal amplitudes of all paramagnetically doped samples were determined by first fitting the DNP enhanced buildup curves with monoexponential functions. The preexponential factor was then divided by the enhancement factor which was determined by on-/off-signal amplitude comparison of spectra measured with a polarization period of $1.26 \times T_B$. Amplitudes are then normalized to the amplitude of the respective undoped sample (compare Fig. S2 and Table S1). The obtained normalized signal amplitudes are shown in Fig. S3. This procedure saves a significant amount of experimental time since no off-signal buildup-curve has to be measured for each doped sample. However, it introduces a small error in the case of polarizing agents allowing for SE DNP due to a minor shortening of T_B with respect to T_1 and therefore leads to an overestimation of the respective enhancement factor. Another study has shown a shortening ratio of ~ 0.87 under similar conditions for 40 mM trityl, leading to an error in the enhancement factor of less than 7%. Since this sample yielded the most efficient SE and therefore is supposed to induce the strongest buildup time shortening, 7% marks the upper limit of the error introduced due to this analysis.

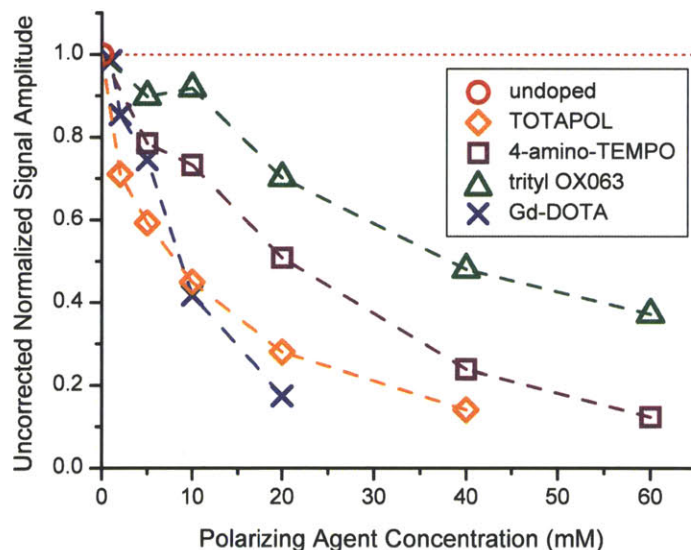


Figure S3. Uncorrected signal amplitude of all paramagnetically doped samples. Amplitudes are normalized to those of the respective undoped samples.

Correction for varying polarization times used in measurement of internal standard signal amplitude of undoped samples

For all paramagnetically doped samples the recorded off-signal was used for internal standard amplitude determination (see Figure S4 left). Because the off-signals were measured using

various polarization periods t (see Figure S4 right), which were partly shorter than $5 \times T_1$ of the standard signal, the standard signal amplitude had to be corrected for this.

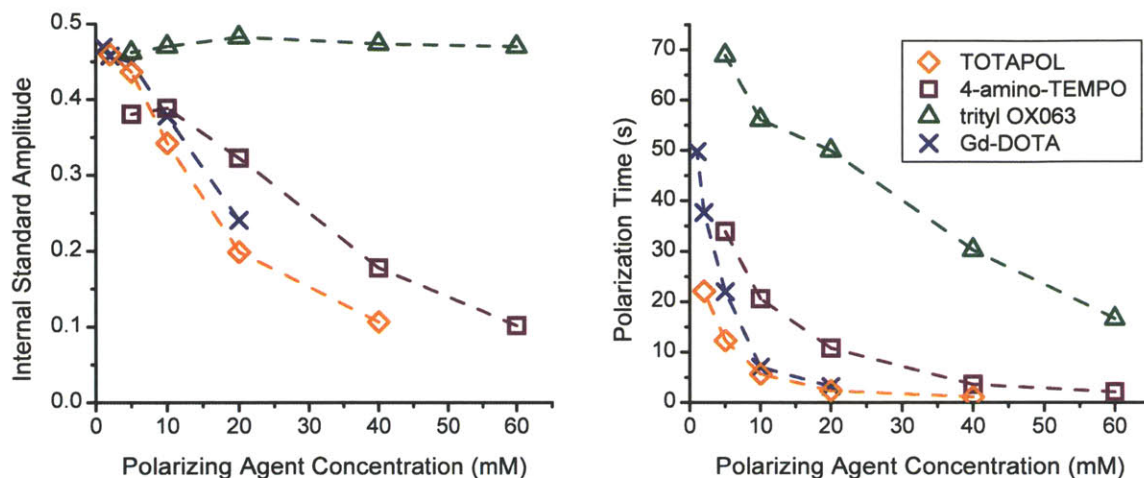


Figure S4. Signal amplitude of the internal standard signal (left). Data was obtained by ^{13}C CP-MAS without microwave (off-spectrum). The polarization time used is shown in the right graph.

Since it is assumed that the standard signal's T_1 does not change between different samples, the T_1 of the internal standard signal was determined by monoexponential fitting of the respective buildup curve (Fig. S2). The time constant was then used to calculate the internal standard signal amplitude at infinite polarization time for each doped sample using

$$I_0 = \frac{I}{1 - \exp\left(-\frac{t}{T_1}\right)}. \quad (8.11)$$

The resulting corrected internal standard amplitude I_0 is depicted in Fig. S5.

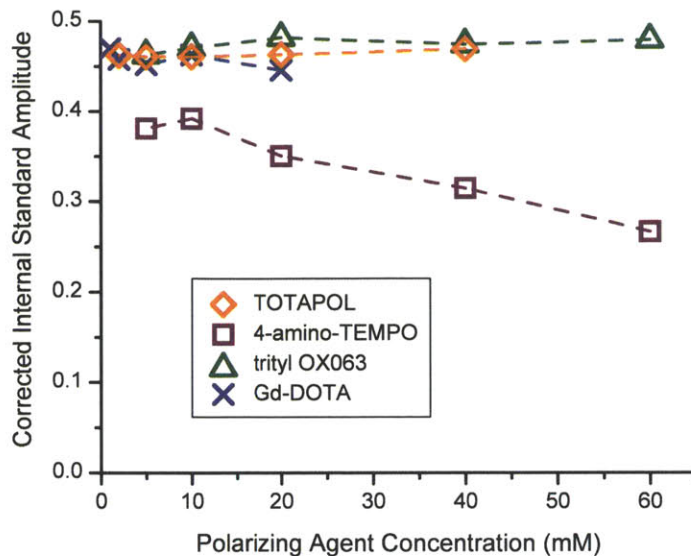


Figure S5. Internal standard amplitude corrected for variation in polarization time.

Final correction of NMR signal bleaching data using internal standard signal amplitude

The ^{13}C -urea amplitudes were corrected for spectrometer sensitivity variation by division by the respective internal standard signal amplitude obtained for each sample following

$$1 - \xi = \frac{I}{I_0} \frac{C_0}{C}, \quad (8.12)$$

where I and C are the uncorrected urea signal amplitude and the correction factor of a doped sample, and I_0 and C_0 describe the respective parameters for the undoped reference sample. The final corrected and normalized signal amplitudes are shown in Fig. S6.

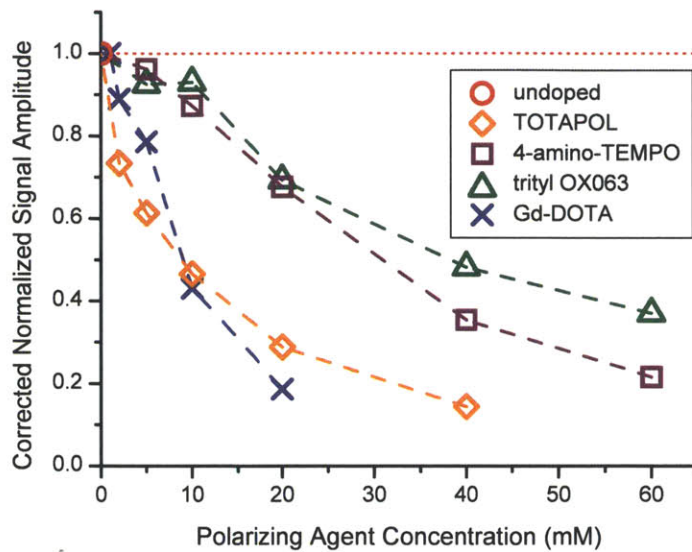


Figure S6. Corrected and normalized signal amplitude.

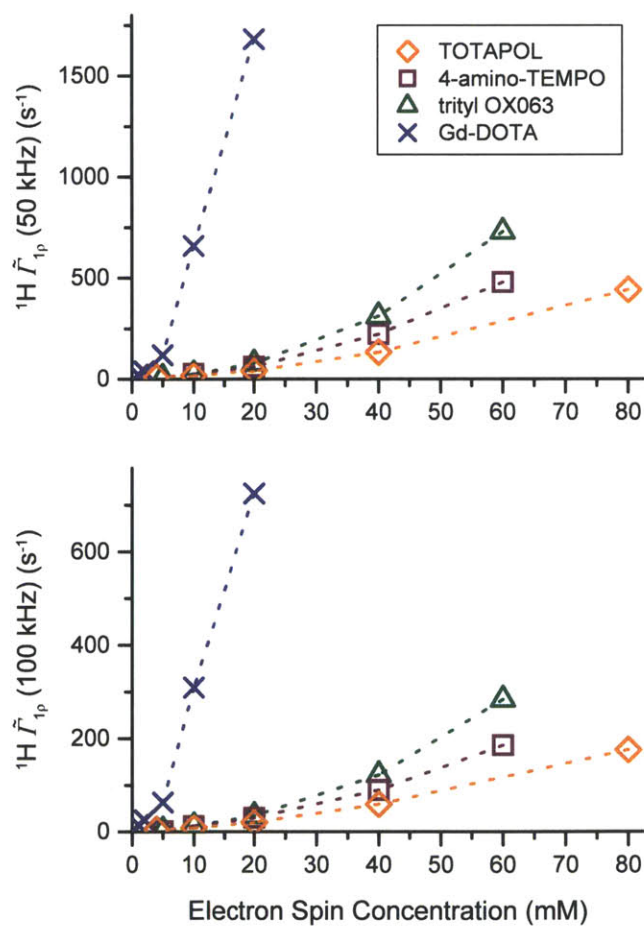


Figure S7. ${}^1\text{H } \tilde{T}_{1p}$ at a spin-lock fields of $\omega_{SL}/2\pi = 50$ kHz (top) and 100 kHz (bottom) as function of electron spin concentration of various polarizing agents.

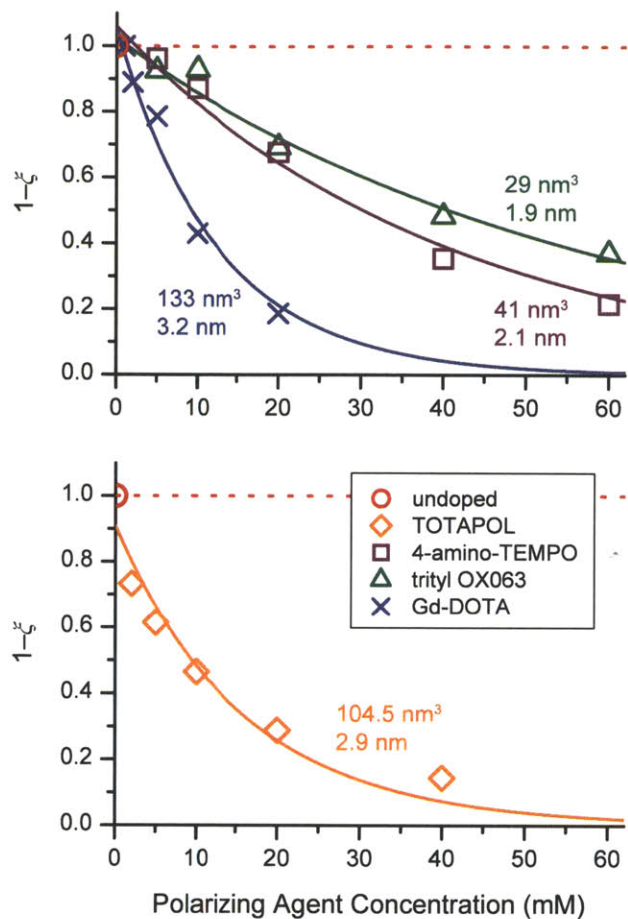


Figure S8. Exponential fit of the bleaching effect $1-\xi$ using equation 8.9, following the void volume model described in the text. Void volume around each polarizing agent molecule inside which NMR signals are quenched are given, together with the radius of a spherically shaped volume. The signal quenching induced by TOTAPOL cannot be perfectly described with this model; the rather unsatisfactory least-square fit is shown in the bottom graph.

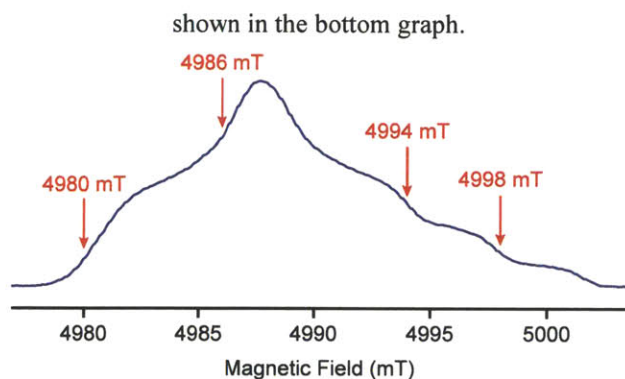


Figure S9. EPR spectrum of TOTAPOL with field positions used for T_{1S} and T_{2S} measurements in the case of TOTAPOL and 4-amino-TEMPO.

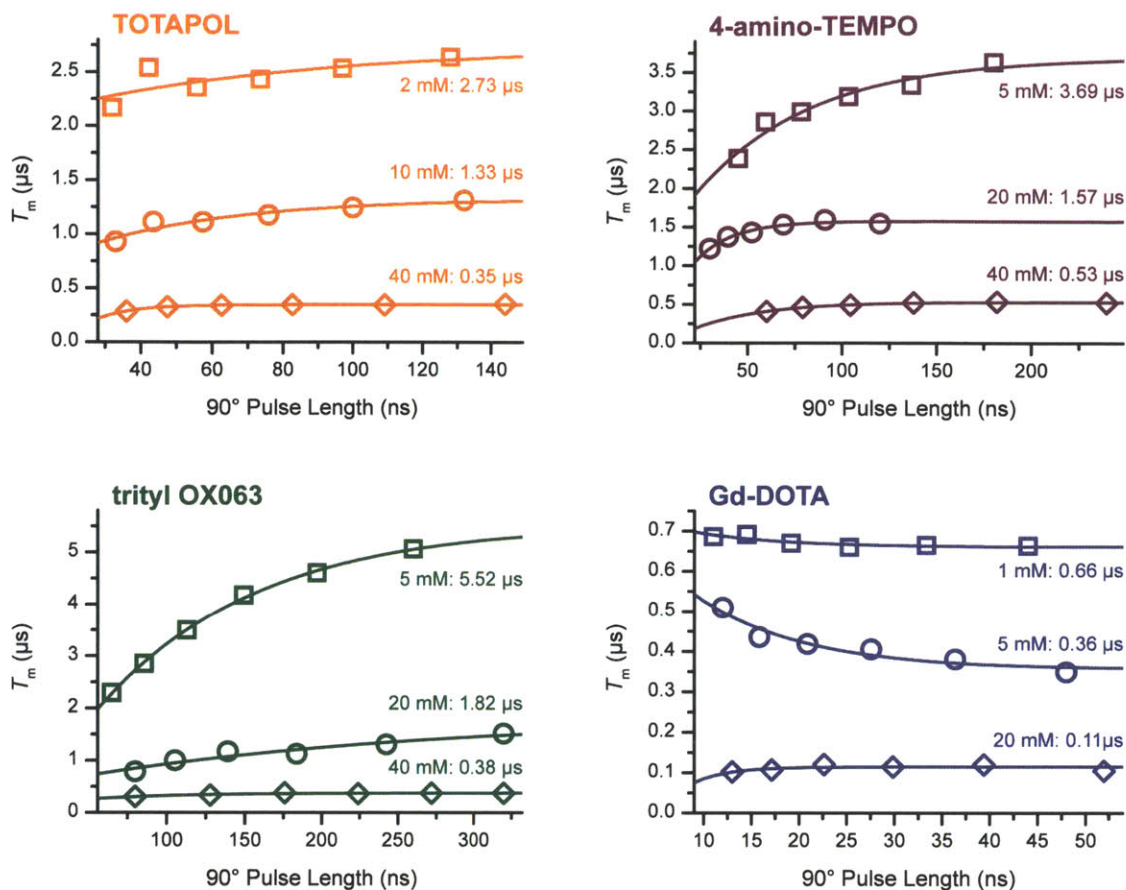


Figure S10. Determination of electron spin transverse relaxation time constant T_{2S} by extrapolation of excitation bandwidth dependent phase memory time T_m to infinite flip pulse length.

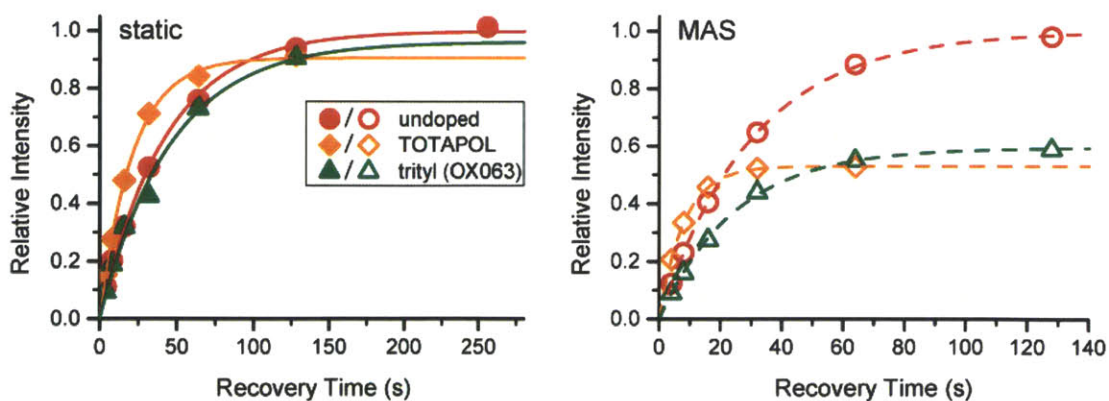


Figure S11. Build up of polarization under static and MAS conditions for an undoped sample, 10 mM TOTAPOL, and 20 mM Trityl recorded at 380 MHz and 80 K. The sample was a 30/30/30/10 mixture (vol) of 2- ^{13}C ,D8 Glycerol / D8 Glycerol / D $_2\text{O}$ / H $_2\text{O}$. The MAS spinning frequency was 4975 Hz.

Supplementary Tables

Table S1. PRE and DNP data for various polarizing agents at different concentrations. Data recorded at 5 T and ~84 K under ~8 W of 140 GHz microwave irradiation.

c_{PA} (mM)	T_B (s)	$^{13}C T_2$ (ms)	$^1H T_{1p}$ (50 kHz) (ms)	$^1H T_{1p}$ (100 kHz) (ms)	$^{13}C T_{1p}$ (50 kHz) (ms)	$^1H \tilde{\Gamma}_1$ (s ⁻¹)	$^{13}C \tilde{\Gamma}_2$ (s ⁻¹)	$^1H \tilde{\Gamma}_{1p}$ (50 kHz) (s ⁻¹)	$^1H \tilde{\Gamma}_{1p}$ (100 kHz) (s ⁻¹)	$^{13}C \tilde{\Gamma}_{1p}$ (50 kHz) (s ⁻¹)	ϵ	κ^c	$1-\xi$	E
undoped														
0	54.59 ^a	14.69	– ^b	– ^b	– ^b	0	0	0	0	0	1	1	1	1
TOTAPOL														
2 ^c	17.50	13.15	103.9	194.1	492.8	0.039	8.0	9.6	5.2	2.0	96.3	1.77	0.73	124.7
5 ^c	9.74	11.11	61.0	113.5	325.9	0.084	22.0	16.4	8.8	3.1	119.6	2.37	0.61	174.0
10 ^c	4.48	7.22	25.1	50.4	153.3	0.205	70.5	39.9	19.8	6.5	139.0	3.49	0.47	225.9
20 ^c	1.84	3.84	7.6	17.0	63.6	0.525	192.1	131.0	58.7	15.7	138.3	5.45	0.29	217.3
40 ^c	0.85	2.22	2.3	5.7	25.1	1.164	381.5	441.0	174.8	39.9	122.5	8.04	0.14	141.3
4-amino-TEMPO														
5	26.88 ^d	11.98	– ^b	– ^b	– ^b	0.019	15.4	– ^b	– ^b	– ^b	14.9	1.43	0.96	20.4
10	16.37 ^d	8.72	39.59	83.53	445.7	0.043	46.7	25.3	12.0	2.24	26.8	1.83	0.87	42.8
20	8.66 ^d	5.09	16.67	33.48	147.5	0.097	128.3	60.0	29.9	67.8	48.7	2.51	0.68	82.6
40	2.82 ^d	2.62	4.527	11.21	51.0	0.336	313.0	220.9	89.2	19.6	78.5	4.40	0.35	122.0
60	1.64 ^d	1.74	2.093	5.414	27.3	0.592	508.3	477.8	184.7	36.7	106.9	5.77	0.22	133.2
trityl OX063														
5	49.09 ^d	11.74	122.2	287.9	709.6	0.002	17.1	8.2	3.5	1.4	19.1	1.05	0.93	18.7
10	44.52	8.07	40.3	81.1	261.7	0.004	55.9	24.8	12.3	3.8	29.7	1.11	0.93	30.6
20	39.68	4.97	12.8	29.2	108.4	0.007	133.1	78.1	34.2	9.2	52.5	1.17	0.69	42.7
40	24.02	3.01	3.2	8.2	35.9	0.023	264.7	311.8	121.7	27.8	62.0	1.51	0.48	45.1
60	13.20	2.20	1.4	3.5	18.0	0.057	387.5	729.4	283.0	55.7	37.7	2.03	0.37	28.4
Gd-DOTA														
1	39.55	13.39	43.4	67.0	272.6	0.007	6.6	23.0	14.9	3.7	5.9	1.17	1.00	6.9
2	29.88	11.78	25.6	40.2	185.9	0.015	16.9	39.0	24.9	5.4	8.2	1.35	0.89	9.8
5	17.47	8.90	8.4	15.8	70.5	0.039	44.3	118.6	63.2	14.2	11.0	1.77	0.79	15.2
10	5.60	5.42	1.5	3.2	20.7	0.160	116.5	658.7	309.6	48.2	10.5	3.12	0.43	14.1
20	2.55	3.54	0.6	1.4	9.2	0.374	214.4	682.1	725.0	109.1	6.3	4.63	0.19	5.4

^aThis value actually represents T_1^* . ^bData could not be determined because fitting did not yield physically meaningful results due to limited spin-lock time.

^cPolarizing agent concentration of the biradical; electron concentration is twice the given value. ^dData was acquired using a different buffer solution with $T_1 = 61.57$ s. T_B was normalized to the same T_1^* given in the table by the relation $1/T_{B,a} - 1/T_{B,b} = 1/T_{1,a}^* - 1/T_{1,b}^*$.

Table S2. T_{1S} of TOTAPOL and 4-amino-TEMPO in 60/30/10 (v/v) d_8 -glycerol/D₂O/H₂O (incl. 1 M ¹³C-urea) at various concentrations and magnetic fields positions at 80 K.

<i>c</i> (mM)	T_{1S} (ms)				mean
	4980 mT	4986 mT	4994 mT	4998 mT	
TOTAPOL					
2	0.248	0.250	0.463	0.686	0.412
10	0.212	0.209	0.399	0.649	0.367
40	0.125	0.160	0.243	0.334	0.216
4-amino-TEMPO					
5	0.319	0.314	0.593	0.892	0.530
20	0.240	0.207	0.381	0.741	0.392
60	0.180	0.165	0.297	0.444	0.272

Table S3. T_{2S} of TOTAPOL and 4-amino-TEMPO in 60/30/10 (v/v) d_8 -glycerol/D₂O/H₂O (incl. 1 M ¹³C-urea) at various concentrations and magnetic fields positions at 80 K.

<i>c</i> (mM)	T_{2S} (μs)				mean
	4980 mT	4986 mT	4994 mT	4998 mT	
TOTAPOL					
2	3.13	2.73	2.82	4.39	3.27
10	1.58	1.33	1.80	2.04	1.68
40	0.38	0.35	0.40	0.42	0.39
4-amino-TEMPO					
5	4.02	3.69	4.35	4.29	4.09
20	1.97	1.57	1.91	2.76	2.05
60	0.60	0.53	0.73	0.85	0.68

Table S4. T_{1S} and T_{2S} of trityl OX063 in 60/30/10 (v/v) d_8 -glycerol/D₂O/H₂O (incl. 1 M ¹³C-urea) at various concentrations at 80 K.

<i>c</i> (mM)	T_{1S} (ms)	T_{2S} (μs)
trityl OX063		
5	1.88	5.52
20	1.50	1.82
60	1.47	0.38

Table S5. T_{1S} and T_{2S} of Gd-DOTA in 60/30/10 (v/v) d_8 -glycerol/D₂O/H₂O (incl. 1 M ¹³C-urea) at various concentrations at 80 K.

<i>c</i> (mM)	T_{1S} (μs)	T_{1S} (μs)	T_{2S} (μs)
	fast comp.	slow comp.	
Gd-DOTA			
1	2.65	6.55	0.66
5	1.48	7.94	0.36
20	4.51	4.84	0.11

8.6 Conclusions

We have presented the effects of several DNP polarizing agents upon nuclear T_1 , T_2 , and $T_{1\rho}$ relaxation times and show that the results may guide the choice of polarizing agent and its concentration. In multidimensional MAS experiments, relaxation of magnetization occurs, for example during coherent mixing periods, evolution of spin coherence, or multiple CP contacts and the details of the type and duration of magnetization transfer will impact the choice of polarizing agent concentration. Polarizing agents employing the SE DNP mechanism generally show a longer longitudinal polarization build-up time compared with CE polarizing agents, which utilize efficient CR for DNP build-up but also for spin-lattice relaxation. Interestingly, the laboratory frame T_2 is less affected by the choice of polarizing agent and is practically invariant of the nature of the electron spin since it shows quantitatively similar polarizing agent concentration dependence for all polarizing agents studied. It is clear from the T_2 measurements that lower polarizing agent concentrations will be optimal when applying long transverse mixing, such as in a REDOR or TEDOR experiment, than would be used based solely on the sensitivity of a CP experiment. In addition, we have characterized the reduction in non-DNP enhanced signal due to paramagnetic dopants and presented a simple model for the concentration dependence of this effect. We present a measure of overall DNP sensitivity gain that includes the signal quenching, the enhancement factor, and the build-up rate that can be used to optimize a DNP experiment. For multidimensional experiments aimed at providing structural information, the empirically determined relaxation times will determine the optimal combination of experiment, polarizing agent, and its concentration to achieve maximum sensitivity. The results presented here clearly demonstrate that much work remains to be done in the design and implementation of efficient polarizing agents for MAS DNP.

Acknowledgments

The authors thank V. K. Michaelis, E. Daviso, and A.B. Barnes for helpful discussions. This work was financially supported by NIH grants EB-002804 and EB-002026. B.C. acknowledges the receipt of a research fellowship (CO802/1-1) by the Deutsche Forschungsgemeinschaft (DFG). We thank C. Luchinat and I. Bertini (CERM, Florence, Italy) for providing samples of Gd-DOTA.

8.7 References

1. Andreas, L. B.; Eddy, M. T.; Pielak, R. M.; Chou, J.; Griffin, R. G., Magic Angle Spinning NMR Investigation of Influenza A M2(18-60): Support for an Allosteric Mechanism of Inhibition. *Journal of the American Chemical Society* **2010**, *132* (32), 10958-10960.
2. Cady, S. D.; Schmidt-Rohr, K.; Wang, J.; Soto, C. S.; DeGrado, W. F.; Hong, M., Structure of the amantadine binding site of influenza M2 proton channels in lipid bilayers. *Nature* **2010**, *463* (7281), 689.
3. Castellani, F.; van Rossum, B.; Diehl, A.; Schubert, M.; Rehbein, K.; Oschkinat, H., Structure of a protein determined by solid-state magic-angle-spinning NMR spectroscopy. *Nature* **2002**, *420* (6911), 98-102.
4. Jaroniec, C. P.; MacPhee, C. E.; Bajaj, V. S.; McMahon, M. T.; Dobson, C. M.; Griffin, R. G., High-resolution molecular structure of a peptide in an amyloid fibril determined by magic angle spinning NMR spectroscopy. *Proceedings of the National Academy of Sciences of the United States of America* **2004**, *101* (3), 711-716.
5. McDermott, A., Structure and Dynamics of Membrane Proteins by Magic Angle Spinning Solid-State NMR. *Annual Review of Biophysics* **2009**, *38*, 385-403.
6. Rienstra, C. M.; Tucker-Kellogg, L.; Jaroniec, C. P.; Hohwy, M.; Reif, B.; McMahon, M. T.; Tidor, B.; Lozano-Perez, T.; Griffin, R. G., De novo determination of peptide structure with solid-state magic-angle spinning NMR spectroscopy. *Proceedings of the National Academy of Sciences of the United States of America* **2002**, *99* (16), 10260-10265.
7. Wasmer, C.; Lange, A.; Van Melckebeke, H.; Siemer, A. B.; Riek, R.; Meier, B. H., Amyloid fibrils of the HET-s(218-289) prion form a beta solenoid with a triangular hydrophobic core. *Science* **2008**, *319* (5869), 1523-1526.
8. Abragam, A.; Goldman, M., Principles of dynamic nuclear-polarization. *Reports on Progress in Physics* **1978**, *41* (3), 395-467.
9. Barnes, A. B.; De Paepe, G.; van der Wel, P. C. A.; Hu, K. N.; Joo, C. G.; Bajaj, V. S.; Mak-Jurkauskas, M. L.; Sirigiri, J. R.; Herzfeld, J.; Temkin, R. J.; Griffin, R. G., High-field dynamic nuclear polarization for solid and solution biological NMR. *Applied Magnetic Resonance* **2008**, *34* (3-4), 237-263.
10. Maly, T.; Debelouchina, G. T.; Bajaj, V. S.; Hu, K. N.; Joo, C. G.; Mak-Jurkauskas, M. L.; Sirigiri, J. R.; van der Wel, P. C. A.; Herzfeld, J.; Temkin, R. J.; Griffin, R. G., Dynamic nuclear polarization at high magnetic fields. *Journal of Chemical Physics* **2008**, *128* (5), 19.
11. Griffin, R. G.; Prisner, T. F., High field dynamic nuclear polarization-the renaissance. *Physical Chemistry Chemical Physics* **2010**, *12* (22), 5737-5740.
12. Maly, T.; Cui, D. T.; Griffin, R. G.; Miller, A. F., ¹H Dynamic Nuclear Polarization Based on an Endogenous Radical. *J. Phys. Chem. B* **2012**, *116*, 7055-7065.
13. Gerfen, G. J.; Becerra, L. R.; Hall, D. A.; Griffin, R. G.; Temkin, R. J.; Singel, D. J., High-Frequency (140 GHz) Dynamic Nuclear-Polarization - Polarization Transfer to a Solute in Frozen Aqueous-Solution. *Journal of Chemical Physics* **1995**, *102* (24), 9494-9497.
14. van der Wel, P. C. A.; Hu, K. N.; Lewandowski, J.; Griffin, R. G., Dynamic nuclear polarization of amyloidogenic peptide nanocrystals: GNNQQNY, a core segment of the yeast prion protein Sup35p. *J Am Chem Soc* **2006**, *128* (33), 10840-10846.
15. Debelouchina, G. T.; Bayro, M. J.; Wel, P. C. A. v. d.; Caporini, M. A.; Barnes, A. B.; Rosay, M.; Maas, W. E.; Griffin, R. G., Dynamic nuclear polarization-enhanced solid-state NMR spectroscopy of GNNQQNY nanocrystals and amyloid fibrils. *Phys. Chem. Chem. Phys.* **2010**, *12*.

16. Rossini, A. J.; Zagdoun, A.; Hegner, F.; Schwarzwälder, M.; Gajan, D.; Copéret, C.; Lesage, A.; Emsley, L., Dynamic Nuclear Polarization NMR Spectroscopy of Microcrystalline Solids. *J Am Chem Soc* **2012**, *134* (40), 16899-16908.
17. Lesage, A.; Lelli, M.; Gajan, D.; Caporini, M. A.; Vitzthum, V.; Miéville, P.; Alauzun, J.; Roussey, A.; Thieuleux, C.; Mehdi, A.; Bodenhausen, G.; Copéret, C.; Emsley, L., Surface Enhanced NMR Spectroscopy by Dynamic Nuclear Polarization. *J Am Chem Soc* **2010**, *132* (44), 15459-15461.
18. Kobayashi, T.; Lafon, O.; Thankamony, A. S. L.; Slowing, I. I.; Kandel, K.; Carnevale, D.; Vitzthum, V.; Vezin, H.; Amoureux, J.-P.; Bodenhausen, G.; Pruski, M., Analysis of sensitivity enhancement by dynamic nuclear polarization in solid-state NMR: a case study of functionalized mesoporous materials. *Phys. Chem. Chem. Phys.* **2013**, *15*, 5553--5562.
19. Rosay, M.; Weis, V.; Kreisler, K. E.; Temkin, R. J.; Griffin, R. G., Two-dimensional ^{13}C - ^{13}C correlation spectroscopy with magic angle spinning and dynamic nuclear polarization. *J Am Chem Soc* **2002**, *124* (13), 3214-3215.
20. Akbey, Ü.; Corzilius, B.; Griffin, R. G.; Oschkinat, H., Dynamic nuclear polarization enhanced NMR spectroscopy in the solid-state: Application to deuterated and protonated proteins. *Journal of Magnetic Resonance* **2011**, to be submitted.
21. Barnes, A. B.; Corzilius, B.; Mak-Jurkauskas, M. L.; Andreas, L. B.; Bajaj, V. S.; Matsuki, Y.; Belenky, M. L.; Lugtenburg, J.; Sirigiri, J. R.; Temkin, R. J.; Herzfeld, J.; Griffin, R. G., Resolution and polarization distribution in cryogenic DNP/MAS experiments. *Physical Chemistry Chemical Physics* **2010**, *12* (22), 5861-5867.
22. Rosay, M. M. Sensitivity Enhanced Nuclear Magnetic Resonance of Biological Solids. Ph.D., Massachusetts Institute of Technology, Cambridge, MA, 2001.
23. Bajaj, V. S.; Farrar, C. T.; Hornstein, M. K.; Mastovsky, I.; Viereg, J.; Bryant, J.; Elena, B.; Kreisler, K. E.; Temkin, R. J.; Griffin, R. G., Dynamic nuclear polarization at 9T using a novel 250 GHz gyrotron microwave source. *J. Mag. Res.* **2003**, *160*, 85-90.
24. Hu, K. N.; Yu, H. H.; Swager, T. M.; Griffin, R. G., Dynamic nuclear polarization with biradicals. *J Am Chem Soc* **2004**, *126* (35), 10844-10845.
25. Matsuki, Y.; Maly, T.; Ouari, O.; Lyubenova, S.; Herzfeld, J.; Prisner, T.; Tordo, P.; Griffin, R. G., Dynamic Nuclear Polarization using a Rigid Biradical. *Angewandte Chemie* **2009**, *48*, 4996-5000.
26. Song, C.; Hu, K.-N.; Joo, C.-G.; Swager, T. M.; Griffin, R. G., TOTAPOL: A Biradical Polarizing Agent for Dynamic Nuclear Polarization Experiments in Aqueous Media. *J Am Chem Soc* **2006**, *128* (35), 11385-11390.
27. Hu, K.-N.; Song, C.; Yu, H.-h.; Swager, T. M.; Griffin, R. G., High-Frequency Dynamic Nuclear Polarization Using Biradicals: A Multifrequency EPR Lineshape Analysis. *J. Chem. Phys.* **2008**, *128*, 052321.
28. Jeffries, C. D., Polarization of Nuclei by Resonance Saturation in Paramagnetic Crystals. *Physical Review* **1957**, *106* (1), 164-165.
29. Abraham, M.; Kedzie, R. W.; Jeffries, C. D., Gamma-Ray Anisotropy of Co60 Nuclei Polarized by Paramagnetic Resonance Saturation. *Physical Review* **1957**, *106* (1), 165-166.
30. Jeffries, C. D., Dynamic Orientation of Nuclei by Forbidden Transitions in Paramagnetic Resonance. *Physical Review* **1960**, *117* (4), 1056-1069.
31. Abragam, A., Principles of nuclear magnetism. *Oxford University Press, New York* **1961**.
32. Corzilius, B.; Smith, A. A.; Griffin, R. G., Solid effect in magic angle spinning dynamic nuclear polarization. *Journal of Chemical Physics* **2012**, *137* (5).
33. Smith, A. A.; Corzilius, B.; Barnes, A. B.; Maly, T.; Griffin, R. G., Solid effect dynamic nuclear polarization and polarization pathways. *Journal of Chemical Physics* **2012**, *136* (1).
34. Hovav, Y.; Feintuch, A.; Vega, S., Theoretical aspects of dynamic nuclear polarization in the solid state - The solid effect. *Journal of Magnetic Resonance* **2010**, *207* (2), 176-189.

35. Abragam, A.; Proctor, W. G., Une Nouvelle Methode De Polarisation Dynamique Des Noyaux Atomiques Dans Les Solides. *Comptes Rendus Hebdomadaires Des Seances De L Academie Des Sciences* **1958**, *246* (15), 2253-2256.
36. Ardenkjær-Larsen, J. H.; Laursen, I.; Leunbach, I.; Ehnholm, G.; Wistrand, L. G.; Petersson, J. S.; Golman, K., EPR and DNP properties of certain novel single electron contrast agents intended for oximetric imaging. *Journal of Magnetic Resonance* **1998**, *133* (1), 1-12.
37. Koelsch, C. F., SYNTHESSES WITH TRIARYLVINYLMAGNESIUM BROMIDES - ALPHA,GAMMA-BISDIPHENYLENE-BETA-PHENYLALLYL, A STABLE FREE RADICAL. *J Am Chem Soc* **1957**, *79* (16), 4439-4441.
38. Haze, O.; Corzilius, B.; Smith, A. A.; Griffin, R. G.; Swager, T. M., Water-Soluble Organic Radicals as Polarizing Agents for High Field Dynamic Nuclear Polarization. *J Am Chem Soc* **2012**, *134*, 14287-14290.
39. Magerstädt, M.; Gansow, O. A.; Brechbiel, M. W.; Colcher, D.; Baltzer, L.; Knop, R. H.; Girton, M. E.; Naegele, M., Gd(DOTA): An alternative to Gd(DTPA) as a T_{1,2} relaxation agent for NMR imaging or spectroscopy. *Magnetic Resonance in Medicine* **1986**, *3* (5), 808-812.
40. Corzilius, B.; Smith, A. A.; Griffin, R. G., Solid Effect in Magic Angle Spinning Dynamic Nuclear Polarization. *Journal of Chemical Physics* **2012**, *137*, 054201.
41. Kessenikh, A. V.; Lushchikov, V. I.; Manenkov, A. A.; Taran, Y. V., Proton polarization in irradiated polyethylenes. *Soviet Physics-Solid State* **1963**, *5* (2), 321-329.
42. Hwang, C. F.; Hill, D. A., New effect in dynamic polarization. *Physical Review Letters* **1967**, *18* (4), 110-&.
43. Hwang, C. F.; Hill, D. A., Phenomenological model for new effect in dynamic polarization. *Physical Review Letters* **1967**, *19* (18), 1011-&.
44. Wollan, D. S., Dynamic nuclear-polarization with an inhomogeneously broadened ESR line. 1. Theory. *Physical Review B* **1976**, *13* (9), 3671-3685.
45. Wollan, D. S., Dynamic nuclear-polarization with an inhomogeneously broadened ESR line. 2. Experiment. *Physical Review B* **1976**, *13* (9), 3686-3696.
46. Hu, K.-N.; Debelouchina, G. T.; Smith, A. A.; Griffin, R. G., Quantum mechanical theory of dynamic nuclear polarization in solid dielectrics. *J. Chem. Physics* **2011**, *134*, 125105.
47. Hu, K. N., Polarizing agents and mechanisms for high-field dynamic nuclear polarization of frozen dielectric solids. *Solid State Nuclear Magnetic Resonance* **2011**, *40* (2), 31-41.
48. Hu, K. N.; Bajaj, V. S.; Rosay, M.; Griffin, R. G., High-frequency dynamic nuclear polarization using mixtures of TEMPO and trityl radicals. *Journal of Chemical Physics* **2007**, *126* (4), 7.
49. Thurber, K. R.; Tycko, R., Theory for cross effect dynamic nuclear polarization under magic-angle spinning in solid state nuclear magnetic resonance: The importance of level crossings. *The Journal of Chemical Physics* **2012**, *137* (8), 084508-14.
50. Mentink-Vigier, F.; Akbey, Ü.; Hovav, Y.; Vega, S.; Oschkinat, H.; Feintuch, A., Fast passage dynamic nuclear polarization on rotating solids. *Journal of Magnetic Resonance* **2012**, *224* (0), 13-21.
51. Bloembergen, N., On the interaction of nuclear spins in a crystalline lattice. *Physica* **1949**, *15* (3-4), 386-426.
52. Bloembergen, N.; Morgan, L. O., Proton relaxation times in paramagnetic solutions effects of electron spin relaxation. *Journal of Chemical Physics* **1961**, *34* (3), 842.
53. Bloembergen, N.; Purcell, E. M.; Pound, R. V., Relaxation effects in nuclear magnetic resonance absorption. *Physical Review* **1948**, *73* (7), 679-712.
54. Solomon, I., Relaxation processes in a system of 2 spins. *Physical Review* **1955**, *99* (2), 559-565.
55. Blumberg, W. E., Nuclear Spin-Lattice Relaxation Caused by Paramagnetic Impurities. *Physical Review* **1960**, *119* (1), 79-84.

56. Farrar, C. T.; Hall, D. A.; Gerfen, G. J.; Inati, S. J.; Griffin, R. G., Mechanism of dynamic nuclear polarization in high magnetic fields. *Journal of Chemical Physics* **2001**, *114* (11), 4922-4933.
57. Smith, A. A.; Corzilius, B.; Barnes, A. B.; Maly, T.; Griffin, R. G., Solid Effect Dynamic Nuclear Polarization and Polarization Pathways. *Journal of Chemical Physics* **2012**, *136* (1), 015101.
58. Corzilius, B.; Smith, A. A.; Barnes, A. B.; Luchinat, C.; Bertini, I.; Griffin, R. G., High-Field Dynamic Nuclear Polarization with High-Spin Transition Metal Ions. *J Am Chem Soc* **2011**, *133* (15), 5648-5651.
59. Bousquet, J. C.; Saini, S.; Stark, D. D.; Hahn, P. F.; Nigam, M.; Wittenberg, J.; Ferrucci, J. T., Gd-DOTA - Characterization of a new paramagnetic complex. *Radiology* **1988**, *166* (3), 693-698.
60. Knop, R. H.; Frank, J. A.; Dwyer, A. J.; Girton, M. E.; Naegele, M.; Schrader, M.; Cobb, J.; Gansow, O.; Maegerstadt, M.; Brechbiel, M.; Baltzer, L.; Doppman, J. L., Gadolinium cryptelates as MR contrast agents. *Journal of Computer Assisted Tomography* **1987**, *11* (1), 35-42.
61. Benmelouka, M.; Van Tol, J.; Borel, A.; Port, M.; Helm, L.; Brunel, L. C.; Merbach, A. E., A high-frequency EPR study of frozen solutions of Gd-III complexes: Straightforward determination of the zero-field splitting parameters and simulation of the NMRD profiles. *J Am Chem Soc* **2006**, *128* (24), 7807-7816.
62. Barnes, A. B.; Mak-Jurkauskas, M. L.; Matsuki, Y.; Bajaj, V. S.; van der Wel, P. C. A.; DeRocher, R.; Bryant, J.; Sirigiri, J. R.; Temkin, R. J.; Lugtenburg, J.; Herzfeld, J.; Griffin, R. G., Cryogenic sample exchange NMR probe for magic angle spinning dynamic nuclear polarization. *Journal of Magnetic Resonance* **2009**, *198* (2), 261-270.
63. Becerra, L. R.; Gerfen, G. J.; Temkin, R. J.; Singel, D. J.; Griffin, R. G., Dynamic nuclear-polarization with a cyclotron-resonance maser at 5-T. *Physical Review Letters* **1993**, *71* (21), 3561-3564.
64. Becerra, L. R.; Gerfen, G. J.; Bellew, B. F.; Bryant, J. A.; Hall, D. A.; Inati, S. J.; Weber, R. T.; Un, S.; Prisner, T. F.; McDermott, A. E.; Fishbein, K. W.; Kreisler, K. E.; Temkin, R. J.; Singel, D. J.; Griffin, R. G., A Spectrometer for Dynamic Nuclear-Polarization and Electron-Paramagnetic-Resonance at High-Frequencies. *J. Magn. Reson. Ser. A* **1995**, *117* (1), 28-40.
65. Joye, C. D.; Griffin, R. G.; Hornstein, M. K.; Hu, K. N.; Kreisler, K. E.; Rosay, M.; Shapiro, M. A.; Sirigiri, J. R.; Temkin, R. J.; Woskov, P. P., Operational characteristics of a 14-W 140-GHz gyrotron for dynamic nuclear polarization. *Ieee T Plasma Sci* **2006**, *34* (3), 518-523.
66. Smith, A. A.; Corzilius, B.; Bryant, J. A.; DeRocher, R.; Woskov, P. P.; Temkin, R. J.; Griffin, R. G., A 140 GHz Pulsed EPR/212 MHz NMR Spectrometer for DNP Studies. *Journal of Magnetic Resonance* **2012**, *223*, 170-179.
67. Lange, S.; Linden, A. H.; Akbey, Ü.; Trent Franks, W.; Loening, N. M.; Rossum, B.-J. v.; Oschkinat, H., The effect of biradical concentration on the performance of DNP-MAS-NMR. *Journal of Magnetic Resonance* **2012**, *216* (0), 209-212.
68. Bennett, A. E.; Rienstra, C. M.; Auger, M.; Lakshmi, K. V.; Griffin, R. G., Heteronuclear decoupling in rotating solids. *Journal of Chemical Physics* **1995**, *103* (16), 6951-6958.
69. Gordon-Grossman, M.; Kaminker, I.; Gofman, Y.; Shai, Y.; Goldfarb, D., W-Band pulse EPR distance measurements in peptides using Gd³⁺-dipicolinic acid derivatives as spin labels. *Physical Chemistry Chemical Physics* **2011**, *13* (22), 10771-10780.
70. Ernst, R. R.; Bodenhausen, G.; Wokaun, A., *Principles of Nuclear Magnetic Resonance in One and Two Dimensions*. Oxford University Press: Oxford, 1987.
71. Linden, A.; Franks, W. T.; Akbey, Ü.; Lange, S.; van Rossum, B.-J.; Oschkinat, H., Cryogenic temperature effects and resolution upon slow cooling of protein preparations in solid state NMR. *Journal of Biomolecular NMR* **2011**, 1-10.

72. Ni, Q. Z.; Daviso, E.; Cana, T. V.; Markhasin, E.; Jawla, S. K.; Temkin, R. J.; Herzfeld, J.; Griffin, R. G., High Frequency Dynamic Nuclear Polarization *Accounts of Chem Research* **2013**, (*in press*).
73. Weissberg, H. L., Effective diffusion coefficient in porous media. *Journal of Applied Physics* **1963**, *34* (9), 2636-&.

Chapter 9: High-Resolution Solid-State NMR Structure of Alanyl-Prolyl-Glycine

Adapted from Barnes, AB; Andreas, LB; Huber, M; Ramachandran, R; van der Wel, PCA; Veshtort, M Griffin, RG; Mehta, MA J. Mag. Res. 2009,200(1),95-100

9.1 Introduction

Determining the high-resolution structures (backbone RMSD < 0.1 Å) of uniformly labelled polypeptides with solid-state NMR is often prohibitively difficult due to a lack of precision available with homonuclear broadbanded recoupling techniques such as RAD¹, DARR² and TSAR³. Although these experiments can define the secondary and tertiary structure and yield a clear global structure of the protein, the lack of high-precision measurements can leave detail of the active site and mechanisms that are of broader interest to the biological community still undefined. More precise techniques such as REDOR⁴, RFDR⁵, DRAWS⁶, and local field correlations yield sub-angstrom precision, but are often limited to spin-pair labelled systems.

A previous study on the polypeptide, N-*f*-MLF-OH, demonstrated the use of FS-REDOR, and torsion angle constraints to determine a high-resolution *de novo* structure⁷. Since the publication of that structure, additional high-resolution techniques applicable to uniformly ¹³C, ¹⁵N labelled systems have been developed, such as Rotational Resonance Width (R²W)^{8,9} and DANTE-REDOR¹⁰. DANTE-REDOR can yield high quality restrictions on torsion angles, in addition to heteronuclear distance constraints. R²W utilizes band selective R² to recouple homonuclear spin pairs and can separate weaker dipolar oscillations (from long distance, structurally relevant spin pairs) from relaxation processes using a constant mixing time strategy and has been recently applied to measure distances in uniformly labelled proteins¹¹. However, Ramachandran *et. al*¹² discussed the effect of the relative CSA orientation of the two spins in extracting accurate distances from R²W experiments. To make R²W a truly *de novo*, precise, and accurate technique for making homonuclear distance measurements, one must obtain the relative CSA orientation of the spin pair experimentally.

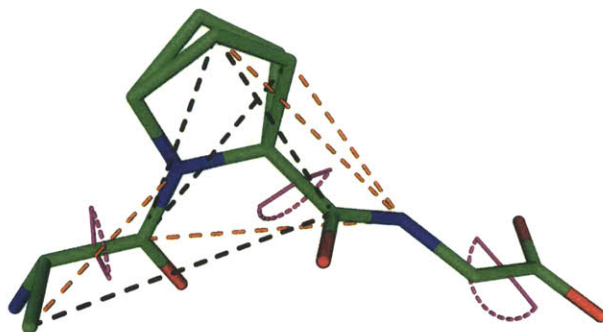


Figure 9.1. Crystal structure of APG¹³ showing the 11 SSNMR experimental constraints used in the structural refinement. Torsion angles are displayed in violet, REDOR distances in orange and R²W constraints in black. Note that the proline ring has a split occupancy between two conformers in the crystal structure.

We demonstrate the utility of an iterative approach to structure determination of uniformly labelled polypeptides using various solid-state NMR methods. Namely, ψ torsion angle and ¹³C-¹⁵N distances from NCCN¹⁴ and DANTE-REDOR measurements are first used to establish a structure from which approximate relative CSA orientations are available. Those orientations are then utilized into the fitting routines of R²W profiles to also obtain precise and accurate ¹³C-¹³C distances. Finally all experimentally determined homonuclear, heteronuclear, and torsion angles constraints are used in a final energy minimization that yields a high-quality *de novo* structure. We further discuss the effect of each sub-group of structural constraints on the structural quality as judged by self-consistent backbone RMSD and comparison to the known crystal structure.

9.2 Results and Discussion

Figure 9.1 shows the 11 constraints determined for APG listed in **Tab. 1**. Comparison with the X-ray crystal structure indicates the level of accuracy achieved in each measurement. Two of the restrictions on ϕ dihedral angles were determined with a local field NCCN experiment¹⁴. DANTE-REDOR was used to determine the glycine ϕ angle, and 4 ¹³C-¹⁵N internuclear distances. The four carbon internuclear distances were extracted using R²W.

CSA parameters for precise R²W fitting

The CSA magnitude and relative orientation of the two spins being recoupled by R² has a profound impact on the spin dynamics¹⁵ and accuracy of the distances extracted using R²W¹². For example **Figure 9.2b** shows the distribution of distances resulting using different CSA orientations taken from an ensemble of structures generated from simulated annealing without experimental constraints. The range of motion displayed in unconstrained simulated annealing is large enough even in this small molecule to cause substantial deviation in the final R² calculations, which demonstrates the importance of first calculating a lower resolution structure.

ψ Torsion Angles	X-ray	SSNMR
ψ_{Gly}	178°	180° ± 15°
ψ_{Ala}	153°	152° ± 5°
ψ_{Pro}	157°	162° ± 5°
Distances	X-ray (Å)	SSNMR (Å)
Pro N - Ala C ^β	3.2	3.2 ± 0.1
Gly N - Pro C ^β	3.2	3.2 ± 0.15
Pro C' - Pro C ^γ	3.3/3.6	3.9 ± 0.39
Ala C' - Pro C ^β	3.6	3.8 ± 0.38
Ala C' - Pro C ^γ	3.6	3.9 ± 0.39
Gly N - Ala C'	4.1	4.1 ^{+0.6-0.3}
Gly N - Pro C ^γ	4.5/4.3	4.2 ^{+0.6-0.3}
Pro C' - Ala C ^β	4.7	4.4 ± 0.44

Table 9.1. Experimental solid-state NMR constraints used in the structure calculation and corresponding values from the crystal structure from all NMR experiments; DANTE-REDOR (orange), NCCN torsion angles and R²W distances (black).

As a starting point in the R²W fitting routine, an initial structure based on REDOR and torsion angle measurements was first calculated. The relative CSA orientation from this structure was then used as an input for the R²W fitting routine, which is derived from a multipole multimode floquet theory (MMFT) treatment of the two spins¹⁶. The ¹³C-¹³C distances from these R²W fits were then used together with the REDOR and torsion angle constraints to calculate a final structure. R²W fits generated with relative CSA orientations found in the final structure yielded the same distance as those generated from the initial

REDOR-torsion angle structure. Thus we found it unnecessary to perform further iterations in which the structure generated with initial R²W distance constraints is used to refine these constraints.

The default values from SIMMOL were used for relative CSA - molecular orientations, the span and skew of carbonyl carbons were extracted from a 4 kHz CP-MAS spectrum according to Herzfeld and Berger¹⁷, and aliphatic carbon span and skew values were taken from Ye et al.¹⁸

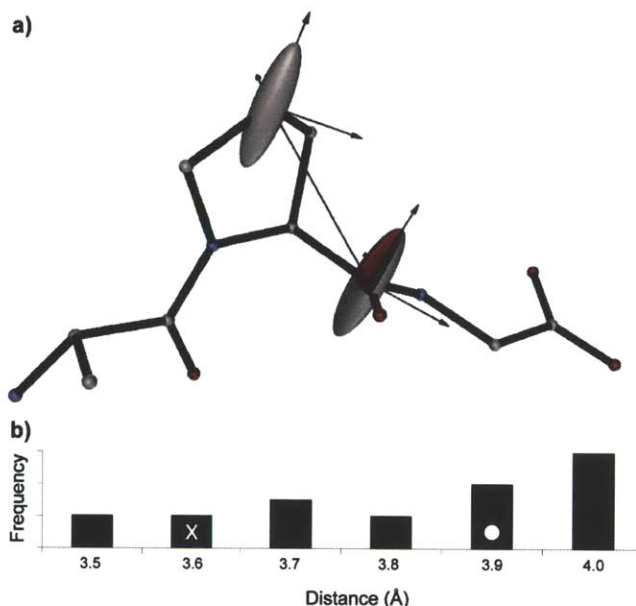


Figure 9.2. a) Relative orientations of the Proline C' and C_γ CSAs are shown superimposed on the initial structure calculated using REDOR and torsion angle constraints. b) Histogram displaying the range of Pro C'-Pro C_γ distances calculated from an ensemble of accessible structures generated using simulated annealing (CNS) without any constraints. X-ray (x) and reported NMR (o) distances are indicated. This graphic was produced with SIMMOL¹⁹.

Carboxyl terminus

The carboxyl terminus is not well defined due to the absence of ¹³C-¹³C constraints to the Gly carboxyl carbon (see **Figure 9.1**). This is predominantly due to intermolecular and dipolar truncation effects complicating any ¹³C-¹³C distance measurements between the Gly C' and the Pro C^α and Pro C^β. The Pro C^β carbon to Gly C' carbon intermolecular distance is 5.5 Å in the crystal structure, but there are 3 other intermolecular Pro C^β to Gly C' separations that are less than 5.4 Å (See **Figure 9.3**). The crystals consisted of 10% ¹³C-labeled peptide diluted with natural abundance APG to reduce the number of intermolecular contacts, however there still appears to be enough coupling between intermolecular Pro C^β - Gly C' pairs to substantially effect the R²W profile and result in a fitting of the data to 4.7 Å rather than 5.5 Å seen in the crystal structure.

Furthermore, the one-bond Pro C' – Pro C^α dipolar coupling truncates the Pro C'- Gly C^α coupling which would also constrain the carboxyl terminus. Even though R²W is a band-selective recoupling technique and thus usually does not suffer from dipolar truncation²⁰, the single bond coupling is an order of magnitude stronger than the coupling of interest and is also recoupled when the spinning frequency is set to the N=2 recoupling condition for the Pro C' to Gly C^α interaction; the stronger coupling dominates and insufficient polarization is transferred to the Gly C^α. We note that the dipolar truncation should not be as pronounced at higher magnetic fields where the resonances are more separated and the recoupling condition is thus more selective.

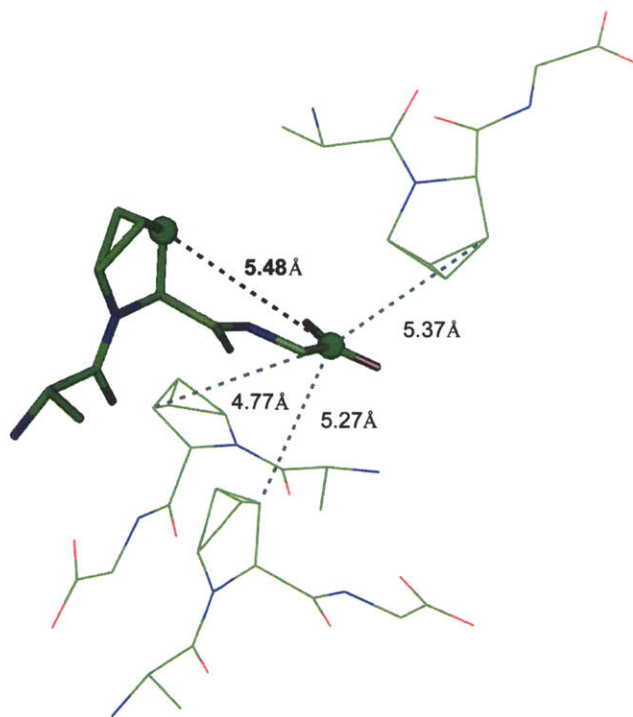


Figure 9.3. Crystal lattice of APG showing competing intermolecular distances to the long-range internuclear distance that could be used for structural refinement.

Constraints effect on structural quality

The standard annealing protocol in the program CNS^{21,22} was used to generate 40 APG structures in order to generate an ensemble that shows both an average geometry and demonstrates the degree of conformational variability allowed by the geometrical constraints.

In order to compare the usefulness of different structural constraints, a backbone RMSD among the 40 structures of each ensemble was calculated. This shows the level of precision attained by the different NMR experiments, indicating their ability to define overall conformation in this peptide. The results are summarized in **Figure 9.4** and show excellent agreement with the crystal structure. Since we were not able to perform a measurement that constrains the Ψ_{Gly} angle, the Gly carboxyl group was omitted from the RMSD calculations. The final NMR structure and the crystal structure agree to within an RMSD of 0.09 Å.

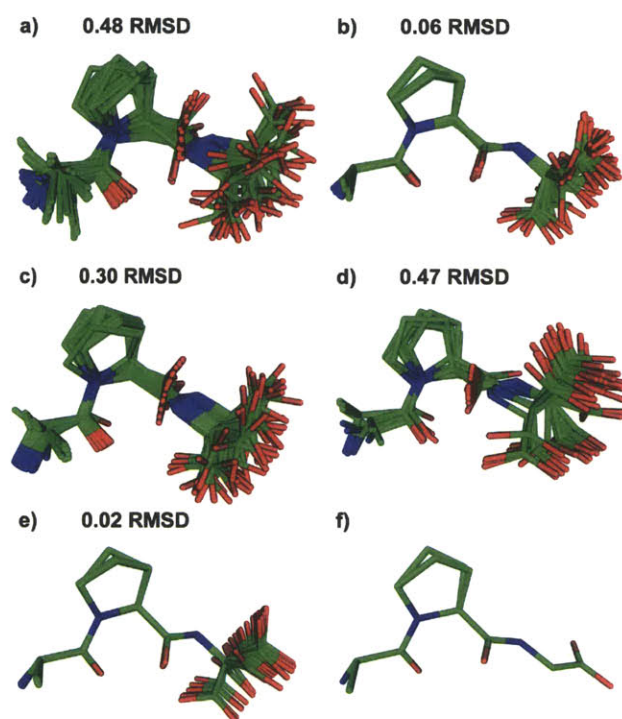


Figure 9.4. 20 lowest energy structures of APG using simulated annealing a) no constraints b) 2 ϕ angles from NCCN measurements c) 4 ^{13}C - ^{13}C distance constraints d) 4 ^{13}C - ^{15}N heteronuclear constraints e) all 11 constraints f) crystal structure.

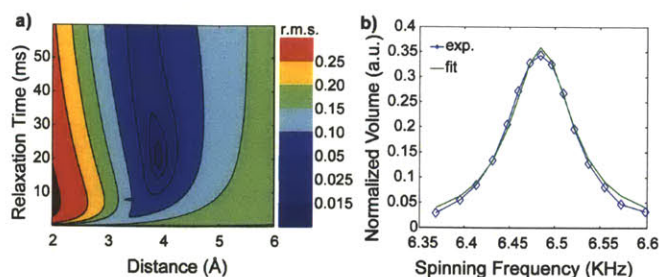


Figure 9.5. a) Contour plot of the root mean square deviation between experimental and simulated R²W profiles for P_O to P_γ as a function of distance and relaxation. b) Magnetization transfer from Pro C' to Pro C'' in R²W as a function of spinning frequency. The experimental data is shown in blue, and the fit in green.

9.3 Conclusions

Precise ¹³C-¹³C, ¹³C-¹⁵N, and ψ torsion angles were measured in a uniformly ¹³C, ¹⁵N labeled peptide using R²W in a de novo manner, DANTE-REDOR and local field NCCN experiments. Using these sub-angstrom structural constraints we were able to determine a high quality structure of APG. The 0.02 Å backbone RMSD structure was sufficient to observe the same conformational heterogeneity of the proline ring that is seen in the x-ray structure at 100 K. The ability to discriminate the two conformers by using structural constraints with sub-angstrom precision and CNS could be applied to address biological questions that require high-resolution structural detail. Furthermore, the short intramolecular contacts present in the tripeptide lattice studied here should not be present in larger proteins and should enable the extension of this *de novo* R²W strategy to distances up to 8 Å.

Finally, the NCCN torsion and many of the internuclear distances that were experimentally determined with SSNMR are indicative of trans-proline. Although proline is almost always in the trans isomer, the isomerization to the cis can play an important role in mitotic regulation²³, and we emphasize the strategies for structure determination presented here could be used to further investigate the biological function of proline isomerization.

9.4 Experimental Methods

Sample preparation

Experiments were performed on a sample of uniformly ^{13}C and ^{15}N labeled Alanyl-Prolyl-Glycine (APG) that was diluted to 10% in the corresponding natural abundance tripeptide to attenuate intermolecular dipolar couplings. The tripeptide was synthesized by CS Bio (CA) with labeled amino acids from Cambridge Isotopes (Andover, MA) and natural abundance material from BaChem (Switzerland). A 9:1 natural abundance to labeled APG mixture was dissolved in a minimal amount of water (solubility was approximately 45 mg/ml). The aqueous solution was placed in a desiccator next to a container of excess ethylene glycol. After a week, crystals were collected, crushed and packed into a rotor.

Assignments

To assign the ^{13}C resonances, a 2D ^{13}C - ^{13}C SPC-5²⁴ spectrum was recorded spinning at $\omega_r/2\pi = 7.5$ kHz using TPPM decoupling²⁵. γB_1 for ^{13}C was set to 37.5 kHz required by the recoupling condition. The mixing time was 1.07 ms corresponding to 16 rotor cycles, during which time a 120 kHz continuous wave γB_1 field was applied on the proton channel for decoupling. 256 time points were recorded in the indirect dimension using 16 scans for each t_1 point. The overall measurement time was 7 hours. The direct and indirect dimensions were linearly predicted forward to 1024 points, zero-filled to 2048 points and Fourier transformed using NMRPIPE²⁶.

NCCN Local Field Correlations

The torsion angles, ϕ_{Ala} and ϕ_{Pro} were determined with the double-quantum heteronuclear local field experiment previously described¹⁴. SPC-5²⁴ was used to create the ^{13}C - ^{13}C double quantum coherence. The homonuclear mixing time was 800 μs , corresponding to 8 rotor periods and the ^{13}C carrier was set precisely between the two resonances targeted for recoupling. γB_1 equal to 50 kHz was used for both ^{13}C and ^{15}N during homonuclear mixing and the REDOR²⁷ dephasing pulses. The spinning frequency was 10 kHz and 110 kHz continuous wave γB_1 decoupling field on protons was applied during SPC-5 mixing and REDOR periods; 136 kHz TPPM²⁵ decoupling was used during the acquisition period. 512 scans were taken per dephasing time, and a 3 s recycle delay was used between scans. Each dephasing point was normalized to the intensity of the corresponding resonances absent of REDOR pulses during the dephasing period. The

resonances were integrated and the intensities fit to extract the torsion angle with SPINEVOLUTION²⁸.

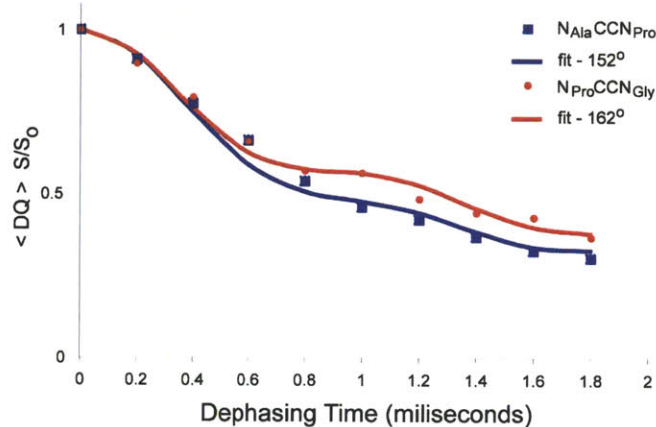


Figure 9.6. Dephasing curves for extraction of Ψ torsion angle. An $N_{Gly}CCN_{Pro}$ Ψ angle of 152° (blue) was extracted compared to 153° from the X-ray data and $N_{Ala}CCN_{Gly}$ Ψ angle was found to be 162° (red) versus 157° from the x-ray data. SPINEVOLUTION²⁸ was used to fit the data.

Rotational Resonance Width

NMR spectra were recorded on a 360 MHz Spectrometer (courtesy of Dr. D. J. Ruben) with a commercial Chemagnetics triple resonance MAS probe equipped with a 4.0 mm Chemagnetics spinning module. Spinning frequencies were regulated with a Bruker MAS controller.

The crosspeak volumes were extracted by automated fitting to two-dimensional Gaussians using NMRPIPE²⁶. All data points in each 2D-slice were normalized to the carbonyl intensities of reference experiments conducted at identical spinning frequencies with zero mixing time.

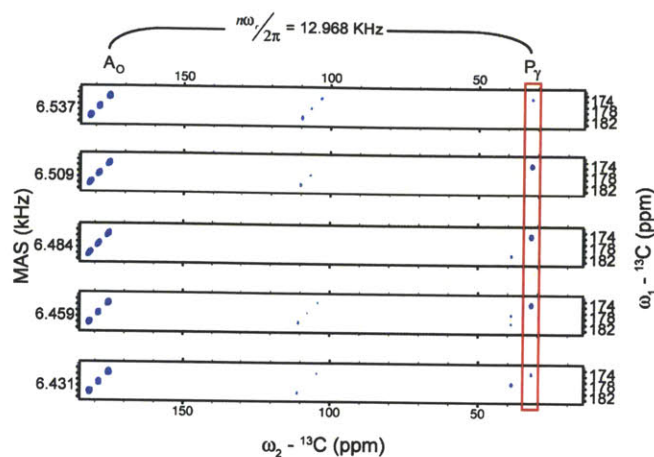


Figure 9.7. R²W spectra at 5 spinning frequencies. The P_γ crosspeak intensifies as the spinning frequency is swept the R² condition between the spin pair.

A Gaussian pulse of 25 μs duration was used, followed by a z-filter of 750 μs to select the carbonyl region of the spectrum. 32 t₁ points were recorded with an increment of 250 μs and 16 scans per point with a recycle delay of 3.1 s leading to a total experimental time of about 50 minutes per two dimensional slice. A series of experiments were performed as a function of the sample spinning frequency under a constant mixing time of 30 ms.

DANTE-REDOR

DANTE-REDOR measurements were carried out on a custom assembled NMR spectrometer with a Discovery console (Tecmag; Houston, TX), 14.1 T magnet (MagneX; Oxford, England), and a 39-channel matrix shim system (Resonance Research, Inc.; Billerica, MA), operating at a proton frequency of 600.377 MHz (150.987 MHz for ¹³C). A doubly tuned 4 mm magic angle spinning probe (Doty Scientific; Columbia, South Carolina) was employed.

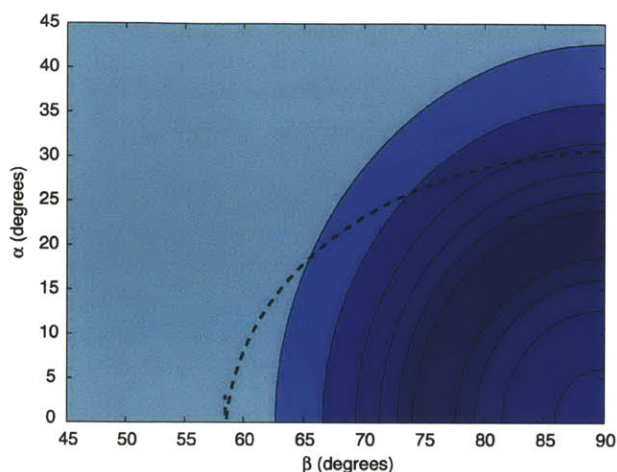


Figure 9.8. The χ^2 surface for azimuthal (α) and polar (β) angles of the CSA-dipole orientation with each contour level 2 times the previous level. Labeled APG was diluted to 10% in natural abundance APG and data were collected at 14.1 Tesla with an MAS spinning frequency of 8929 Hz. The superimposed dashed line shows the allowed azimuthal and polar angles corresponding to a rotation about the terminal ψ dihedral angle, with the best fit at $\alpha=31^\circ$, $\beta=90^\circ$.

The DANTE-REDOR pulse sequence is described in ¹⁰. This sequence adapts the orientation information available in a specifically labelled sample to a uniformly labelled system. By employing a DANTE pulse train as the selective pulse in FS-REDOR, the orientation information in REDOR sidebands is retained. Thus at the end of the REDOR evolution time, the ¹³C spin-echo intensity is modulated only by dipolar couplings to the selected ¹⁵N and the resulting REDOR curve can be fit to the analytical expression for an isolated spin pair. The effects of proton couplings are attenuated with Small Phase Incremental Alternation (SPINAL-64) decoupling ²⁵. The proton decoupling field was 100 kHz, the ¹⁵N REDOR π -pulse width was 16 μ s and the DANTE π -pulse trains consisted of 33 2 μ s rotor synchronized pulses.

Fourier transforms were applied with no apodization and zero filling to twice the acquisition time of 15.36 ms. Only zero order phase correction was used. Dephasing (S) and full-echo (S_0) peak areas were determined by integrating the center band and all observed sidebands. For distance determinations, the sum of all bands in the S and S_0 spectra were used. For extraction of orientation information, the dephasing of each individual band was compared.

Distances were determined by fitting the experimentally observed REDOR curve to the analytical expression, $\Delta S/S_0(\tau) = \lambda[1 - \langle \cos(\omega_{CN}\tau) \rangle]$. $\Delta S/S_0 = 1 - S/S_0$, where S and S_0 are the dipolar dephasing and reference intensities, respectively. The coupling ω_{CN} is a function of the dipolar coupling constant, b_{CN} ,

and $\langle \rangle$ indicates the powder average over a uniform distribution of crystallite orientations. The scaling factor λ accounts for ^{13}C spins without a neighbouring ^{15}N spin, which is a result of imperfect labelling and dilution of the labelled compound in natural abundance material. In the DANTE-REDOR experiment, λ also accounts for imperfect inversion of the ^{15}N spin magnetization by the selective pulse and decay of coherence due to insufficient decoupling.

For each distance measurement, the weighted χ^2 , χ_v^2 , was minimized to fit the data.

$\chi_v^2 \propto \sum_i w_i (s_{i,\text{exp}} - s_{i,\text{sim}})^2$. In this expression, w_i is the inverse uncertainty in each point squared (σ^{-2}).

Since the noise in each data point is approximately constant, w_i was easily determined by propagation of error. In the minimization of χ_v^2 , the coupling constant, b_{CN} , was varied freely and the amplitude scaling factor λ was varied within the narrow range of values determined for strong couplings, for which this parameter can be easily determined. The reported uncertainties are at the 95% confidence level according to the following procedure²⁹. First, b_{CN} and λ are varied to determine the best-fit dipolar coupling, $\chi_{v,\text{min}}^2$. Next, several trial b_{CN} values are selected about the best fit, and the data are re-fit by optimizing λ within the previously defined range. The uncertainties are represented by χ_v^2 values that differ from $\chi_{v,\text{min}}^2$ by $F(v) * \chi_{v,\text{min}}^2$, where $F(v)$ is a constant that depends on the number of degrees of freedom, v , and the confidence level. For the case of 95% confidence, and 2 degrees of freedom, $F(v)=19$.

Each best-fit b_{CN} value was linearly scaled by dividing by 0.95 in order to account for thermal motion at 298 K. Internuclear C–N distances are related to the dipolar coupling constants by the equation

$$b_{\text{CN}} = -\frac{\mu_0 \gamma_{\text{C}} \gamma_{\text{N}} \hbar}{4\pi r_{\text{CN}}^3} \quad 30.$$

The orientation of the nitrogen in the CSA principle axis system was determined by fitting the experimentally observed REDOR curves of each sideband to numerical simulations explained previously³¹. The weighted χ^2 , χ_v^2 , was minimized to fit the data. $\chi_v^2 \propto \sum_{i,N} w (s_{\text{exp}} - s_{\text{sim}})^2$, where the sum is taken over spectral bands N , and mixing times i . As before, w_i is the inverse uncertainty in each point squared (σ^{-2}). The uncertainties in the dipolar and azimuthal angles alpha and beta are represented by χ_v^2 values that differ from $\chi_{v,\text{min}}^2$ by $F(v) * \chi_{v,\text{min}}^2$, where $F(v)$ is a constant that depends on the number of degrees of freedom, v , and the confidence level. The best-fit dipolar coupling is used in this determination, so this is really a three-parameter fit.

However, since the REDOR dephasing is approximately linear in the beginning of the curve (before the first extremum in the REDOR curve, where we fit the data) a small error in the dipolar coupling does not significantly alter the position of the best-fit orientation, and thus can be treated as a two parameter fit.

Acknowledgments:

A.B.B. was supported through an NSF graduate research fellowship. We thank Marvin Bayro for supplying the pulse sequence for the NCCN experiment and Jozef Lewandowski and Matthew Eddy for helpful discussions, and Matthias Zeller (Youngstown State University) for the crystal structure. This research was supported by the National Institutes of Health (EB003151 and EB002026).

9.5 Supporting Information

APG Single Crystal Data

Identification code: 05mz152m

Empirical formula: C₁₀ H₁₉ N₃ O₅

Moiety formula: C₁₀ H₁₇ N₃ O₄, H₂ O

Formula weight: 261.28

Temperature: 298(2) K

Wavelength: 0.71073 Å

Crystal system: Orthorhombic

Space group: P2₁2₁2₁

Unit cell dimensions:

$a = 6.7158(3)$ Å, $\alpha = 90^\circ$

$b = 11.7784(6)$ Å, $\beta = 90^\circ$

$c = 16.2633(8)$ Å, $\gamma = 90^\circ$

Volume, Z : 1286.45(11) Å³, 4

Density (calculated): 1.349 Mg/m³

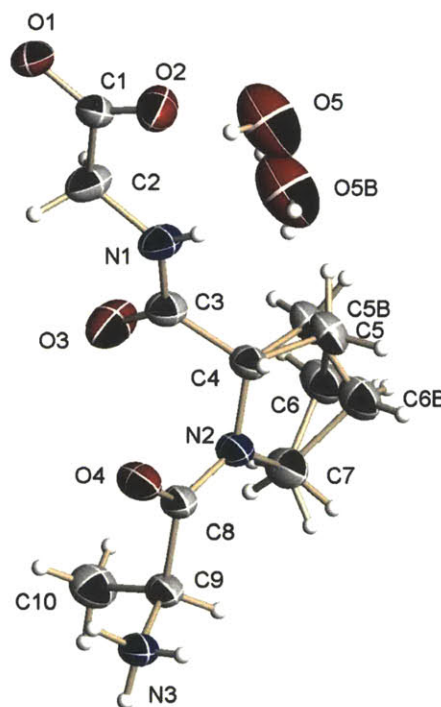
Absorption coefficient: 0.108 mm⁻¹

$F(000)$: 560

Crystal size: 0.39 × 0.31 × 0.30 mm

Crystal shape, colour: block, colourless

θ range for data collection: 1.63 to 28.28°



Limiting indices: $-8 \leq h \leq 8$, $-15 \leq k \leq 15$, $-21 \leq l \leq 21$

Reflections collected: 13006

Independent reflections: 1844 ($R(\text{int}) = 0.0236$)

Completeness to $\theta = 28.28^\circ$: 99.9 %

Absorption correction: multi-scan

Max. and min. transmission: 0.97 and 0.8073

Refinement method: Full-matrix least-squares on F^2

Data / restraints / parameters: 1844 / 1 / 185

Goodness-of-fit on F^2 : 1.052

Final R indices [$I > 2\sigma(I)$]: $R1 = 0.0398$, $wR2 = 0.1055$

R indices (all data): $R1 = 0.0422$, $wR2 = 0.1073$

Largest diff. peak and hole: 0.297 and $-0.171 \text{ e} \times \text{\AA}^{-3}$

Refinement of F^2 against ALL reflections. The weighted R-factor wR and goodness of fit are based on F^2 , conventional R-factors R are based on F , with F set to zero for negative F^2 . The threshold expression of

$F^2 > 2\sigma(F^2)$ is used only for calculating R-factors

Comments:

Carbon atom C5 and C6 of the proline ring are disordered over two positions with an occupancy ratio of 0.674(5) to 0.326(5). A water solvate molecule is also disordered over two positions with an occupancy ratio of 0.785(6) to 0.215(6).

Treatment of hydrogen atoms:

The water hydrogen atoms were found in the difference density Fourier map and were restraint to have the same O-H and H...H distances within a standard deviation of 0.01. The positions of the minor water hydrogen atoms could only be stable refined with a damping factor of 50. For the final refinement without damping they were set to ride on the adjacent oxygen atom. All other hydrogen atoms were placed in calculated positions. All hydrogen atoms were isotropically refined with a displacement parameter 1.2 (methylene) or 1.5 times (methyl, hydroxyl, ammonium) that of the adjacent carbon, oxygen or nitrogen atom.

Table 2. Atomic coordinates [$\times 10^4$] and equivalent isotropic displacement parameters [$\text{\AA}^2 \times 10^3$] for 05mz152m. U(eq) is defined as one third of the trace of the orthogonalized U_{ij} tensor.

	x	y	z	U(eq)
C(1)	8191(3)	5720(1)	583(1)	37(1)
C(2)	8280(4)	4634(2)	1083(1)	48(1)
C(3)	6602(3)	2831(2)	1203(1)	39(1)
C(4)	4881(3)	2095(1)	908(1)	37(1)
C(5)	2853(7)	2306(4)	1302(3)	43(1)
C(6)	2849(6)	1469(3)	2034(2)	49(1)
C(7)	3890(3)	431(2)	1702(1)	46(1)
C(8)	6737(3)	351(1)	702(1)	35(1)
C(9)	7111(3)	-884(1)	952(1)	38(1)
C(10)	8516(4)	-937(2)	1685(1)	55(1)
C(5B)	3222(16)	2397(10)	1571(6)	43(1)
C(6B)	2119(12)	1304(6)	1648(5)	49(1)
C(7B)	3890(3)	431(2)	1702(1)	46(1)
N(1)	6777(3)	3830(1)	826(1)	43(1)
N(2)	5262(2)	895(1)	1084(1)	36(1)
N(3)	8024(3)	-1463(1)	237(1)	41(1)
O(1)	9505(2)	6449(1)	762(1)	49(1)
O(2)	6932(2)	5827(1)	36(1)	55(1)
O(3)	7714(3)	2545(1)	1759(1)	68(1)
O(4)	7799(2)	806(1)	182(1)	47(1)
O(5)	2152(6)	3791(4)	6798(2)	100(1)
O(5B)	1870(20)	2885(15)	6634(7)	100(1)

All esds (except the esd in the dihedral angle between two l.s. planes) are estimated using the full covariance matrix. The cell esds are taken

into account individually in the estimation of esds in distances, angles and torsion angles; correlations between esds in cell parameters are only used when they are defined by crystal symmetry. An approximate (isotropic) treatment of cell esds is used for estimating esds involving l.s. planes.

Table 3. Bond lengths [Å] and angles [deg] for 05mz152m.

C(1)-O(2)	1.234(2)	C(8)-C(9)	1.531(2)
C(1)-O(1)	1.265(2)	C(9)-N(3)	1.482(2)
C(1)-C(2)	1.517(2)	C(9)-C(10)	1.522(3)
C(2)-N(1)	1.446(3)	C(9)-H(9)	0.9800
C(2)-H(2A)	0.9700	C(10)-H(10A)	0.9600
C(2)-H(2B)	0.9700	C(10)-H(10B)	0.9600
C(3)-O(3)	1.220(2)	C(10)-H(10C)	0.9600
C(3)-N(1)	1.332(2)	C(5B)-C(6B)	1.491(15)
C(3)-C(4)	1.522(3)	C(5B)-H(5D)	0.9700
C(4)-N(2)	1.465(2)	C(5B)-H(5C)	0.9700
C(4)-C(5)	1.525(5)	C(6B)-H(6C)	0.9700
C(4)-C(5B)	1.590(11)	C(6B)-H(6D)	0.9700
C(4)-H(4)	0.9800	N(1)-H(1)	0.78(2)
C(5)-C(6)	1.545(6)	N(3)-H(3A)	0.8900
C(5)-H(5A)	0.9700	N(3)-H(3B)	0.8900
C(5)-H(5B)	0.9700	N(3)-H(3C)	0.8900
C(6)-C(7)	1.509(4)	O(5)-H(5E)	0.78(3)
C(6)-H(6A)	0.9700	O(5)-H(5F)	0.78(3)
C(6)-H(6B)	0.9700	O(5B)-H(5E)	0.93(4)
C(7)-N(2)	1.469(2)	O(5B)-H(5G)	0.7821
C(7)-H(7A)	0.9700	O(5B)-H(5H)	0.7820
C(7)-H(7B)	0.9700		
C(8)-O(4)	1.228(2)	O(2)-C(1)-O(1)	125.05(16)
C(8)-N(2)	1.333(2)	O(2)-C(1)-C(2)	119.95(16)

O(1)-C(1)-C(2)	114.98(16)	N(2)-C(7)-H(7A)	111.1
N(1)-C(2)-C(1)	111.75(16)	C(6)-C(7)-H(7A)	111.1
N(1)-C(2)-H(2A)	109.3	N(2)-C(7)-H(7B)	111.1
C(1)-C(2)-H(2A)	109.3	C(6)-C(7)-H(7B)	111.1
N(1)-C(2)-H(2B)	109.3	H(7A)-C(7)-H(7B)	109.0
C(1)-C(2)-H(2B)	109.3	O(4)-C(8)-N(2)	122.90(15)
H(2A)-C(2)-H(2B)	107.9	O(4)-C(8)-C(9)	120.10(16)
O(3)-C(3)-N(1)	122.04(18)	N(2)-C(8)-C(9)	116.98(15)
O(3)-C(3)-C(4)	122.76(17)	N(3)-C(9)-C(10)	109.83(16)
N(1)-C(3)-C(4)	115.17(16)	N(3)-C(9)-C(8)	107.24(14)
N(2)-C(4)-C(3)	110.81(14)	C(10)-C(9)-C(8)	110.44(15)
N(2)-C(4)-C(5)	103.4(2)	N(3)-C(9)-H(9)	109.8
C(3)-C(4)-C(5)	116.9(2)	C(10)-C(9)-H(9)	109.8
N(2)-C(4)-C(5B)	101.9(5)	C(8)-C(9)-H(9)	109.8
C(3)-C(4)-C(5B)	101.0(4)	C(9)-C(10)-H(10A)	109.5
N(2)-C(4)-H(4)	108.5	C(9)-C(10)-H(10B)	109.5
C(3)-C(4)-H(4)	108.5	H(10A)-C(10)-H(10B)	109.5
C(5)-C(4)-H(4)	108.5	C(9)-C(10)-H(10C)	109.5
C(5B)-C(4)-H(4)	125.6	H(10A)-C(10)-H(10C)	109.5
C(4)-C(5)-C(6)	102.8(3)	H(10B)-C(10)-H(10C)	109.5
C(4)-C(5)-H(5A)	111.2	C(6B)-C(5B)-C(4)	102.2(7)
C(6)-C(5)-H(5A)	111.2	C(6B)-C(5B)-H(5D)	111.3
C(4)-C(5)-H(5B)	111.2	C(4)-C(5B)-H(5D)	111.3
C(6)-C(5)-H(5B)	111.2	C(6B)-C(5B)-H(5C)	111.3
H(5A)-C(5)-H(5B)	109.1	C(4)-C(5B)-H(5C)	111.3
C(7)-C(6)-C(5)	103.9(3)	H(5D)-C(5B)-H(5C)	109.2
C(7)-C(6)-H(6A)	111.0	C(5B)-C(6B)-H(6C)	111.5
C(5)-C(6)-H(6A)	111.0	C(5B)-C(6B)-H(6D)	111.5
C(7)-C(6)-H(6B)	111.0	H(6C)-C(6B)-H(6D)	109.4
C(5)-C(6)-H(6B)	111.0	C(3)-N(1)-C(2)	120.52(17)
H(6A)-C(6)-H(6B)	109.0	C(3)-N(1)-H(1)	118.6(19)
N(2)-C(7)-C(6)	103.52(19)	C(2)-N(1)-H(1)	120.8(19)

C(8)-N(2)-C(4)	120.12(14)	C(9)-N(3)-H(3C)	109.5
C(8)-N(2)-C(7)	127.36(15)	H(3A)-N(3)-H(3C)	109.5
C(4)-N(2)-C(7)	112.52(15)	H(3B)-N(3)-H(3C)	109.5
C(9)-N(3)-H(3A)	109.5	H(5E)-O(5)-H(5F)	104(5)
C(9)-N(3)-H(3B)	109.5	H(5G)-O(5B)-H(5H)	100.2
H(3A)-N(3)-H(3B)	109.5		

Table 4. Anisotropic displacement parameters [$\text{\AA}^2 \times 10^3$] for 05mz152m. The anisotropic displacement factor exponent takes the form: $-2 \pi^2 [(h a^*)^2 U_{11} + \dots + 2 h k a^* b^* U_{12}]$

	U11	U22	U33	U23	U13	U12
C(1)	37(1)	28(1)	47(1)	-1(1)	3(1)	3(1)
C(2)	61(1)	33(1)	50(1)	4(1)	-16(1)	-8(1)
C(3)	45(1)	31(1)	43(1)	3(1)	-1(1)	0(1)
C(4)	35(1)	29(1)	46(1)	5(1)	5(1)	3(1)
C(5)	36(2)	49(2)	43(2)	5(2)	4(2)	13(1)
C(6)	43(2)	50(1)	53(2)	6(2)	14(1)	8(1)
C(7)	42(1)	40(1)	57(1)	9(1)	19(1)	-1(1)
C(8)	32(1)	27(1)	45(1)	3(1)	4(1)	-1(1)
C(9)	34(1)	27(1)	52(1)	6(1)	9(1)	-1(1)
C(10)	59(1)	48(1)	57(1)	10(1)	-4(1)	7(1)
C(5B)	36(2)	49(2)	43(2)	5(2)	4(2)	13(1)
C(6B)	43(2)	50(1)	53(2)	6(2)	14(1)	8(1)
C(7B)	42(1)	40(1)	57(1)	9(1)	19(1)	-1(1)
N(1)	53(1)	29(1)	46(1)	4(1)	-11(1)	-5(1)
N(2)	34(1)	27(1)	48(1)	5(1)	8(1)	-1(1)
N(3)	41(1)	27(1)	57(1)	2(1)	5(1)	1(1)
O(1)	49(1)	31(1)	66(1)	1(1)	-8(1)	-4(1)
O(2)	47(1)	47(1)	70(1)	17(1)	-14(1)	-5(1)

O(3)	79(1)	49(1)	75(1)	24(1)	-34(1)	-15(1)
O(4)	47(1)	34(1)	59(1)	11(1)	19(1)	4(1)
O(5)	92(2)	138(3)	71(2)	36(2)	24(2)	32(3)
O(5B)	92(2)	138(3)	71(2)	36(2)	24(2)	32(3)

Table 5. Hydrogen coordinates ($\times 10^4$) and isotropic displacement parameters ($\text{\AA}^2 \times 10^3$) for 05mz152m.

	x	y	z	U(eq)
H(2A)	9586	4293	1021	58
H(2B)	8092	4813	1660	58
H(4)	4749	2188	312	44
H(5A)	1781	2140	921	51
H(5B)	2730	3085	1489	51
H(6A)	3565	1782	2500	58
H(6B)	1499	1290	2203	58
H(7A)	4610	37	2134	56
H(7B)	2947	-90	1453	56
H(9)	5845	-1250	1092	45
H(10A)	8736	-1716	1834	82
H(10B)	7936	-539	2141	82
H(10C)	9763	-590	1542	82
H(5D)	3814	2619	2091	51
H(5C)	2359	3001	1378	51
H(6C)	1288	1163	1170	58
H(6D)	1303	1288	2139	58
H(7C)	4485	424	2246	56
H(7D)	3462	-331	1560	56
H(1)	6010(40)	3990(20)	480(16)	56
H(5E)	2240(70)	3280(30)	7100(20)	69
H(5F)	3120(50)	3760(40)	6530(20)	69
H(3A)	9111	-1087	81	62

H(3B)	7157	-1480	-177	62
H(3C)	8354	-2169	376	62
H(5G)	1911	2719	6169	151
H(5H)	1828	2282	6835	151

Table 6. Hydrogen bonds for 05mz152m [\AA and deg].

D-H...A	d(D-H)	d(H...A)	d(D...A)	\angle (DHA)
N(1)-H(1)...O(4)#1	0.78(2)	2.42(2)	3.164(2)	158(2)
N(3)-H(3A)...O(2)#2	0.89	1.93	2.765(2)	155.8
N(3)-H(3B)...O(1)#1	0.89	2.02	2.868(2)	158.8
N(3)-H(3B)...O(5B)#3	0.89	2.57	3.139(11)	122.6
N(3)-H(3C)...O(1)#4	0.89	1.91	2.787(2)	169.0
N(3)-H(3C)...O(2)#4	0.89	2.61	3.292(2)	134.6
O(5)-H(5E)...O(3)#5	0.78(3)	2.11(3)	2.851(4)	158(4)
O(5)-H(5F)...O(1)#6	0.78(3)	2.04(3)	2.821(4)	174(4)
O(5B)-H(5G)...N(3)#7	0.78	2.48	3.139(11)	142.7
O(5B)-H(5H)...O(3)#5	0.78	2.37	2.721(12)	108.3

Symmetry transformations used to generate equivalent atoms:

#1 $x-1/2, -y+1/2, -z$ #2 $x+1/2, -y+1/2, -z$ #3 $-x+1, y-1/2, -z+1/2$

#4 $x, y-1, z$ #5 $x-1/2, -y+1/2, -z+1$ #6 $-x+3/2, -y+1, z+1/2$

#7 $-x+1, y+1/2, -z+1/2$

9.6 References

1. Morcombe, C. R.; Gaponenko, V.; Byrd, R. A.; Zilm, K. W., *Journal of the American Chemical Society* **2004**, *126* (23), 7196-7197.
2. Takegoshi, K.; Nakamura, S.; Terao, T., *Chemical Physics Letters* **2001**, *344* (5-6), 631-637.
3. Lewandowski, J. R.; de Paepe, G.; Griffin, R. G., *J. Am Chem. Soc* **2007**, *129* (4), 728-729.
4. Gullion, T.; Schaefer, J., *J. Magn. Reson.* **1989**, *81*, 196-200.
5. Bennett, A. E.; Rienstra, C. M.; Griffiths, J. M.; Zhen, W. G.; Lansbury, P. T.; Griffin, R. G., *Journal of Chemical Physics* **1998**, *108* (22), 9463-9479.
6. Gregory, D. M.; Mitchell, D. J.; Stringer, J. A.; Kiihne, S.; Shiels, J. C.; Callahan, J.; Mehta, M. A.; Drobny, G. P., *Chem. Phys. Lett.* **1995**, *246*, 654.
7. Rienstra, C. M.; Tucker-Kellogg, L.; Jaroniec, C. P.; Hohwy, M.; Reif, B.; McMahon, M. T.; Tidor, B.; Lozano-Perez, T.; Griffin, R. G., *Proc. Natl. Acad. Sci. U. S. A.* **2002**, *99* (16), 10260-10265.
8. Ramachandran, R.; Ladizhansky, V.; Bajaj, V. S.; Griffin, R. G., *J. Amer. Chem. Soc.* **2003**, *125*, 15623-15629.
9. Costa, P.; Sun, B.; Griffin, R. G., *J. Magn. Resonance* **2003**, *164*, 92-103.
10. Andreas, L. B.; Mehta, A. K.; Mehta, M. A., *Journal of the American Chemical Society* **2007**, *129* (49), 15233-15239.
11. van der Wel, P. C. A.; Eddy, M. T.; Ramachandran, R.; Griffin, R. G., *Physical Chemistry and Chemical Physics* **2009**, submitted.
12. Ramachandran, R.; Lewandowski, J. R.; van der Wel, P. C. A.; Griffin, R. G., *J. Chem. Phys.* **2006**, *124*, 214107.
13. Wu, S.; Declercq, J. P.; Tinant, B.; Vanmeerssche, M., *Bulletin Des Societes Chimiques Belges* **1987**, *96* (7), 515-520.
14. Costa, P. R.; Gross, J. D.; Hong, M.; Griffin, R. G., *Chem. Phys. Lett* **1997**, *280* (1-2), 95-103.
15. Levitt, M. H.; Raleigh, D. P.; Creuzet, F.; Griffin, R. G., *Journal of Chemical Physics* **1990**, *92* (11), 6347-6364.
16. Ramachandran, R.; Griffin, R., *The Journal of chemical physics* **2005**, *122*, 164502.
17. Herzfeld, J.; Berger, A. E., *Journal of Chemical Physics* **1980**, *73* (12), 6021-6030.
18. Ye, C.; Fu, R.; Hu, J.; Hou, L.; Ding, S., *MAGNETIC RESONANCE IN CHEMISTRY* **1993**, *31* (8), 699-704.
19. Bak, M.; Schultz, R.; Vosegaard, T.; Nielsen, N. C., *Journal of Magnetic Resonance* **2002**, *154* (1), 28-45.
20. Bayro, M. J. H., M.; Ramachandran, R.; Davenport, T. C.; Meier, B. H.; Ernst, M.; Griffin, R. G., *J. Chem. Phys.* **2009**, To be published.
21. Brunger, A. T.; Adams, P. D.; Clore, G. M.; DeLano, W. L.; Gros, P.; Grosse-Kunstleve, R. W.; Jiang, J. S.; Kuszewski, J.; Nilges, M.; Pannu, N. S.; Read, R. J.; Rice, L. M.; Simonson, T.; Warren, G. L., *Acta Crystallographica Section D-Biological Crystallography* **1998**, *54*, 905-921.
22. Brunger, A. T., *Nature Protocols* **2007**, *2* (11), 2728-2733.
23. Yaffe, M. B.; Schutkowski, M.; Shen, M.; Zhou, X. Z.; Stukenberg, P. T.; Rahfeld, J.-U.; Xu, J.; Kuang, J.; Kirschner, M. W.; Fischer, G.; Cantley, L. C.; Lu, K. P., *Science* **1997**, *278* (5345), 1957-1960.
24. Hohwy, M.; Rienstra, C. M.; Jaroniec, C. P.; Griffin, R. G., *Journal of Chemical Physics* **1999**, *110* (16), 7983-7992.

25. Bennett, A. E.; Rienstra, C. M.; Auger, M.; Lakshmi, K. V.; Griffin, R. G., *Journal of Chemical Physics* **1995**, *103*, 6951.
26. Delaglio, F.; Grzesiek, S.; Vuister, G. W.; Zhu, G.; Pfeifer, J.; Bax, A., *Journal of Biomolecular Nmr* **1995**, *6* (3), 277-293.
27. Gullion, T.; Schaefer, J., *Journal of Magnetic Resonance* **1989**, *81* (1), 196-200.
28. Veshtort, M.; Griffin, R. G., *Journal of Magnetic Resonance* **2006**, *178*, 248-282
29. Shoemaker, D. P.; Garland, C. W.; Nibler, J. W., **1989**.
30. Jaroniec, C. P.; Tounge, B. A.; Herzfeld, J.; Griffin, R. G., *Journal Of The American Chemical Society* **2001**, *123* (15), 3507-3519.
31. O'connor, R. D.; Schaefer, J., *Journal of Magnetic Resonance* **2002**, *154* (1), 46-52.

Curriculum Vitae

2007-2013

Physical Chemistry PhD Program

Massachusetts Institute of Technology, Cambridge, MA. GPA: 5.0/5.0

(Thesis to be submitted September 2013)

Advisor: Prof. Robert G. Griffin

Bachelor of Arts

2002-2007

Oberlin College, Oberlin, Ohio. Major: Chemistry, GPA: 3.99/4.0

Advisor: Prof. Manish M. Mehta

Publications

(9) Björn Corzilius, Loren B. Andreas, Albert A. Smith, Qing Zhe Ni, Robert G. Griffin. *Paramagnet Induced Signal Quenching in MAS-DNP experiments on Homogeneous Solutions*. J. Magn. Reson, accepted.

(1) Loren B. Andreas, Alexander B. Barnes, Bjorn Corzilius, James J. Chou, Eric A. Miller, Marc Caporini, Melanie Rosay, and Robert Griffin *Dynamic Nuclear Polarization Study of Inhibitor Binding to the M2₁₈₋₆₀ Proton Transporter from Influenza A* Biochemistry, **2013**, 52(16):2774-82.

(2) Eugenio Daviso, Matthew T. Eddy, Loren B. Andreas, Robert G. Griffin, Judith Herzfeld. *Efficient resonance assignment of proteins in MAS NMR by simultaneous intra- and inter-residue 3D correlation spectroscopy*. J. Biomol. NMR, **2013**, 55(3):257-65.

(3) Loren B. Andreas, Rafal M. Pielak, James J. Chou Robert G. Griffin *Magic-Angle-Spinning NMR of the Drug Resistant S31N M2 Proton Transporter from Influenza A*. J. Am. Chem. Soc., **2012**, 134(17):7215-8.

(4) Loren B. Andreas, Matthew T. Eddy, Rafal M. Pielak, James J. Chou Robert G. Griffin. *Magic Angle Spinning NMR Investigation of Influenza A M2(18-60): Support for an Allosteric Mechanism of Inhibition*. J. Am. Chem. Soc., **2010**, 132(32):10958-60.

(5) Thorsten Maly, Loren B. Andreas, Albert A. Smith and Robert G. Griffin *²H-DNP-enhanced ²H-¹³C solid-state NMR correlation spectroscopy* Phys. Chem. Chem. Phys., **2010**, 12(22):5872-8.

(6) Alexander B. Barnes, Björn Corzilius, Melody L Mak-Jurkauskas, Loren B. Andreas, Vikram S. Bajaj, Yoh Matsuki, Marina L Belenky, Johan Lugtenburg, Jagadishwar R. Sirigiri, Richard J. Temkin, Judith Herzfeld, Robert G. Griffin. *Resolution and polarization distribution in cryogenic DNP/MAS experiments*. Phys. Chem. Chem. Phys., **2010**, 12(22):5861-7.

(7) Alexander B. Barnes, Loren B. Andreas, Matthias Huber, Ramesh Ramachandran, Patrick C.A. van der Wel, Mikhail Veshtort, Robert G. Griffin and Manish A. Mehta *High Resolution solid-state NMR structure of Alanyl-Prolyl-Glycine*. J. Magn. Reson., **2009**, 200(1):95-100.

(8) Loren B. Andreas, Anil K. Mehta, Manish A. Mehta. *Determination of Global Structure from Distance and Orientation Constraints in Biological Solids using Solid-State NMR*. J. Am. Chem. Soc., **2007**, 129(49):15233-9.

Awards

Ritchey Award 2013

Experimental NMR Conference, Pacific Grove, CA

NSF Graduate Research Fellowship (\$30,000 per year) 2008-2011

National Fellowship

Finalist, Hertz Foundation Fellowship, 2005.

National Fellowship

Barry M. Goldwater Excellence in Education, National Scholarship (\$5000 award) 2005-2006.

National Award